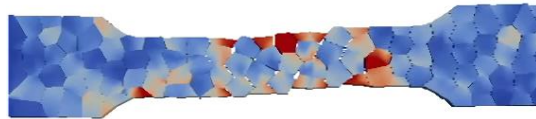
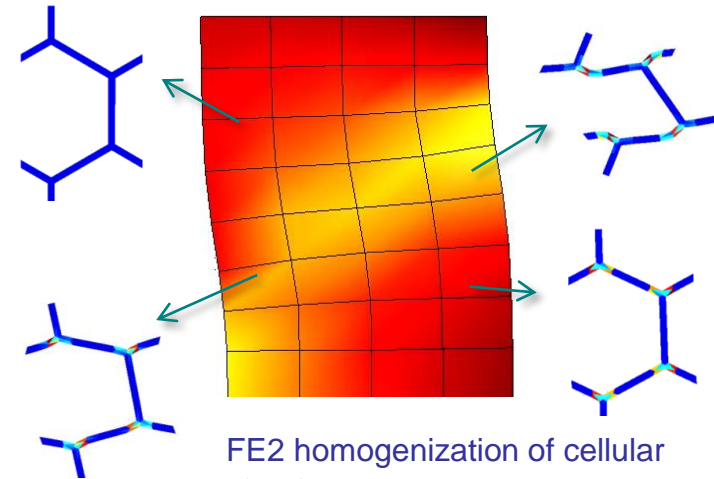


Non-local damage mean-field-homogenization

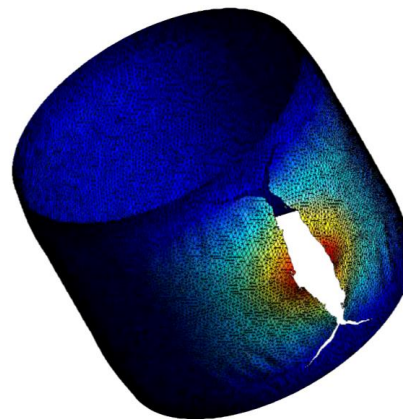
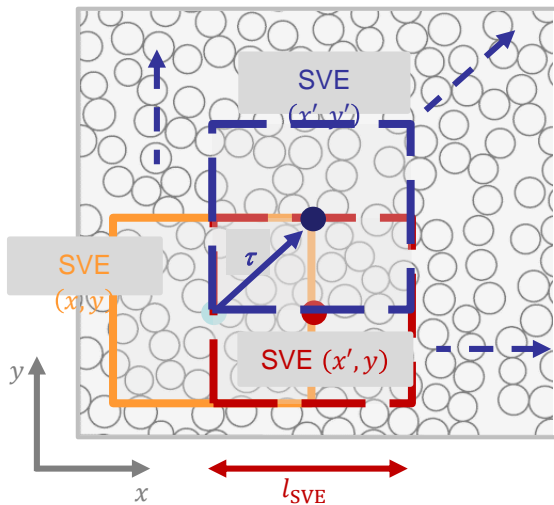
Stochastic multi-scale methods



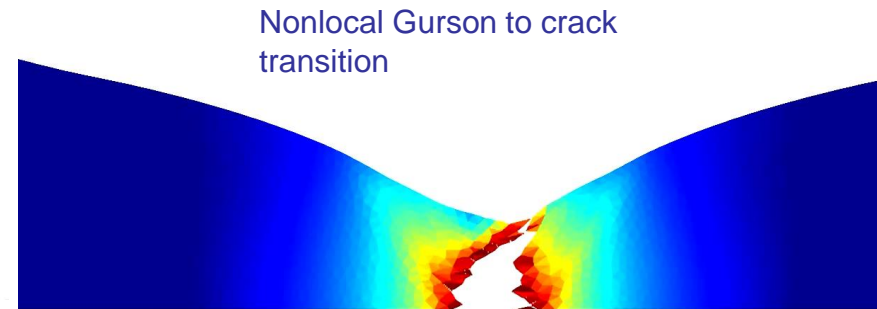
QC-based 2-scale method



FE2 homogenization of cellular structures

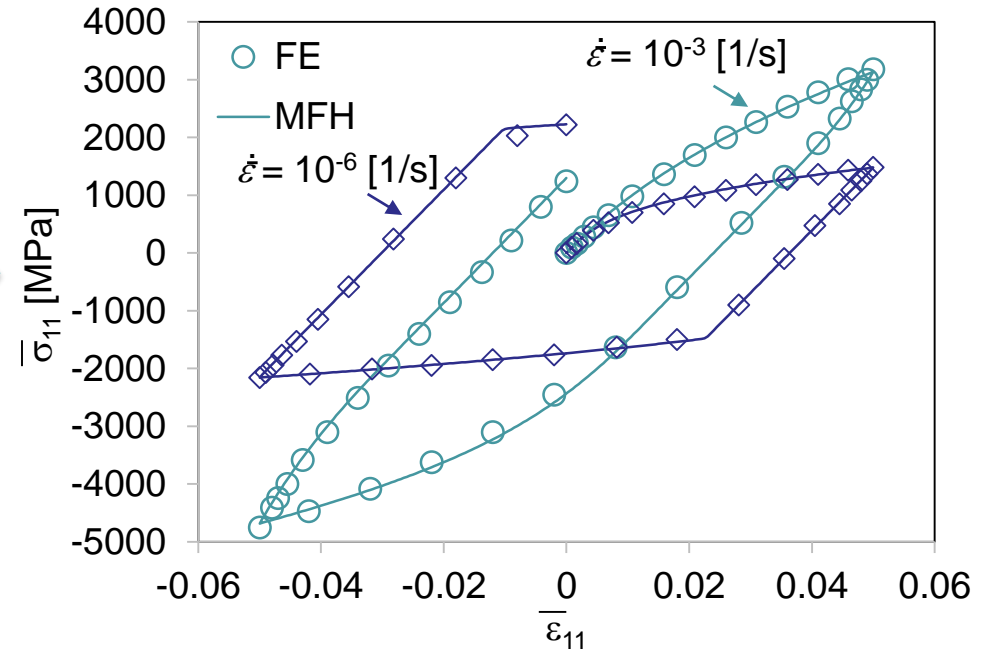
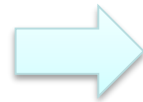
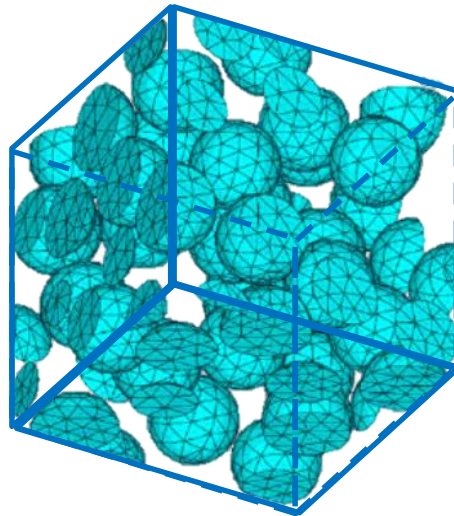


DG-based fracture



Nonlocal Gurson to crack transition

- [Mean-Field-Homogenization for Elasto-Visco-Plastic Composites](#)
- [Micro-structural simulation of fiber-reinforced highly crosslinked epoxy](#)
- [Stochastic Homogenization of Composite Materials](#)
- [Bayesian identification of stochastic MFH model parameters](#)
- [Non-Local Damage Mean-Field-Homogenization](#)
- [Boundary conditions and tangent operator in multi-physics FE²](#)
- [Computational Homogenization For Cellular Materials](#)
- [Stochastic 3-Scale Models for Polycrystalline Materials](#)
- [DG-Based Fracture](#)
 - [DG-Based Multi-Scale Fracture](#)
 - [DG-Based Dynamic Fracture](#)
 - [DG-Based Damage elastic damage to crack transition](#)
- [Non-local Gurson damage model to crack transition](#)
- [Stochastic Multi-Scale Fracture of Polycrystalline Films](#)
- [Smart Composite Materials – Shape Memory Effects](#)
- [Multi-Scale Modeling of Nano-Crystal Grain Boundary Sliding](#)
- [Stochastic Multi-Scale Model to Predict MEMS Stiction](#)



Mean-Field-Homogenization for Elasto-Visco-Plastic Composites

SIMUCOMP The research has been funded by the Walloon Region under the agreement no 1017232 (CT-EUC 2010-10-12) in the context of the ERA-NET +, Matera + framework.

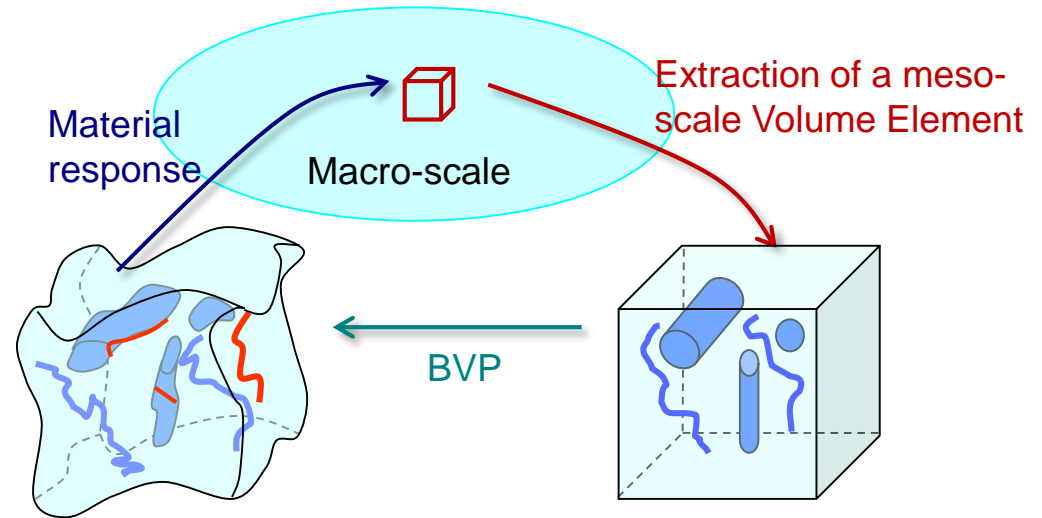
The authors gratefully acknowledge the financial support from F.R.S-F.N.R.S. under the project number PDR T.1015.14

STOMMMAC The research has been funded by the Walloon Region under the agreement no 1410246-STOMMMAC (CT-INT 2013-03-28) in the context of M-ERA.NET Joint Call 2014.

Mean-Field-Homogenization for elasto-visco-plastic composites

- Multi-scale modeling

- 2 problems are solved concurrently
 - The macro-scale problem
 - The meso-scale problem (on a meso-scale Volume Element)



- Length-scales separation

$$L_{\text{macro}} \gg L_{\text{VE}} \gg L_{\text{micro}}$$

For accuracy: Size of the meso-scale volume element smaller than the characteristic length of the macro-scale loading

To be statistically representative: Size of the meso-scale volume element larger than the characteristic length of the micro-structure

Mean-Field-Homogenization for elasto-visco-plastic composites

- Incremental-secant mean-field-homogenization

- Linear Comparison Composite material
 - Defined from unloaded state
- Solve iteratively the system

$$\left\{ \begin{array}{l} \Delta \bar{\boldsymbol{\varepsilon}}^r = \nu_0 \Delta \boldsymbol{\varepsilon}_0^r + \nu_I \Delta \boldsymbol{\varepsilon}_I^r \\ \Delta \boldsymbol{\varepsilon}_I^r = \Delta \boldsymbol{\varepsilon}_I + \Delta \boldsymbol{\varepsilon}_I^{\text{unload}} \\ \Delta \boldsymbol{\varepsilon}_0^r = \Delta \boldsymbol{\varepsilon}_0 + \Delta \boldsymbol{\varepsilon}_0^{\text{unload}} \\ \Delta \boldsymbol{\varepsilon}_I^r = \mathbf{B}^\varepsilon(\mathbf{I}, \bar{\mathbf{C}}_0^{\text{Sr}}, \bar{\mathbf{C}}_I^{\text{Sr}}) : \Delta \boldsymbol{\varepsilon}_0^r \end{array} \right.$$

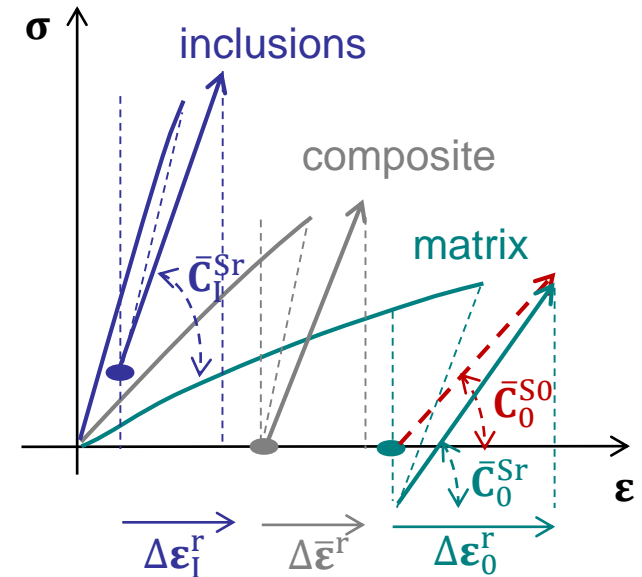
- With the stress tensors

$$\left\{ \begin{array}{l} \bar{\boldsymbol{\sigma}} = \nu_0 \boldsymbol{\sigma}_0 + \nu_I \boldsymbol{\sigma}_I \\ \boldsymbol{\sigma}_I = \boldsymbol{\sigma}_I^{\text{res}} + \bar{\mathbf{C}}_I^{\text{Sr}} : \Delta \boldsymbol{\varepsilon}_I^r \\ \boldsymbol{\sigma}_0 = \boldsymbol{\sigma}_0^{\text{res}} + \bar{\mathbf{C}}_0^{\text{Sr}} : \Delta \boldsymbol{\varepsilon}_0^r \end{array} \right.$$

- For soft matrix response

- Remove residual stress in matrix
- Or use second moment estimates

$$\Delta \boldsymbol{\varepsilon}_I^r = \mathbf{B}^\varepsilon(\mathbf{I}, \bar{\mathbf{C}}_0^{\text{S}0}, \bar{\mathbf{C}}_I^{\text{Sr}}) : \Delta \boldsymbol{\varepsilon}_0^r \quad \& \quad \boldsymbol{\sigma}_0 = \bar{\mathbf{C}}_0^{\text{S}0} : \Delta \boldsymbol{\varepsilon}_0^r$$



For elasto-plasticity: $f(\sigma^{\text{eq}}, p) = 0$

&

For elasto-visco-plasticity: $\Delta p = g_v(\sigma^{\text{eq}}, p) \Delta t$

Mean-Field-Homogenization for elasto-visco-plastic composites

- Incremental-secant mean-field-homogenization

- Stress tensor (2 forms)

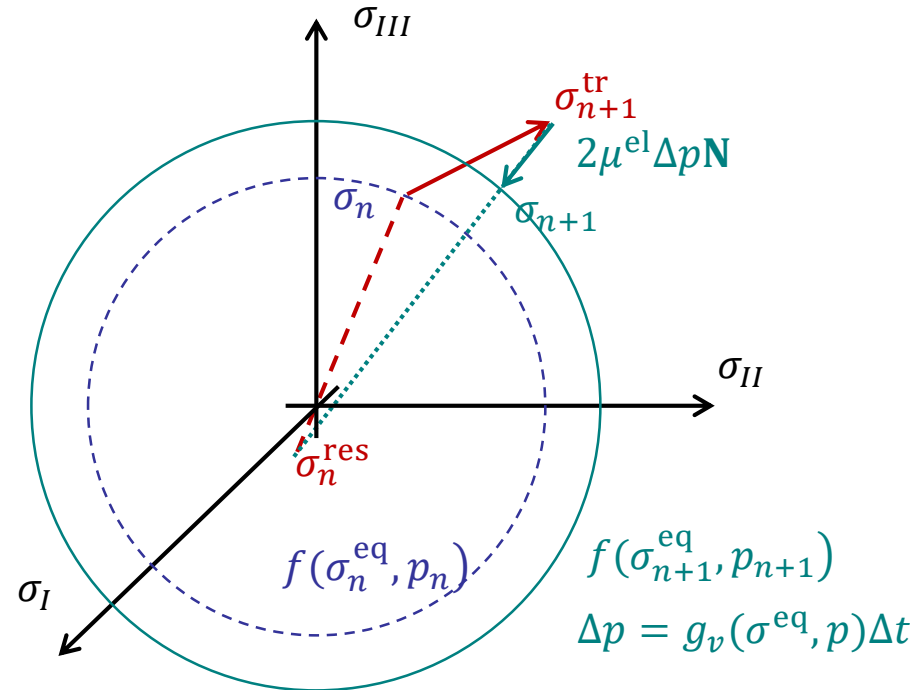
$$\left\{ \begin{array}{l} \boldsymbol{\sigma}_{I/0} = \boldsymbol{\sigma}_{I/0}^{\text{res}} + \bar{\mathbf{C}}_{I/0}^{\text{Sr}} : \Delta \boldsymbol{\varepsilon}_{I/0}^{\text{r}} \\ \boldsymbol{\sigma}_{I/0} = \bar{\mathbf{C}}_{I/0}^{\text{S0}} : \Delta \boldsymbol{\varepsilon}_{I/0}^{\text{r}} \end{array} \right.$$

- Radial return direction toward residual stress

- First order approximation in the strain increment (and not in the total strain)
- Exact for the zero-incremental-secant method

- The secant operators are naturally isotropic

$$\left\{ \begin{array}{l} \bar{\mathbf{C}}^{\text{Sr}} = 3\kappa^{\text{el}} \mathbf{I}^{\text{vol}} + 2 \left(\mu^{\text{el}} - 3 \frac{\mu^{\text{el}2} \Delta p}{(\boldsymbol{\sigma}_{n+1} - \boldsymbol{\sigma}_n^{\text{res}})^{\text{eq}}} \right) \mathbf{I}^{\text{vol}} \\ \bar{\mathbf{C}}^{\text{S0}} = 3\kappa^{\text{el}} \mathbf{I}^{\text{vol}} + 2 \left(\mu^{\text{el}} - 3 \frac{\mu^{\text{el}2} \Delta p}{\boldsymbol{\sigma}_{n+1}^{\text{eq}}} \right) \mathbf{I}^{\text{vol}} \end{array} \right.$$



Mean-Field-Homogenization for elasto-visco-plastic composites

- Incremental-secant mean-field-homogenization

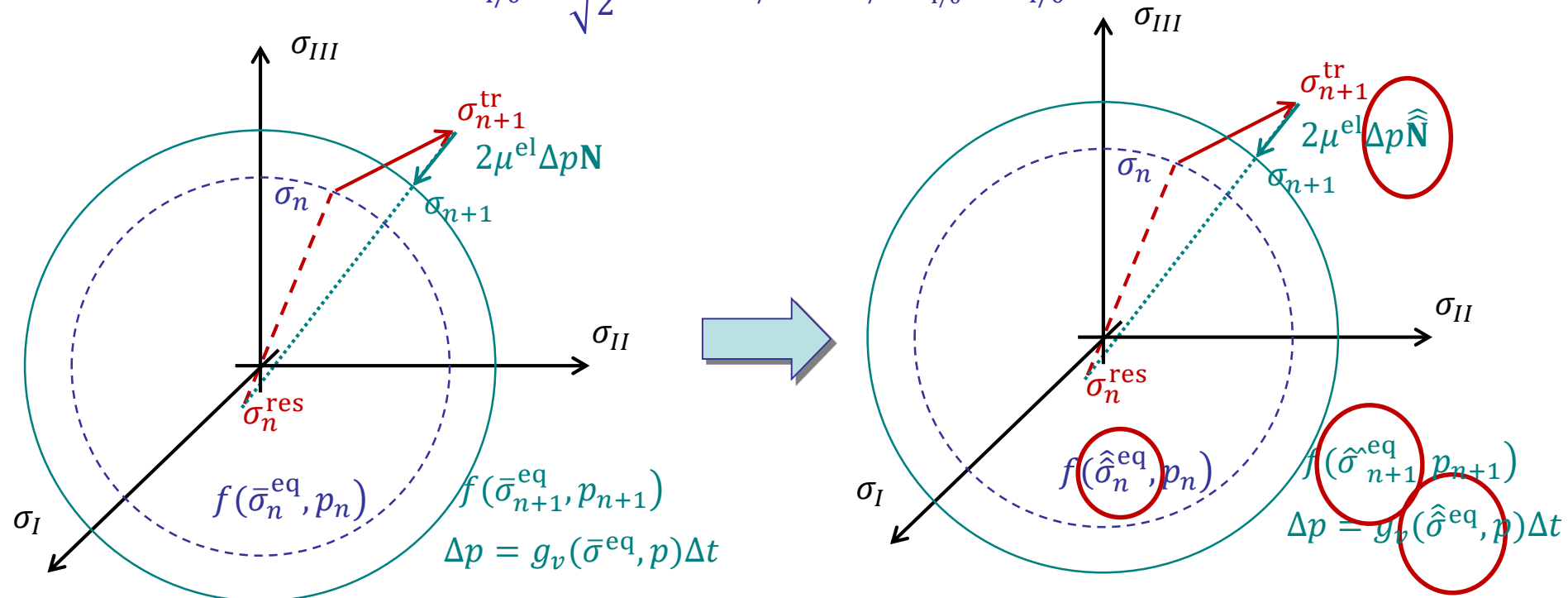
- Second-statistical moment estimation of the von Mises stress

- First statistical moment (mean value) not fully representative

$$\bar{\sigma}_{I/0}^{eq} = \sqrt{\frac{3}{2} \bar{\sigma}_{I/0}^{dev} : \bar{\sigma}_{I/0}^{dev}}$$

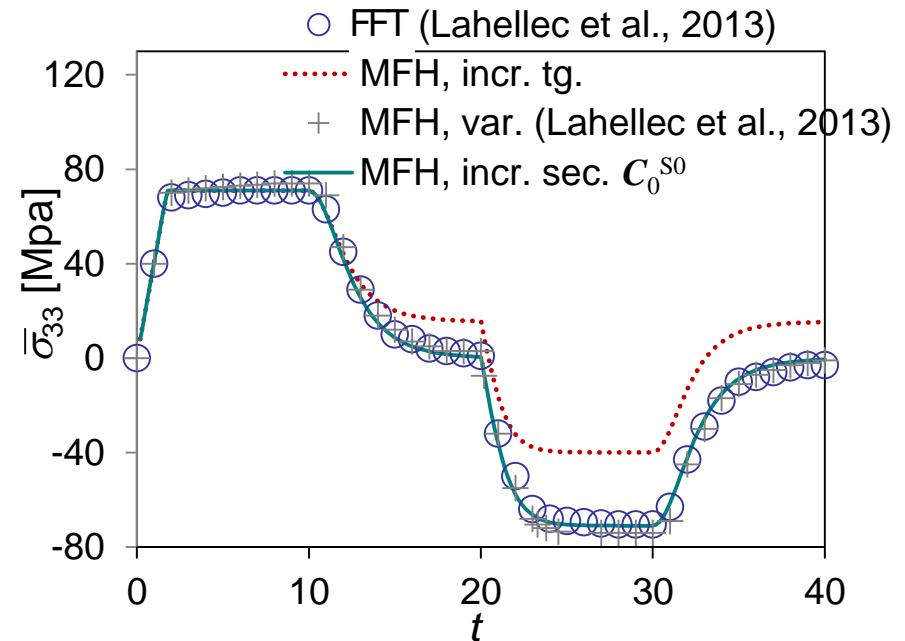
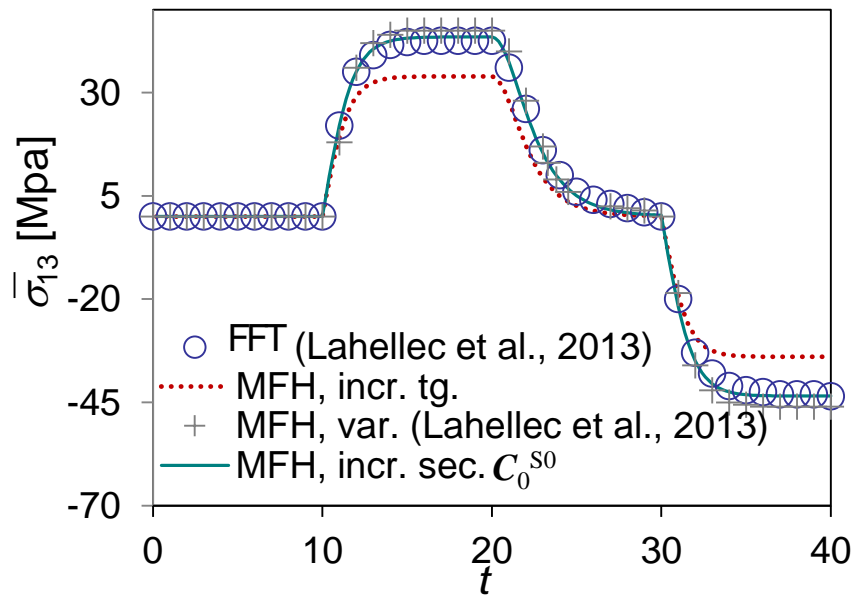
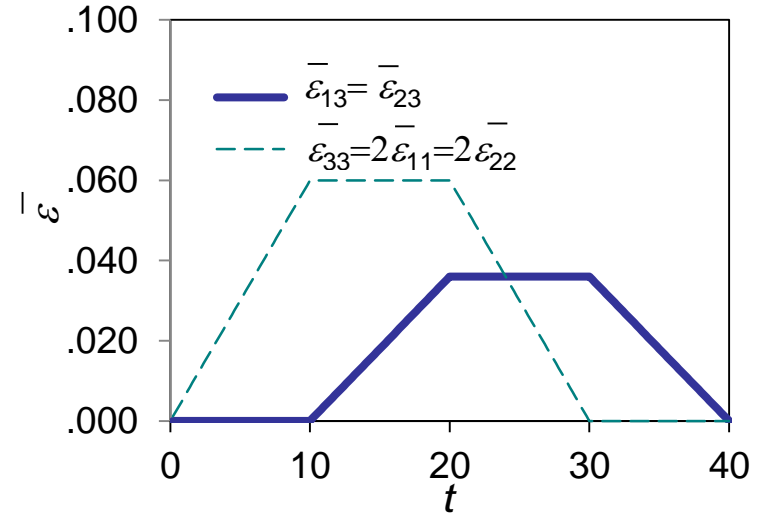
- Use second statistical moment estimations to define the yield surface

$$\hat{\sigma}_{I/0}^{eq} = \sqrt{\frac{3}{2} \mathbf{I}^{dev} :: \langle \sigma_{I/0} \otimes \sigma_{I/0} \rangle_{\omega_{I/0}} \geq \bar{\sigma}_{I/0}^{eq}}$$



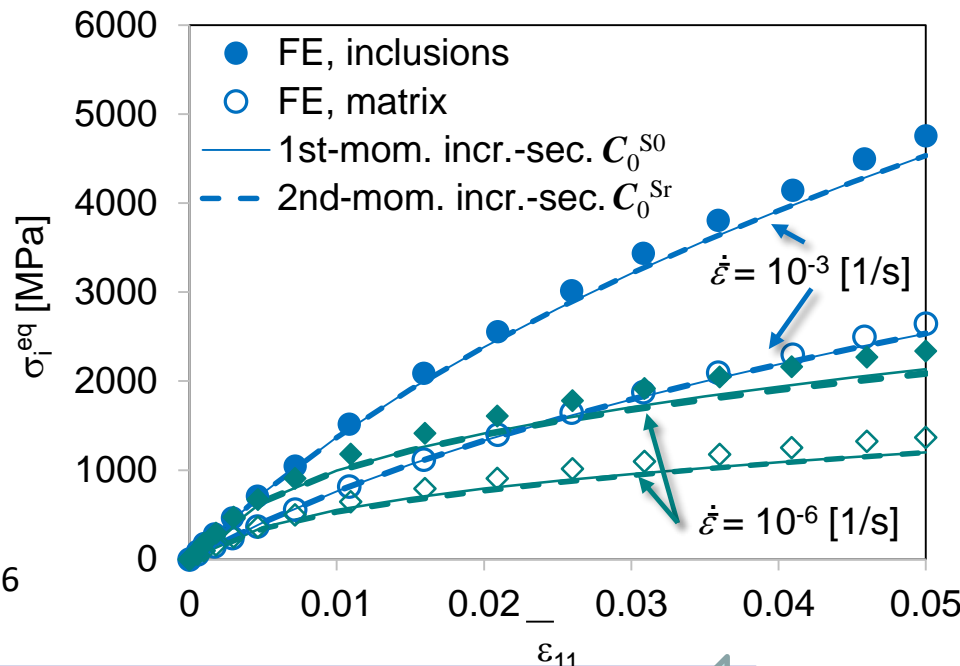
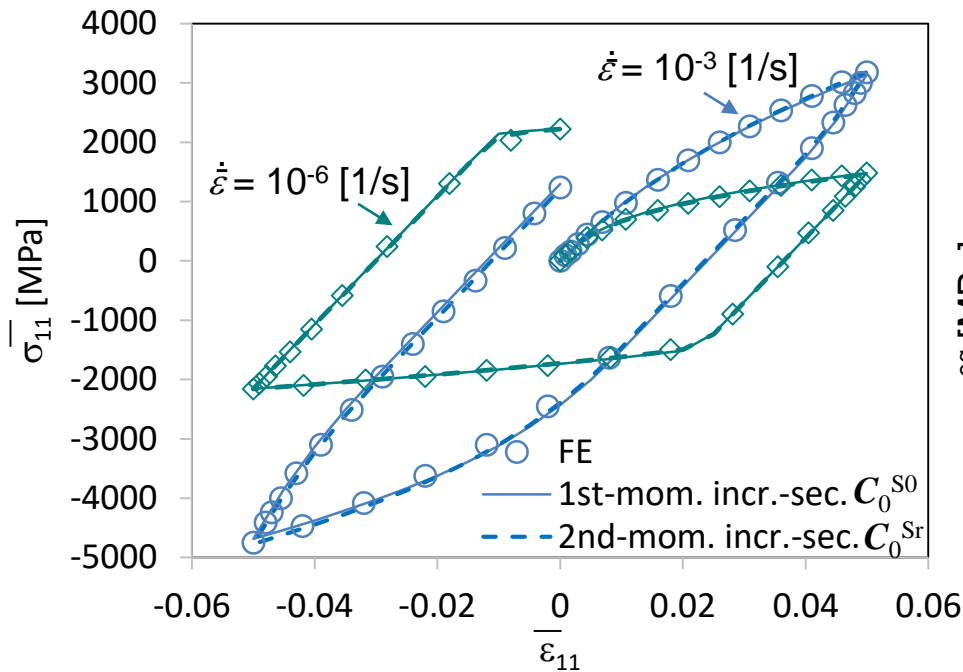
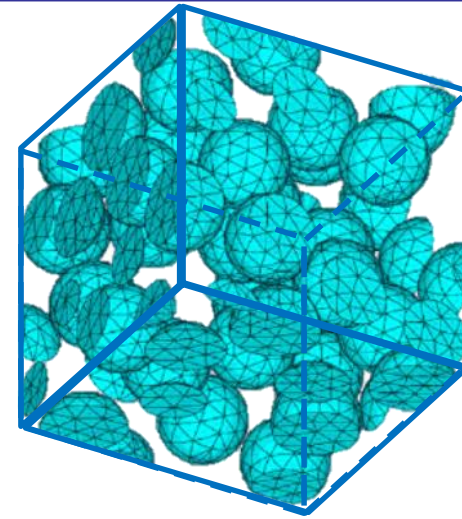
Mean-Field-Homogenization for elasto-visco-plastic composites

- Non-proportional loading
 - Spherical inclusions
 - 17 % volume fraction
 - Elastic
 - Elastic-perfectly-plastic matrix



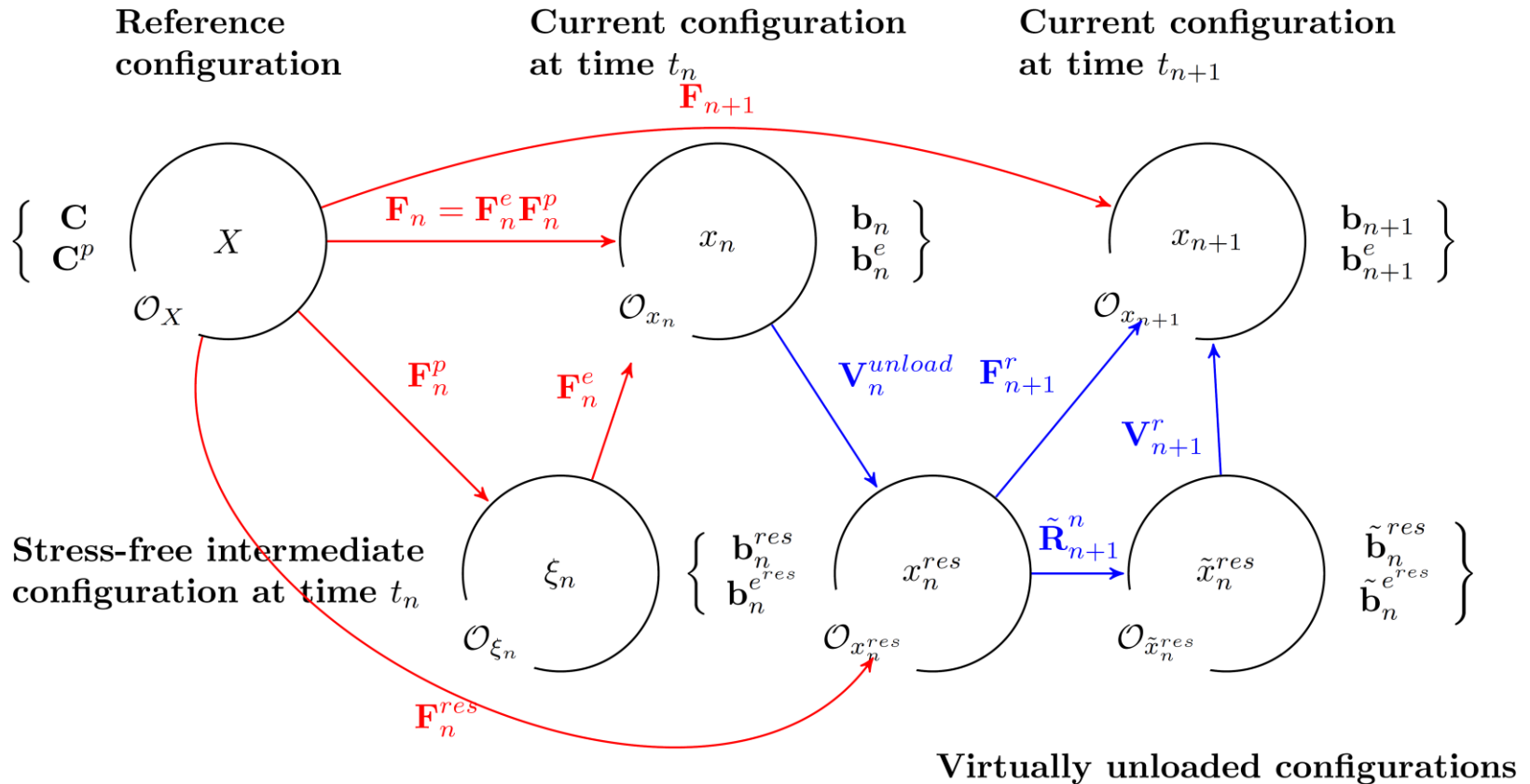
Mean-Field-Homogenization for elasto-visco-plastic composites

- Elasto-visco-plasticity
 - Elasto-visco-plastic short fibres
 - Spherical
 - 30 % volume fraction
 - Elasto-visco-plastic matrix



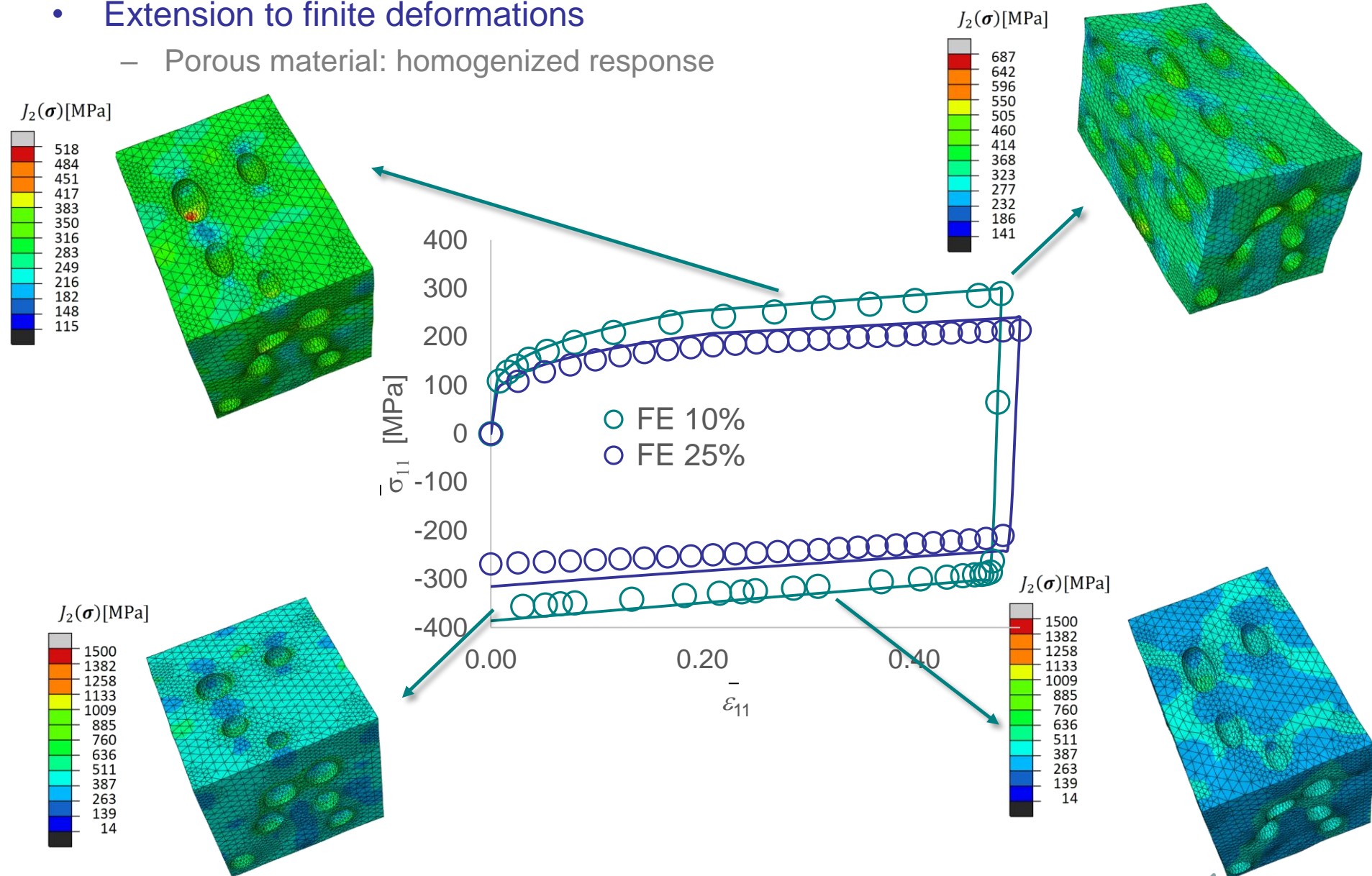
Mean-Field-Homogenization for elasto-visco-plastic composites

- Extension to finite deformations
 - Formulate everything in terms of elastic left Cauchy-Green tensor



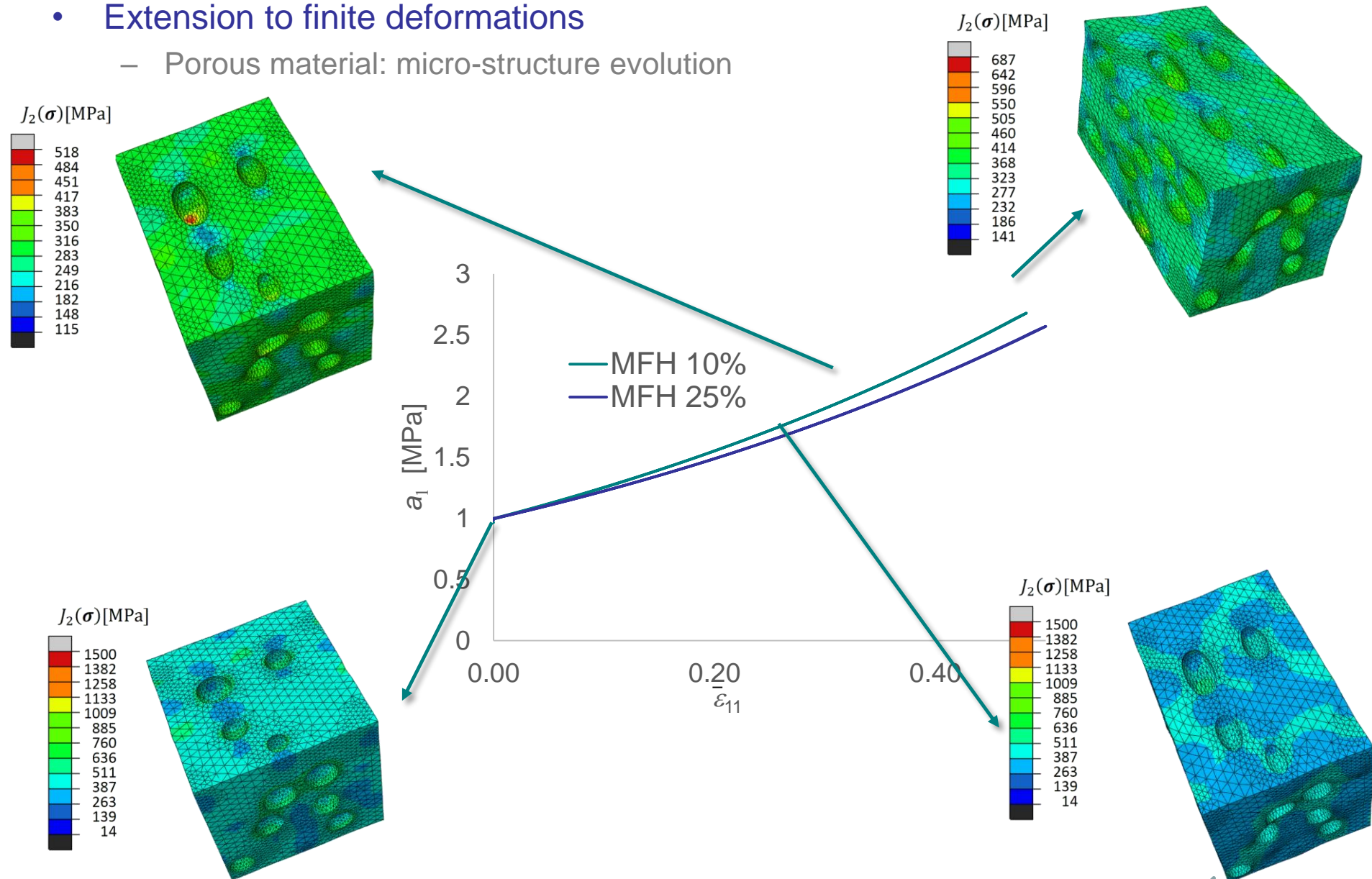
Mean-Field-Homogenization for elasto-visco-plastic composites

- Extension to finite deformations
 - Porous material: homogenized response



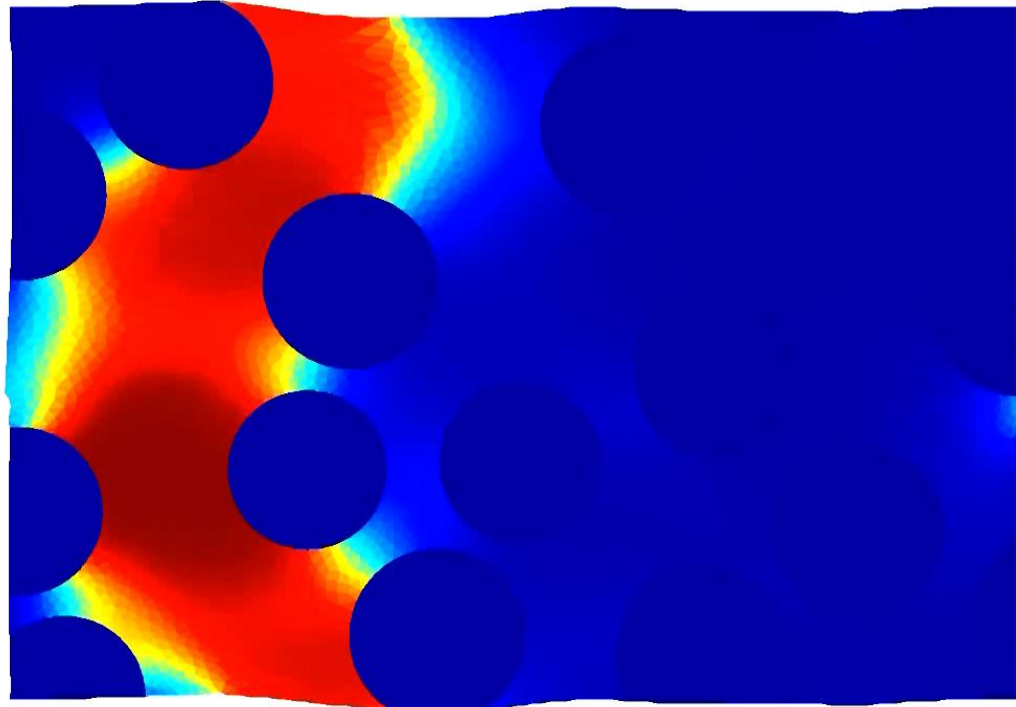
Mean-Field-Homogenization for elasto-visco-plastic composites

- Extension to finite deformations
 - Porous material: micro-structure evolution



Mean-Field-Homogenization for elasto-visco-plastic composites

- SIMUCOMP ERA-NET project (incremental secant MFH)
 - e-Xstream, CENAERO, ULiège (Belgium)
 - IMDEA Materials (Spain)
 - CRP Henri-Tudor (Luxemburg)
- PDR T.1015.14 project (MFH with second-order moments)
 - ULiège, UCL (Belgium)
- STOMMMAC M.ERA-NET project (MFH for elasto-visco-plastic composites)
 - e-Xstream, ULiège (Belgium)
 - BATZ (Spain)
 - JKU, AC (Austria)
 - U Luxembourg (Luxemburg)
- Publications (doi)
 - [10.1016/j.mechmat.2017.08.006](https://doi.org/10.1016/j.mechmat.2017.08.006)
 - [10.1080/14786435.2015.1087653](https://doi.org/10.1080/14786435.2015.1087653)
 - [10.1016/j.ijplas.2013.06.006](https://doi.org/10.1016/j.ijplas.2013.06.006)
 - [10.1016/j.cma.2018.12.007](https://doi.org/10.1016/j.cma.2018.12.007)

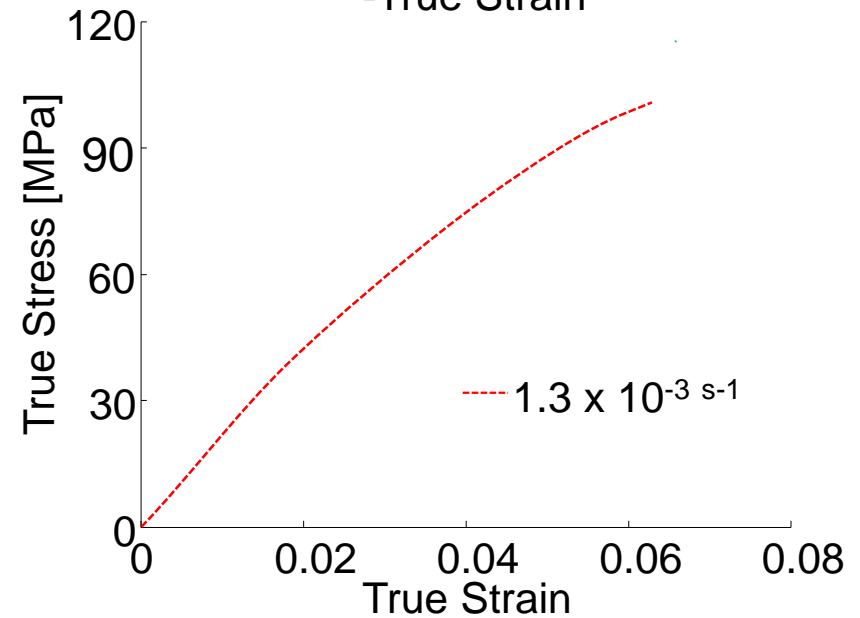
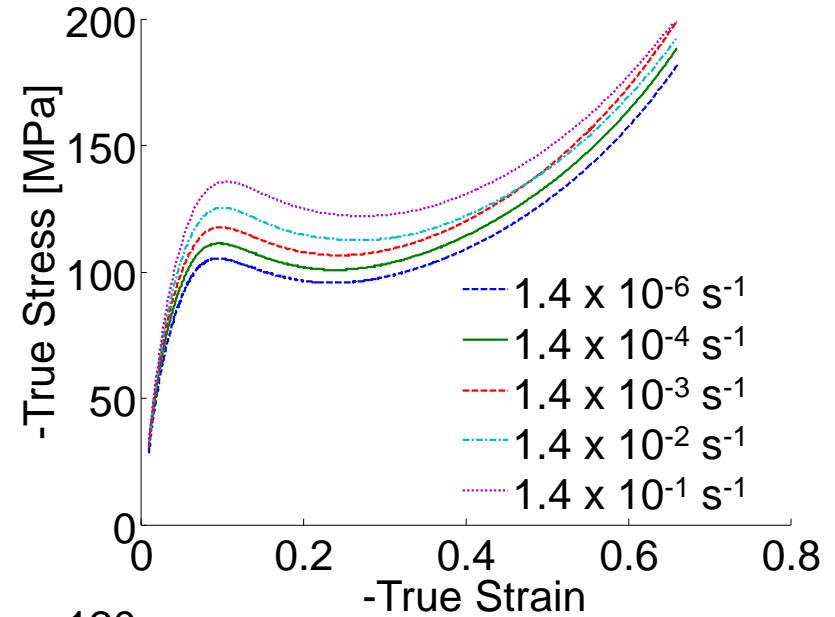
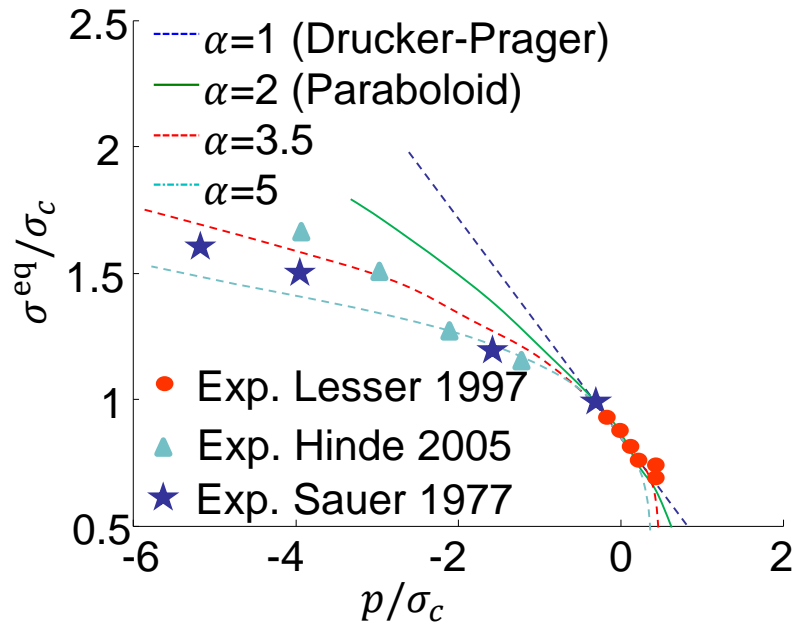


Micro-structural characterization and simulation of fiber-reinforced highly crosslinked epoxy

The authors gratefully acknowledge the financial support from F.R.S-F.N.R.S. under the project number PDR T.1015.14

Micro-structural simulation of fiber-reinforced highly crosslinked epoxy

- Resin behavior (experiments UCL)
 - Viscoelasto-Viscoplasticity
 - Saturated softening
 - Asymmetry tension-compression
 - Pressure-dependent yield
- To used in micro-structural analysis
 - Behavior in composite is different
 - Introduce a length-scale effect



Micro-structural simulation of fiber-reinforced highly crosslinked epoxy

- Material changes represented via internal variables

- Constitutive law $\mathbf{P}(\mathbf{F}; \mathbf{Z}(t'))$

- Internal variables $\mathbf{Z}(t')$

- Multi-damage strategy

$$\mathbf{P} = (\mathbf{1} - D_s)(\mathbf{1} - D_f)\hat{\mathbf{P}}$$

- Resin model implementation:

- Requires non-local form [Bažant 1988]

- Introduction of characteristic length l_c

- Weighted average: $\tilde{Z}(\mathbf{x}) = \int_{V_c} W(\mathbf{y}; \mathbf{x}, l_c) Z(\mathbf{y}) d\mathbf{y}$

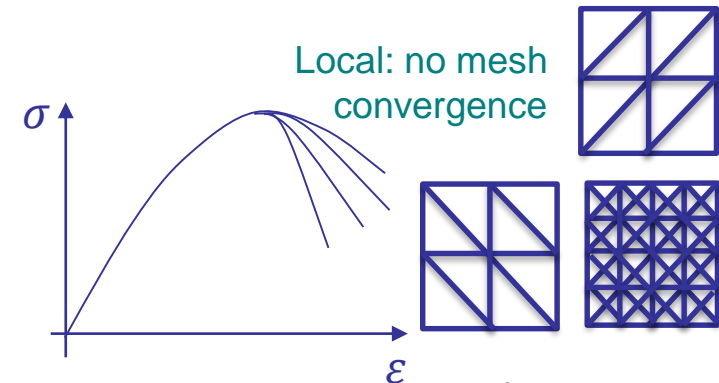
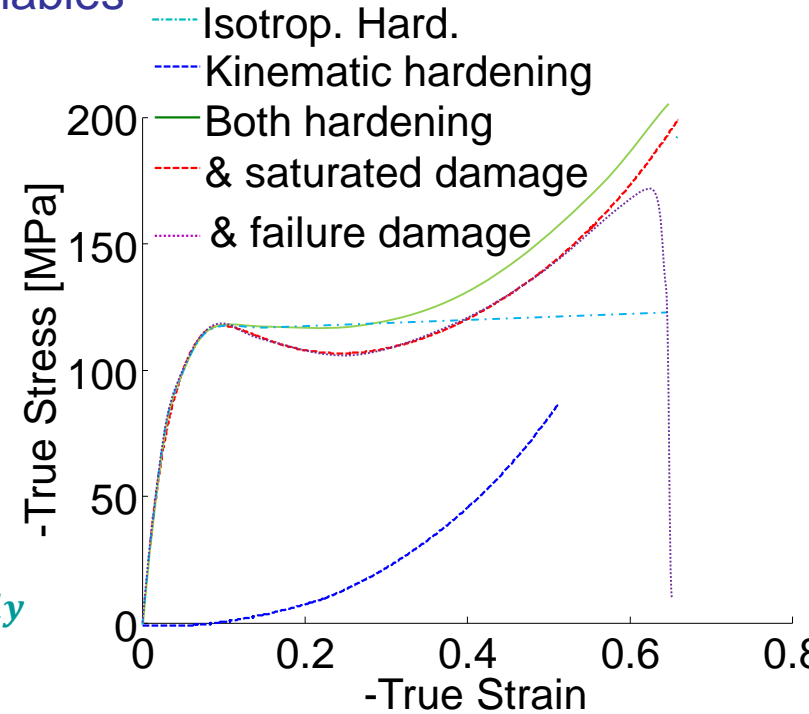
- Implicit form [Peerlings et al. 1998]

- New degrees of freedom: \tilde{Z}

- New Helmholtz-type equations: $\tilde{Z} - l_c^2 \Delta \tilde{Z} = Z$

- Damage evolution laws

$$\left\{ \begin{array}{l} \dot{D}_{s/f} = D_{s/f}(D_{s/f}, \mathbf{F}(t), \chi_{s/f}(t); Z(\tau), \tau \in [0, t]) \dot{\chi}_{s/f} \\ \chi_{s/f}(t) = \max_{\tau} (\tilde{\gamma}_{s/f}(\tau)) \\ \tilde{\gamma}_{s/f} - l_{s/f}^2 \Delta \tilde{\gamma}_{s/f} = \gamma_{s/f} \end{array} \right.$$



Micro-structural simulation of fiber-reinforced highly crosslinked epoxy

- Resin model: hyperelastic-based formulation

- Multiplicative decomposition

$$\mathbf{F} = \mathbf{F}^{ve} \cdot \mathbf{F}^{vp}, \quad \mathbf{C}^{ve} = \mathbf{F}^{veT} \cdot \mathbf{F}^{ve}, \quad J^{ve} = \det(\mathbf{F}^{ve})$$

- Undamaged stress tensor definition

- Elastic potential $\psi(\mathbf{C}^{ve})$
- Undamaged first Piola-Kirchhoff stress tensor

$$\hat{\mathbf{P}} = 2\mathbf{F}^{ve} \cdot \frac{\partial \psi(\mathbf{C}^{ve})}{\partial \mathbf{C}^{ve}} \cdot \mathbf{F}^{vp-T}$$

- Undamaged Kirchhoff stress tensors

- In current configuration

$$\hat{\boldsymbol{\kappa}} = \hat{\mathbf{P}} \cdot \mathbf{F}^T = 2\mathbf{F}^{ve} \cdot \frac{\partial \psi(\mathbf{C}^{ve})}{\partial \mathbf{C}^{ve}} \cdot \mathbf{F}^{veT}$$

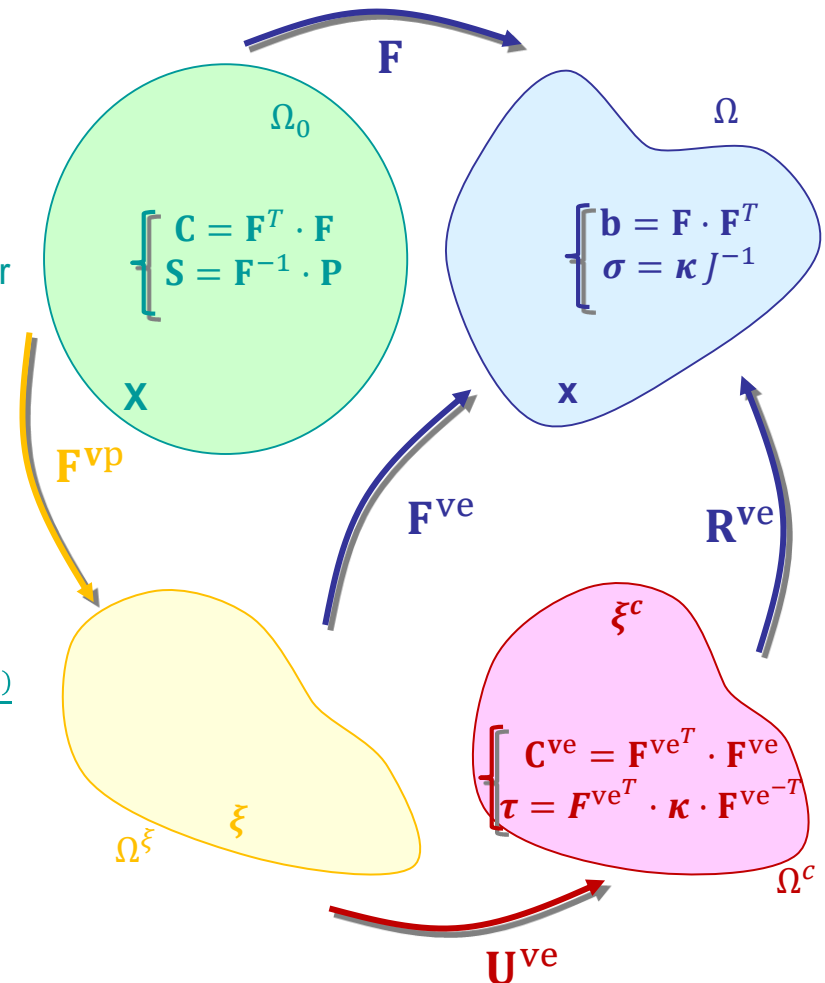
- In co-rotational space

$$\hat{\boldsymbol{\tau}} = \mathbf{C}^{ve} \cdot \mathbf{F}^{ve-1} \cdot \hat{\boldsymbol{\kappa}} \cdot \mathbf{F}^{ve-T} = 2\mathbf{C}^{ve} \cdot \frac{\partial \psi(\mathbf{C}^{ve})}{\partial \mathbf{C}^{ve}}$$

- Apparent stress tensor

- Piola-Kirchhoff stress

$$\mathbf{P} = (\mathbf{1} - D_s)(\mathbf{1} - D_f)\hat{\mathbf{P}}$$



Micro-structural simulation of fiber-reinforced highly crosslinked epoxy

- Resin model: logarithmic visco-elasticity

- Elastic potentials ψ_i :

$$\psi_i(\mathbf{C}^{\text{ve}}) = \frac{K_i}{2} \ln^2(J^{\text{ve}}) + \frac{G_i}{4} (\ln(\mathbf{C}^{\text{ve}}))^{\text{dev}} : (\ln(\mathbf{C}^{\text{ve}}))^{\text{dev}}$$

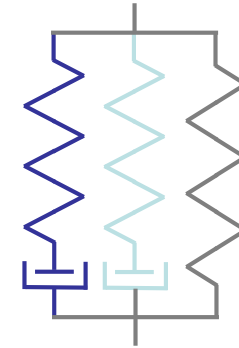
- Dissipative potentials Υ_i

$$\Upsilon_i(\mathbf{C}^{\text{ve}}, \mathbf{q}_i) = -\mathbf{q}_i : \ln(\mathbf{C}^{\text{ve}}) + \left[\frac{1}{18K_i} \text{tr}^2(\mathbf{q}_i) + \frac{1}{4G_i} \mathbf{q}_i^{\text{dev}} : \mathbf{q}_i^{\text{dev}} \right]$$

$$\left\{ \begin{array}{l} \dot{\mathbf{q}}_i^{\text{dev}} = \frac{2G_i}{g_i} (\ln(\mathbf{C}^{\text{ve}}))^{\text{dev}} - \frac{1}{g_i} \mathbf{q}_i^{\text{dev}} \\ \text{tr}(\dot{\mathbf{q}}_i) = \frac{3K_i}{k_i} \ln^2(J^{\text{ve}}) - \frac{1}{k_i} \text{tr}(\mathbf{q}_i) \end{array} \right.$$

- Total potential ψ :

$$\left\{ \begin{array}{l} \psi(\mathbf{C}^{\text{ve}}; \mathbf{q}_i) = \psi_\infty(\mathbf{C}^{\text{ve}}) + \sum_i [\psi_i(\mathbf{C}^{\text{ve}}) + \Upsilon_i(\mathbf{C}^{\text{ve}}, \mathbf{q}_i)] \\ \hat{\mathbf{P}} = 2\mathbf{F}^{\text{ve}} \cdot \frac{\partial \psi(\mathbf{C}^{\text{ve}})}{\partial \mathbf{C}^{\text{ve}}} \cdot \mathbf{F}^{\text{vp}-T} \end{array} \right.$$



Micro-structural simulation of fiber-reinforced highly crosslinked epoxy

- Resin model: visco-plasticity

- Stress, back-stress

$$\boldsymbol{\varphi} = \hat{\boldsymbol{\tau}} - \hat{\boldsymbol{b}}$$

- Perzina plastic flow rule

$$\mathbf{D}^{vp} = \dot{\mathbf{F}}^{vp} \cdot \mathbf{F}^{vp} = \frac{1}{\eta} \langle \phi \rangle^{\frac{1}{p}} \frac{\partial P}{\partial \hat{\boldsymbol{\tau}}}$$

- Pressure dependent yield surface

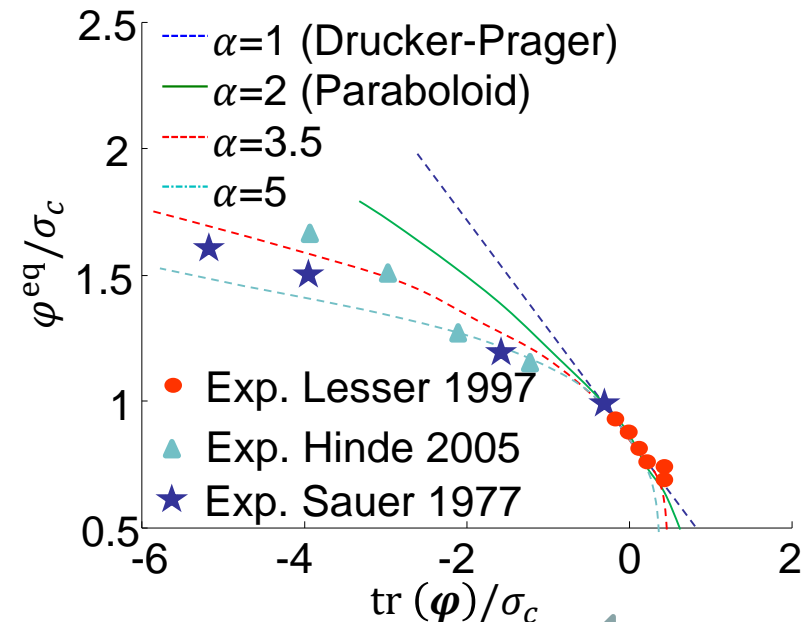
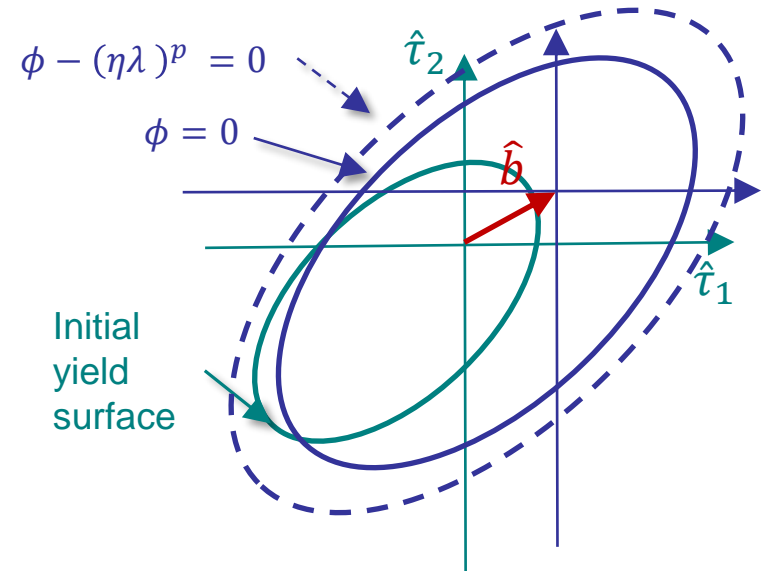
$$\left\{ \begin{array}{l} \phi = \left(\frac{\varphi^{eq}}{\sigma_c} \right)^\alpha - \frac{m^\alpha - 1}{m+1} \frac{\text{tr} \boldsymbol{\varphi}}{\sigma_c} - \frac{m^\alpha + m}{m+1} \leq 0 \\ m = \frac{\sigma_t}{\sigma_c} \end{array} \right.$$

- Non-associated flow potential

$$P = (\varphi^{eq})^2 + \beta \left(\frac{\text{tr} \boldsymbol{\varphi}}{3} \right)^2$$

- Equivalent plastic strain rate:

$$\left\{ \begin{array}{l} \dot{\gamma} = \frac{\sqrt{\mathbf{D}^{vp} : \mathbf{D}^{vp}}}{\sqrt{1 + 2v_p^2}} \\ v_p = \frac{9 - 2\beta}{18 + 2\beta} \end{array} \right.$$



Micro-structural simulation of fiber-reinforced highly crosslinked epoxy

- Resin model: saturated softening

- Damage evolution

$$\begin{cases} \dot{D}_s = H_s (\chi_s - \chi_{s0})^{\zeta_s} (D_{s\infty} - D_s) \dot{\chi}_s \\ \chi_s = \max_{\tau} (\chi_{s0}, \tilde{\gamma}_s(\tau)) \\ \tilde{\gamma}_s - l_s^2 \Delta \tilde{\gamma}_s = \gamma \end{cases}$$

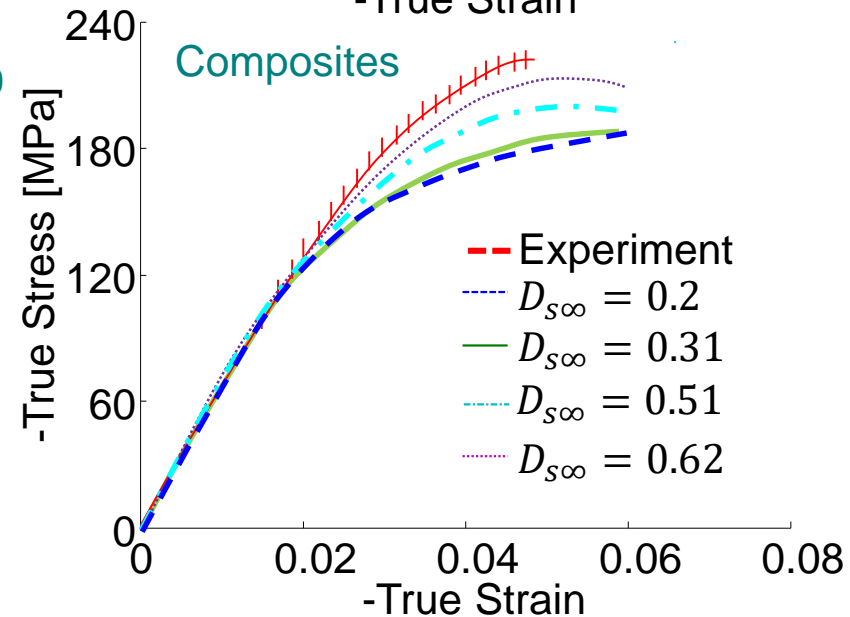
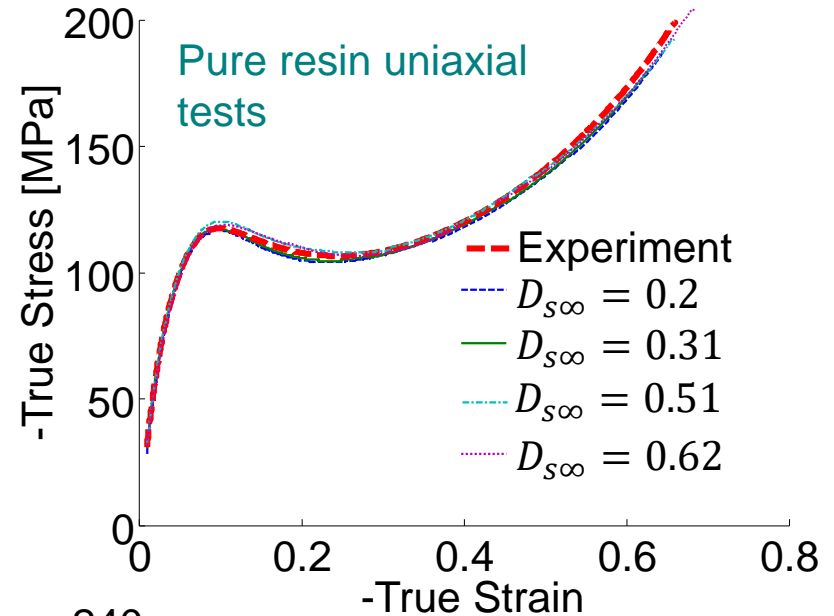
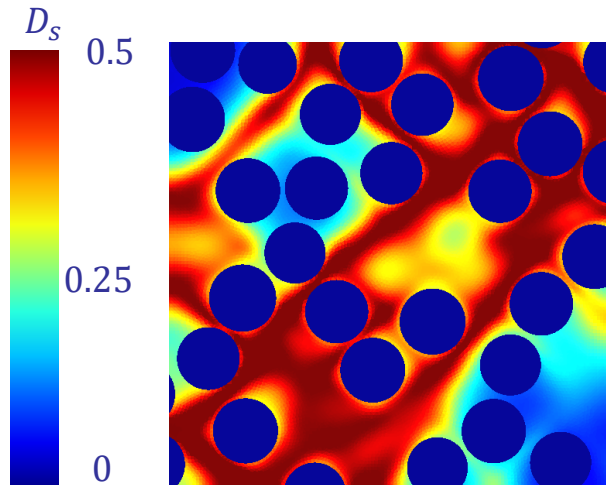
- Calibration

- Several hardening/softening combinations
 - Requires composite material tests

- Length scale effect

$$l_s = 3\mu\text{m} \left(1 - \frac{D_s}{D_{s\infty}}\right)$$

- Non-local BC at fiber interface $[[\dot{\gamma}_s]] = 0$



Micro-structural simulation of fiber-reinforced highly crosslinked epoxy

- Resin model: failure softening

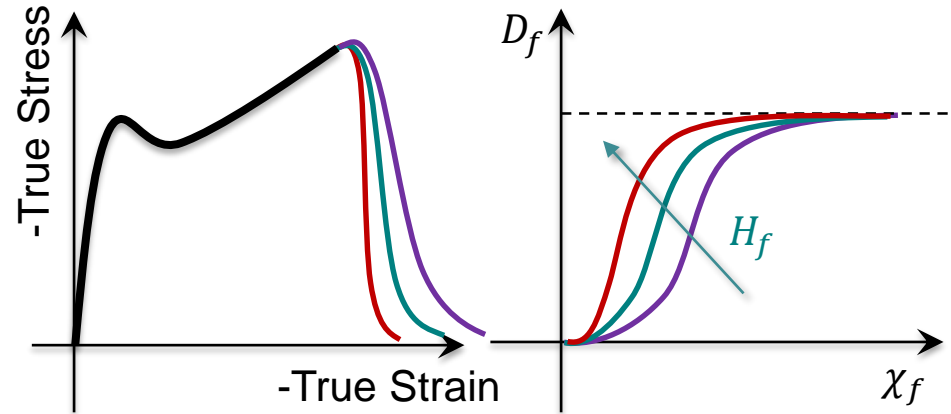
- Failure surface

$$\left\{ \begin{array}{l} \phi_f = \gamma - a \exp\left(-b \frac{\text{tr}(\hat{\boldsymbol{\tau}})}{3\hat{\boldsymbol{\tau}}^{eq}}\right) - c \\ \phi_f - r \leq 0; \dot{r} \geq 0; \text{ and } \dot{r}(\phi_f - r) = 0 \\ \dot{\gamma}_f = \dot{r} \end{array} \right.$$

- Damage evolution

$$\left\{ \begin{array}{l} \dot{D}_f = H_f(\chi_f)^{\zeta_f} (1 - D_f)^{-\zeta_a} \dot{\chi}_f \\ \chi_f = \max_{\tau} (\tilde{\gamma}_f(\tau)) \\ \tilde{\gamma}_f - l_f^2 \Delta \tilde{\gamma}_f = \gamma_f \\ l_f = 3 \mu\text{m} \quad \nabla_0 \tilde{\gamma}_f \cdot \mathbf{N} = 0 \end{array} \right.$$

- Affect ductility



Micro-structural simulation of fiber-reinforced highly crosslinked epoxy

- Resin model: failure softening (2)

- Damage evolution

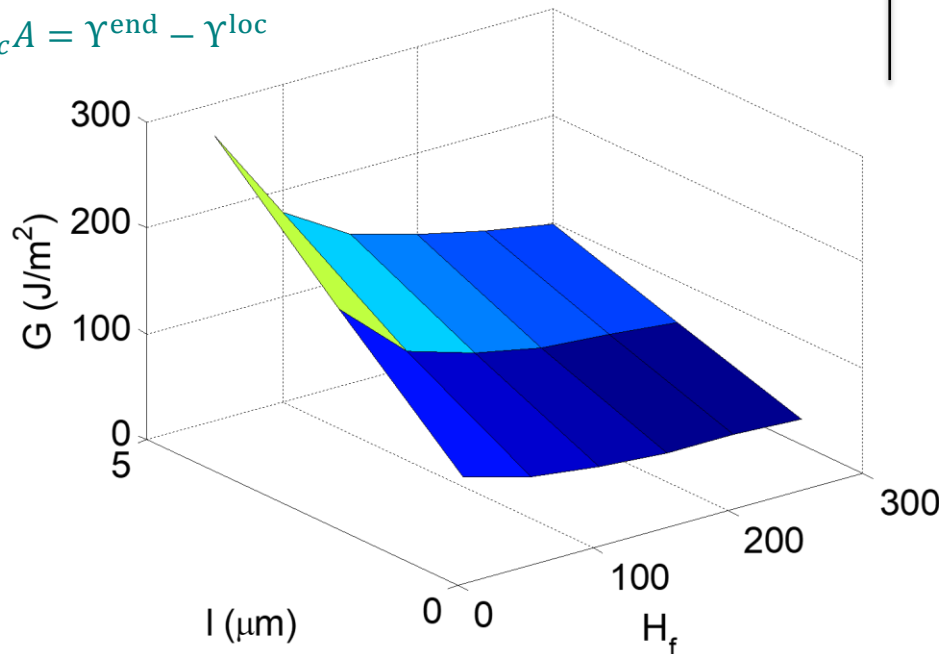
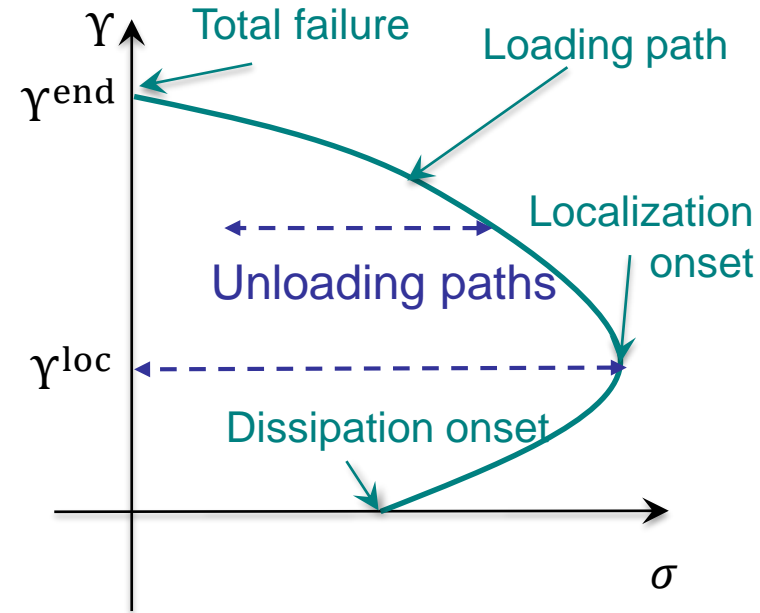
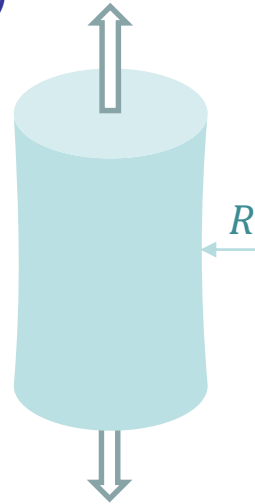
$$\dot{D}_f = H_f (\chi_f)^{\zeta_f} (1 - D_f)^{-\zeta_d} \dot{\chi}_f$$

$$\tilde{\gamma}_f - l_f^2 \Delta \tilde{\gamma}_f = \gamma_f$$

- Calibration

- Recover the epoxy G_c
- From localization simulation

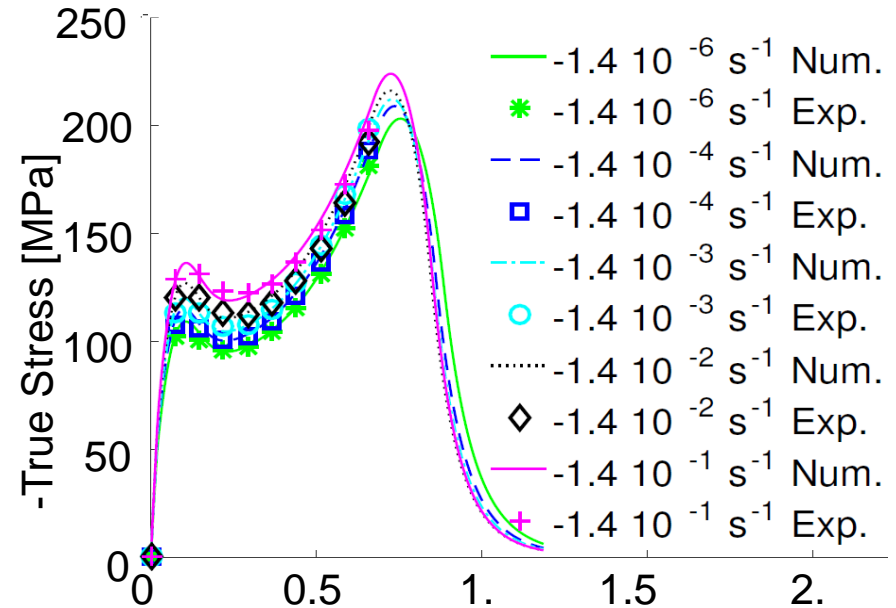
$$G_c A = \gamma^{\text{end}} - \gamma^{\text{loc}}$$



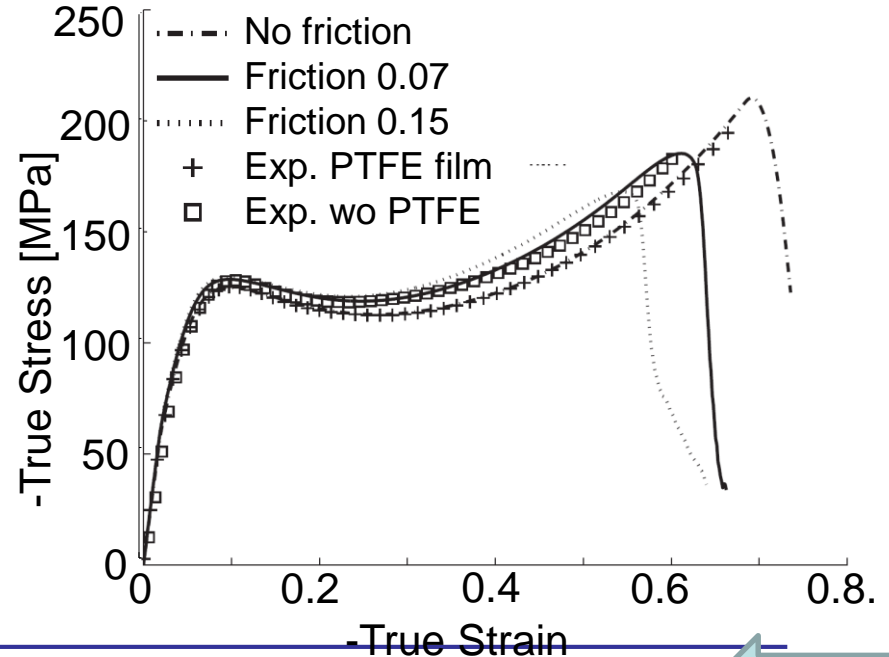
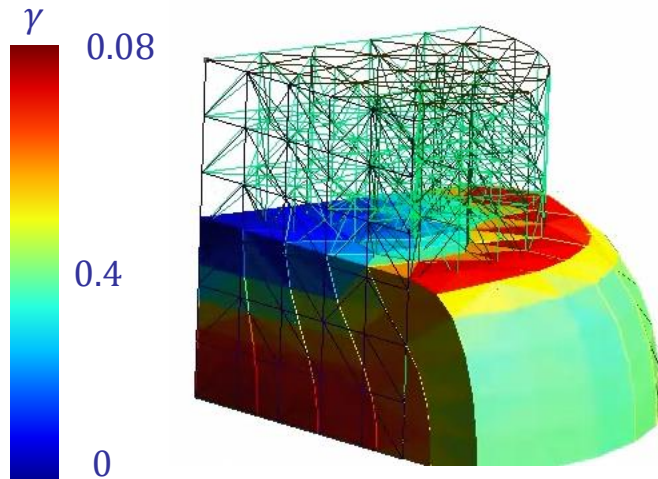
Micro-structural simulation of fiber-reinforced highly crosslinked epoxy

- Resin model: Validation

- Compression without barrelling effect

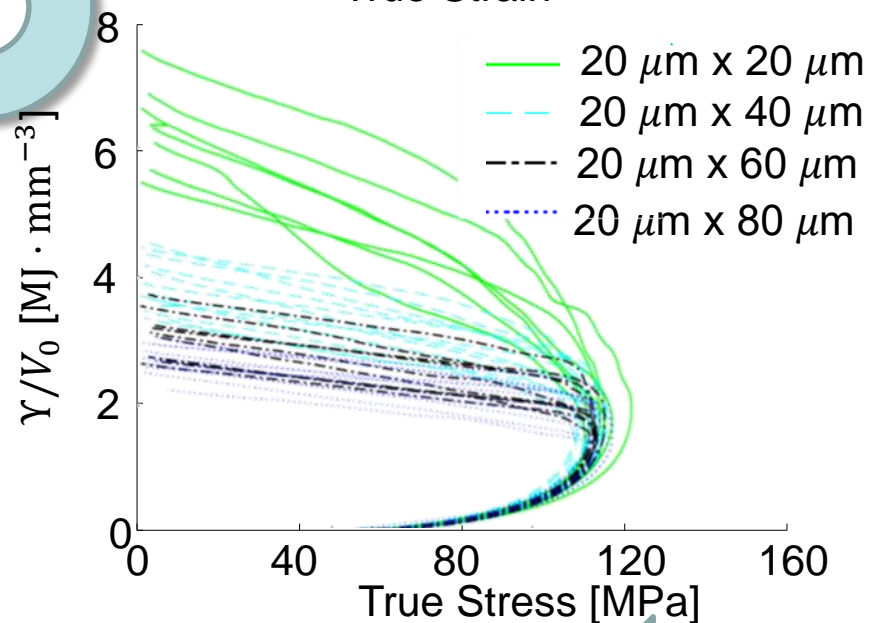
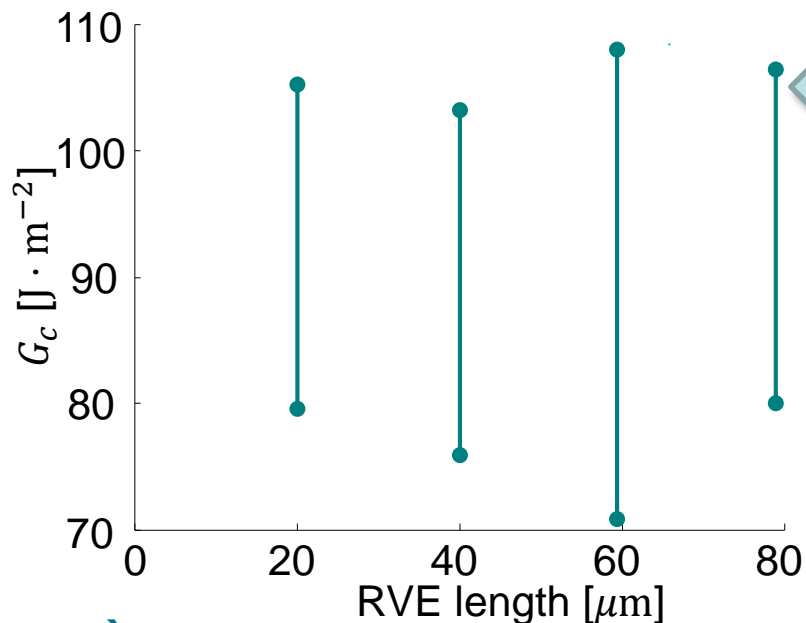
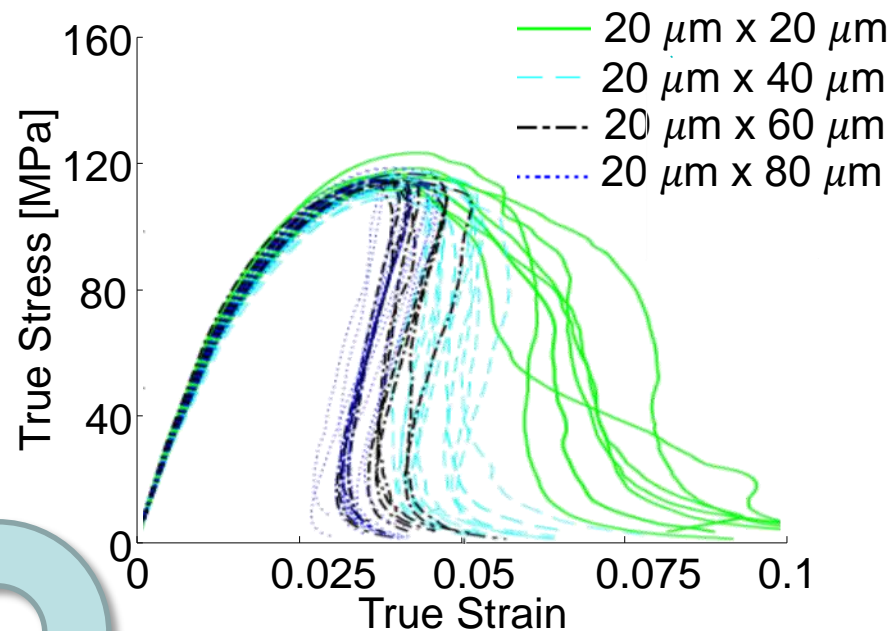
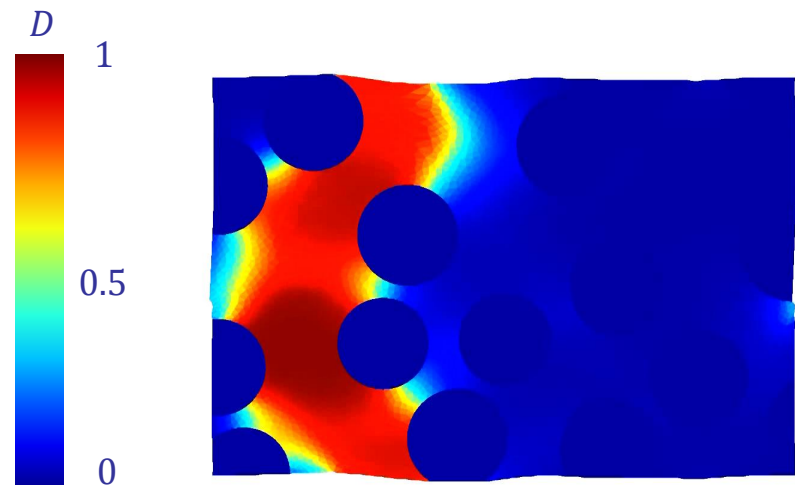


- With barrelling effect



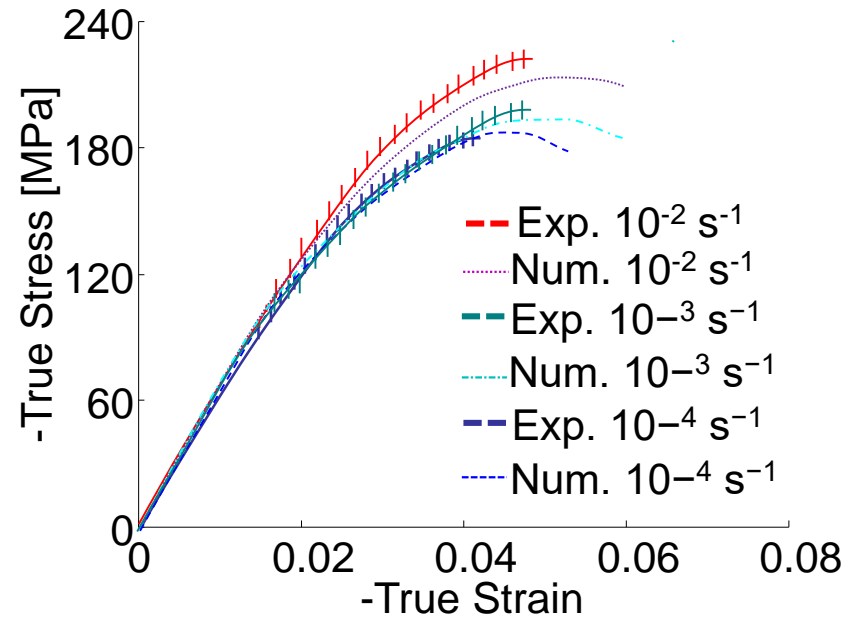
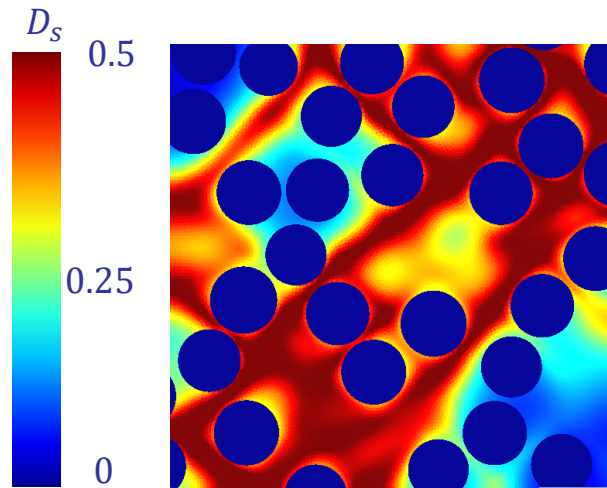
Micro-structural simulation of fiber-reinforced highly crosslinked epoxy

- Composite model: Extraction of G_c

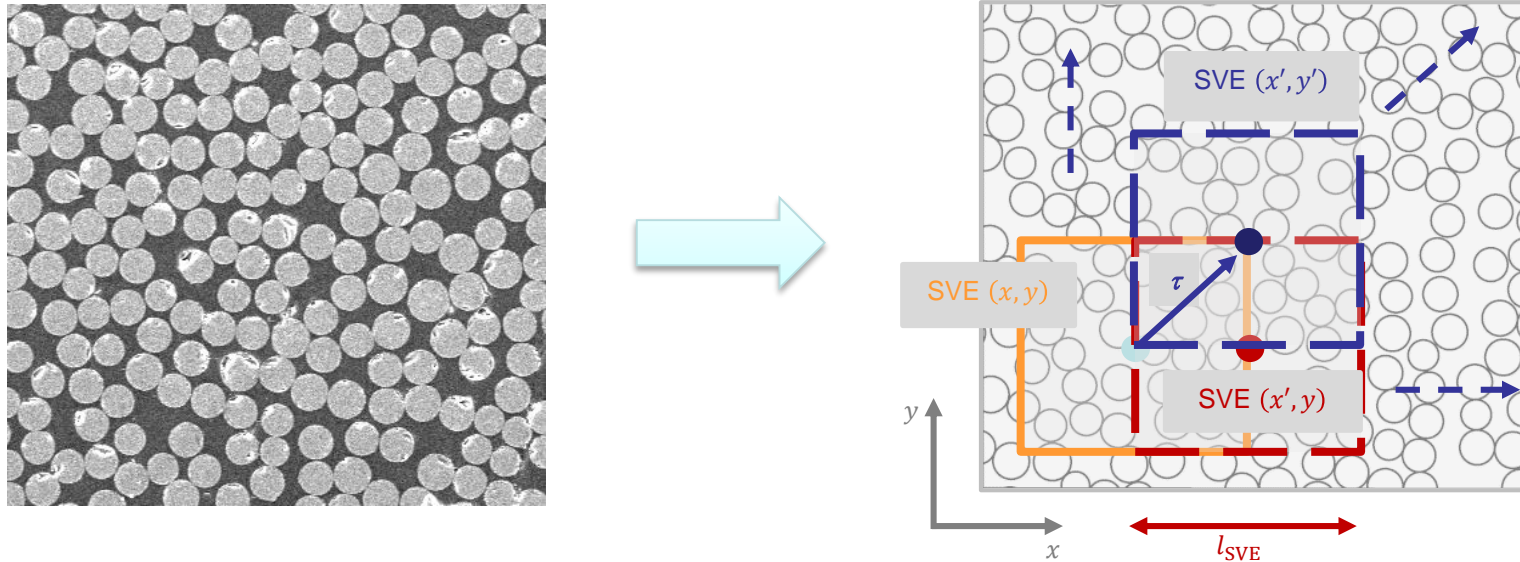


Micro-structural simulation of fiber-reinforced highly crosslinked epoxy

- Composite model: Validation
 - Compression test



- PDR T.1015.14 project
 - ULiège, UCL (Belgium)
- Publications
 - [10.1016/j.ijsolstr.2016.06.008](https://doi.org/10.1016/j.ijsolstr.2016.06.008)
 - [10.1016/j.mechmat.2019.02.017](https://doi.org/10.1016/j.mechmat.2019.02.017)



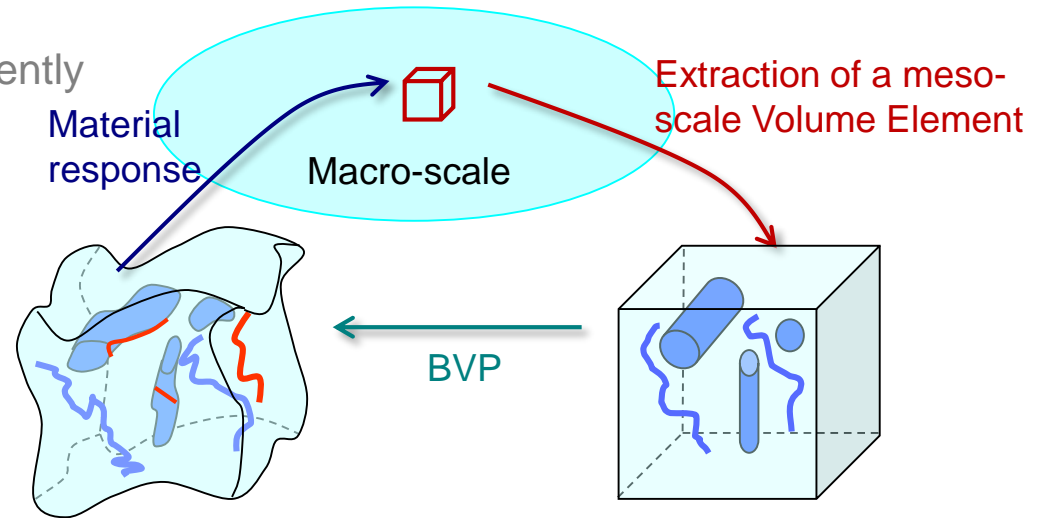
Stochastic Homogenization of Composite Materials

STOMMMAC The research has been funded by the Walloon Region under the agreement no 1410246-STOMMMAC (CT-INT 2013-03-28) in the context of M-ERA.NET Joint Call 2014.

Stochastic Homogenization of Composite Materials

- Multi-scale modeling

- 2 problems are solved concurrently
 - The macro-scale problem
 - The meso-scale problem (on a meso-scale Volume Element)



- For structures not several orders larger than the micro-structure size

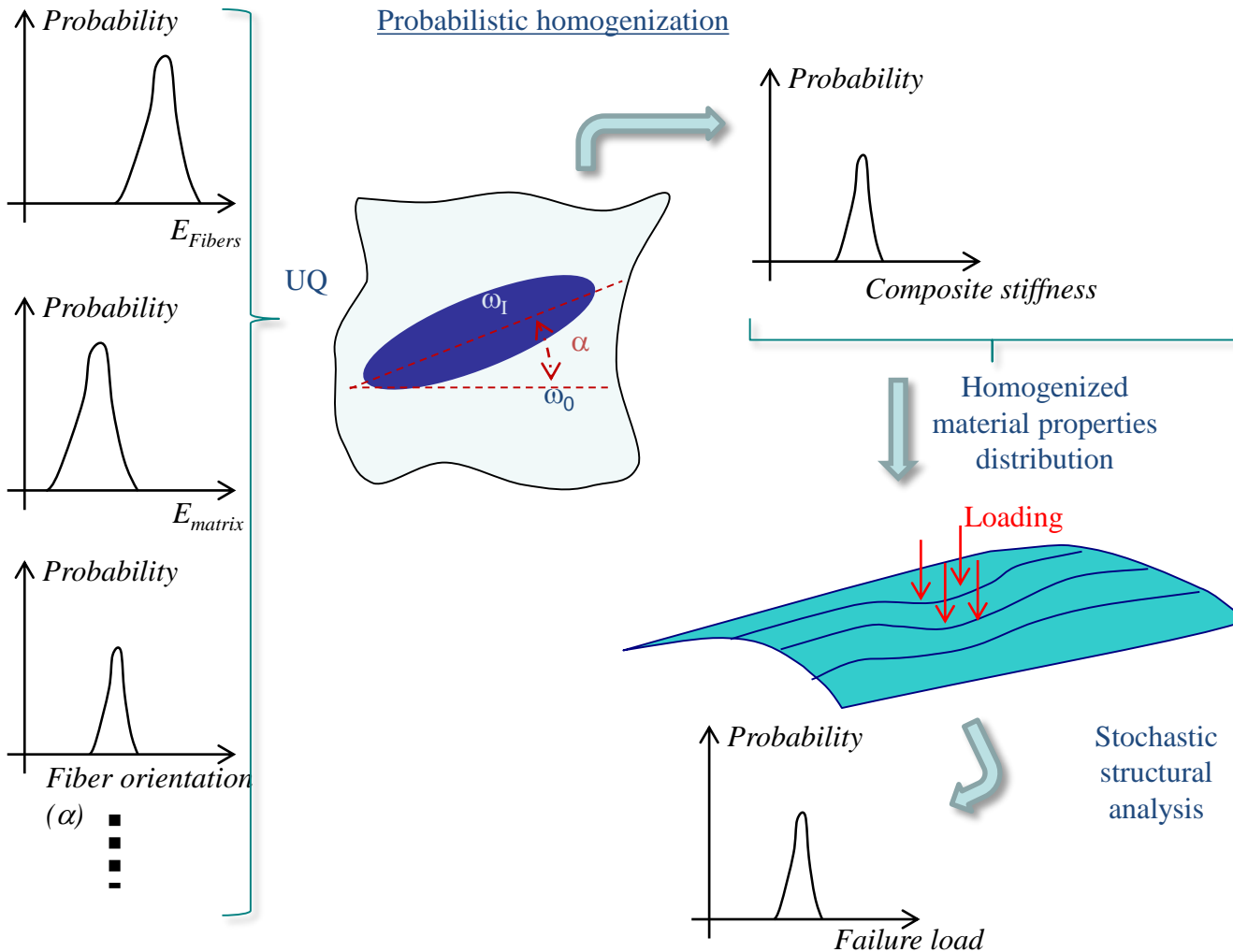
$$L_{\text{macro}} \gg L_{\text{VE}} \sim L_{\text{micro}}$$

For accuracy: Size of the meso-scale volume element smaller than the characteristic length of the macro-scale loading

Meso-scale volume element no longer statistically representative:
• Stochastic Volume Elements

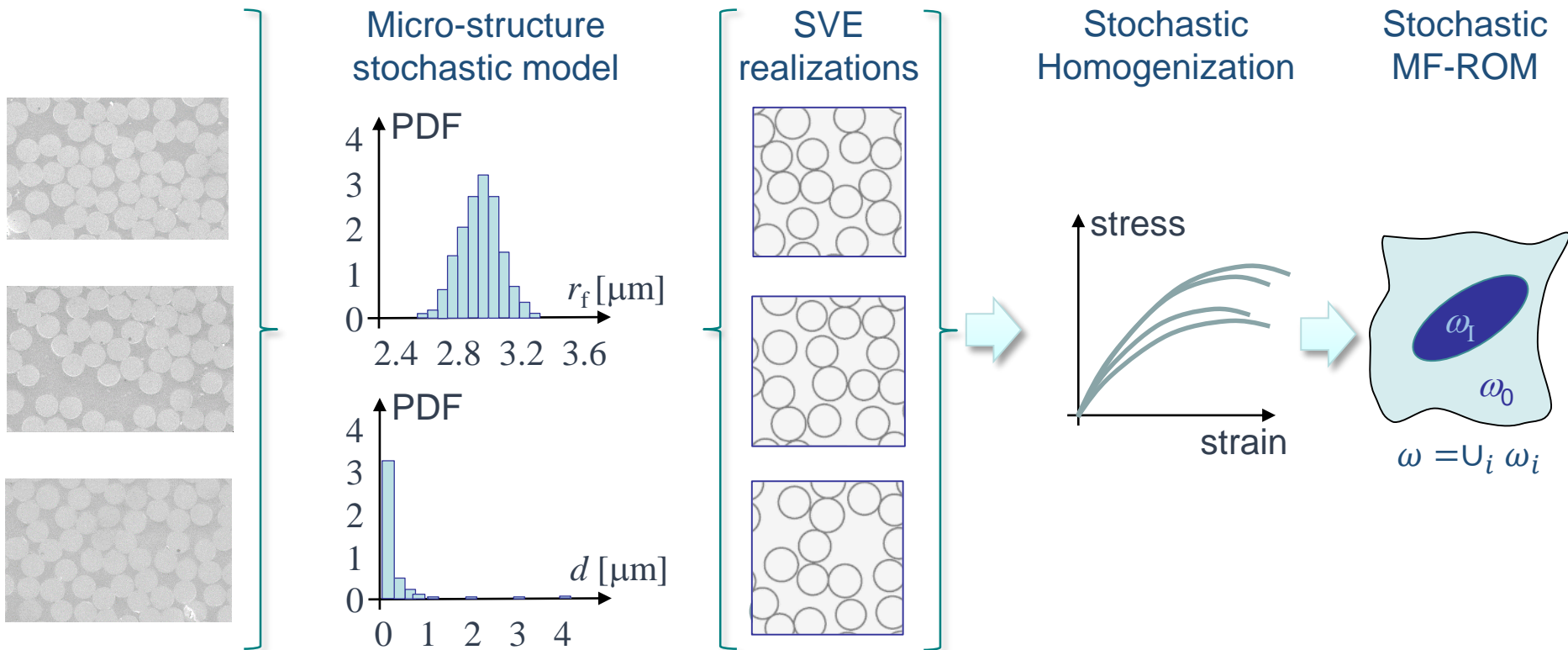
Stochastic Homogenization of Composite Materials

- Material uncertainties affect structural behaviors



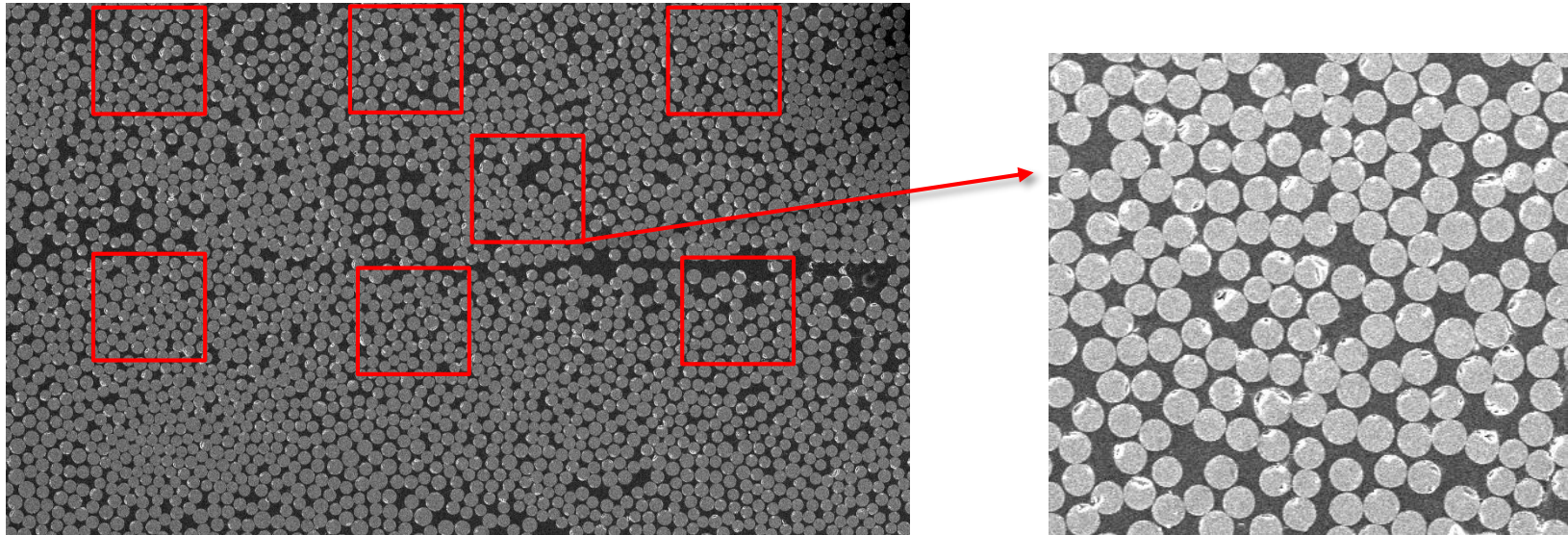
Stochastic Homogenization of Composite Materials

- Proposed methodology for material:
 - To develop a stochastic Mean Field Homogenization method able to predict the probabilistic distribution of material response at an intermediate scale from micro-structural constituents characterization

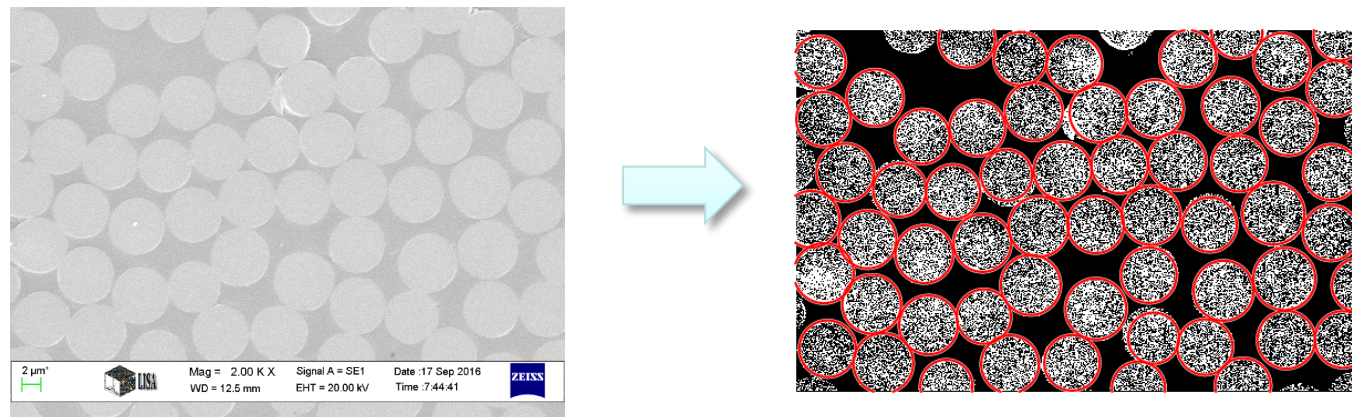


Stochastic Homogenization of Composite Materials

- Micro-structure stochastic model
 - 2000x and 3000x SEM images



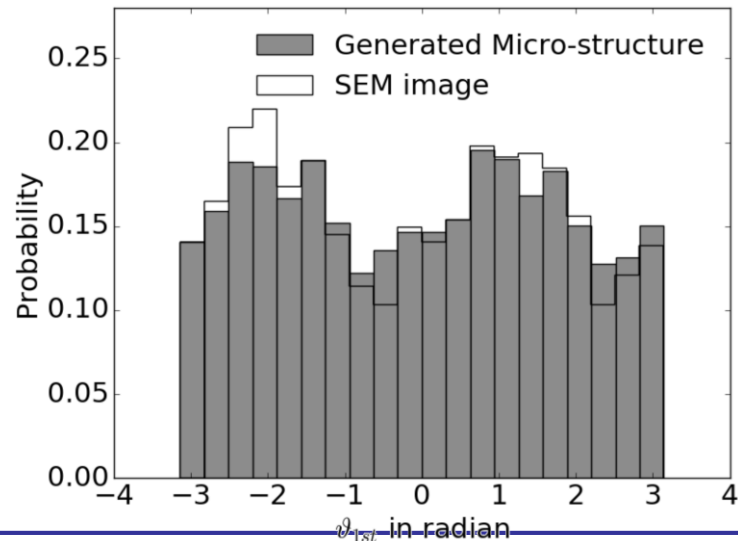
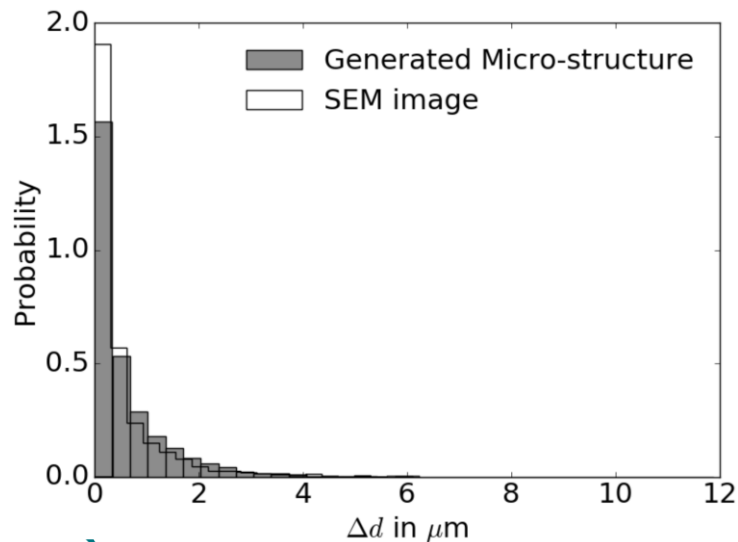
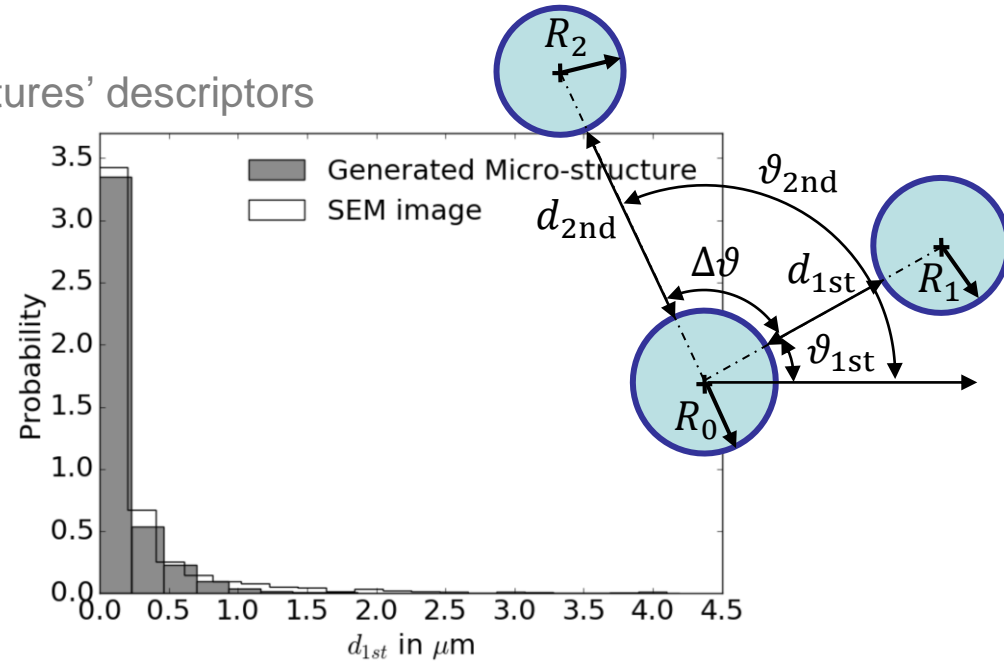
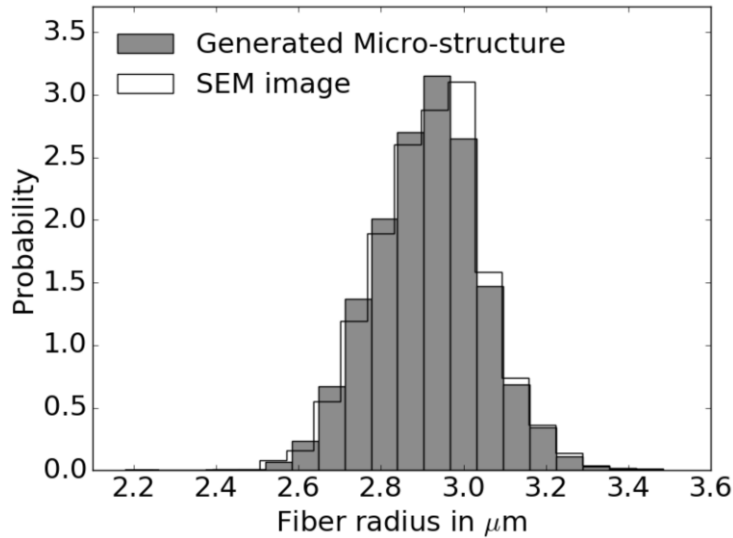
- Fibers detection



Stochastic Homogenization of Composite Materials

- Micro-structure stochastic model

– Histograms of random micro-structures' descriptors



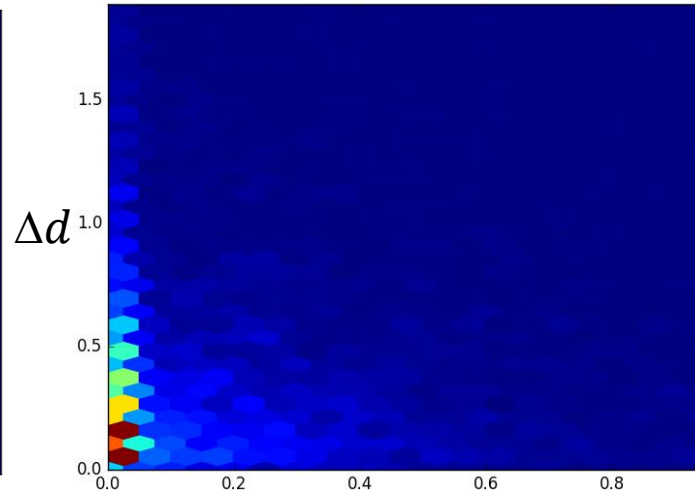
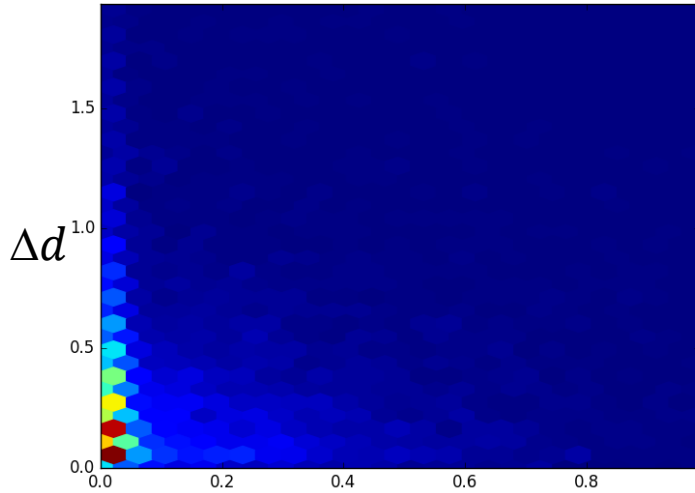
Stochastic Homogenization of Composite Materials

- Micro-structure stochastic model

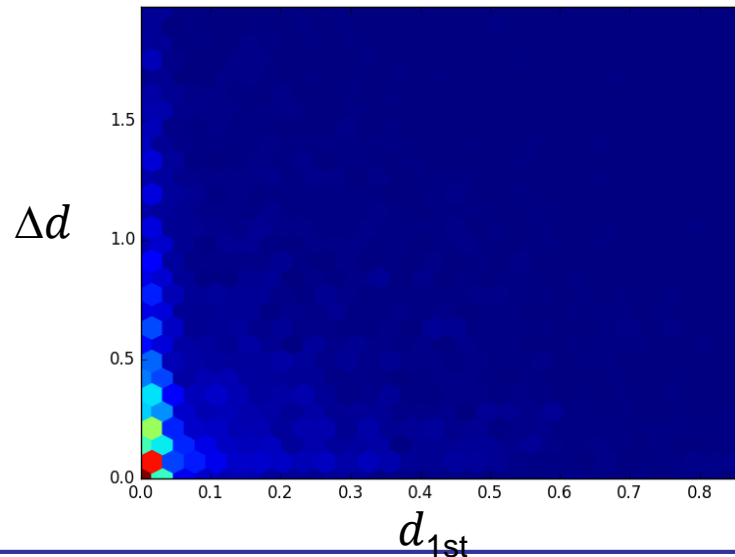
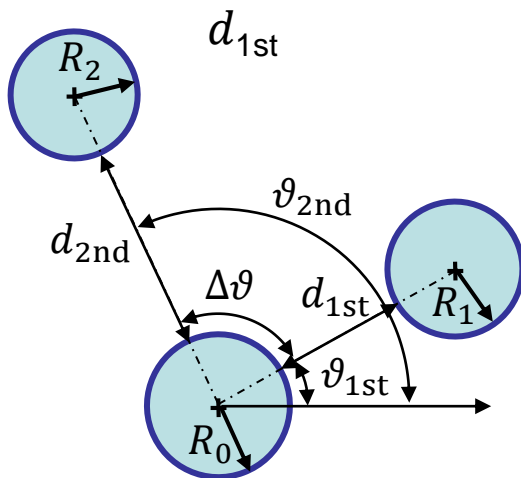
- Dependent variables generated using their empirical copula

SEM sample

Generated sample



Directly from
copula generator



Statistic result from
generated SVE

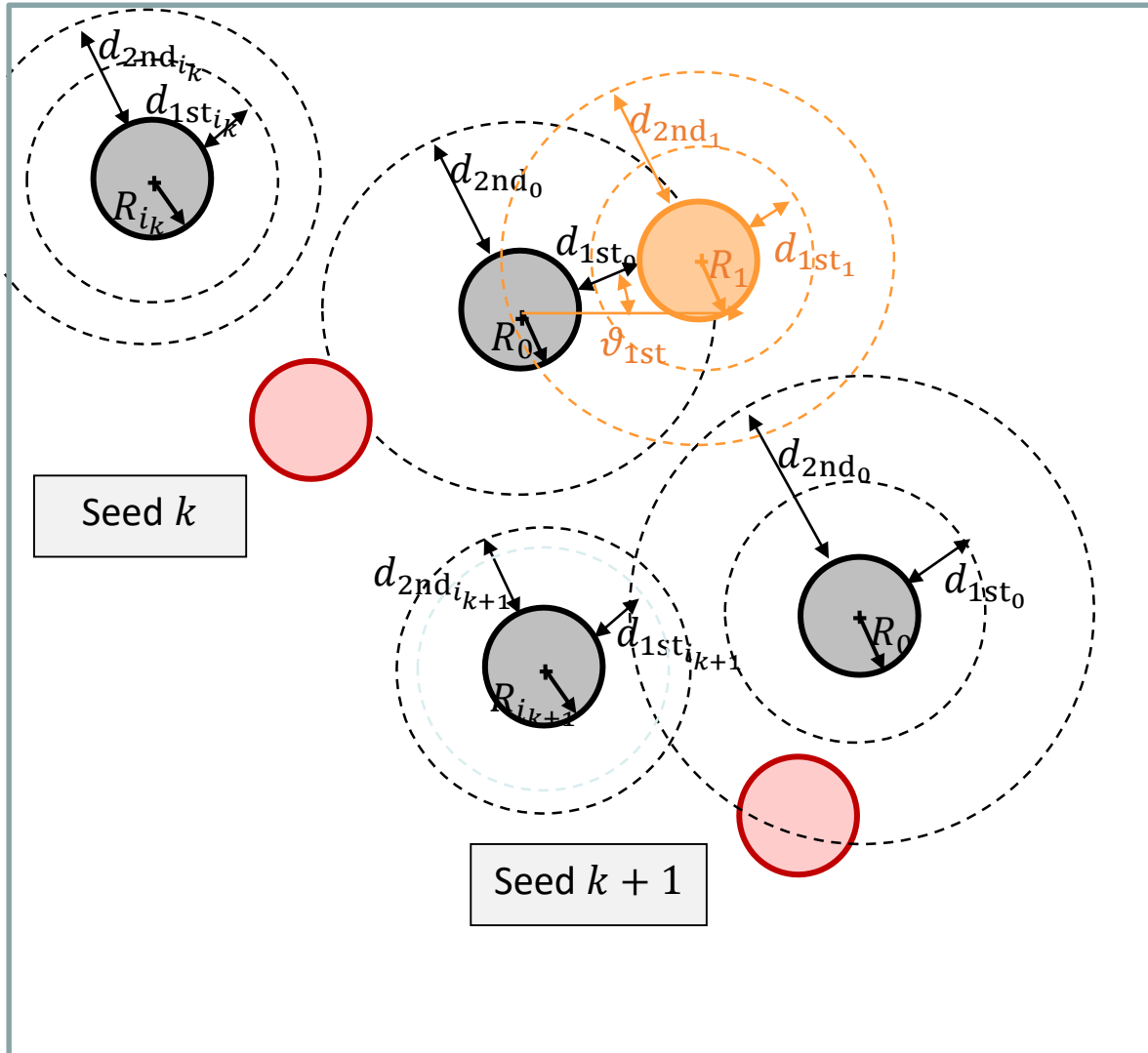
Stochastic Homogenization of Composite Materials

- Micro-structure stochastic model

- Dependent variables generated using their empirical copula

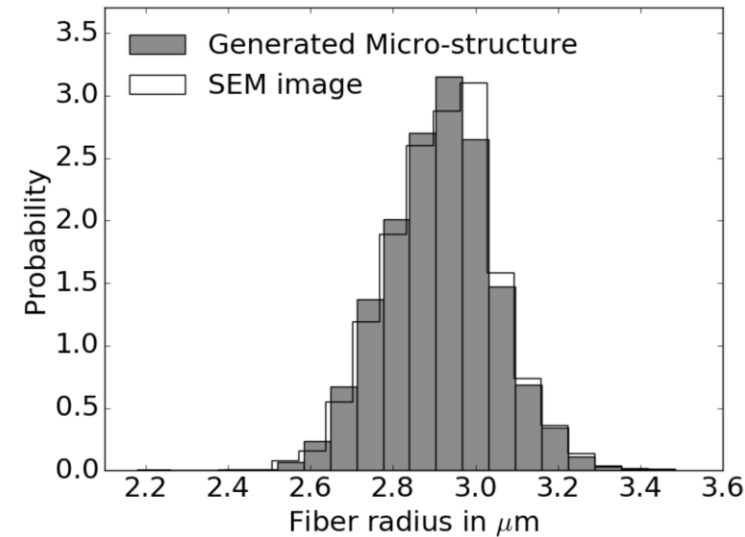
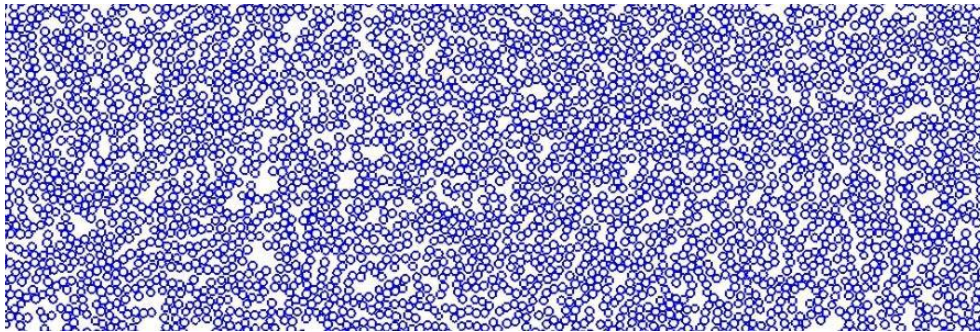
- Fiber additive process

- 1) Define N seeds with first and second neighbors distances
- 2) Generate first neighbor with its own first and second neighbors distances
- 3) Generate second neighbor with its own first and second neighbors distances
- 4) Change seeds & then change central fiber of the seeds

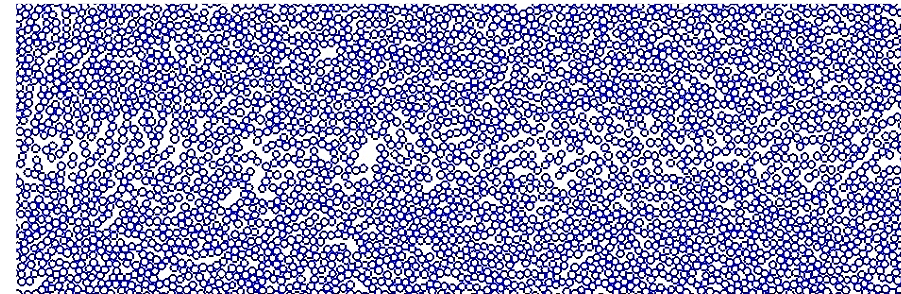
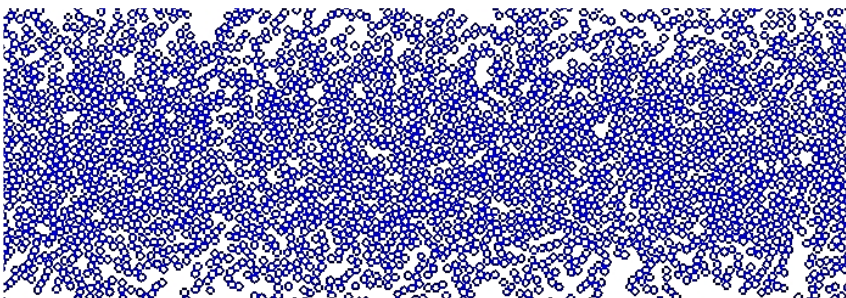


Stochastic Homogenization of Composite Materials

- Micro-structure stochastic model
 - Arbitrary size
 - Arbitrary number



- Possibility to generate non-homogenous distributions



- Stochastic homogenization of SVEs

- Extraction of Stochastic Volume Elements

- 2 sizes considered: $l_{SVE} = 10 \mu m$ & $l_{SVE} = 25 \mu m$
- Window technique to capture correlation

$$R_{rs}(\boldsymbol{\tau}) = \frac{\mathbb{E}[(r(\mathbf{x}) - \mathbb{E}(r))(s(\mathbf{x} + \boldsymbol{\tau}) - \mathbb{E}(s))]}{\sqrt{\mathbb{E}[(r - \mathbb{E}(r))^2]} \sqrt{\mathbb{E}[(s - \mathbb{E}(s))^2]}}$$

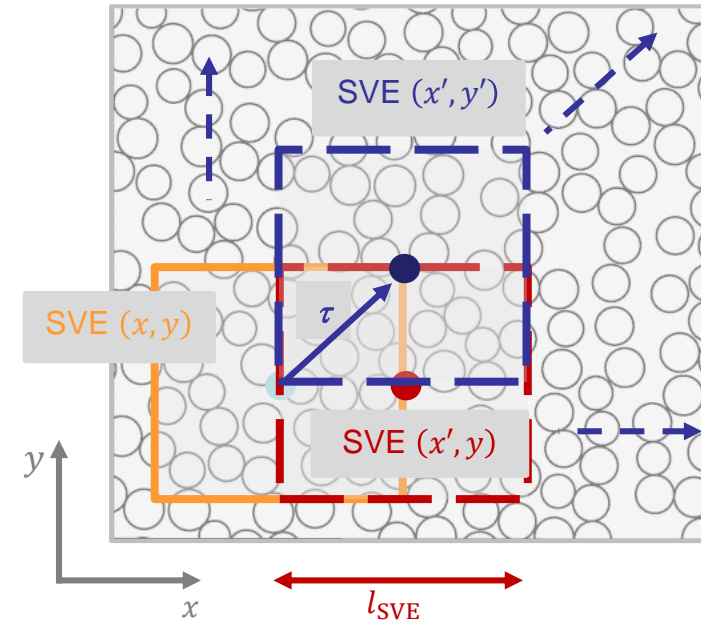
- For each SVE

- Extract apparent homogenized material tensor \mathbb{C}_M

$$\left\{ \begin{array}{l} \boldsymbol{\varepsilon}_M = \frac{1}{V(\omega)} \int_{\omega} \boldsymbol{\varepsilon}_m d\omega \\ \boldsymbol{\sigma}_M = \frac{1}{V(\omega)} \int_{\omega} \boldsymbol{\sigma}_m d\omega \\ \mathbb{C}_M = \frac{\partial \boldsymbol{\sigma}_M}{\partial \mathbf{u}_M \otimes \nabla_M} \end{array} \right.$$

- Consistent boundary conditions:

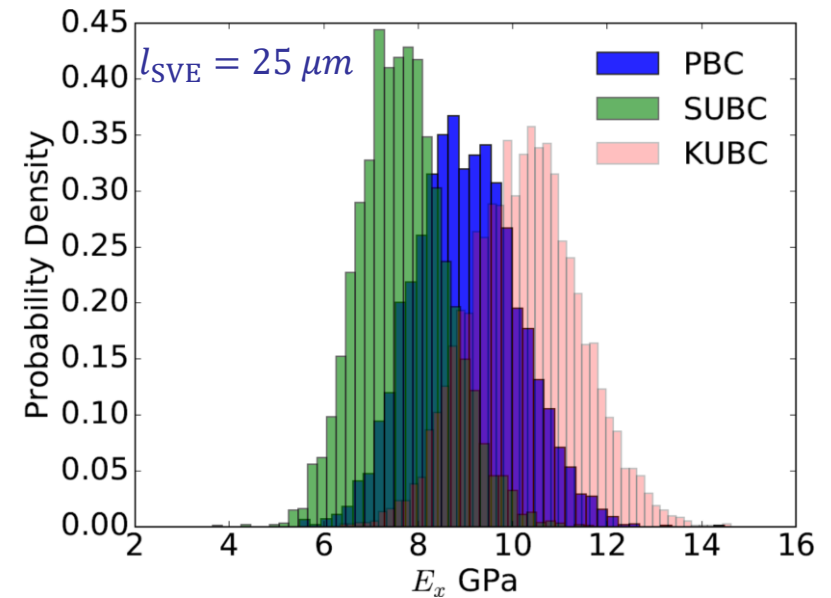
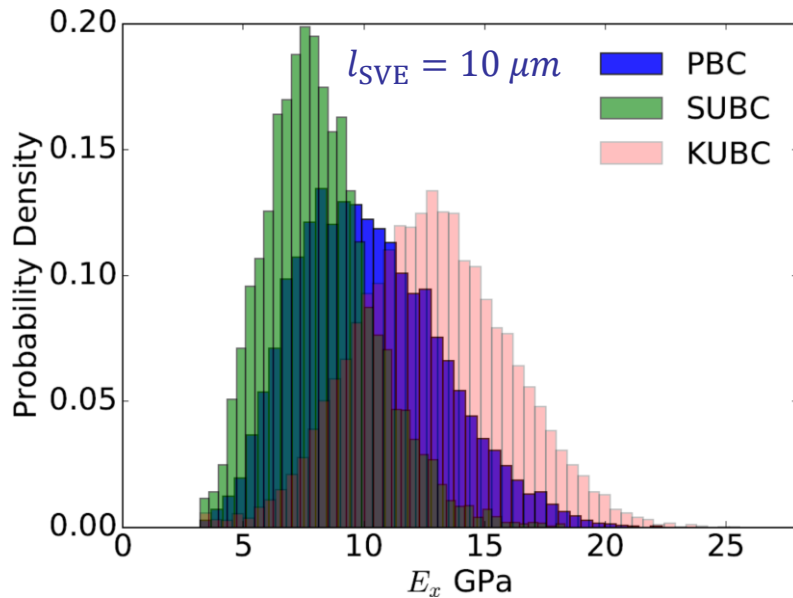
- Periodic (PBC)
- Minimum kinematics (SUBC)
- Kinematic (KUBC)



Stochastic Homogenization of Composite Materials

- Stochastic homogenization of SVEs

- Apparent properties



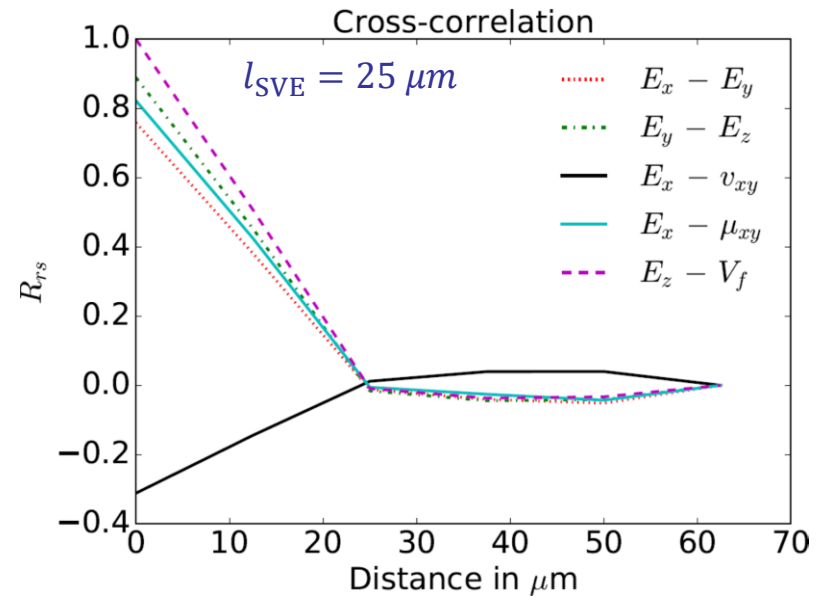
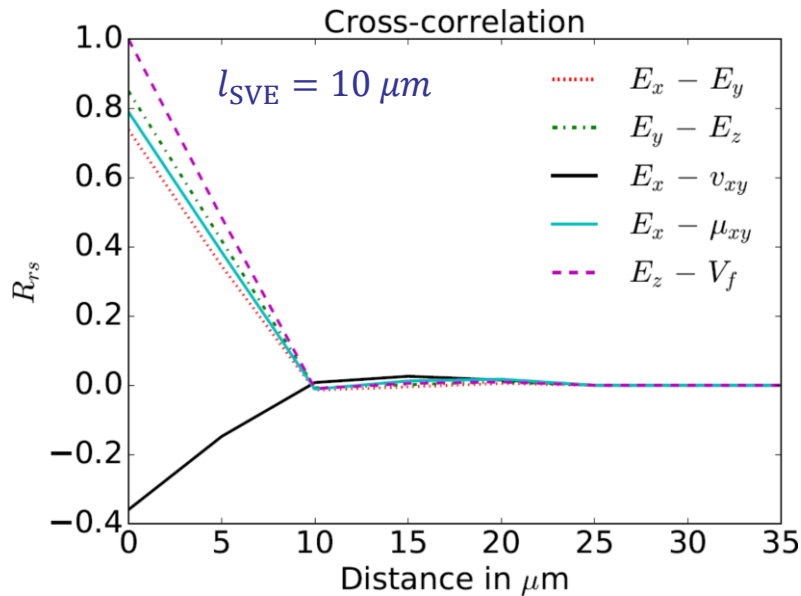
Increasing l_{SVE}

When l_{SVE} increases

- Average values for different BCs get closer (to PBC one)
- Distributions narrow
- Distributions get closer to normal

- Stochastic homogenization of SVEs

- Correlation study



- (1) Auto/cross correlation vanishes at $\tau = l_{SVE}$
- (2) When l_{SVE} increases, distributions get closer to normal

(1)+(2) Apparent properties are independent random variables
However the distribution depend on

- l_{SVE}
- The boundary conditions

Stochastic Homogenization of Composite Materials

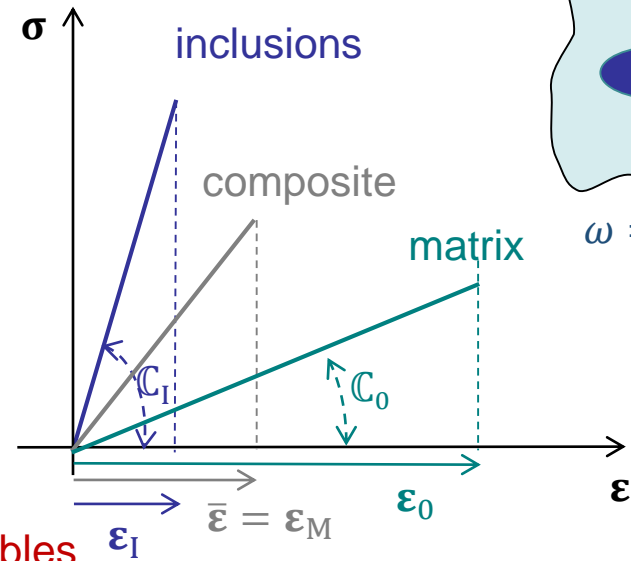
- Mean-Field-homogenization (MFH)

- Linear composites

$$\left\{ \begin{array}{l} \sigma_M = \bar{\sigma} = v_0 \sigma_0 + v_1 \sigma_1 \\ \varepsilon_M = \bar{\varepsilon} = v_0 \varepsilon_0 + v_1 \varepsilon_1 \\ \varepsilon_1 = \mathbb{B}^\varepsilon(I, C_0, C_I) : \varepsilon_0 \end{array} \right.$$

→ $\hat{C}_M = \hat{C}_M(I, C_0, C_I, v_1)$

Defined as random variables



- Consider an equivalent system

- For each SVE realization i :

→ C_M and v_I known

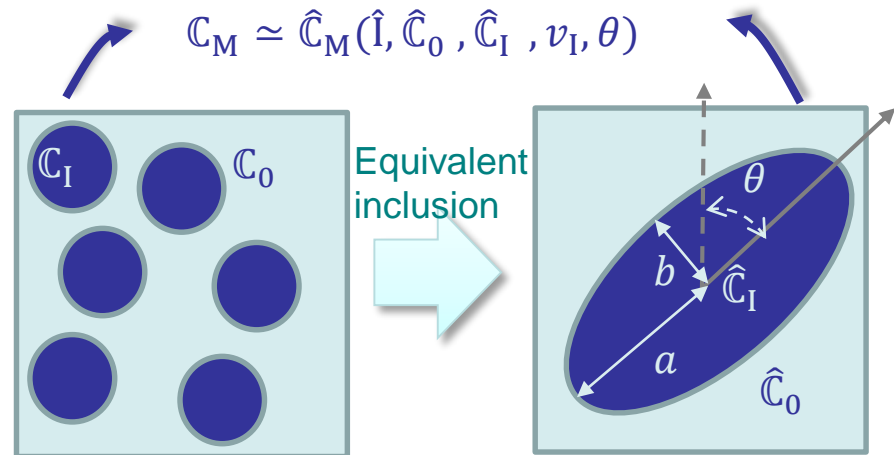
- Anisotropy from C_M^i

→ θ is evaluated

- Fiber behavior uniform

→ \hat{C}_I for one SVE

- Remaining optimization problem:

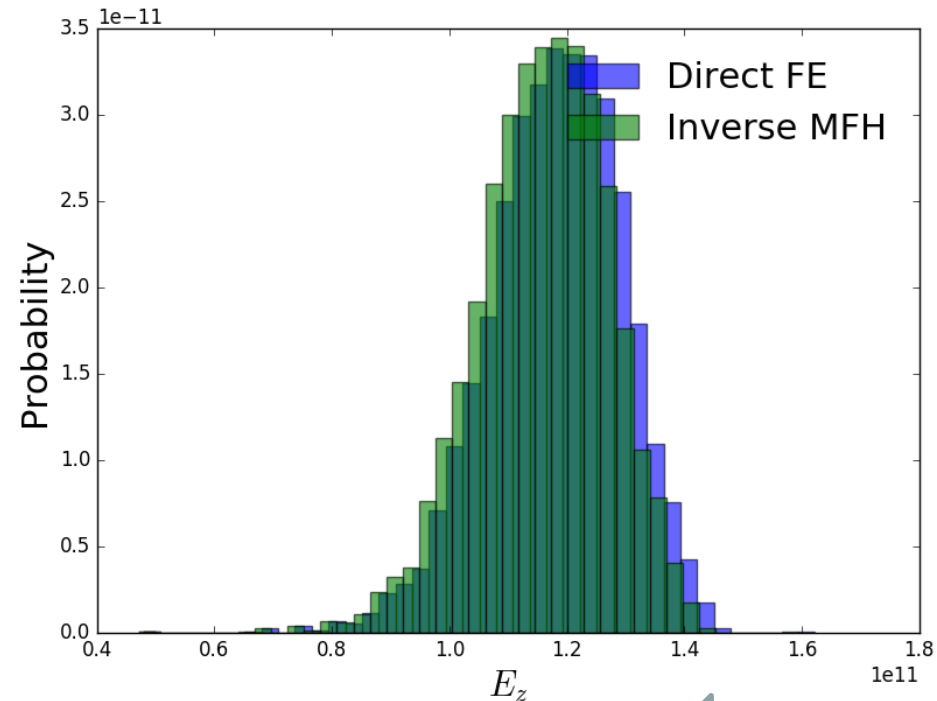
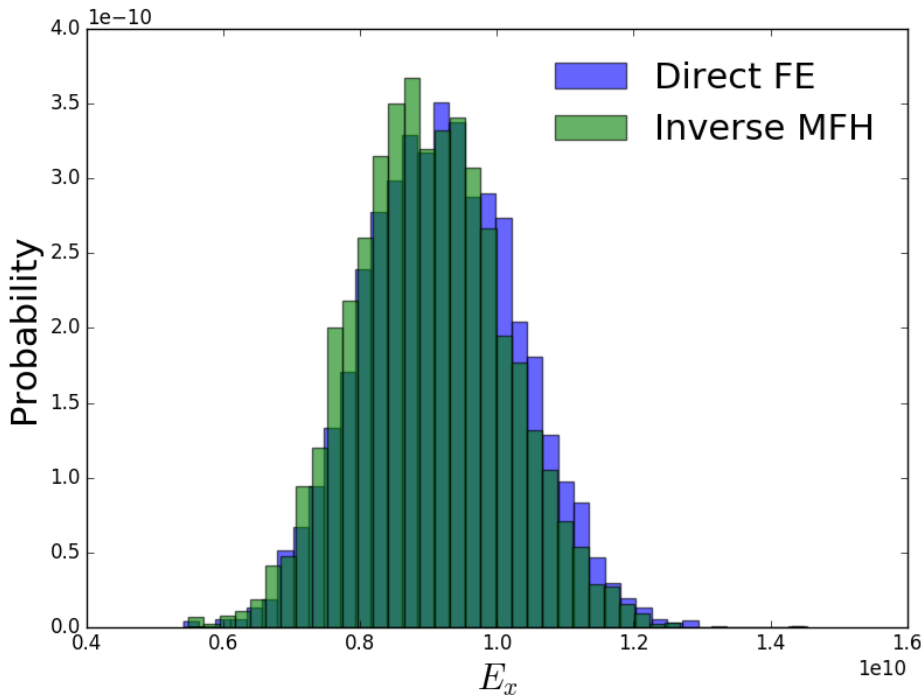
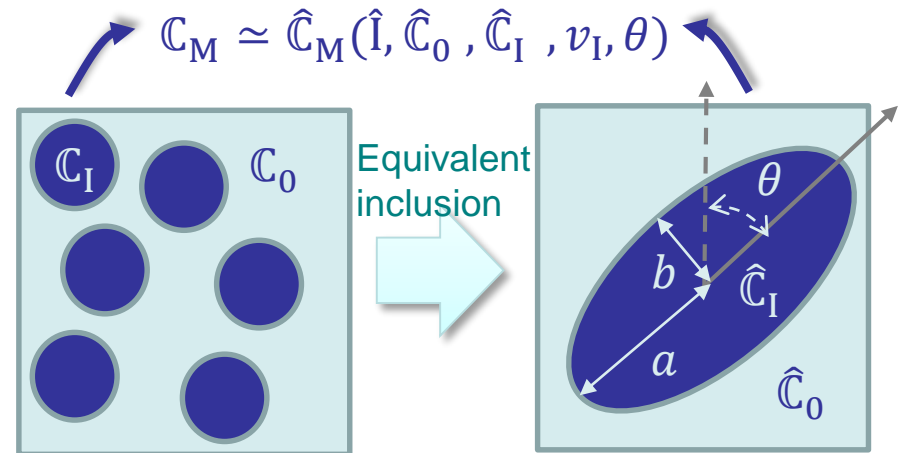


$$\min_{\frac{a}{b}, \hat{E}_0, \hat{\nu}_0} \left\| C_M - \hat{C}_M\left(\frac{a}{b}, \hat{E}_0, \hat{\nu}_0; v_I, \theta, \hat{C}_I\right) \right\|$$

Stochastic Homogenization of Composite Materials

- Inverse stochastic identification

- Comparison of homogenized properties from SVE realizations and stochastic MFH



Stochastic Homogenization of Composite Materials

- Incremental-secant Mean-Field-homogenization

- Virtual elastic unloading from previous state
 - Composite material unloaded to reach the stress-free state
 - Residual stress in components

- Define Linear Comparison Composite

- From unloaded state

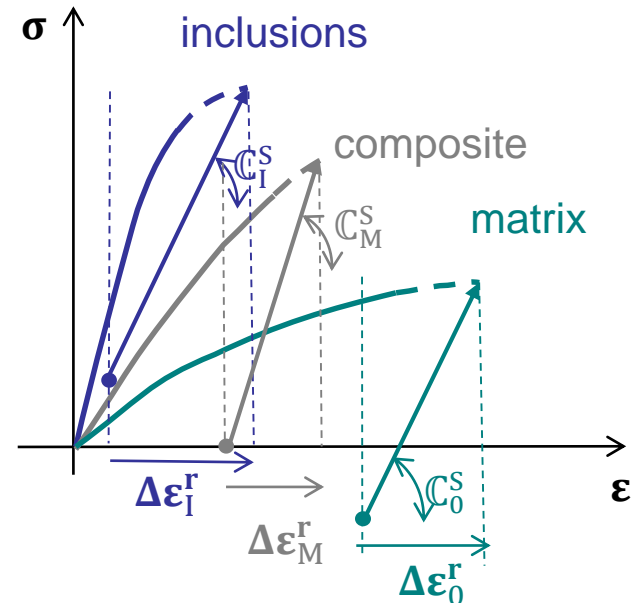
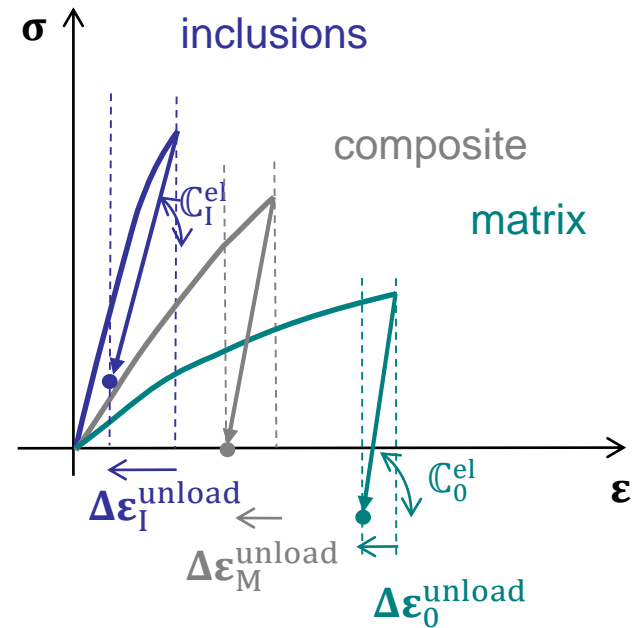
$$\Delta \boldsymbol{\varepsilon}_{I/0}^r = \Delta \boldsymbol{\varepsilon}_{I/0} + \Delta \boldsymbol{\varepsilon}_{I/0}^{\text{unload}}$$

- Incremental-secant loading

$$\left\{ \begin{array}{l} \boldsymbol{\sigma}_M = \bar{\boldsymbol{\sigma}} = \nu_0 \boldsymbol{\sigma}_0 + \nu_1 \boldsymbol{\sigma}_I \\ \Delta \boldsymbol{\varepsilon}_M^r = \bar{\Delta \boldsymbol{\varepsilon}} = \nu_0 \Delta \boldsymbol{\varepsilon}_0^r + \nu_1 \Delta \boldsymbol{\varepsilon}_I^r \\ \Delta \boldsymbol{\varepsilon}_I^r = \mathbb{B}^\varepsilon(I, \mathbb{C}_0^S, \mathbb{C}_I^S) : \Delta \boldsymbol{\varepsilon}_0^r \end{array} \right.$$

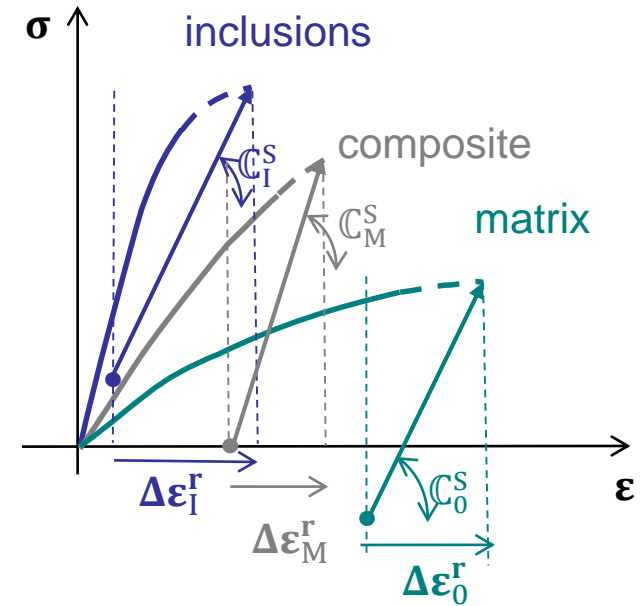
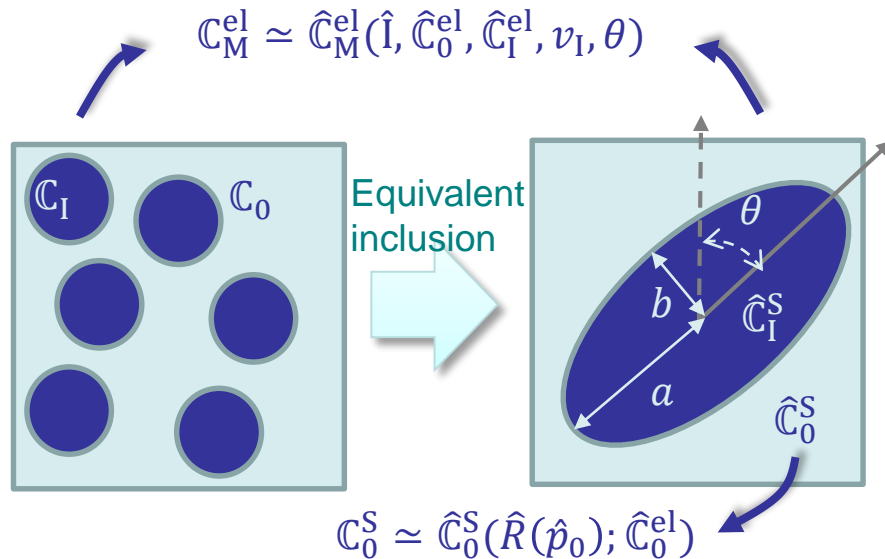
- Incremental secant operator

$$\Rightarrow \Delta \boldsymbol{\sigma}_M = \mathbb{C}_M^S(I, \mathbb{C}_0^S, \mathbb{C}_I^S, \nu_1) : \Delta \boldsymbol{\varepsilon}_M^r$$



Stochastic Homogenization of Composite Materials

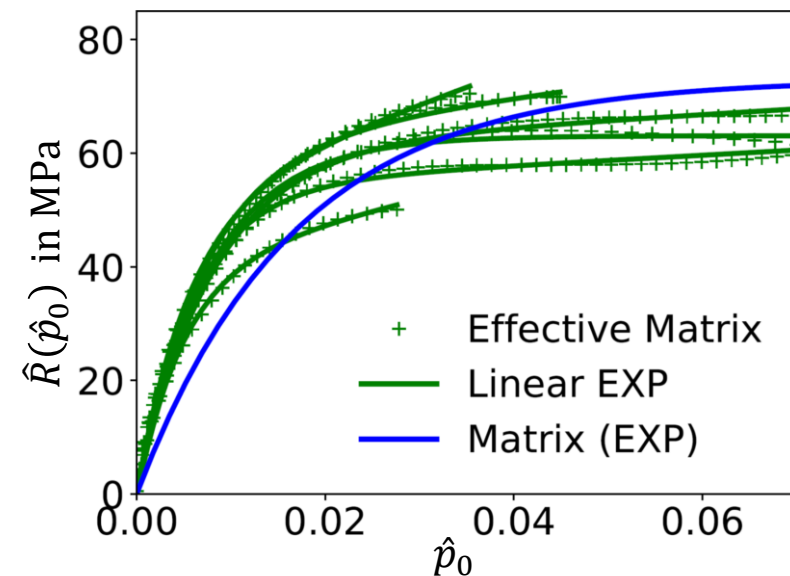
- Non-linear inverse identification
 - First step from elastic response



- Second step from the LCC
 - New optimization problem

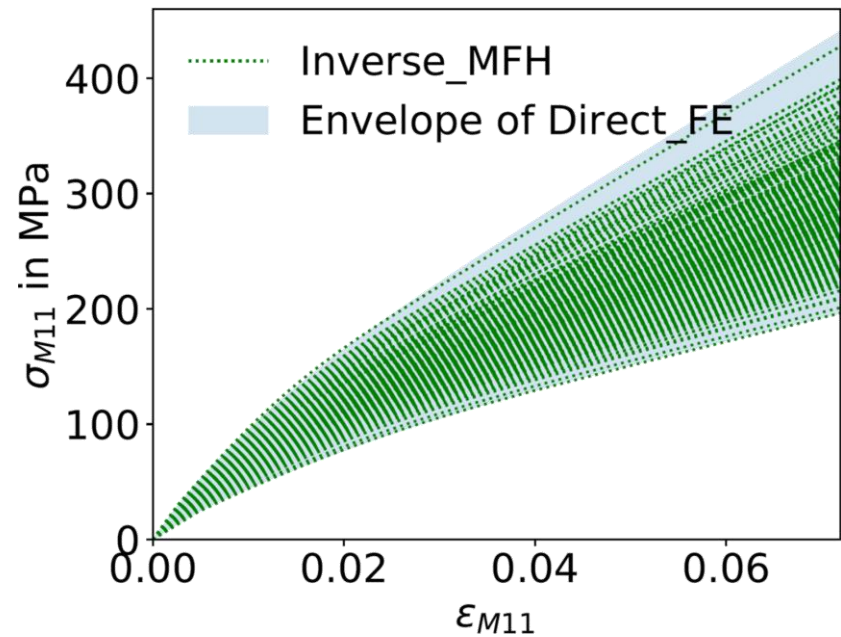
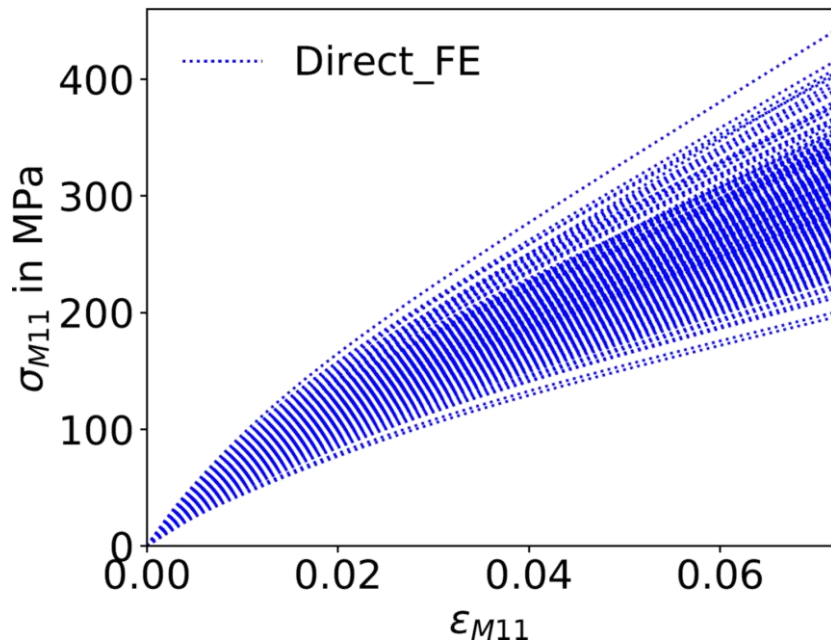
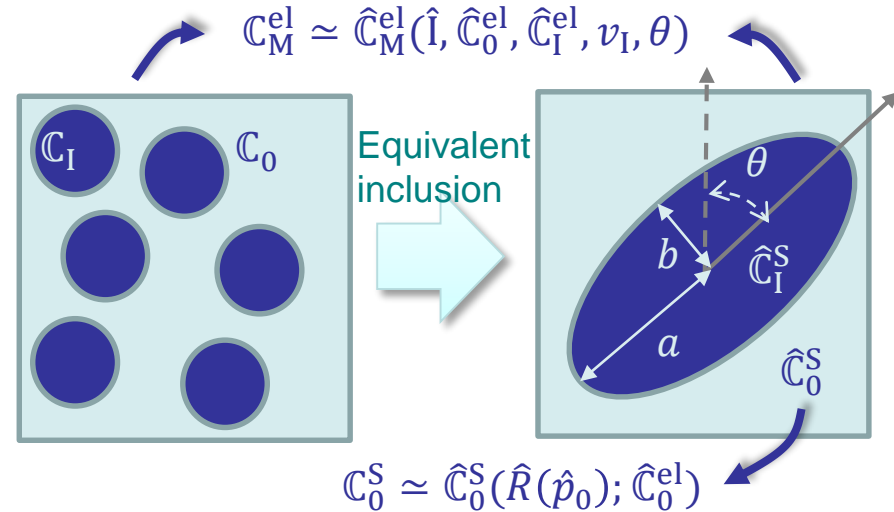
$$\Delta \sigma_M \simeq \hat{\mathbb{C}}_M^S(\hat{\mathbf{I}}, \hat{\mathbb{C}}_0^S, \mathbb{C}_I^S, \nu_I, \theta): \Delta \epsilon_M^r$$
 - Extract the equivalent hardening $\hat{R}(\hat{p}_0)$ from the incremental secant tensor

$$\mathbb{C}_0^S \simeq \hat{\mathbb{C}}_0^S(\hat{R}(\hat{p}_0); \hat{\mathbb{C}}_0^{el})$$



Stochastic Homogenization of Composite Materials

- Non-linear inverse identification
 - Comparison SVE vs. MFH



Stochastic Homogenization of Composite Materials

- **Damage-enhanced Mean-Field-homogenization**

- Virtual elastic unloading from previous state
 - Composite material unloaded to reach the stress-free state
 - Residual stress in components

- Define Linear Comparison Composite

- From elastic state

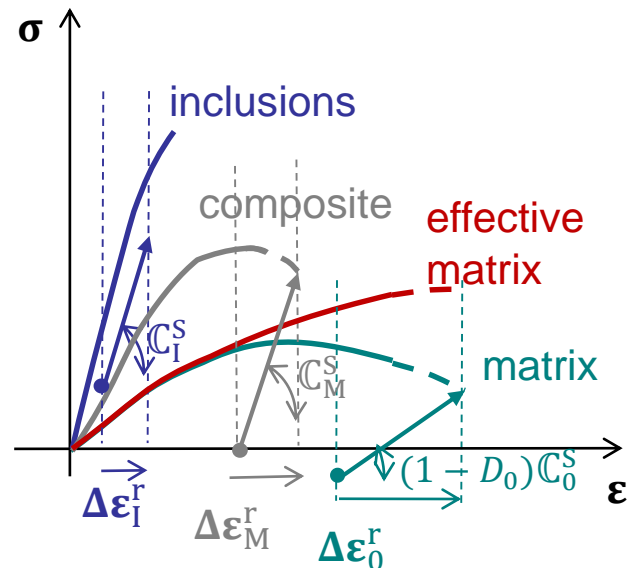
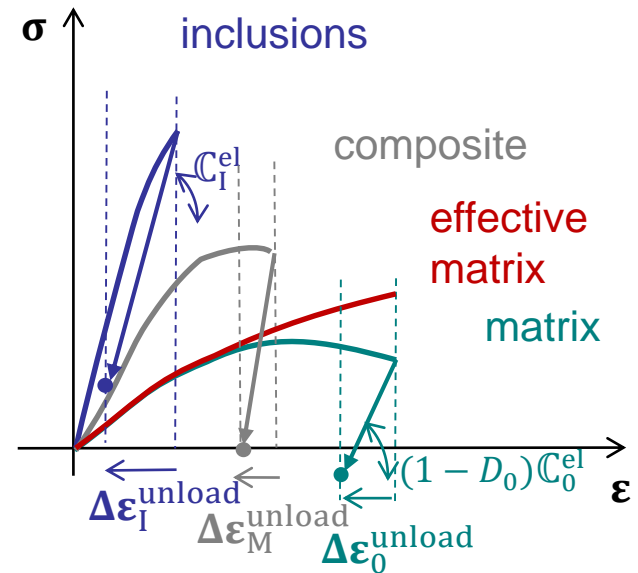
$$\Delta \boldsymbol{\varepsilon}_{I/0}^r = \Delta \boldsymbol{\varepsilon}_{I/0} + \Delta \boldsymbol{\varepsilon}_{I/0}^{\text{unload}}$$

- Incremental-secant loading

$$\left\{ \begin{array}{l} \boldsymbol{\sigma}_M = \bar{\boldsymbol{\sigma}} = v_0 \boldsymbol{\sigma}_0 + v_I \boldsymbol{\sigma}_I \\ \Delta \boldsymbol{\varepsilon}_M^r = \bar{\Delta \boldsymbol{\varepsilon}} = v_0 \Delta \boldsymbol{\varepsilon}_0^r + v_I \Delta \boldsymbol{\varepsilon}_I^r \\ \Delta \boldsymbol{\varepsilon}_I^r = \mathbb{B}^\varepsilon(I, (1 - D_0) \mathbb{C}_0^S, \mathbb{C}_I^S) : \Delta \boldsymbol{\varepsilon}_0^r \end{array} \right.$$

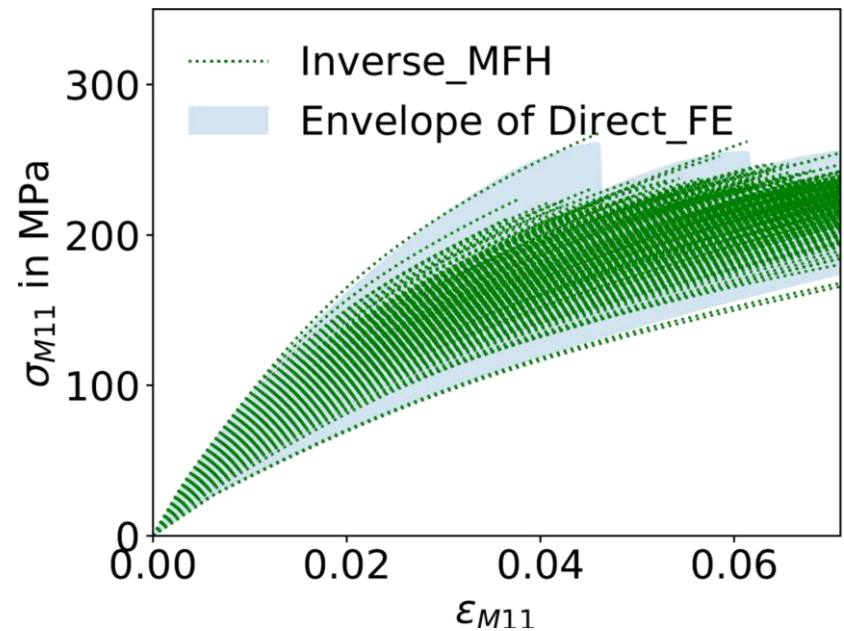
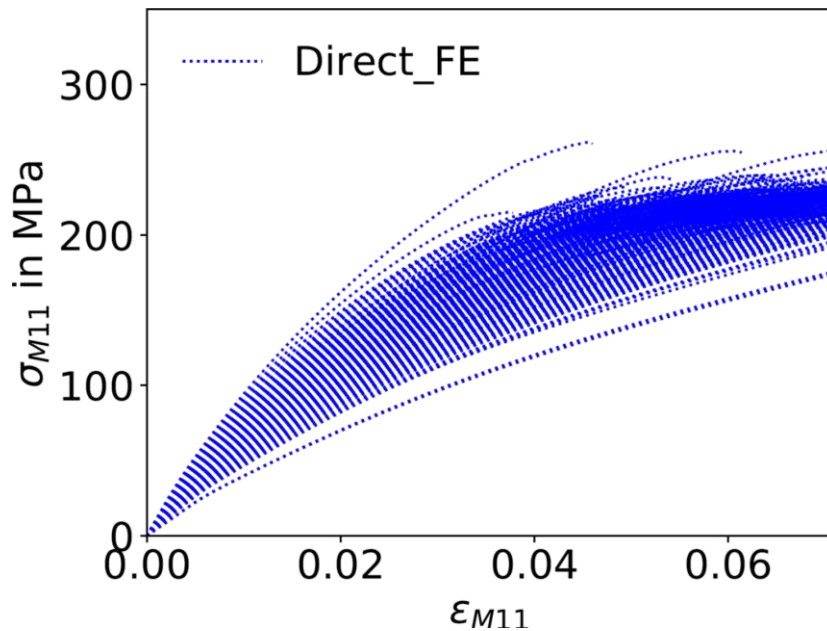
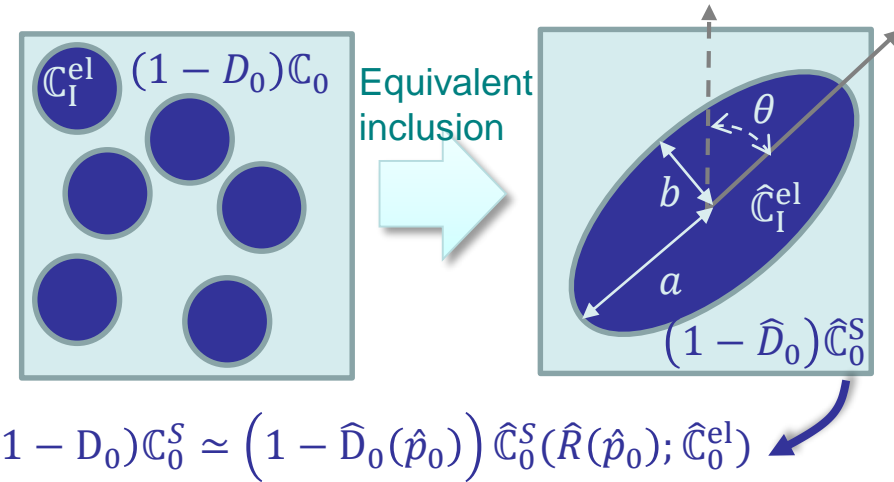
- Incremental secant operator

$$\Rightarrow \Delta \boldsymbol{\sigma}_M = \mathbb{C}_M^S(I, (1 - D_0) \mathbb{C}_0^S, \mathbb{C}_I^S, v_I) : \Delta \boldsymbol{\varepsilon}_M^r$$



Stochastic Homogenization of Composite Materials

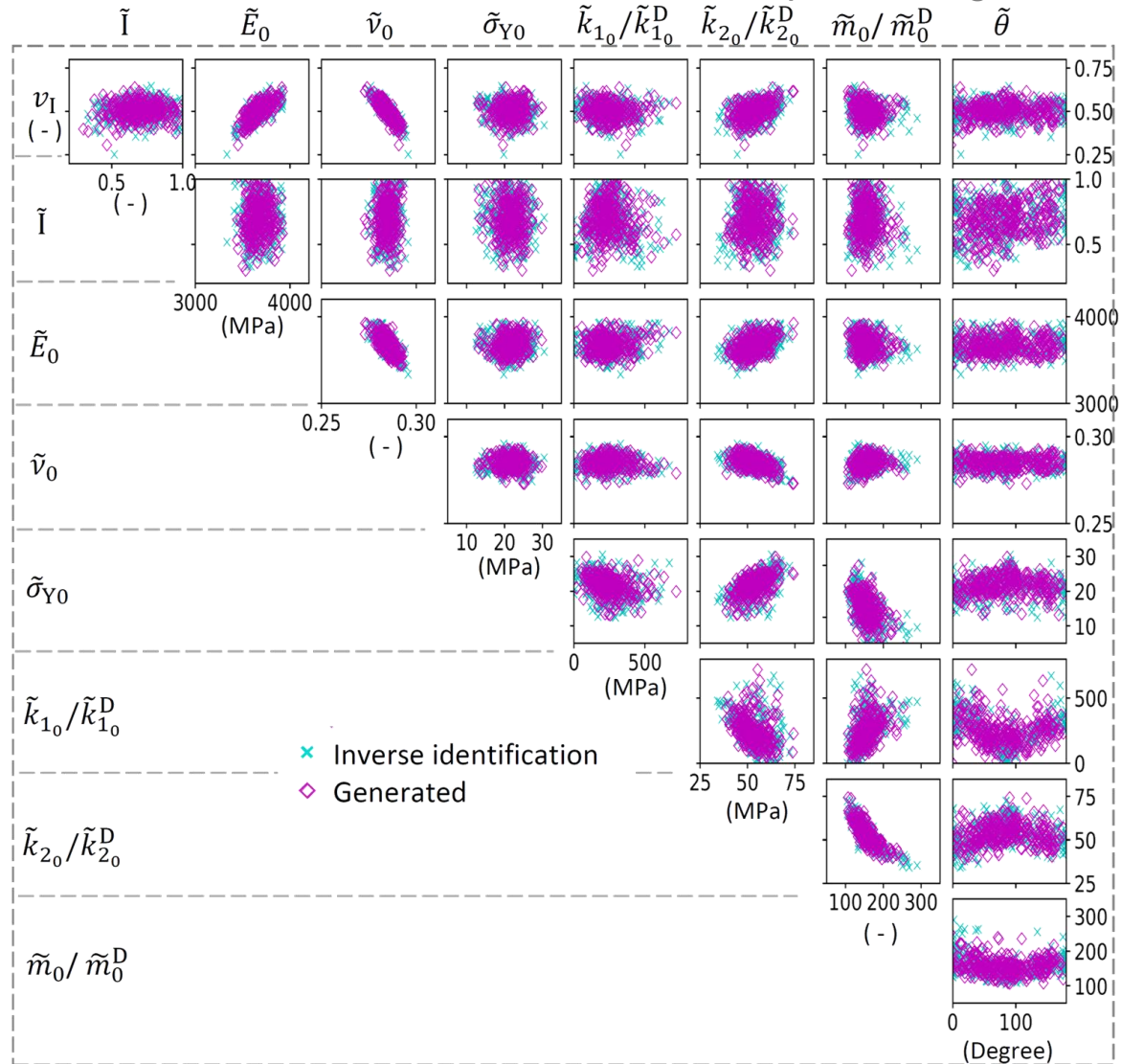
- Damage-enhanced inverse identification
 - Comparison SVE vs. MFH



Stochastic Homogenization of Composite Materials

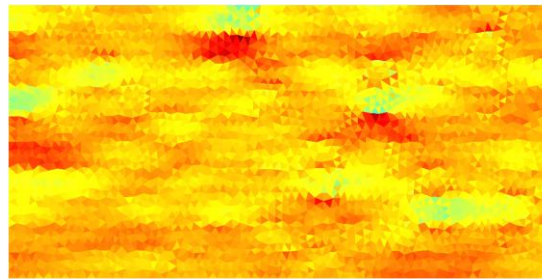
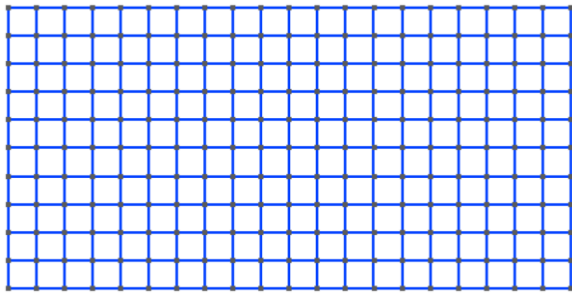
- Generation of random field

- Comparison inverse identification vs. diffusion map –based generator

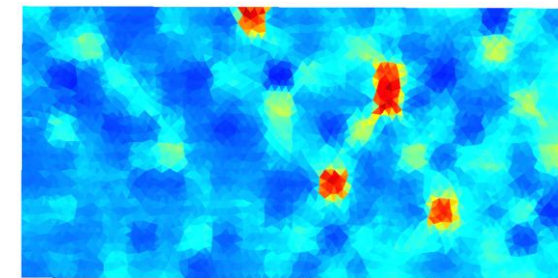


Stochastic Homogenization of Composite Materials

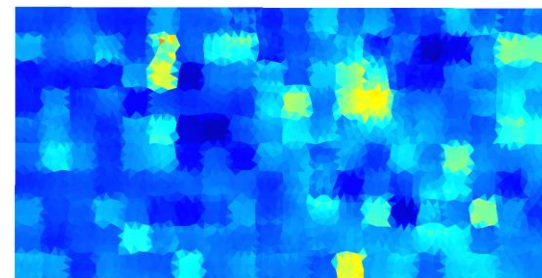
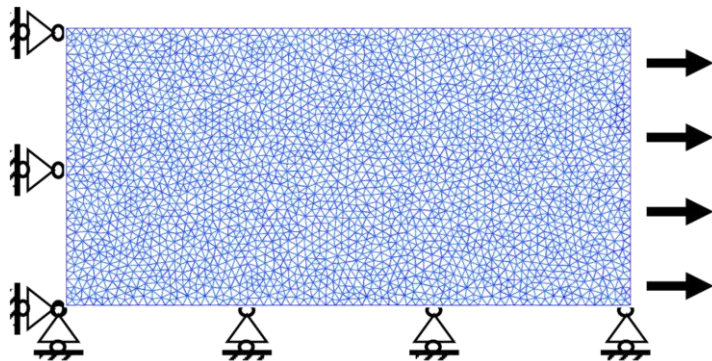
- One single ply loading realization
 - Random field and finite elements discretizations
 - Non-uniform homogenized stress distributions
 - Creates damage localization



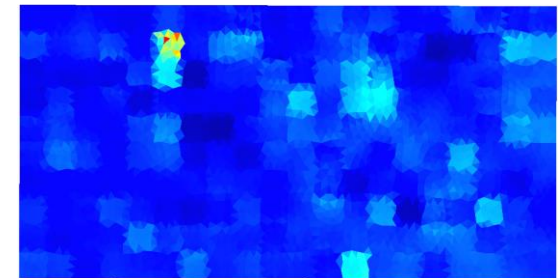
$\sigma_{M_{xx}}$ [Mpa]; $\varepsilon_{M_{xx}} = 2.6\%$
0 108 215



\hat{p}_0 [-]; $\varepsilon_{M_{xx}} = 2.6\%$
0 108 215



\hat{D}_0 [-]; $\varepsilon_{M_{xx}} = 2.4\%$
0 0.025 0.05

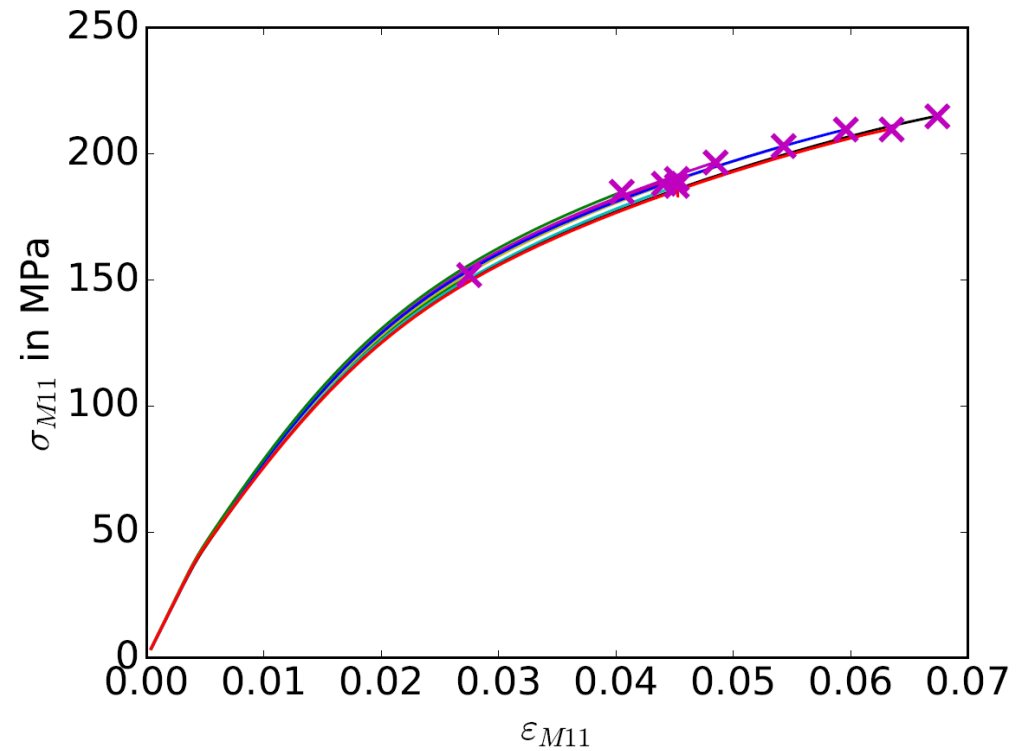
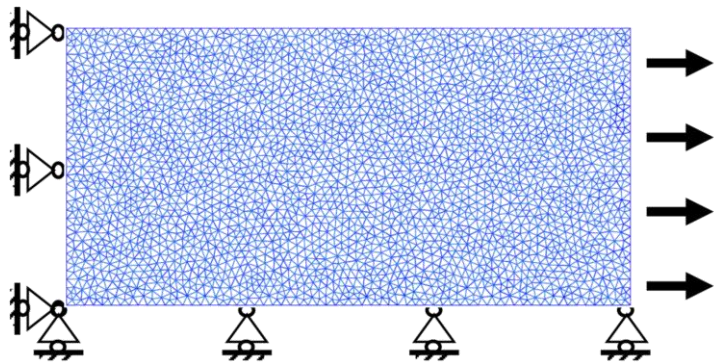
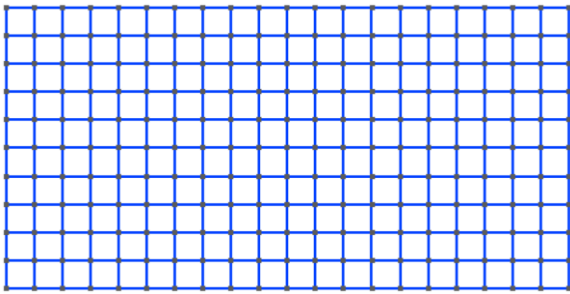


\hat{D}_0 [-]; $\varepsilon_{M_{xx}} = 2.6\%$
0 0.025 0.05



Stochastic Homogenization of Composite Materials

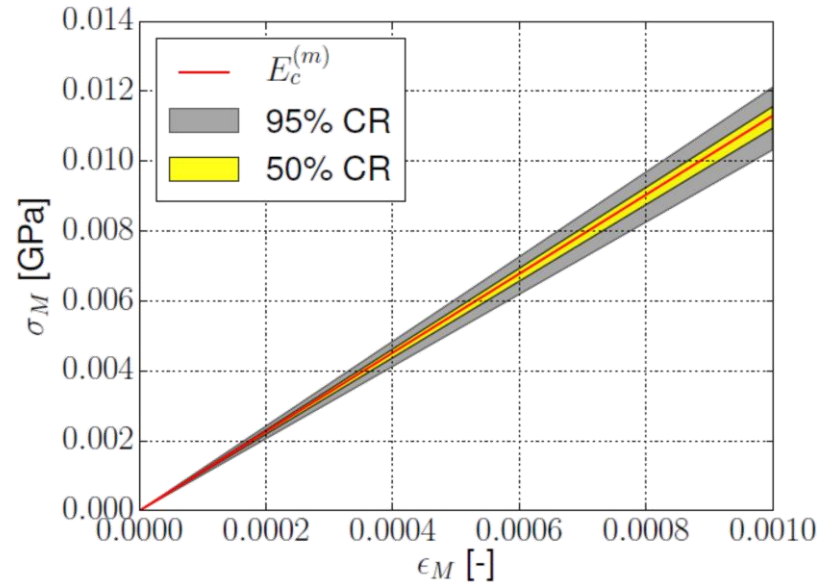
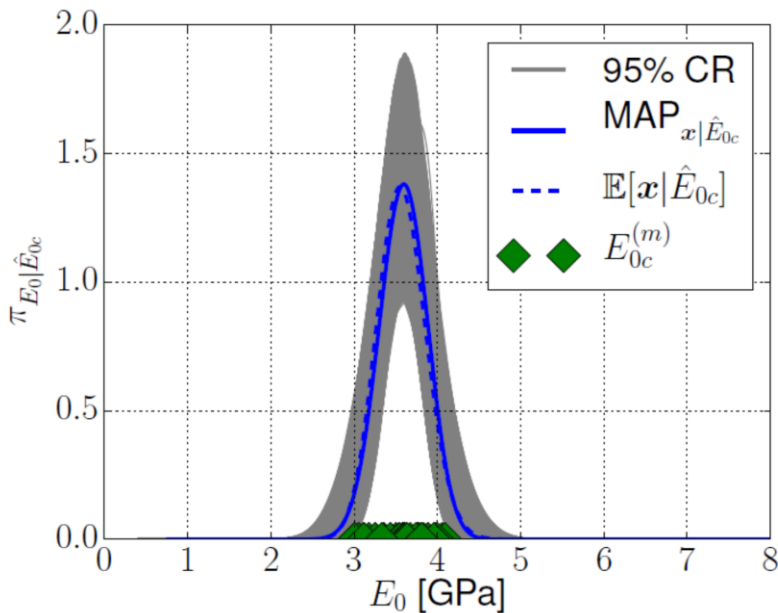
- Ply loading realizations
 - Simple failure criterion at (homogenized stress) loss of ellipticity
 - Discrepancy in failure point



Stochastic Homogenization of Composite Materials

- STOMMMAC M.ERA-NET project (MFH for elasto-visco-plastic composites)
 - e-Xstream, ULiège (Belgium)
 - BATZ (Spain)
 - JKU, AC (Austria)
 - U Luxembourg (Luxemburg)

- Publications (doi)
 - [10.1016/j.compstruct.2018.01.051](https://doi.org/10.1016/j.compstruct.2018.01.051)
 - [10.1002/nme.5903](https://doi.org/10.1002/nme.5903)
 - [10.1016/j.cma.2019.01.016](https://doi.org/10.1016/j.cma.2019.01.016)



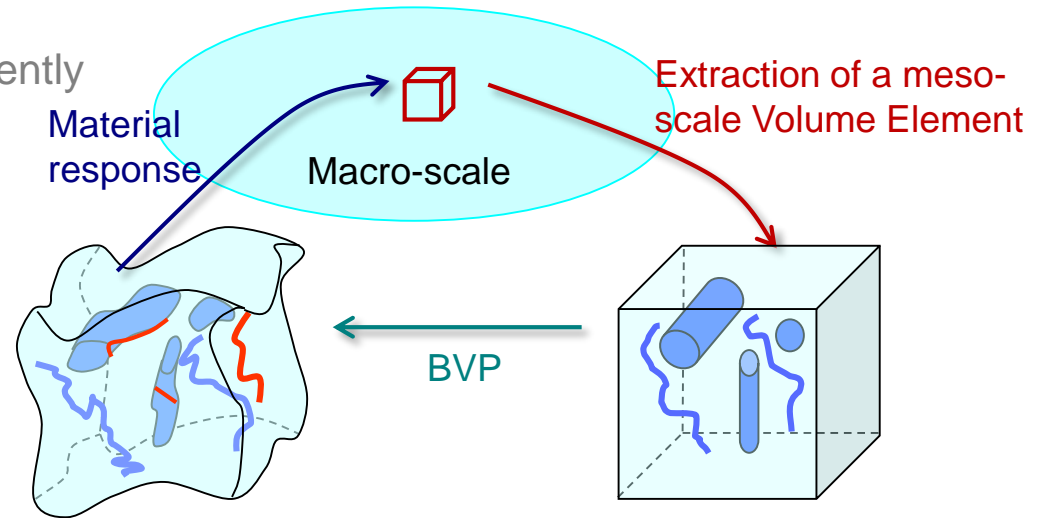
Bayesian identification of stochastic Mean-Field Homogenization model parameters

STOMMMAC The research has been funded by the Walloon Region under the agreement no 1410246-STOMMMAC (CT-INT 2013-03-28) in the context of M-ERA.NET Joint Call 2014.

Bayesian identification of stochastic MFH model parameters

- Multi-scale modeling

- 2 problems are solved concurrently
 - The macro-scale problem
 - The meso-scale problem (on a meso-scale Volume Element)

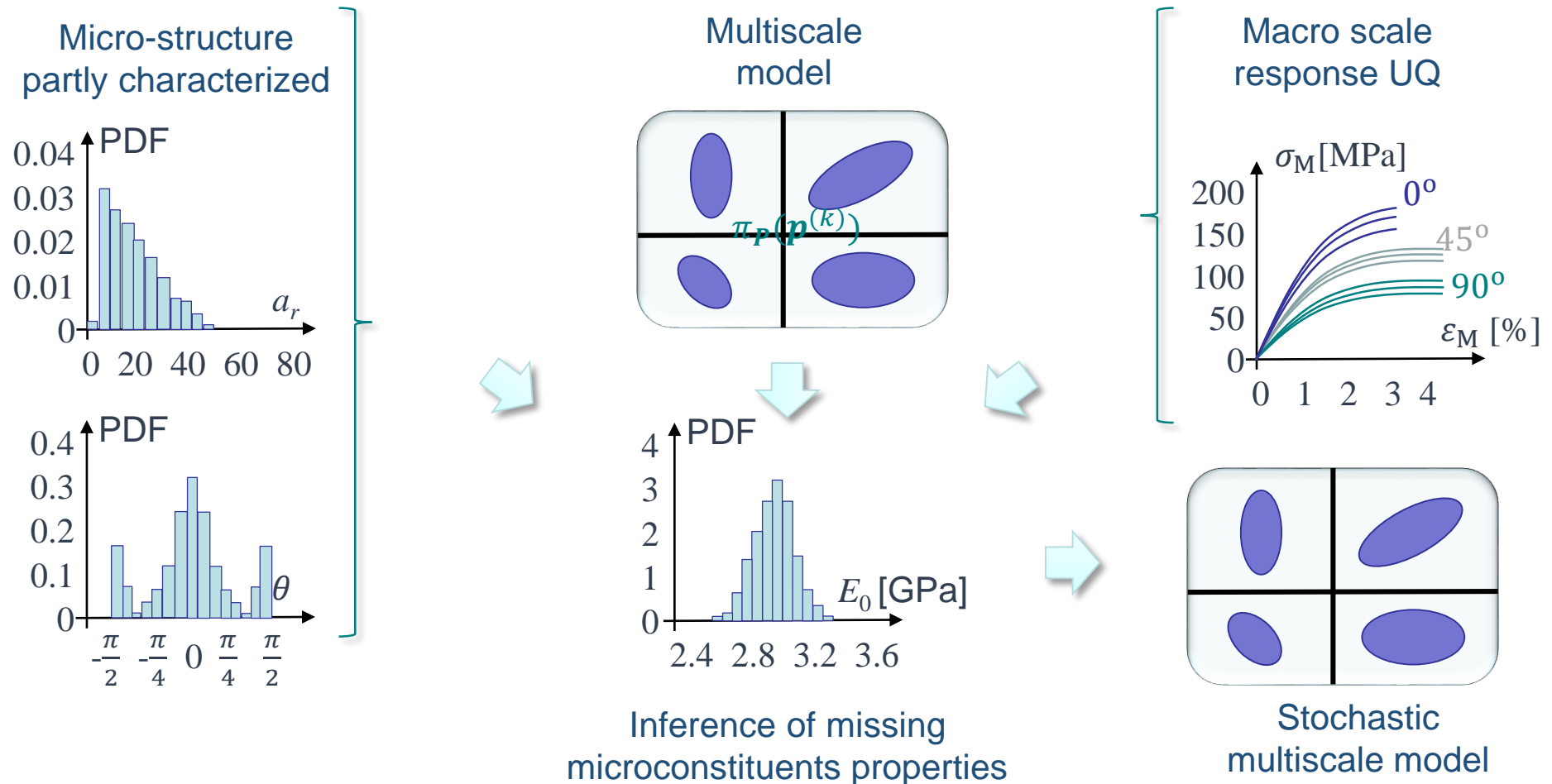


Identification: Requires identification of micro-scale geometrical and material model parameters

Bayesian identification of stochastic MFH model parameters

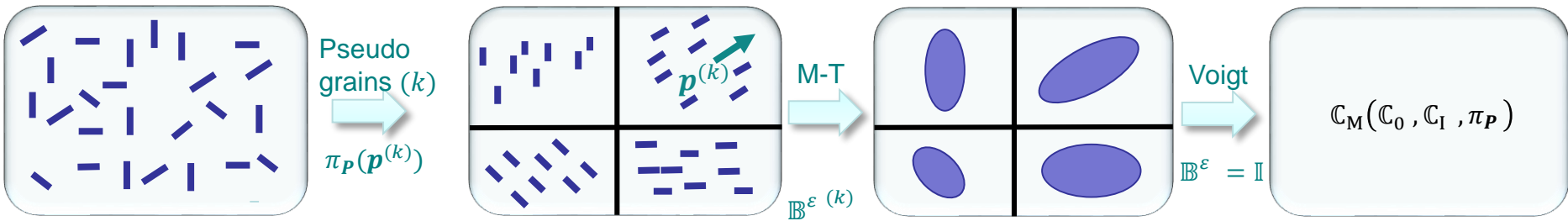
- Proposed methodology

- To develop a stochastic Mean Field Homogenization method whose missing micro-constituents properties are inferred from coupons tests



Bayesian identification of stochastic MFH model parameters

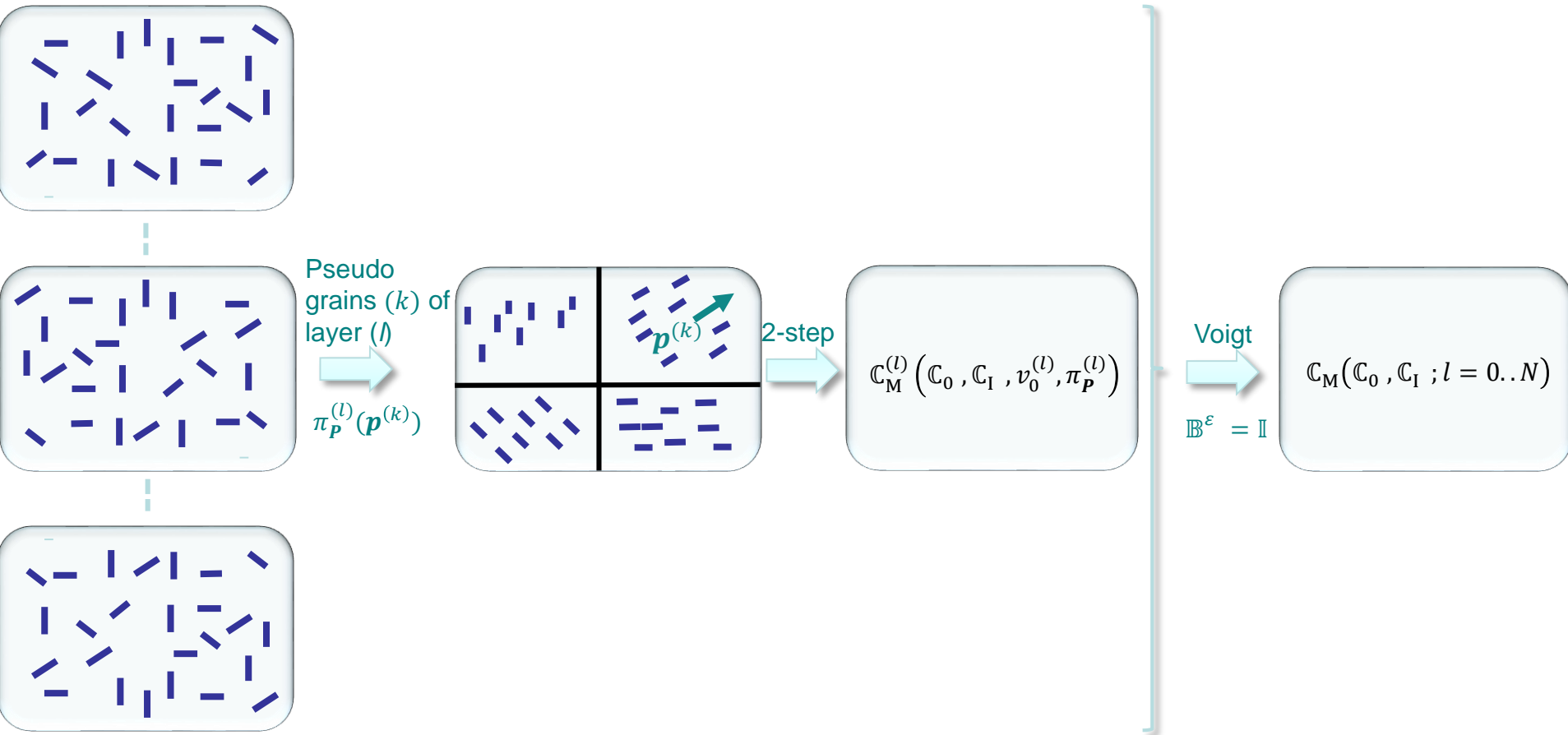
- Fibre distribution effect
 - 2-step homogenization



- For uniaxial tests along direction θ : $\sigma_M = \sigma_M(I(\psi(\mathbf{p})), C_0, C_I; \theta, \varepsilon_M)$

Bayesian identification of stochastic MFH model parameters

- Fibre distribution effect
 - Skin-core effect

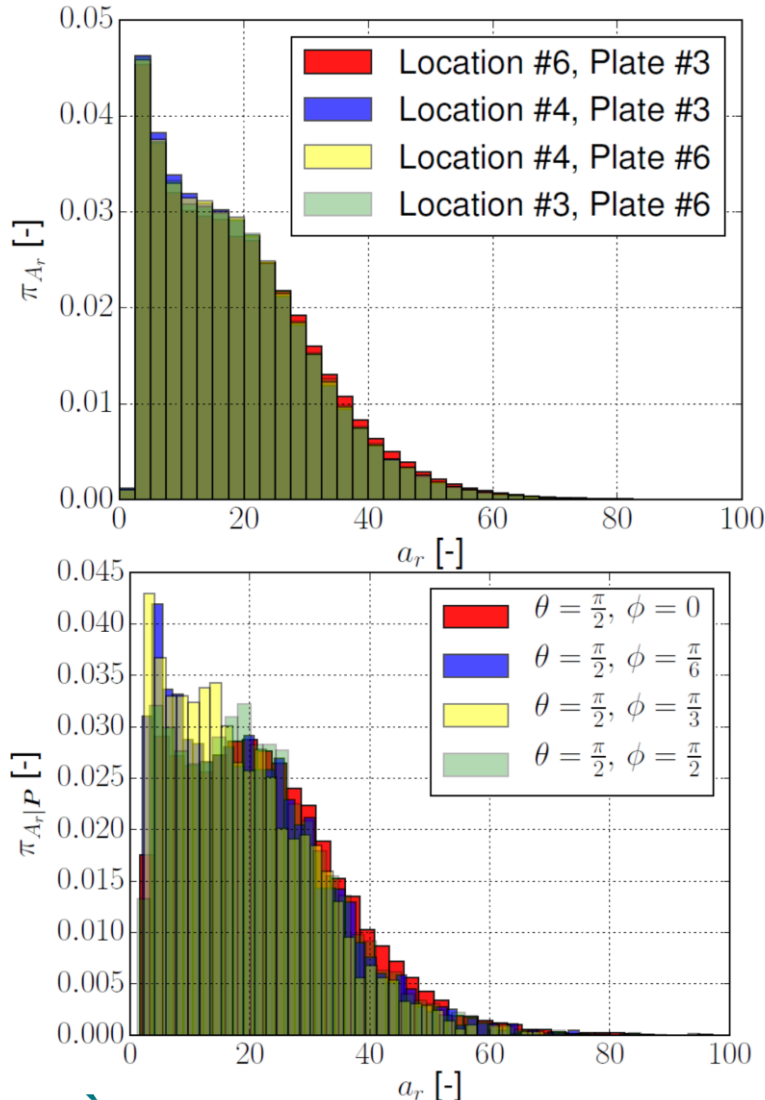


- For uniaxial tests along direction θ : $\sigma_M = \sigma_M(\mathbb{I}(\psi(\mathbf{p})), \mathbb{C}_0, \mathbb{C}_I; \theta, \varepsilon_M)$

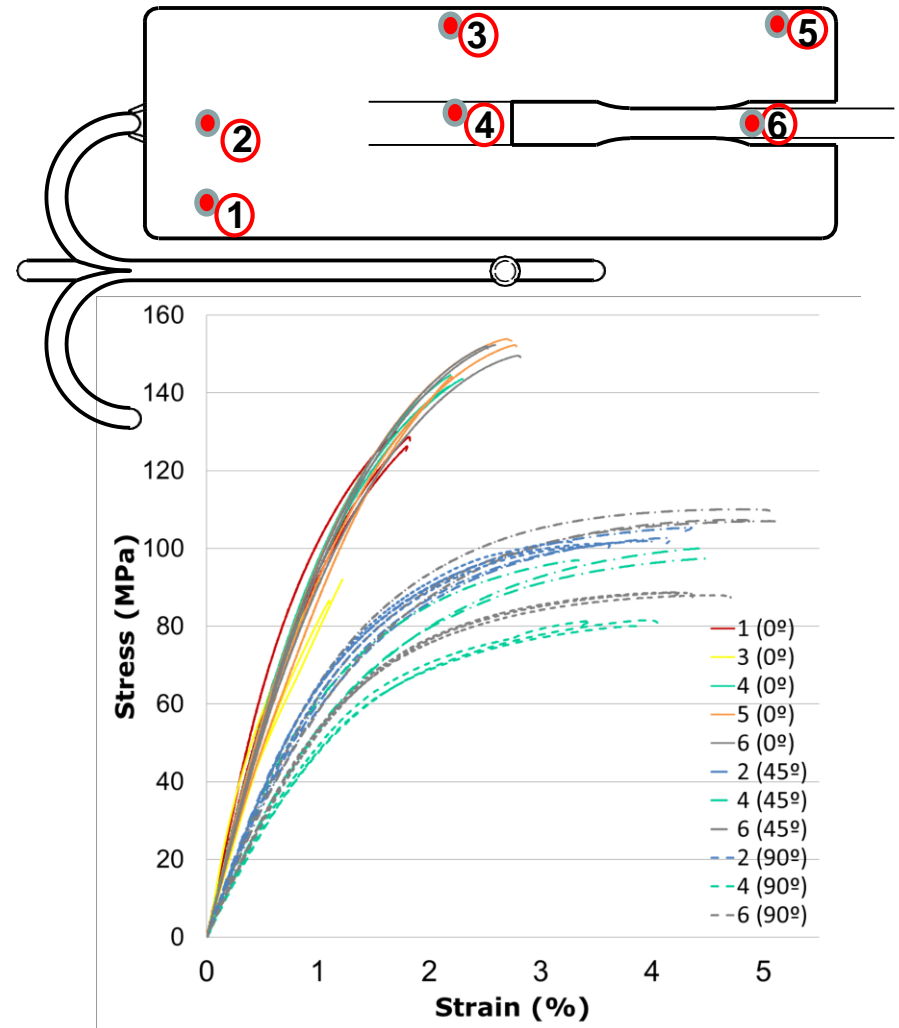
Bayesian identification of stochastic MFH model parameters

- Experimental characterization

Fiber orientation and aspect ratio (JKU)



Composite material response (BATZ)



Bayesian identification of stochastic MFH model parameters

- Assume a distribution of the matrix Young's modulus

- Beta distribution $E_0 \sim \beta_{\alpha,\beta,a,b}$ with $\beta_{\alpha,\beta,a,b}(y) = \frac{(y-a)^{\alpha-1}(y-b)^{\beta-1}}{(b-a)^{\alpha+\beta+1}B(\alpha,\beta)}$

- Matrix Young's modulus corresponding to experimental measurements

- $E_{0c}^{(n)}$ with $n = 1..n_{\text{total}}$, for all directions and positions

- Bayes' theorem

$$\pi_{\text{post}}(\alpha, \beta, a, b | \hat{E}_{0c}) \propto \pi(\hat{E}_{0c} | \alpha, \beta, a, b) \pi_{\text{prior}}(\alpha) \pi_{\text{prior}}(\beta) \pi_{\text{prior}}(a) \pi_{\text{prior}}(b)$$

- Priors: $\pi_{\text{prior}}(x) = \Gamma_{\alpha,\beta,a,c}$ with $\Gamma_{\alpha,\beta,a,c}(y) = \frac{\left(\frac{y-a}{c}\right)^{\alpha-1} \beta^\alpha e^{-\beta\left(\frac{y-a}{c}\right)}}{c\Gamma(\alpha)}$

- Likelihood: $\pi(\hat{E}_{0c} | \alpha, \beta, a, b) = \prod_{n=1}^{n_{\text{total}}} \beta_{\alpha,\beta,a,b}(E_{0c}^{(n)})$

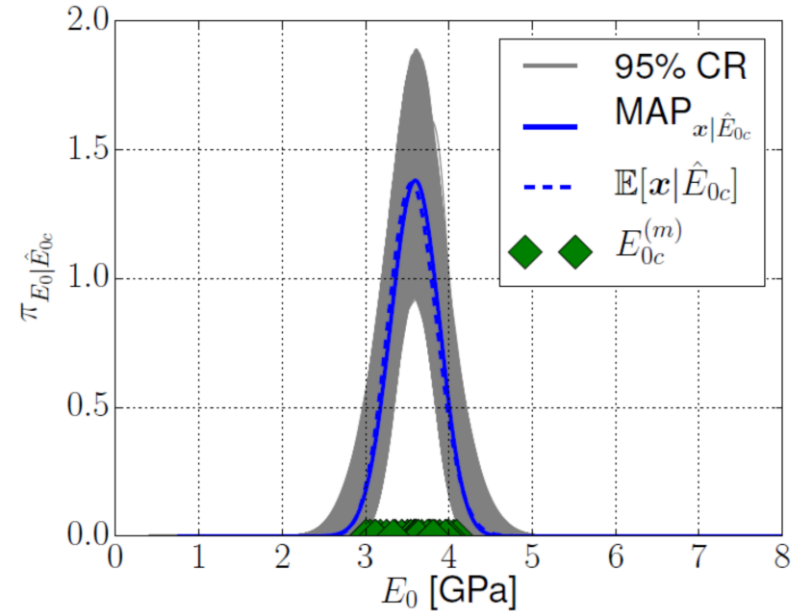
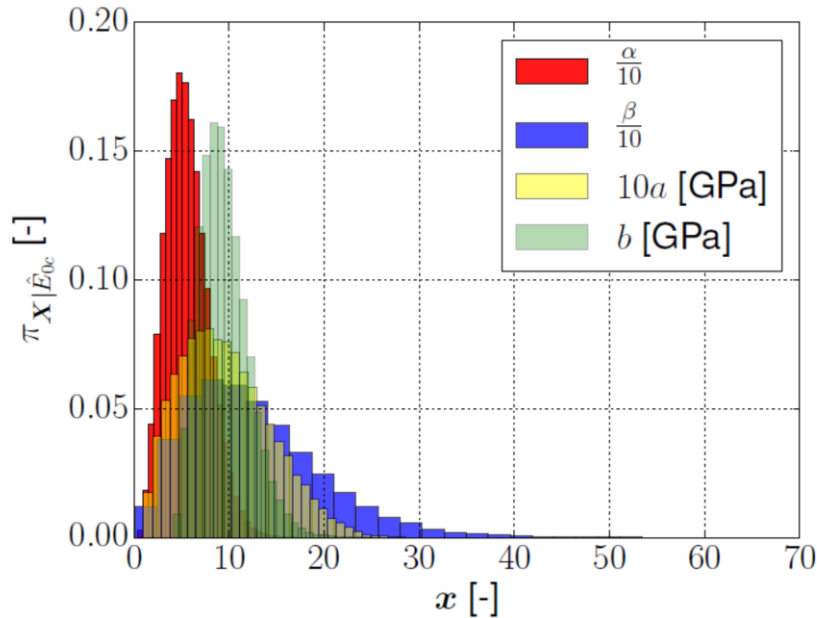
➔
$$\pi_{\text{post}}(\alpha, \beta, a, b | \hat{E}_{0c}) \propto \prod_{n=1}^{n_{\text{total}}} \beta_{\alpha,\beta,a,c}(E_{0c}^{(n)}) \pi_{\text{prior}}(\alpha) \pi_{\text{prior}}(\beta) \pi_{\text{prior}}(a) \pi_{\text{prior}}(b)$$

Bayesian identification of stochastic MFH model parameters

- Assume a distribution of the matrix Young's modulus

– Inference: $\pi_{\text{post}}(\alpha, \beta, a, b | \hat{E}_{0c}) \propto \prod_{n=1}^{n_{\text{total}}} \beta_{\alpha, \beta, a, c}(E_{0c}^{(n)}) \pi_{\text{prior}}(\alpha) \pi_{\text{prior}}(\beta) \pi_{\text{prior}}(a) \pi_{\text{prior}}(b)$

- $i = 1..n_{\text{pos}}$, with n_{pos} the number of positions tested (5, positions #1-#5)



Bayesian identification of stochastic MFH model parameters

- Validation

- Evaluate stochastic response at Position 6

- Perform stochastic homogenization from

$$\pi_{\text{post}}(\alpha, \beta, a, b | \hat{E}_{0c})$$

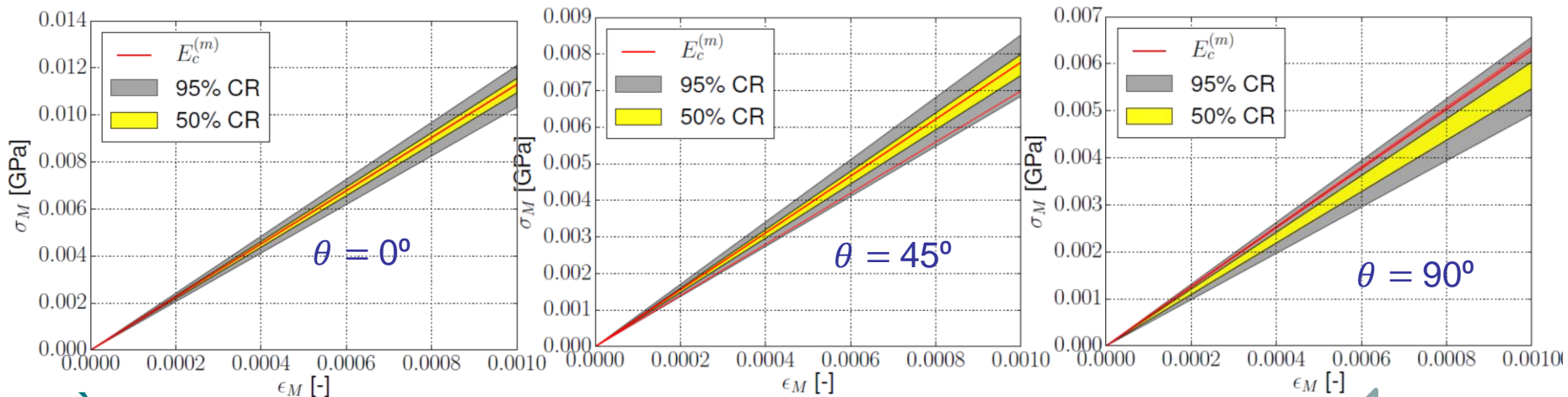
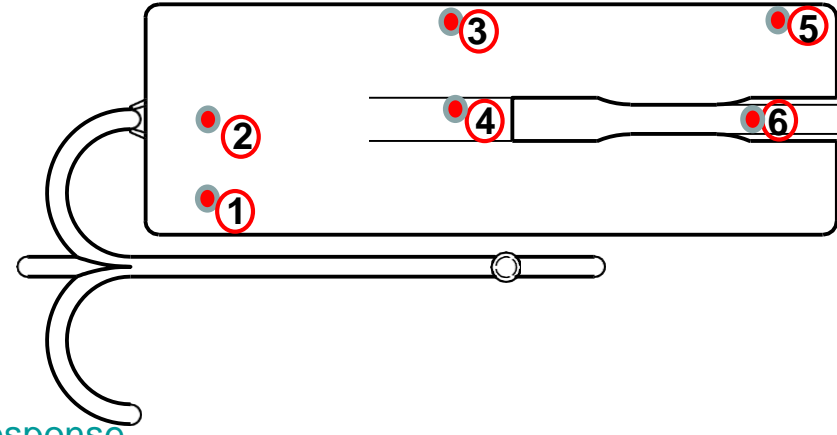
- From sampling of $[\alpha, \beta, a, b]$, evaluate

$$E_0 \sim \beta_{\alpha, \beta, a, b}$$

- From sampling of $[E_0]$, evaluate composite response

$$E_{\text{MFH}} = E_{\text{MFH}}(I(\psi(\mathbf{p}), a_r), E_0, \mathbb{C}_I; \theta)$$

- Compare with experimental measurements $\hat{E}_c^{(6,j)}$



Bayesian identification of stochastic MFH model parameters

- Extension to non-linear behavior
 - More parameters to infer
 - Matrix Young's modulus E_0
 - Matrix yield stress σ_{Y_0}
 - Matrix hardening law

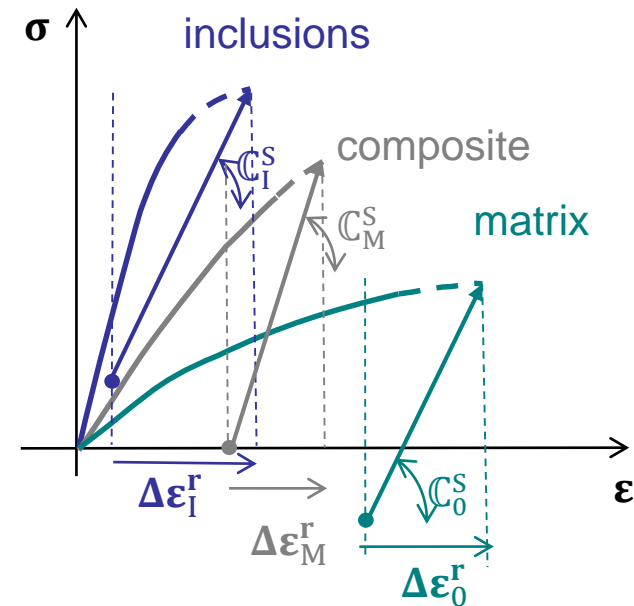
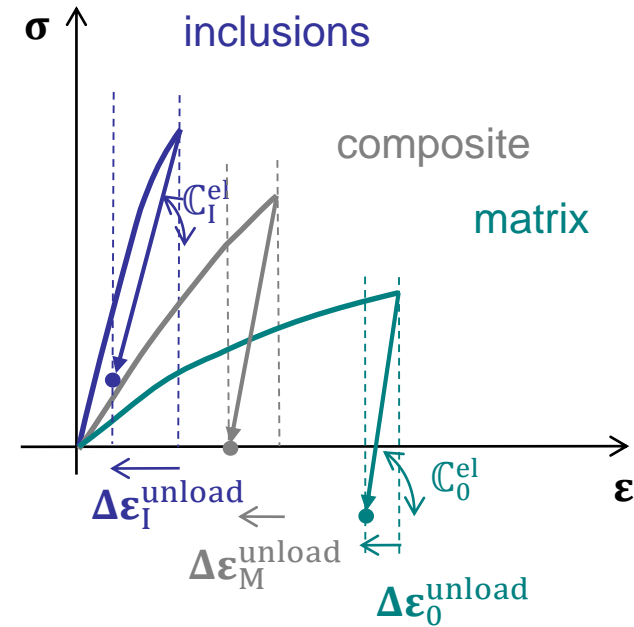
$$R(p_0) = h p_0^{m_1} (1 - \exp(-m_2 p_0))$$
 - Effective aspect ratio a_r
 - 2-Step MFH model requires many iterations
 - Incremental secant approach

$$\left\{ \begin{array}{l} \sigma_M = \bar{\sigma} = v_0 \sigma_0 + v_I \sigma_I \\ \Delta \epsilon_M^r = \bar{\Delta \epsilon} = v_0 \Delta \epsilon_0^r + v_I \Delta \epsilon_I^r \\ \Delta \epsilon_I^r = \mathbb{B}^\epsilon(I, C_0^S, C_I^S) : \Delta \epsilon_0^r \end{array} \right.$$



Too expensive for BI

- Definition of parameters



Bayesian identification of stochastic MFH model parameters

- Speed up the evaluation of the likelihood

- Likelihood

- $\pi(\hat{\sigma}_M(t) | [\varepsilon_M(t' \leq t), \boldsymbol{\vartheta}])$
 - With $\boldsymbol{\vartheta} = [E_0, \sigma_{Y_0}, h, m_1, m_2, a_r]$
 - 2-Step MFH model

$$\begin{aligned} \sigma_{MFH}(t) \\ = \sigma_{MFH}(I(\psi(\mathbf{p}), a_r), E_0 \end{aligned}$$

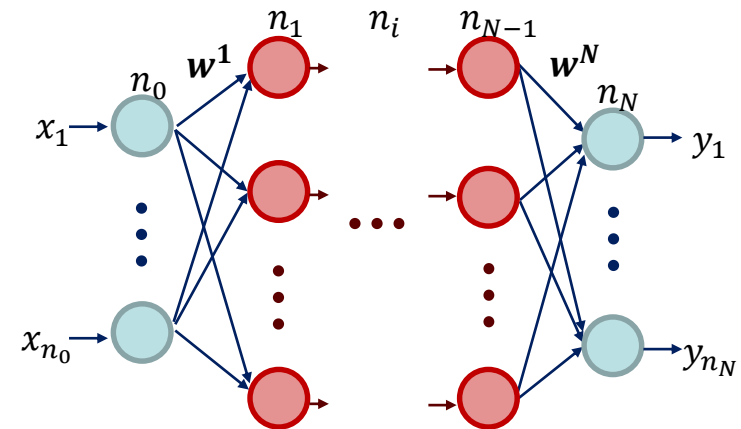
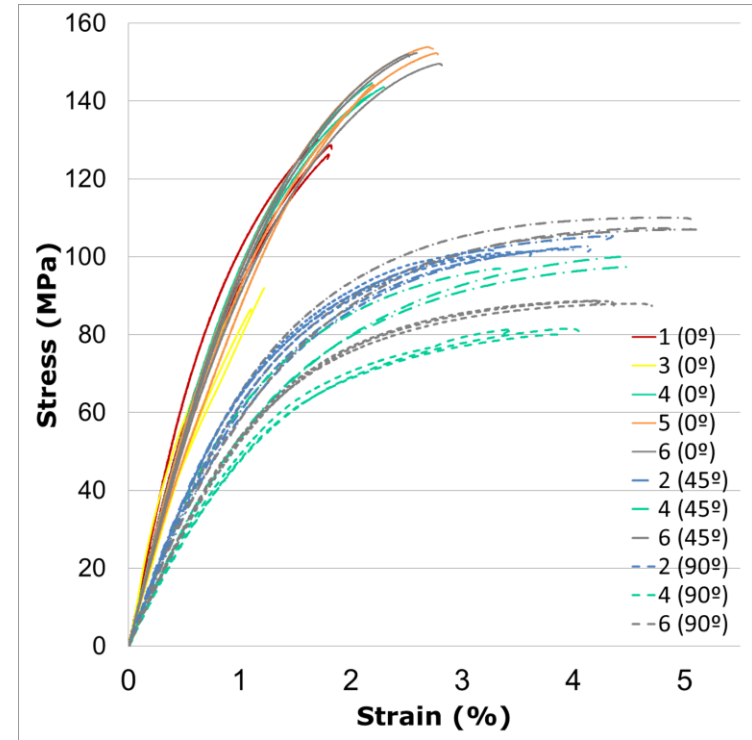


Too expensive for BI

- Use of a surrogate

- $\sigma_{NNW}(t) = \sigma_{NNW}(\varepsilon_M(t), \boldsymbol{\vartheta}, \mathbb{C}_I ; \theta)$
 - Constructed using artificial Neural Network
 - Trained fusing the 2-Step MFH model

$$\begin{aligned} \sigma_{MFH}(t) \\ = \sigma_{MFH}(I(\psi(\mathbf{p}), a_r), E_0 \\ , \quad \mathbb{C}_I, \varepsilon_M(t') \end{aligned}$$



Bayesian identification of stochastic MFH model parameters

- Assume a noise in the measurements & use surrogate model

- Measurements at strain i in direction θ_j :

$$\Sigma_c^{(i,j,k)} = \sigma_{\text{NNW}}^{(i,j)} \left(\boldsymbol{\varepsilon}_M^{(i,j)}, \boldsymbol{\vartheta}, \mathbb{C}_I ; \theta_j \right) + \text{noise}^{(i,j)}$$



$$\begin{aligned} & \pi \left(\Sigma_c^{(i,j,k)} \mid \left[\boldsymbol{\varepsilon}_M^{(i,j)}, \boldsymbol{\vartheta} \right] \right) \\ &= \pi_{\text{noise}}^{(i,j)} \left(\Sigma_c^{(i,j,k)} - \sigma_{\text{NNW}}^{(i,j)} \left(\boldsymbol{\varepsilon}_M^{(i,j)}, \boldsymbol{\vartheta}, \mathbb{C}_I ; \theta_j \right) \right) \end{aligned}$$

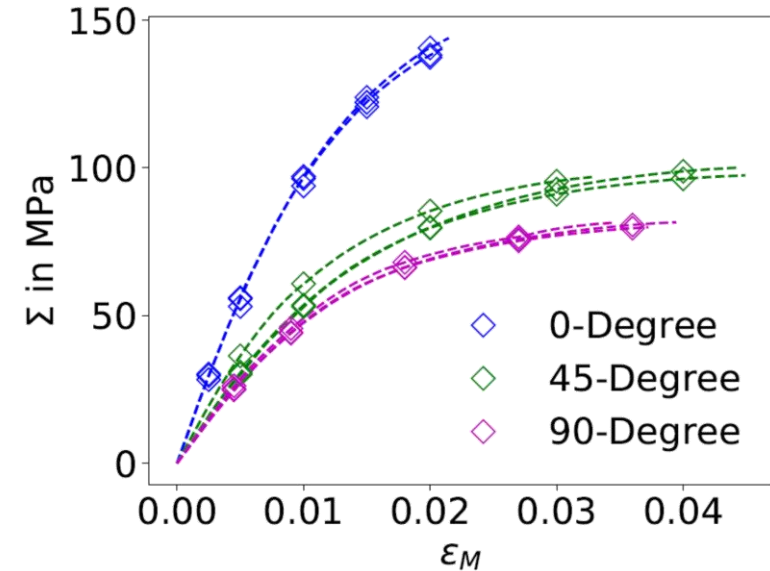
- $j = 1..n_{\text{dir}}$, with
 n_{dir} the number of directions θ_j tested
- $i = 1..n_{\varepsilon}^{(j)}$, with
 n_{ε} the number of stress-strain points
- $k = 1..n_{\text{test}}^{(i,j)}$, with
 $n_{\text{test}}^{(i,j)}$ the number of samples tested at point i along direction θ_j

- Noise function from $n_{\text{test},i,j}$ measurements at strain i in direction θ_j :

$$\pi_{\text{noise}}^{(i,j)}(y) = \frac{1}{\sqrt{2\pi} \sigma_{\Sigma_c^{(i,j)}}} \exp \left(-\frac{y^2}{2\sigma_{\Sigma_c^{(i,j)}}^2} \right)$$

- Bayes' theory:

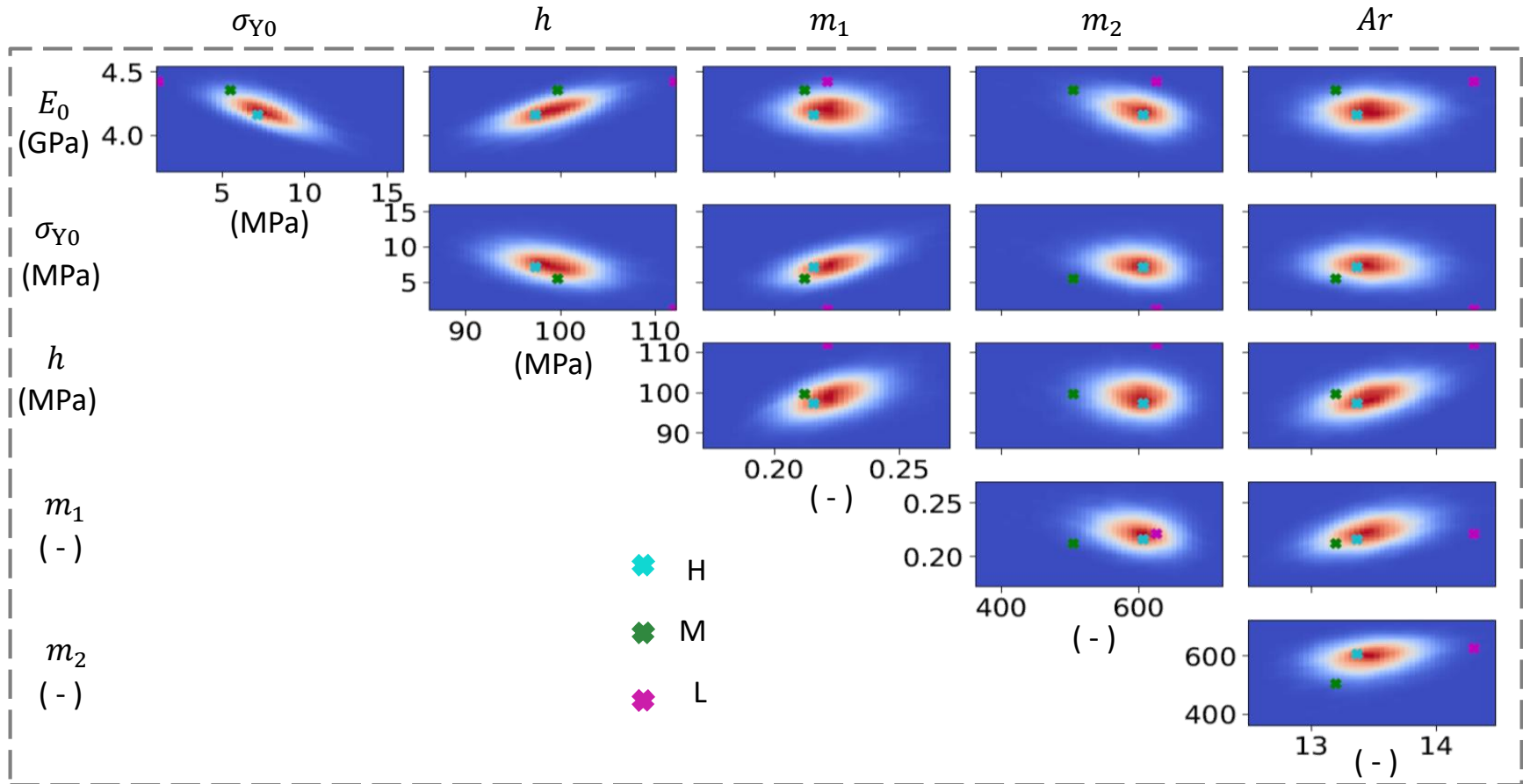
$$\pi_{\text{post}}(\boldsymbol{\vartheta} \mid \hat{\boldsymbol{\varepsilon}}_M, \hat{\Sigma}_c) \propto \pi_{\text{prior}}(\boldsymbol{\vartheta}) \prod_{j=1}^{n_{\text{dir}}} \prod_{i=1}^{n_{\varepsilon}^{(j)}} \prod_{k=1}^{n_{\text{test}}^{(i,j)}} \pi_{\text{noise}}^{(i,j)} \left(\Sigma_c^{(i,j,k)} - \sigma_{\text{NNW}}^{(i,j)} \left(\boldsymbol{\varepsilon}_M^{(i,j)}, \boldsymbol{\vartheta}, \mathbb{C}_I ; \theta_j \right) \right)$$



Bayesian identification of stochastic MFH model parameters

- Results

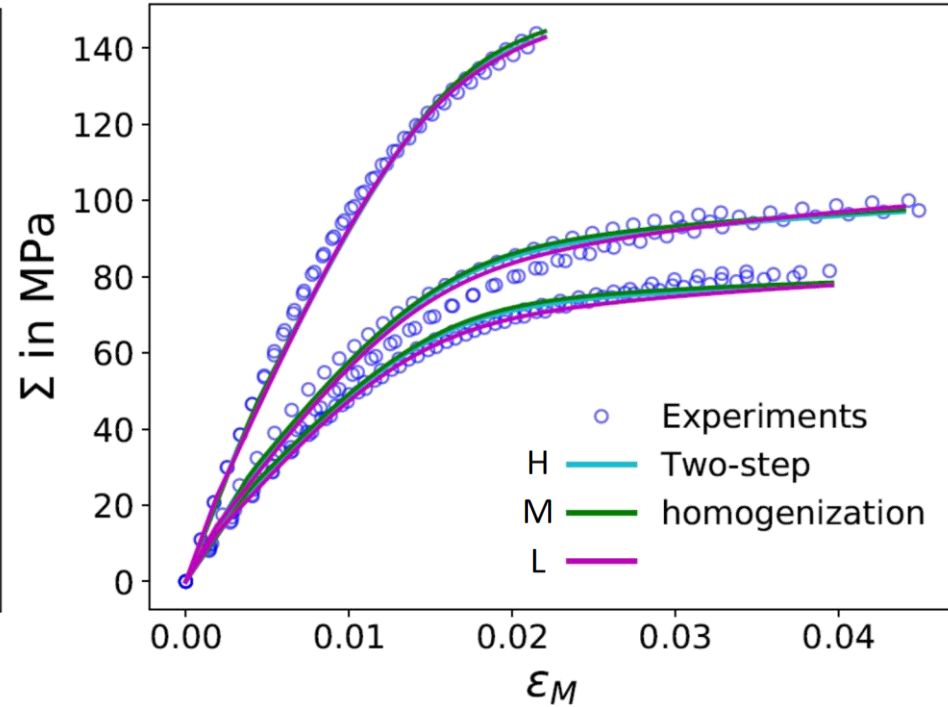
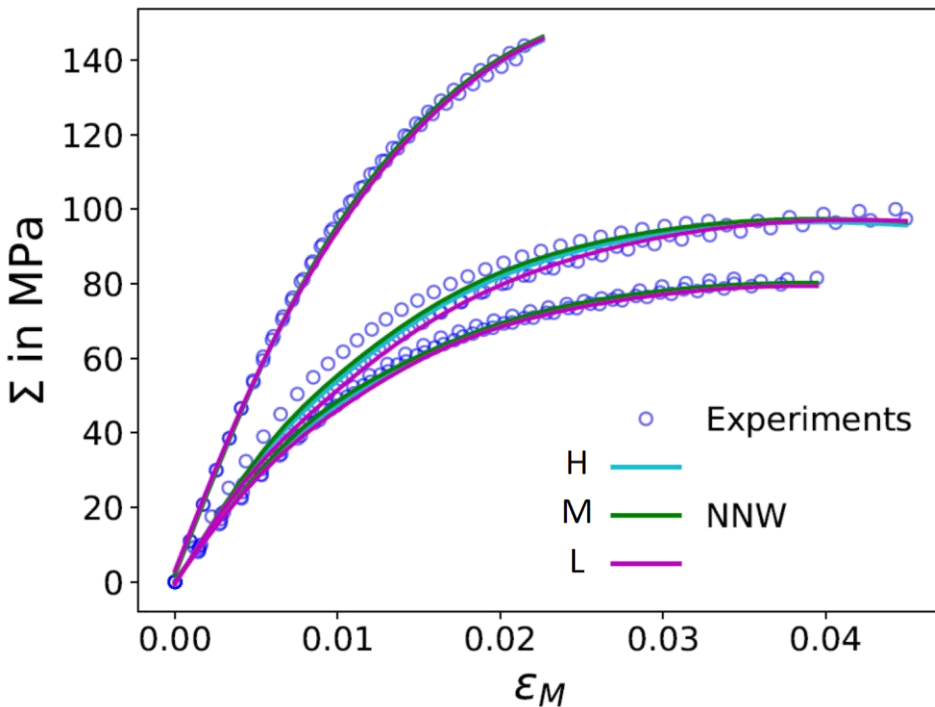
$$\pi_{\text{post}}(\boldsymbol{\vartheta} | \hat{\boldsymbol{\varepsilon}}_{\text{M}}, \hat{\boldsymbol{\Sigma}}_{\text{c}}) \propto \pi_{\text{prior}}(\boldsymbol{\vartheta}) \prod_{j=1}^{n_{\text{dir}}} \prod_{i=1}^{n_{\varepsilon}^{(j)}} \prod_{k=1}^{n_{\text{test}}^{(i,j)}} \pi_{\text{noise}}^{(i,j)} \left(\boldsymbol{\Sigma}_{\text{c}}^{(i,j,k)} - \sigma_{\text{NNW}}^{(i,j)} \left(\boldsymbol{\varepsilon}_{\text{M}}^{(i,j)}, \boldsymbol{\vartheta}, \mathbb{C}_{\text{I}} ; \theta_j \right) \right)$$



Bayesian identification of stochastic MFH model parameters

- Verification

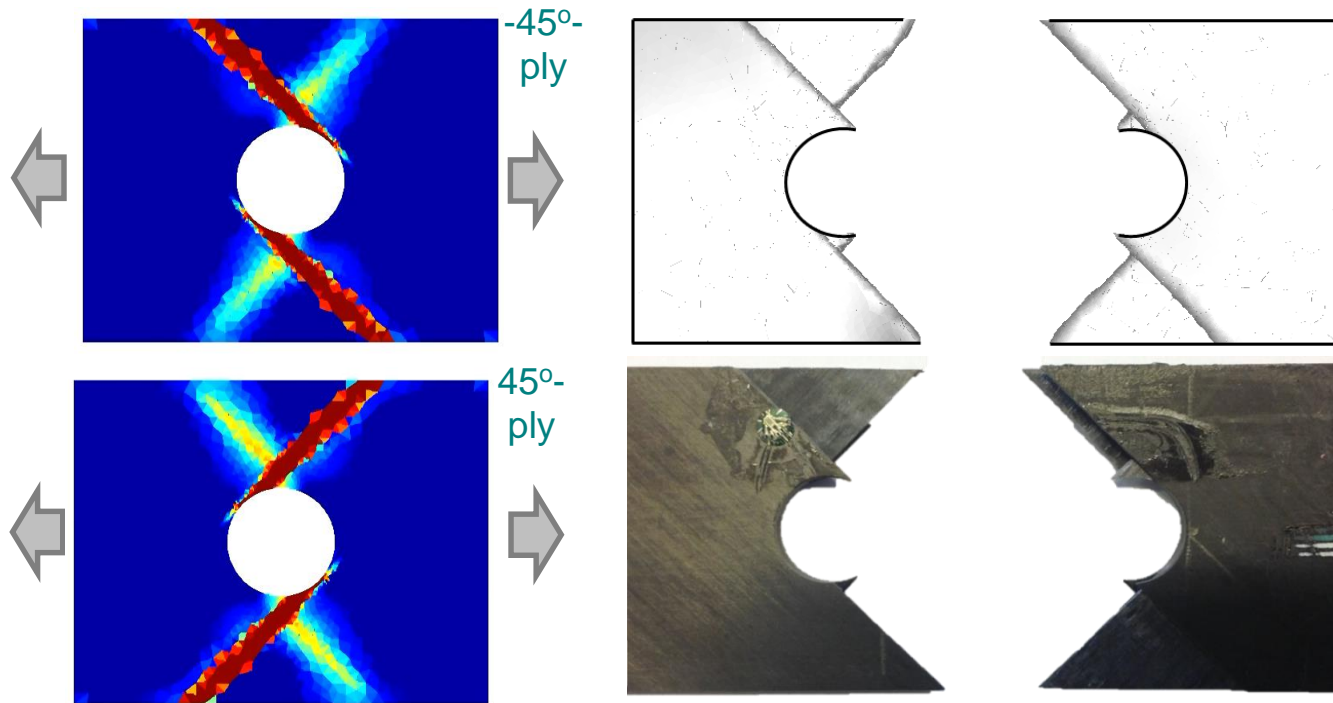
$$\pi_{\text{post}}(\boldsymbol{\vartheta} | \hat{\boldsymbol{\varepsilon}}_{\mathbf{M}}, \hat{\boldsymbol{\Sigma}}_{\mathbf{c}}) \propto \pi_{\text{prior}}(\boldsymbol{\vartheta}) \prod_{j=1}^{n_{\text{dir}}} \prod_{i=1}^{n_{\boldsymbol{\varepsilon}}^{(j)}} \prod_{k=1}^{n_{\text{test}}^{(i,j)}} \pi_{\text{noise}}^{(i,j)} \left(\boldsymbol{\Sigma}_{\mathbf{c}}^{(i,j,k)} - \sigma_{\text{NNW}}^{(i,j)} \left(\boldsymbol{\varepsilon}_{\mathbf{M}}^{(i,j)}, \boldsymbol{\vartheta}, \mathbb{C}_{\mathbf{I}} ; \theta_j \right) \right)$$



Bayesian identification of stochastic MFH model parameters

- STOMMMAC M.ERA-NET project (MFH for elasto-visco-plastic composites)
 - e-Xstream, ULiège (Belgium)
 - BATZ (Spain)
 - JKU, AC (Austria)
 - U Luxembourg (Luxembourg)

- Publications (doi)
 - [10.1016/j.compstruct.2019.03.066](https://doi.org/10.1016/j.compstruct.2019.03.066)



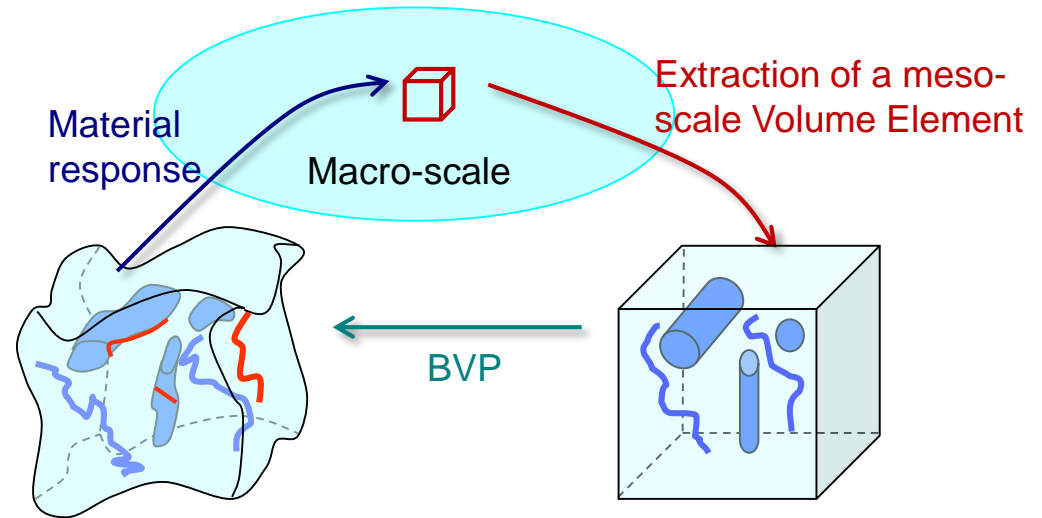
Non-Local Damage Mean-Field-Homogenization

SIMUCOMP The research has been funded by the Walloon Region under the agreement no 1017232 (CT-EUC 2010-10-12) in the context of the ERA-NET +, Matera + framework.

Non-Local Damage Mean-Field-Homogenization

- Multi-scale modeling

- 2 problems are solved concurrently
 - The macro-scale problem
 - The meso-scale problem (on a meso-scale Volume Element)



- Length-scales separation

$$L_{\text{macro}} \gg L_{\text{VE}} \gg L_{\text{micro}}$$

For accuracy: Size of the meso-scale volume element smaller than the characteristic length of the macro-scale loading

To be statistically representative: Size of the meso-scale volume element larger than the characteristic length of the micro-structure

Non-Local Damage Mean-Field-Homogenization

- Materials with strain softening

- Incremental forms

- Strain increments in the same direction

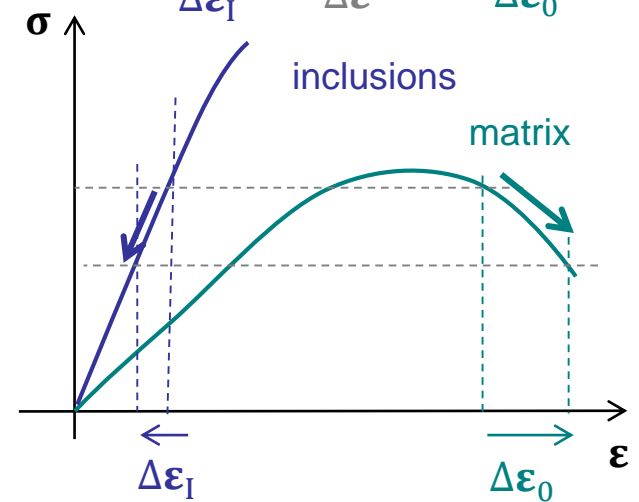
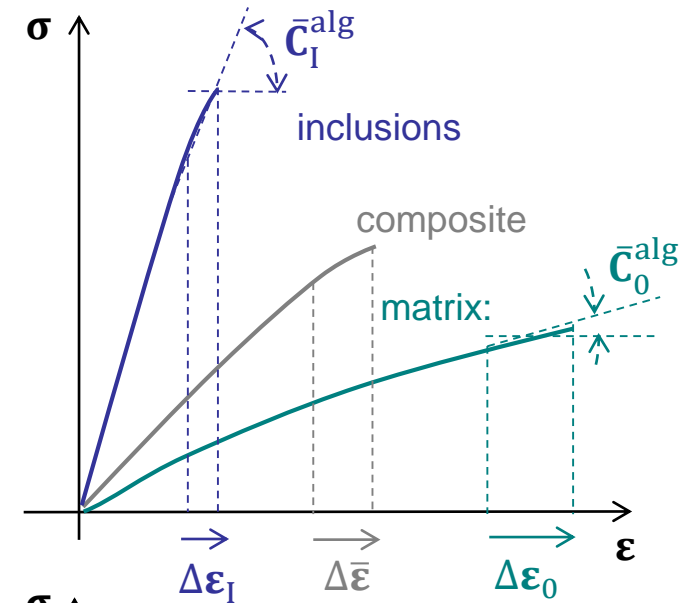
$$\Delta \boldsymbol{\varepsilon}_I = \mathbf{B}^\varepsilon \left(\mathbf{I}, \bar{\mathbf{C}}_0^{\text{alg}}, \bar{\mathbf{C}}_I^{\text{alg}} \right) : \Delta \boldsymbol{\varepsilon}_0$$

- Because of the damaging process, the fiber phase is elastically unloaded during matrix softening



- Solution: new incremental-secant method

- We need to define the LCC from another stress state



Non-Local Damage Mean-Field-Homogenization

- Based on the incremental-secant approach

- Perform a virtual elastic unloading from previous solution
 - Composite material unloaded to reach the stress-free state
 - Residual stress in components
- Apply MFH from unloaded state
 - New strain increments (>0)

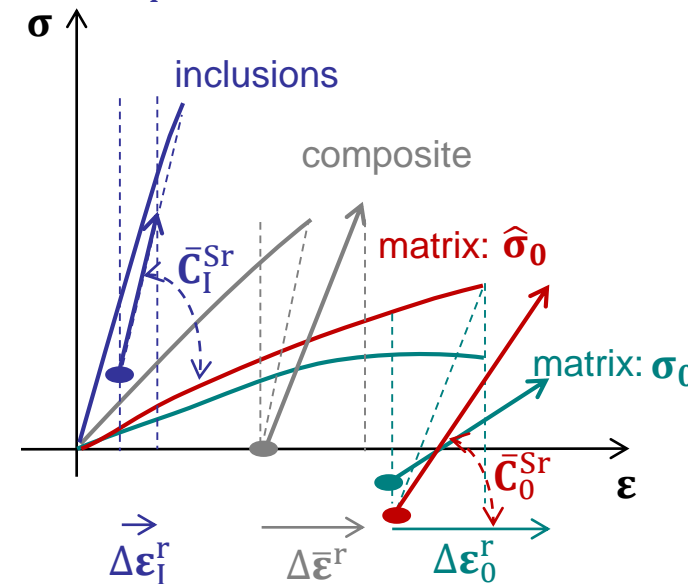
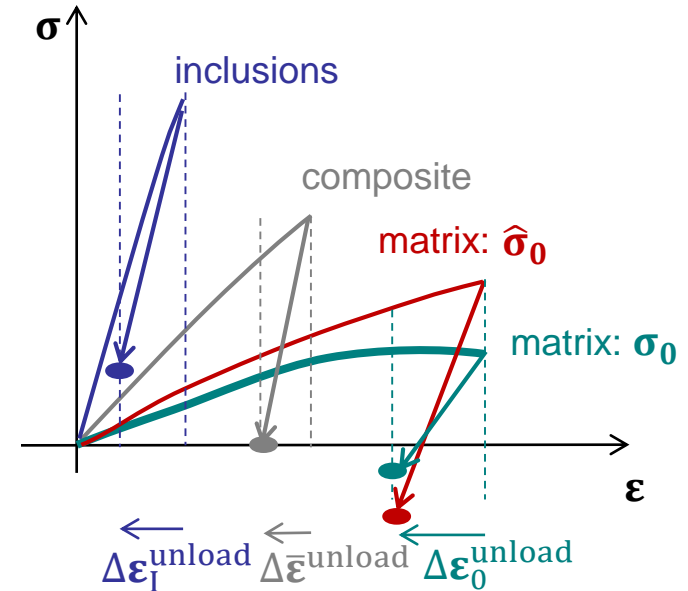
$$\Delta \boldsymbol{\varepsilon}_{I/0}^r = \Delta \boldsymbol{\varepsilon}_{I/0} + \Delta \boldsymbol{\varepsilon}_{I/0}^{\text{unload}}$$

- Use of secant operators

$$\Delta \boldsymbol{\varepsilon}_I^r = \mathbf{B}^\varepsilon (\mathbf{I}, (1 - D) \bar{\mathbf{C}}_0^{\text{Sr}}, \bar{\mathbf{C}}_I^{\text{S}0}) : \Delta \boldsymbol{\varepsilon}_0^r$$

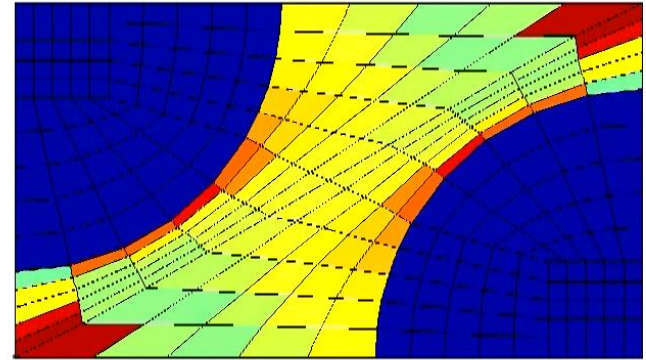
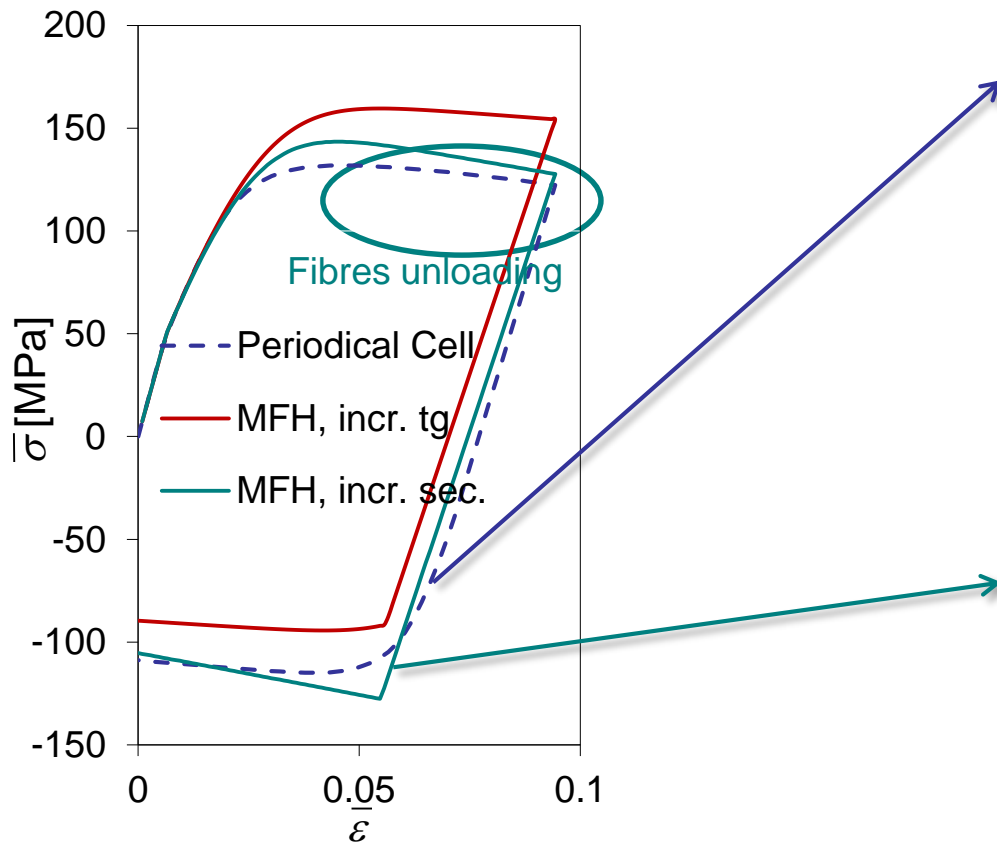
- Possibility of unloading

$$\left\{ \begin{array}{l} \Delta \boldsymbol{\varepsilon}_I^r > \mathbf{0} \\ \Delta \boldsymbol{\varepsilon}_I < \mathbf{0} \end{array} \right.$$



Non-Local Damage Mean-Field-Homogenization

- New results for damage
 - Fictitious composite
 - 50%-UD fibres
 - Elasto-plastic matrix with damage



Non-Local Damage Mean-Field-Homogenization

- Material models

- Elasto-plastic material

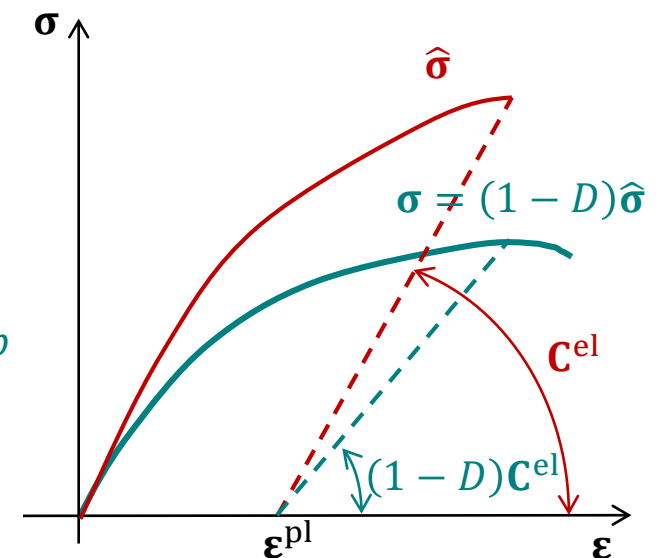
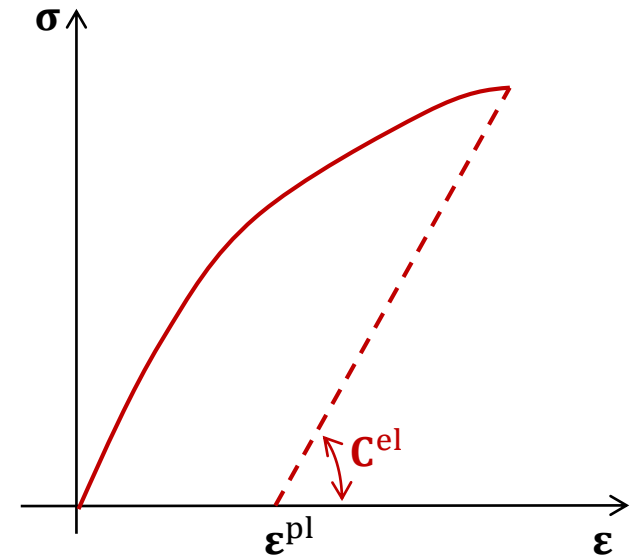
- Stress tensor $\boldsymbol{\sigma} = \mathbf{C}^{\text{el}} : (\boldsymbol{\varepsilon} - \boldsymbol{\varepsilon}^{\text{pl}})$
 - Yield surface $f(\boldsymbol{\sigma}, p) = \boldsymbol{\sigma}^{\text{eq}} - \sigma^Y - R(p) \leq 0$
 - Plastic flow $\Delta \boldsymbol{\varepsilon}^{\text{pl}} = \Delta p \mathbf{N} \quad \& \quad \mathbf{N} = \frac{\partial f}{\partial \boldsymbol{\sigma}}$

- Local damage model

- Apparent-effective stress tensors $\boldsymbol{\sigma} = (1 - D)\hat{\boldsymbol{\sigma}}$
 - Plastic flow in the effective stress space
 - Damage evolution $\Delta D = F_D(\boldsymbol{\varepsilon}, \Delta p)$

- Non-Local damage model [Peerlings et al., 1996]

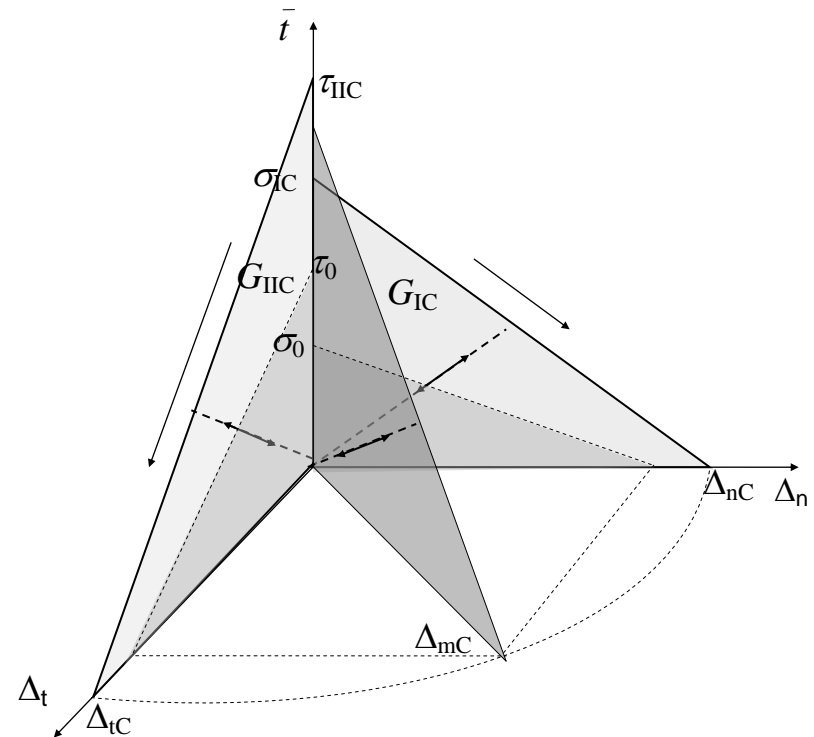
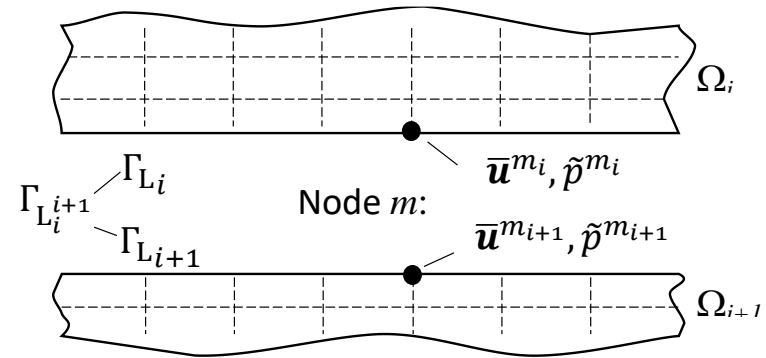
- Damage evolution $\Delta D = F_D(\boldsymbol{\varepsilon}, \Delta \tilde{p})$
 - Anisotropic governing equation $\tilde{p} - \nabla \cdot (\mathbf{c}_g \cdot \nabla \tilde{p}) = p$



Non-Local Damage Mean-Field-Homogenization

- Laminate studies

- Bulk material law
 - Non-local damage-enhanced MFH
 - Intra-laminar failure
 - Account for anisotropy
- Interface
 - DG/Cohesive zone model
 - Inter-laminar failure

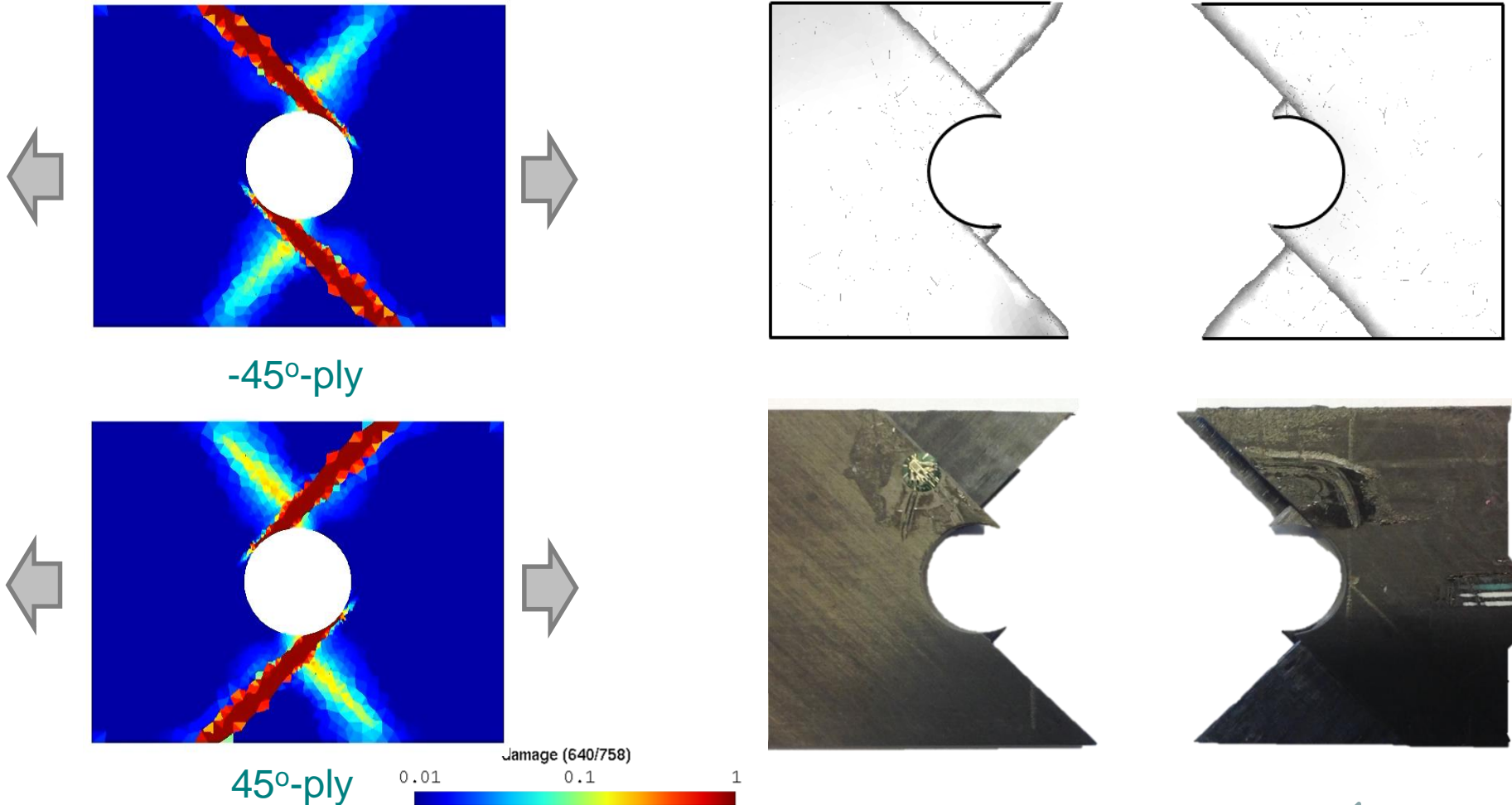


Non-Local Damage Mean-Field-Homogenization

- $[45^\circ_4 / -45^\circ_4]_S$ - open hole laminate (epoxy- with 60% UD CF)

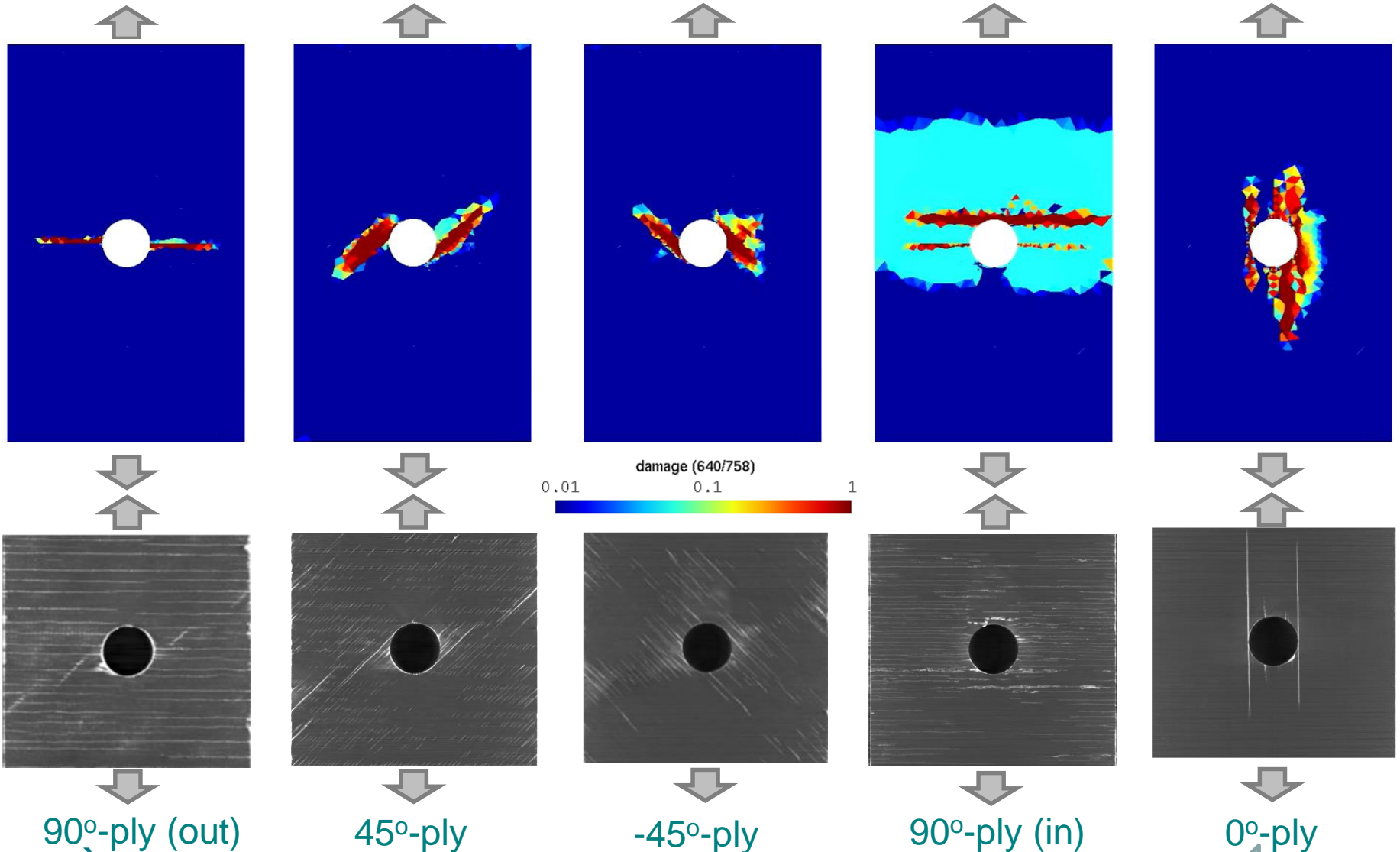
Intra-laminar failure along fiber directions

Inter-laminar failure matches experimental results



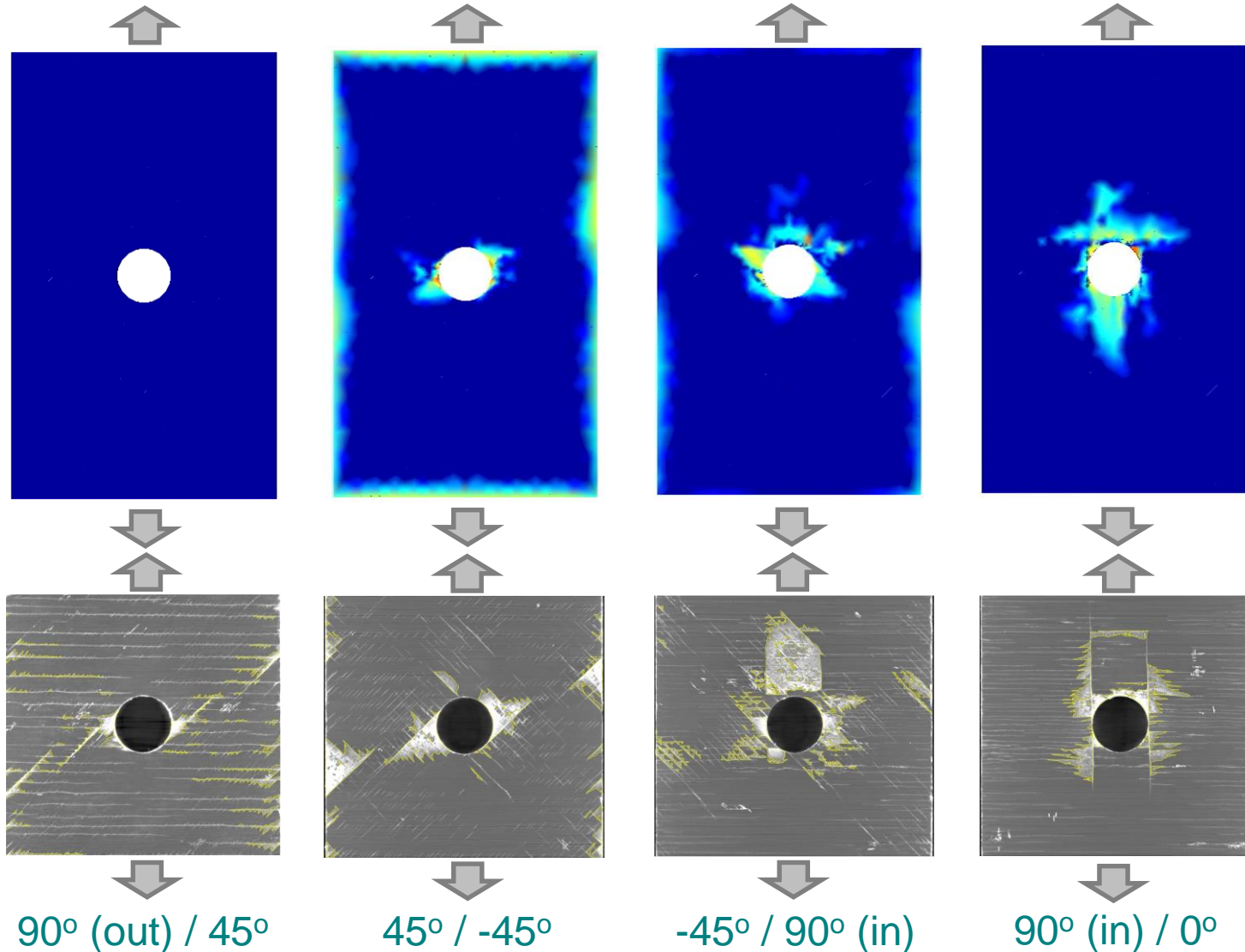
Non-Local Damage Mean-Field-Homogenization

- $[90^\circ / 45^\circ / -45^\circ / 90^\circ / 0^\circ]_S$ - open hole laminate
 - Intra-laminar failure along fiber directions (experiments: IMDEA Materials)



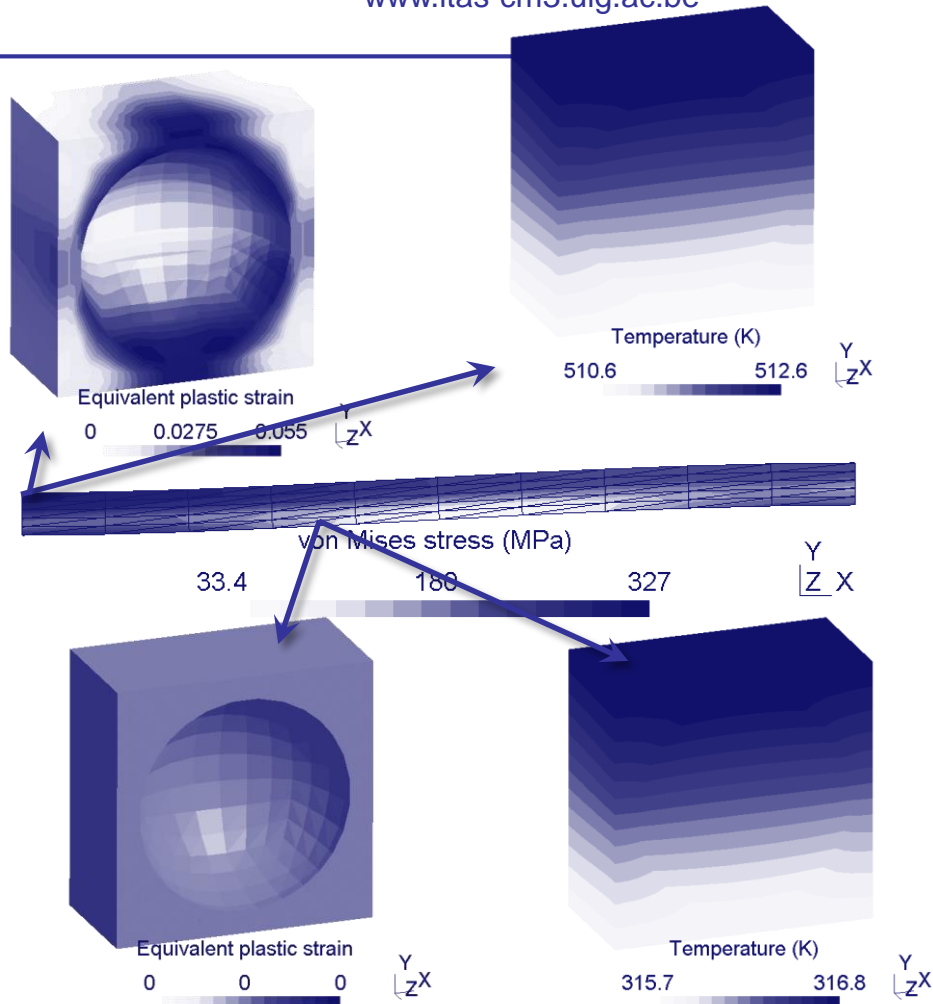
Non-Local Damage Mean-Field-Homogenization

- $[90^\circ / 45^\circ / -45^\circ / 90^\circ / 0^\circ]_S$ - open hole laminate
 - Inter-laminar failure compared to experimental results (experiments: IMDEA Materials)



- SIMUCOMP ERA-NET project
 - e-Xstream, CENAERO, ULiège (Belgium)
 - IMDEA Materials (Spain)
 - CRP Henri-Tudor (Luxemburg)
- Publications (doi)
 - [10.1016/j.compstruct.2015.02.070](https://doi.org/10.1016/j.compstruct.2015.02.070)
 - [10.1016/j.ijsolstr.2013.07.022](https://doi.org/10.1016/j.ijsolstr.2013.07.022)
 - [10.1016/j.ijplas.2013.06.006](https://doi.org/10.1016/j.ijplas.2013.06.006)
 - [10.1016/j.cma.2012.04.011](https://doi.org/10.1016/j.cma.2012.04.011)
 - [10.1007/978-1-4614-4553-1_13](https://doi.org/10.1007/978-1-4614-4553-1_13)

Boundary conditions and
tangent operator in multi-
physics computational
homogenization

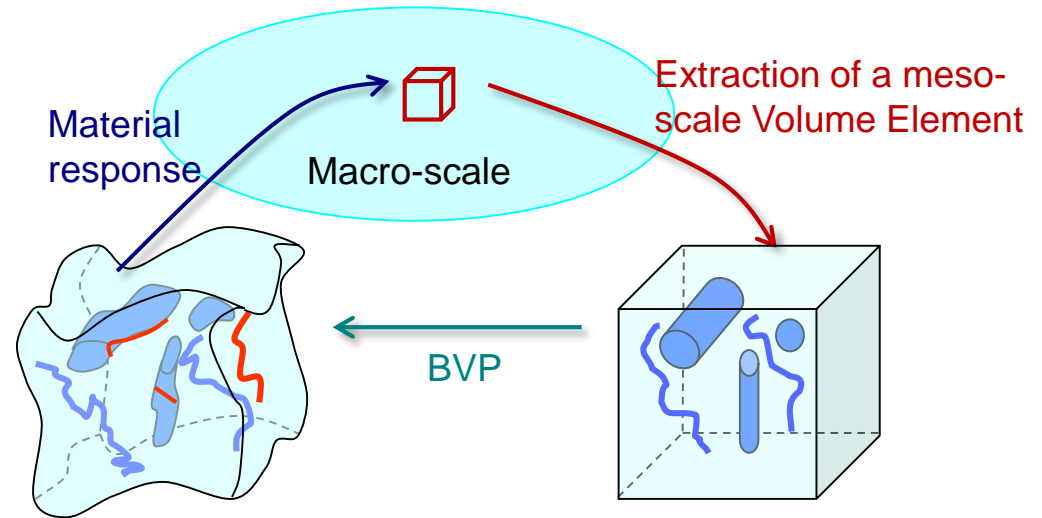


ARC 09/14-02 BRIDGING - From imaging to geometrical modelling of complex micro structured materials: Bridging computational engineering and material science
The authors gratefully acknowledge the financial support from F.R.S-F.N.R.S. under the project number PDR T.1015.14

Boundary conditions and tangent operator in FE²

- Multi-scale modeling

- 2 problems are solved concurrently
 - The macro-scale problem
 - The meso-scale problem (on a meso-scale Volume Element)



- Length-scales separation

$$L_{\text{macro}} \gg L_{\text{VE}} \gg L_{\text{micro}}$$

For accuracy: Size of the meso-scale volume element smaller than the characteristic length of the macro-scale loading

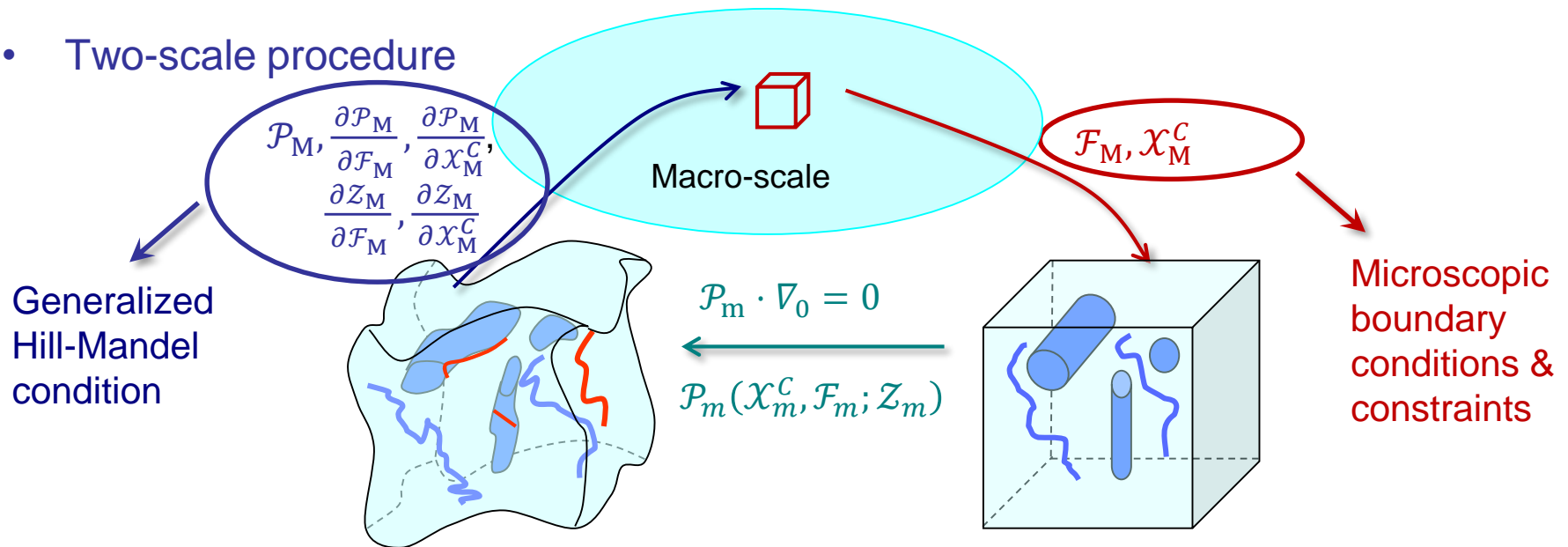
To be statistically representative: Size of the meso-scale volume element larger than the characteristic length of the micro-structure

Boundary conditions and tangent operator in FE²

- Generalized multi-physics representation

- Strong form $\mathcal{P} \cdot \nabla_0 = 0$
- Fully-coupled constitutive law $\mathcal{P} = \mathcal{P}(\chi^C, \mathcal{F}; \mathcal{Z})$
 - \mathcal{F} : generalized deformation gradient, χ^C : fields appearing in the constitutive relations
 - \mathcal{Z} : internal variables
- Tangent operators $\mathcal{L} = \frac{\partial \mathcal{P}}{\partial \mathcal{F}}$ & $\mathcal{J} = \frac{\partial \mathcal{P}}{\partial \chi^C}$ but also $\mathcal{Y}_{\mathcal{F}} = \frac{\partial \mathcal{Z}}{\partial \mathcal{F}}$ & $\mathcal{Y}_{\chi^C} = \frac{\partial \mathcal{Z}}{\partial \chi^C}$

- Two-scale procedure



Boundary conditions and tangent operator in FE²

- Generalized microscopic boundary conditions

- Arbitrary field k kinematics: $\mathcal{X}_m^k = \mathcal{X}_M^k + \mathcal{F}_M^k \cdot X_m + \mathcal{W}_m^k$ Fluctuation

- Constrained field k equivalence: $\int_{\omega_0} C_m^k \mathcal{X}_m^{C^k} d\omega = \int_{\omega_0} C_m^k d\omega \mathcal{X}_M^{C^k}$

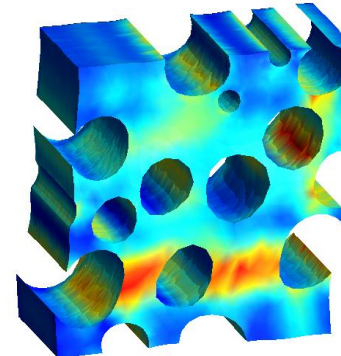
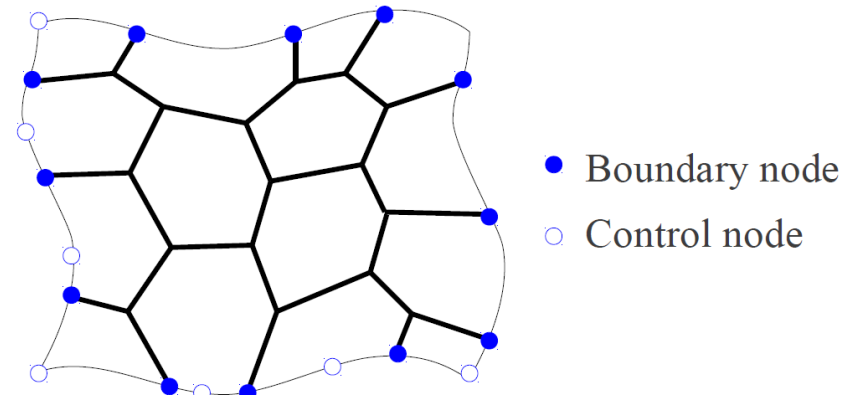
- E.g. periodic boundary conditions

Define an interpolant map

$$\mathbb{S}^i = \sum N_k^i(\mathbf{X}_m) a_k^i$$

Substitute fluctuation fields

$$W_m^k(\mathbf{X}_m^+) = \mathbb{S}^i(\mathbf{X}_m^-) = W_m^k(\mathbf{X}_m^-)$$



- Microscale BVP

- Weak formulation

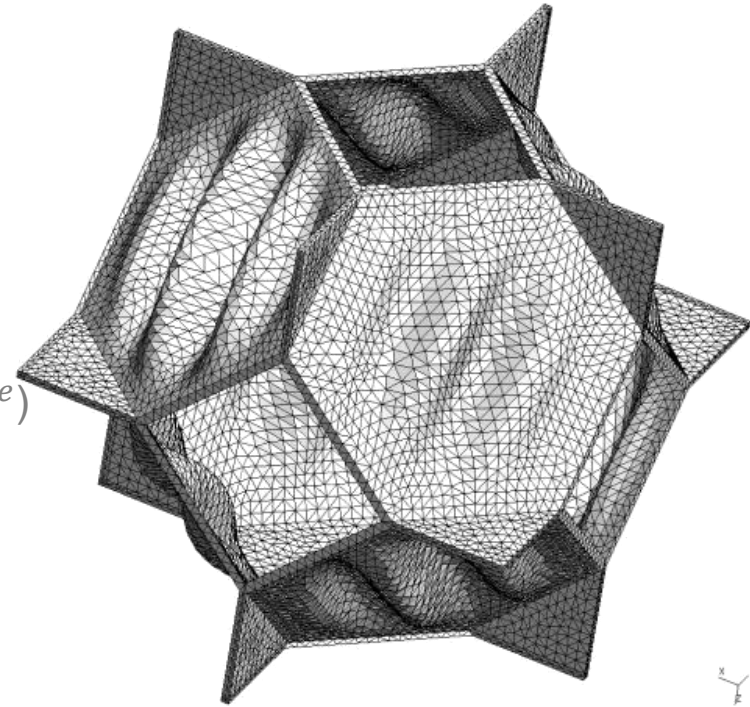
$$\left\{ \begin{array}{l} \mathcal{P}_m \cdot \nabla_0 = 0 \quad \text{with } \mathcal{P}_m(\mathcal{X}_m^C, \mathcal{F}_m; \mathcal{Z}_m) \\ \mathcal{X}_m^k = \mathcal{X}_M^k + \mathcal{F}_M^k \cdot X_m + \mathcal{W}_m^k \\ \int_{\omega_0} C_m^k \mathcal{X}_m^{C^k} d\omega = \int_{\omega_0} C_m^k d\omega \mathcal{X}_M^{C^k} \end{array} \right.$$

- Weak finite element constrained form ($\omega_0 = \cup_e \omega^e$)

$$\left\{ \begin{array}{l} \mathbf{f}_m(\mathbf{u}_m) - \mathbf{C}^T \boldsymbol{\lambda} = 0 \\ \mathbf{C} \mathbf{u}_m - \mathbf{S} \begin{bmatrix} \mathcal{F}_M \\ \mathcal{X}_M^C \end{bmatrix} = 0 \end{array} \right.$$

- System linearization

$$\left\{ \begin{array}{l} \mathbf{Q}^T \frac{\partial \mathbf{f}_m}{\partial \mathbf{u}_m} \mathbf{Q} \delta \mathbf{u}_m + \mathbf{r} - \mathbf{Q}^T \frac{\partial \mathbf{f}_m}{\partial \mathbf{u}_m} \mathbf{C}^T (\mathbf{C} \mathbf{C}^T)^{-1} \left(\mathbf{r}_c - \mathbf{S} \begin{bmatrix} \delta \mathcal{F}_M \\ \delta \mathcal{X}_M^C \end{bmatrix} \right) = 0 \\ \mathbf{C} \delta \mathbf{u}_m + \mathbf{r}_c - \mathbf{S} \begin{bmatrix} \delta \mathcal{F}_M \\ \delta \mathcal{X}_M^C \end{bmatrix} = 0 \quad \& \quad \mathbf{Q} = \mathbf{I} - \mathbf{C}^T (\mathbf{C} \mathbf{C}^T)^{-1} \mathbf{C} \end{array} \right.$$



- Multi-scale resolution

- System linearization

$$\begin{cases} \mathbf{Q}^T \frac{\partial \mathbf{f}_m}{\partial \mathbf{u}_m} \mathbf{Q} \delta \mathbf{u}_m + \mathbf{r} - \mathbf{Q}^T \frac{\partial \mathbf{f}_m}{\partial \mathbf{u}_m} \mathbf{C}^T (\mathbf{C} \mathbf{C}^T)^{-1} \left(\mathbf{r}_c - \mathbf{s} \begin{bmatrix} \delta \mathcal{F}_M \\ \delta \chi_M^c \end{bmatrix} \right) = 0 \\ \mathbf{C} \delta \mathbf{u}_m + \mathbf{r}_c - \mathbf{s} \begin{bmatrix} \delta \mathcal{F}_M \\ \delta \chi_M^c \end{bmatrix} = 0 \end{cases} \quad \& \quad \mathbf{Q} = \mathbf{I} - \mathbf{C}^T (\mathbf{C} \mathbf{C}^T)^{-1} \mathbf{C}$$

- FEM resolution: $\delta \mathcal{F}_M = \delta \chi_M^c = 0$

$$\delta \mathbf{u}_m = -\tilde{\mathbf{K}}^{-1} \left(\mathbf{r} + \left(\mathbf{C}^T - \mathbf{Q}^T \frac{\partial \mathbf{f}_m}{\partial \mathbf{u}_m} \mathbf{C}^T (\mathbf{C} \mathbf{C}^T)^{-1} \right) \mathbf{r}_c \right) \quad \rightarrow \quad \text{Only one matrix to factorize}$$

- Constraints effect: $\mathbf{r} = \mathbf{r}_c = 0$

$$\frac{\partial \mathbf{u}_m}{\partial [\mathcal{F}_M \quad \chi_M^c]^T} = \tilde{\mathbf{K}}^{-1} \left(\mathbf{C}^T - \mathbf{Q}^T \frac{\partial \mathbf{f}_m}{\partial \mathbf{u}_m} \mathbf{C}^T (\mathbf{C} \mathbf{C}^T)^{-1} \right) \mathbf{s} \quad \rightarrow \quad \tilde{\mathbf{K}} = \mathbf{C}^T \mathbf{C} + \mathbf{Q}^T \frac{\partial \mathbf{f}_m}{\partial \mathbf{u}_m} \mathbf{Q}$$

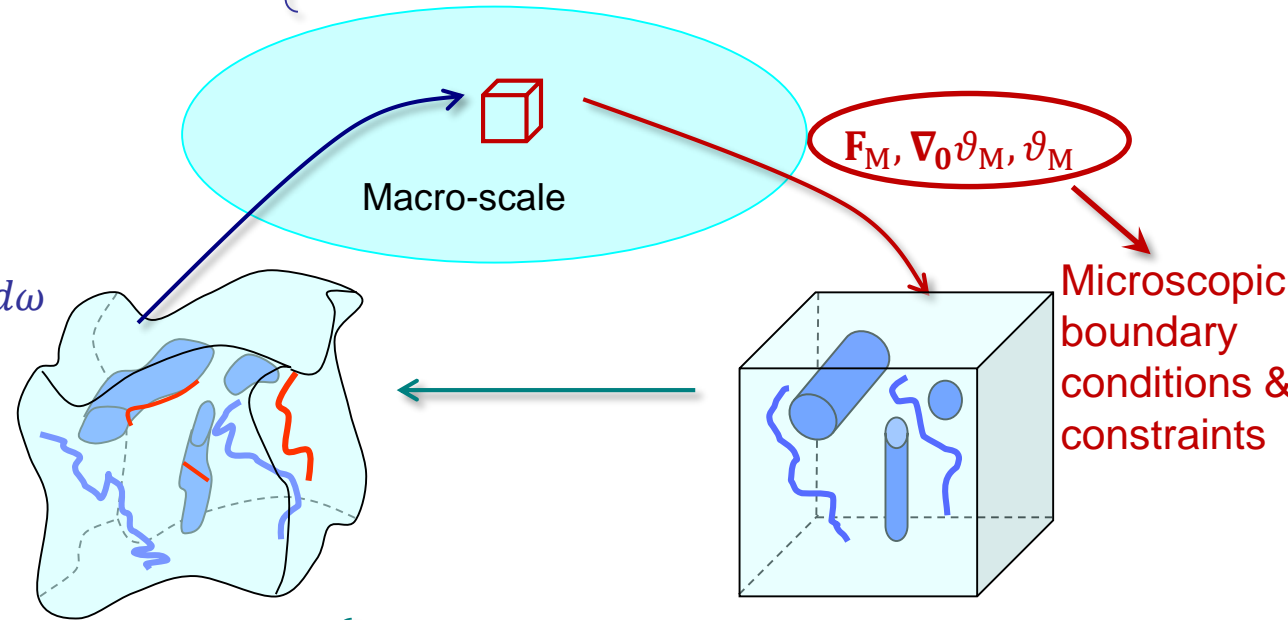
- Macro-scale operators at low cost

$$\begin{bmatrix} \frac{\partial \mathcal{P}_M}{\partial \mathcal{F}_M} & \frac{\partial \mathcal{P}_M}{\partial \chi_M^c} \\ \frac{\partial \mathcal{Z}_M}{\partial \mathcal{F}_M} & \frac{\partial \mathcal{Z}_M}{\partial \chi_M^c} \end{bmatrix} = \left(\bigwedge_{\omega^e} \frac{1}{V(\omega_0)} \int_{\omega_0^e} \begin{bmatrix} \frac{\partial \mathcal{P}_m}{\partial \mathcal{F}_m} \mathbf{B}^e & \frac{\partial \mathcal{P}_m}{\partial \chi_m^c} \mathbf{N}^e \\ \frac{\partial \mathcal{Z}_m}{\partial \mathcal{F}_m} \mathbf{B}^e & \frac{\partial \mathcal{Z}_m}{\partial \chi_m^c} \mathbf{N}^e \end{bmatrix} d\omega \right) \frac{\partial \mathbf{u}_m}{\partial [\mathcal{F}_M \quad \chi_M^c]^T}$$

- Thermo-elasto-plasticity

$$\left\{ \begin{aligned} \mathbf{P}_M &= \frac{1}{V(\omega_0)} \int_{\omega_0} \mathbf{P}_m d\omega \\ \mathbf{q}_M &= \frac{1}{V(\omega_0)} \int_{\omega_0} \mathbf{q}_m d\omega \\ \rho_M c_{vM} &= \frac{1}{V(\omega_0)} \int \rho_m c_{vm} d\omega \\ \mathcal{D}_M &= \frac{1}{V(\omega_0)} \int \mathcal{D}_m d\omega \\ &\& \\ \frac{\partial \mathbf{P}_M}{\partial \mathbf{F}_M}, \frac{\partial \mathbf{P}_M}{\partial \vartheta_M}, \frac{\partial \mathbf{P}_M}{\partial \nabla_0 \vartheta_M}, \\ \frac{\partial \mathbf{q}_M}{\partial \mathbf{F}_M}, \frac{\partial \mathbf{q}_M}{\partial \vartheta_M}, \frac{\partial \mathbf{q}_M}{\partial \nabla_0 \vartheta_M}, \\ \frac{\partial \mathcal{D}_M}{\partial \mathbf{F}_M}, \frac{\partial \mathcal{D}_M}{\partial \vartheta_M}, \frac{\partial \mathcal{D}_M}{\partial \nabla_0 \vartheta_M} \end{aligned} \right.$$

$$\left\{ \begin{aligned} \mathbf{P}_M \cdot \nabla_0 &= 0 \\ \rho_M c_{vM} \dot{\vartheta}_M - \mathcal{D}_M + \mathbf{q}_M \cdot \nabla_0 &= 0 \end{aligned} \right.$$



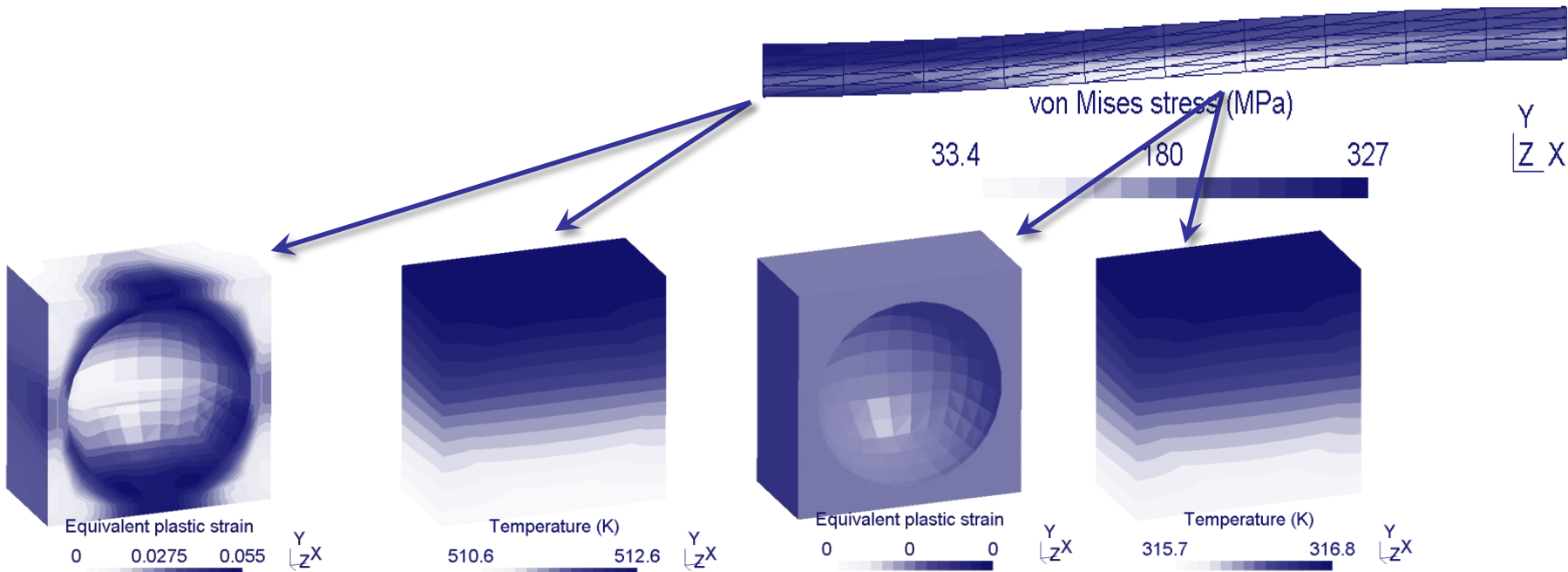
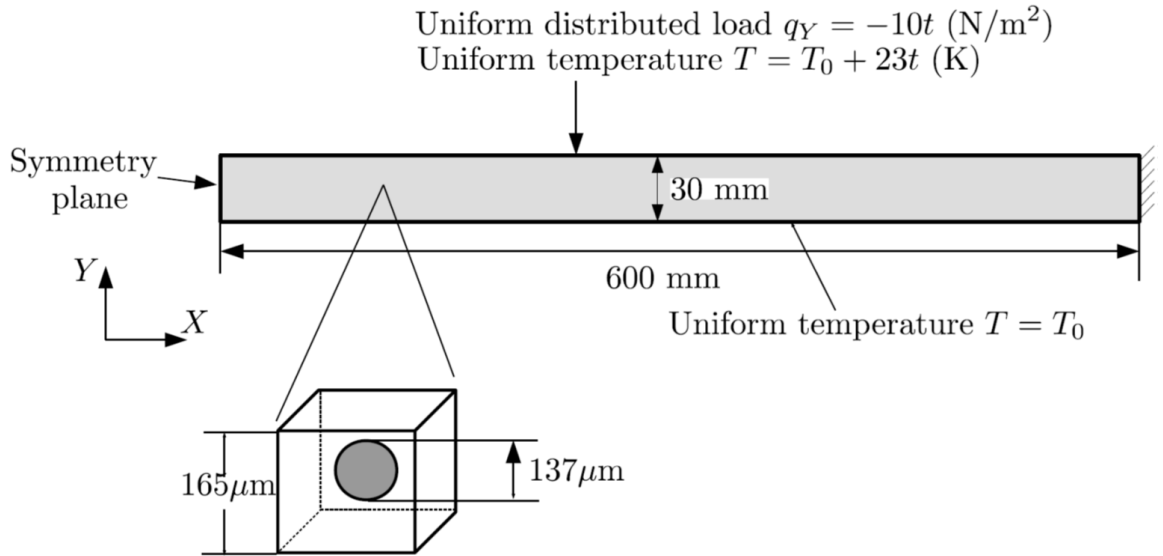
$$\left\{ \begin{aligned} \mathbf{P}_m &= \mathbf{P}_m(\mathbf{F}_m, \nabla_0 \vartheta_m, \vartheta_m; p, \mathbf{F}_m^p) \\ \mathbf{q}_m &= \mathbf{q}_m(\mathbf{F}_m, \nabla_0 \vartheta_m, \vartheta_m; p, \mathbf{F}_m^p) \\ \mathcal{D}_m &= \beta \dot{p} \tau + \vartheta \frac{\partial \dot{W}^{el}}{\partial \vartheta} \\ \mathbf{P}_m \cdot \nabla_0 &= 0 \\ \mathbf{q}_m \cdot \nabla_0 &= 0 \end{aligned} \right.$$

Boundary conditions and tangent operator in FE²

- Thermo-elasto-plasticity

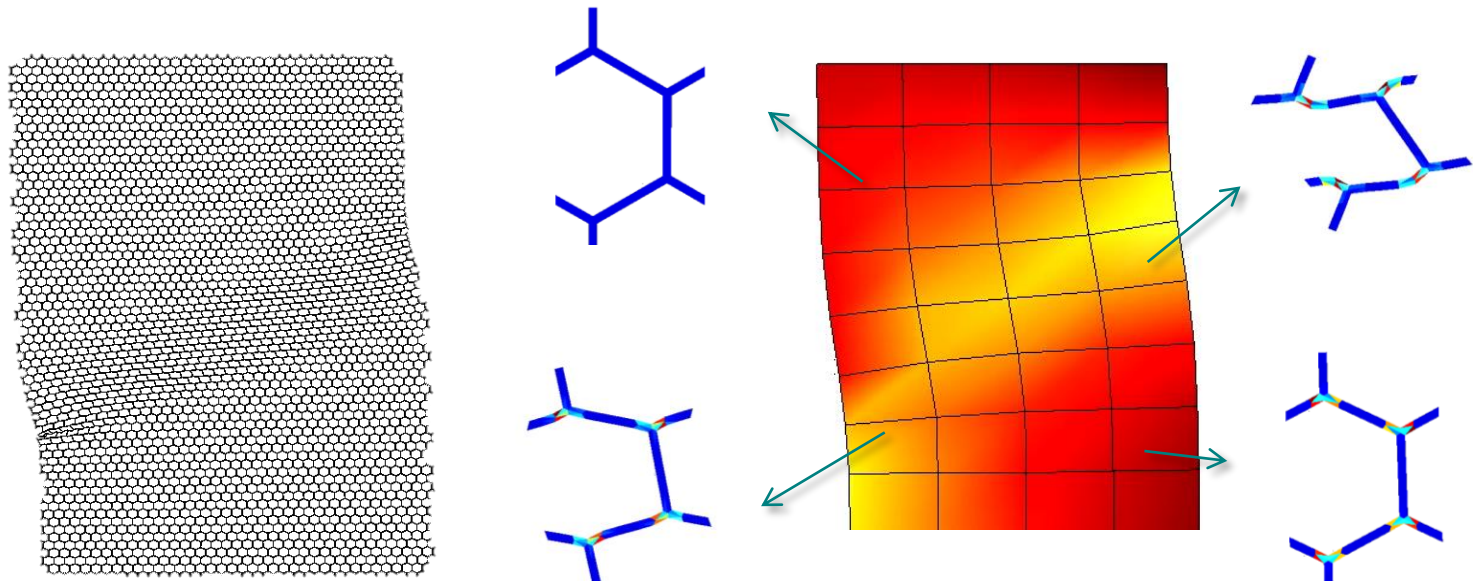
- Thermal-softening hardening

$$\tau = (\sigma_0 + Hp) (1 - \omega_T(T - T_0))$$



Boundary conditions and tangent operator in FE²

- BRIDGING ARC project (Periodic boundary conditions)
 - ULiège, Applied Sciences (A&M, EEI, ICD)
 - ULiège, Sciences (CERM)
- PDR T.1015.14 project (MFH with second-order moments)
 - ULiège, UCL (Belgium)
- Publications
 - [10.1007/s00466-016-1358-z](https://doi.org/10.1007/s00466-016-1358-z)
 - [10.1016/j.commatsci.2011.10.017](https://doi.org/10.1016/j.commatsci.2011.10.017)



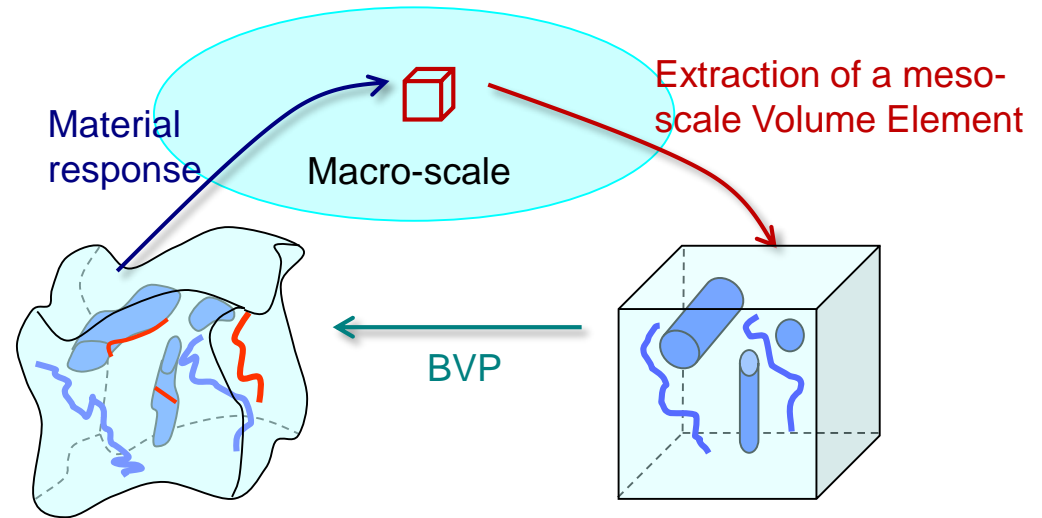
Computational Homogenization For Cellular Materials

ARC 09/14-02 BRIDGING - From imaging to geometrical modelling of complex micro structured materials: Bridging computational engineering and material science

Computational Homogenization For Cellular Materials

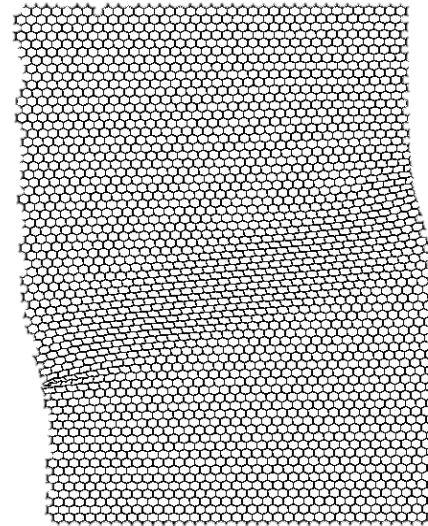
- Multi-scale modeling

- 2 problems are solved concurrently
 - The macro-scale problem
 - The meso-scale problem (on a meso-scale Volume Element)



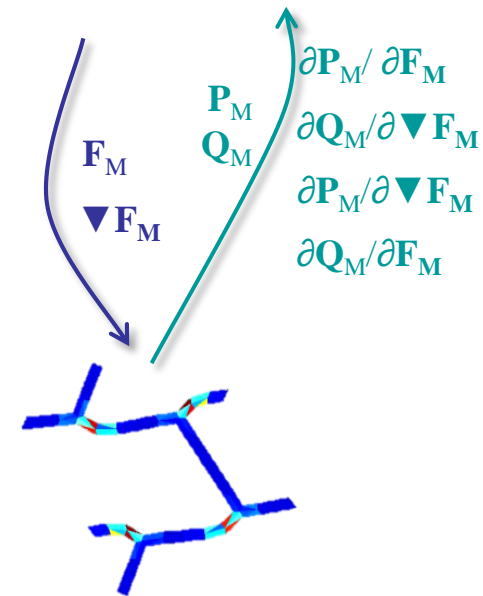
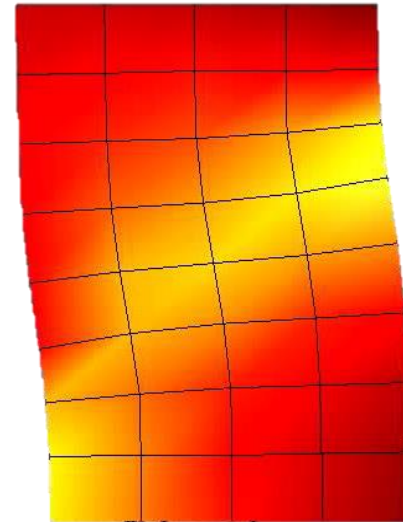
- What if homogenized properties loose ellipticity?

- Buckling of honeycomb structures



Computational Homogenization For Cellular Materials

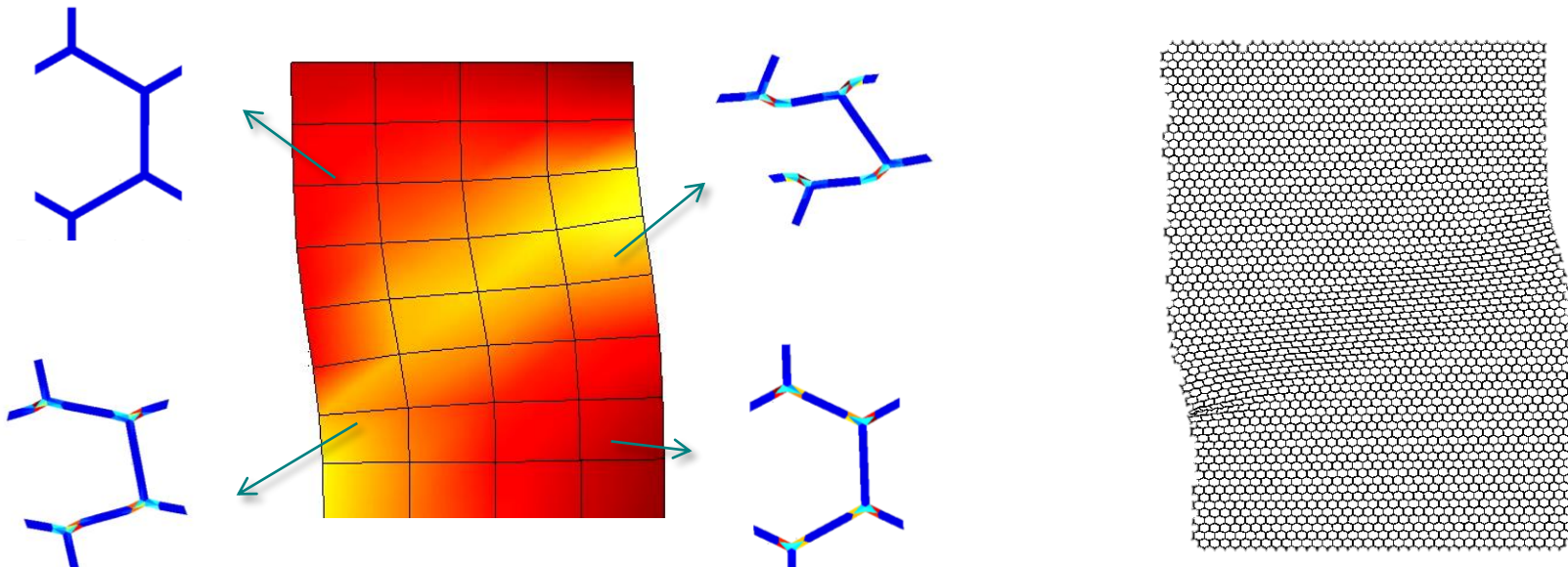
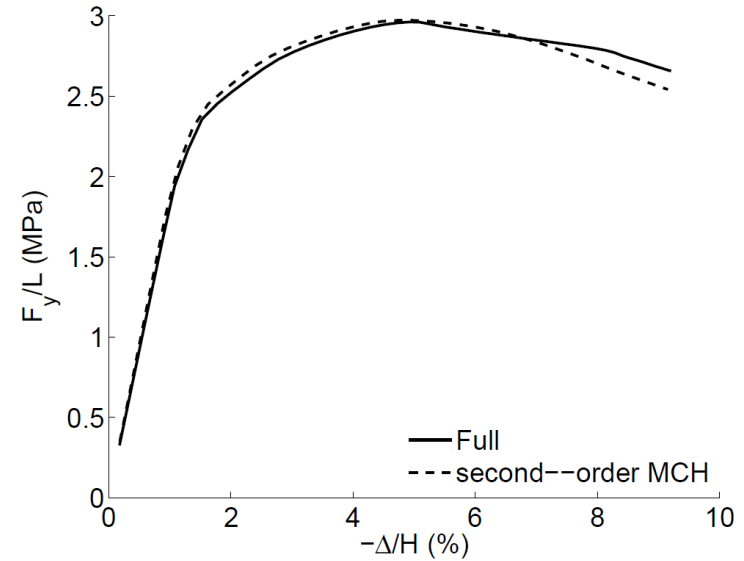
- DG-based second-order FE²
 - Macro-scale
 - High-order Strain-Gradient formulation
 - C¹ weakly enforced by DG
 - Partitioned mesh (//)
 - Transition
 - Gauss points on different processors
 - Each Gauss point is associated to one mesh and one solver
 - Micro-scale
 - Usual 3D finite elements
 - High-order periodic boundary conditions
 - Non-conforming mesh
 - Use of interpolant functions



Computational Homogenization For Cellular Materials

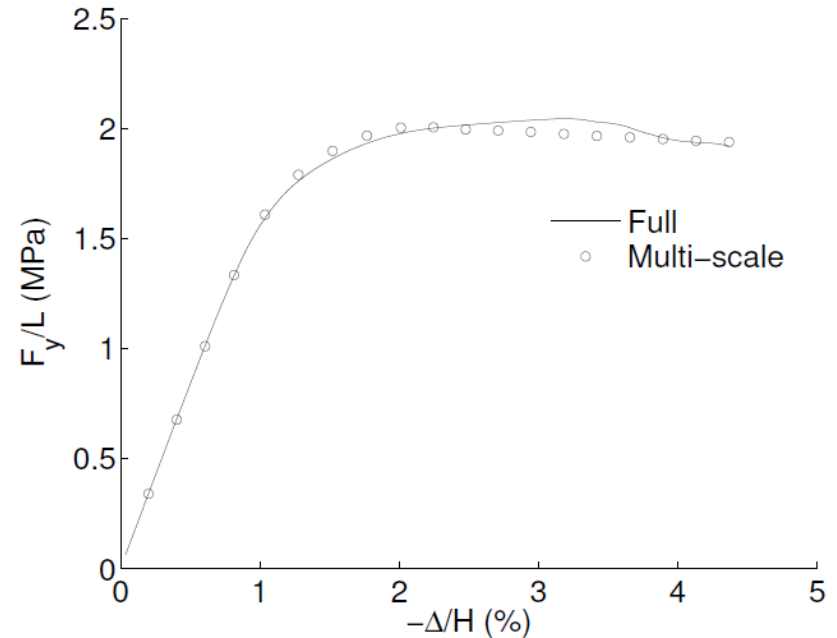
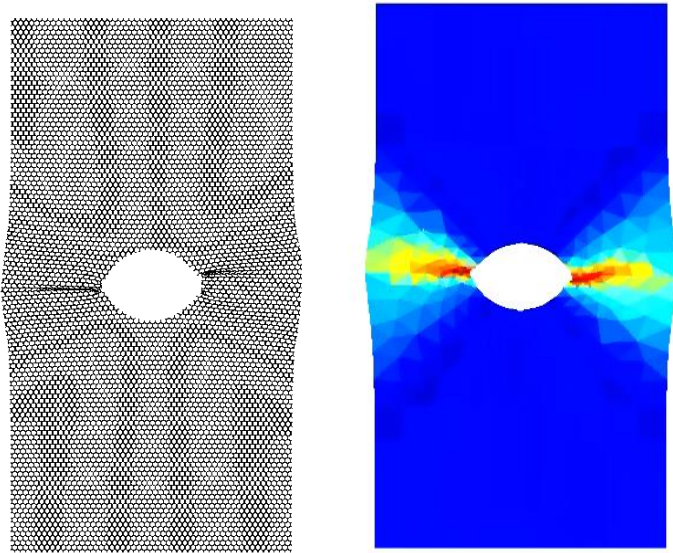
- Instabilities

- Micro-scale: buckling
- Macro-scale: localization bands
- Captured owing to
 - Second-order homogenization
 - Ad-hoc periodic boundary conditions
 - Path following method



Computational Homogenization For Cellular Materials

- Open-hole plate

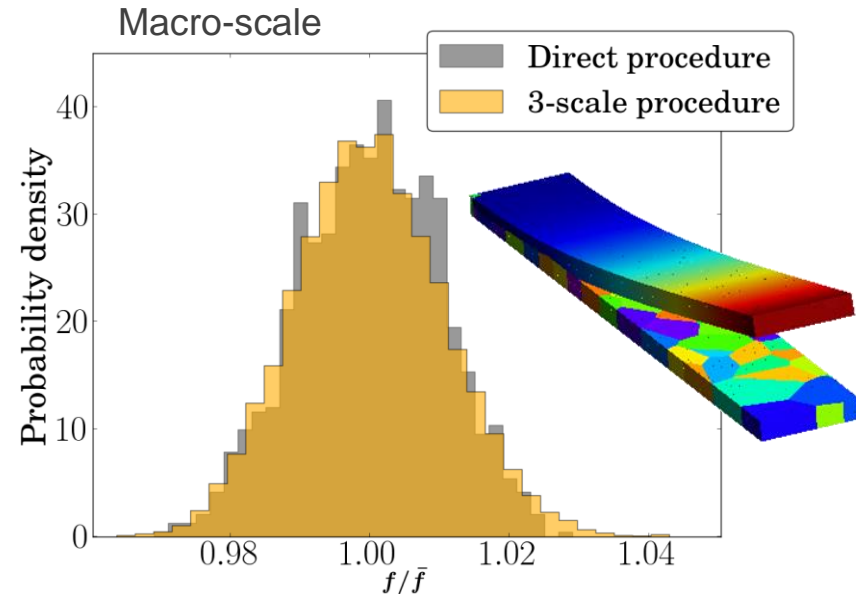
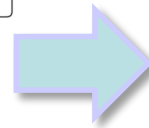
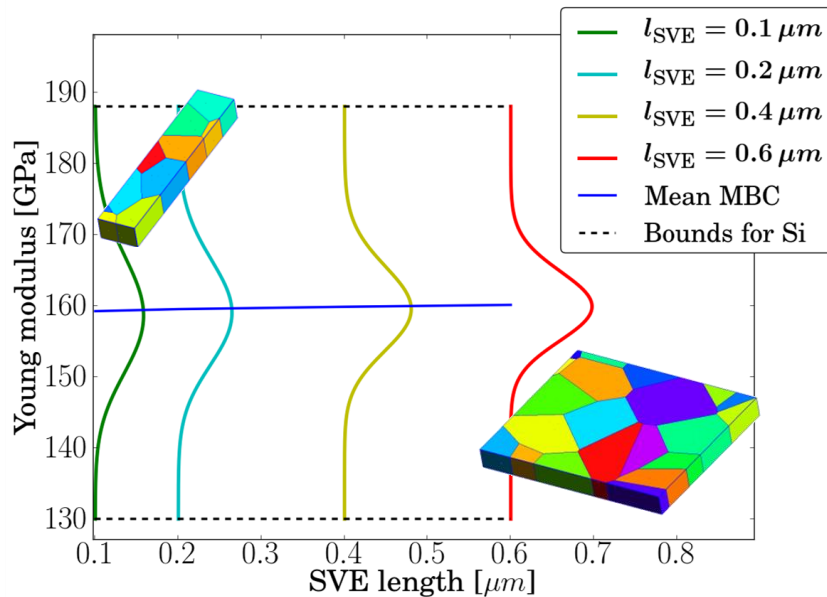


- BRIDGING ARC project

- ULiège, Applied Sciences (A&M, EEI, ICD)
- ULiège, Sciences (CERM)

- Publications

- [10.1016/j.mechmat.2015.07.004](https://doi.org/10.1016/j.mechmat.2015.07.004)
- [10.1016/j.ijsolstr.2014.02.029](https://doi.org/10.1016/j.ijsolstr.2014.02.029)
- [10.1016/j.cma.2013.03.024](https://doi.org/10.1016/j.cma.2013.03.024)



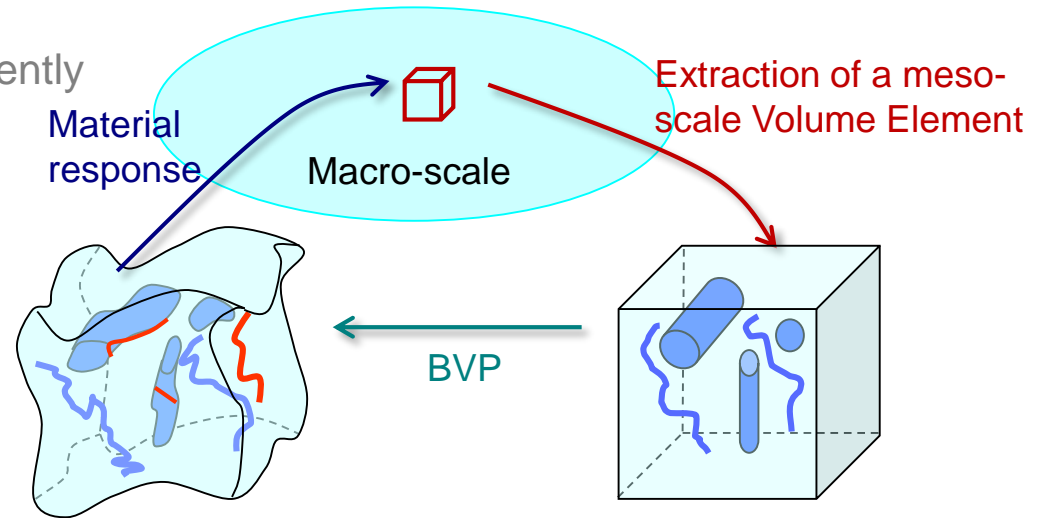
Stochastic 3-Scale Models for Polycrystalline Materials

3SMVIB: The research has been funded by the Walloon Region under the agreement no 1117477 (CT-INT 2011-11-14) in the context of the ERA-NET MNT framework.

Stochastic 3-Scale Models

- Multi-scale modeling

- 2 problems are solved concurrently
 - The macro-scale problem
 - The meso-scale problem (on a meso-scale Volume Element)



- For structures not several orders larger than the micro-structure size

$$L_{\text{macro}} \gg L_{\text{VE}} \sim L_{\text{micro}}$$

For accuracy: Size of the meso-scale volume element smaller than the characteristic length of the macro-scale loading

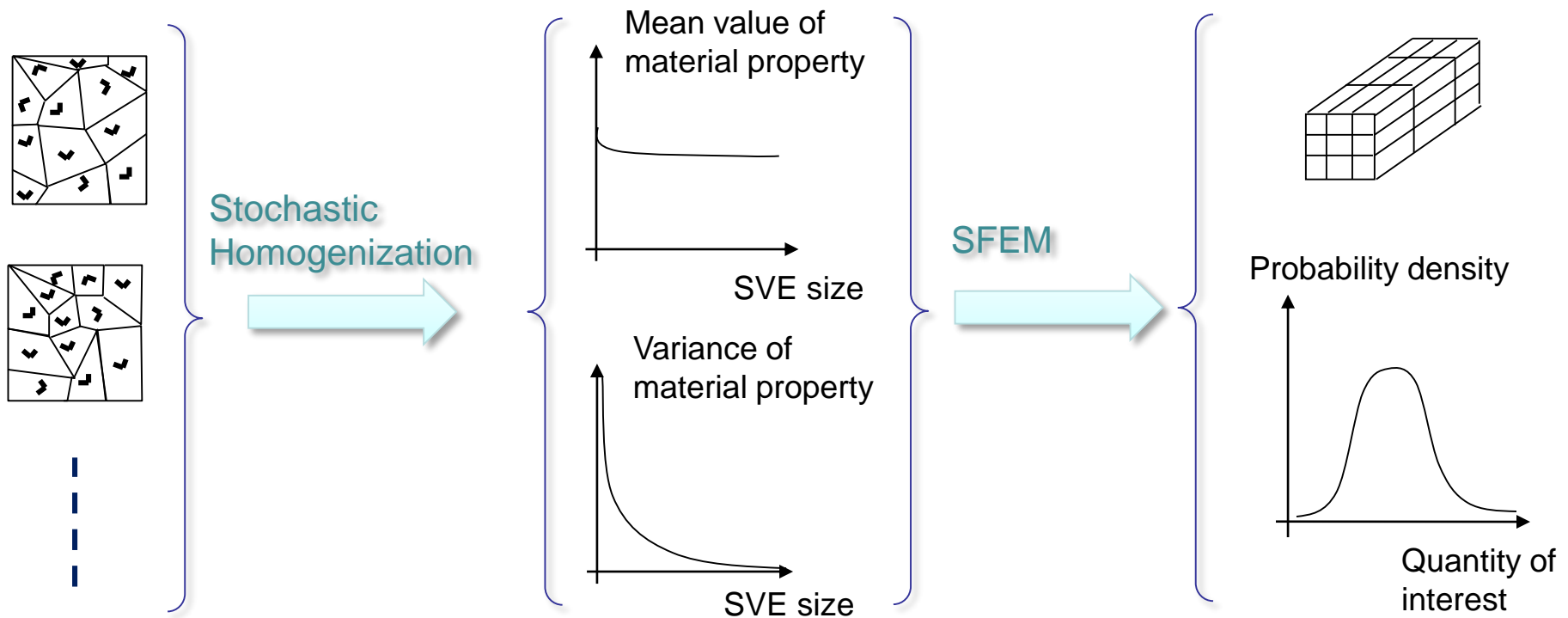
Meso-scale volume element no longer statistically representative:

- Stochastic Volume Elements

Stochastic 3-Scale Models

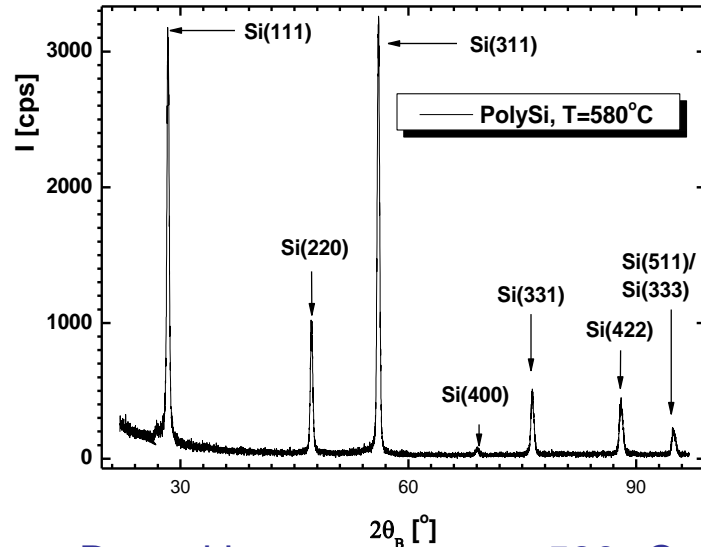
- Key idea

Micro-scale	Meso-scale	Macro-scale
<ul style="list-style-type: none"> ➤ Samples of stochastic volume elements ➤ Random microstructure 	<ul style="list-style-type: none"> ➤ Intermediate scale ➤ The distribution of the material property $\mathbb{P}(\mathcal{C})$ is defined 	<ul style="list-style-type: none"> ➤ Uncertainty quantification of the macro-scale quantity ➤ Quantity of interest distribution $\mathbb{P}(Q)$

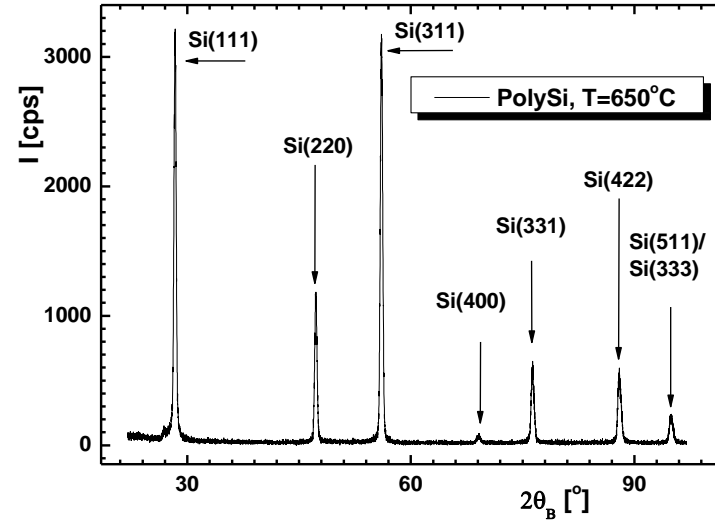


Stochastic 3-Scale Models

- Material structure: grain orientation distribution
 - Grain orientation by XRD (X-ray Diffraction) measurements on 2 μm -thick poly-silicon films



Deposition temperature: 580 °C



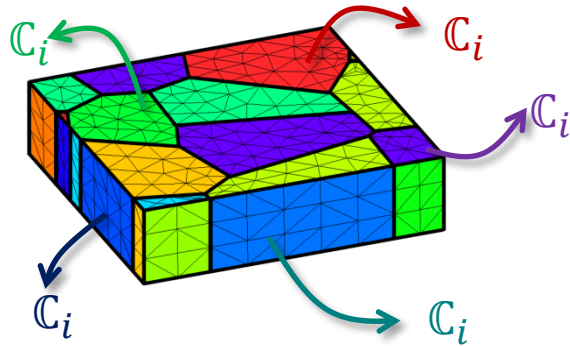
Deposition temperature: 630 °C

Deposition temperature [°C]	580	610	630	650
$\langle 111 \rangle$ [%]	12.57	19.96	12.88	11.72
$\langle 220 \rangle$ [%]	7.19	13.67	7.96	7.59
$\langle 311 \rangle$ [%]	42.83	28.83	39.08	38.47
$\langle 400 \rangle$ [%]	4.28	5.54	3.13	3.93
$\langle 331 \rangle$ [%]	17.97	18.14	21.32	20.45
$\langle 422 \rangle$ [%]	15.15	13.86	15.63	17.84

XRD images provided by IMT Bucharest, Rodica Voicu, Angela Baracu, Raluca Muller

Stochastic 3-Scale Models

- Application to polycrystalline materials: The micro-scale to meso-scale transition
 - Stochastic homogenization



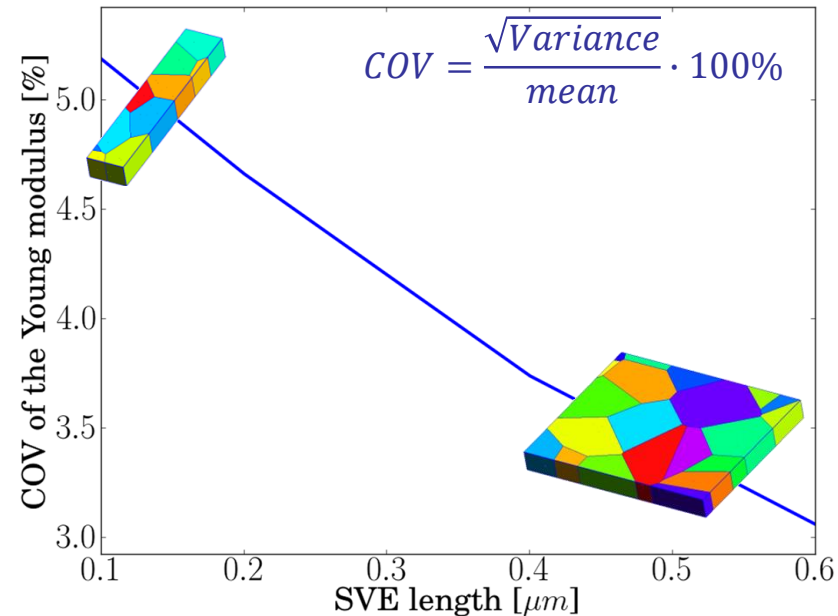
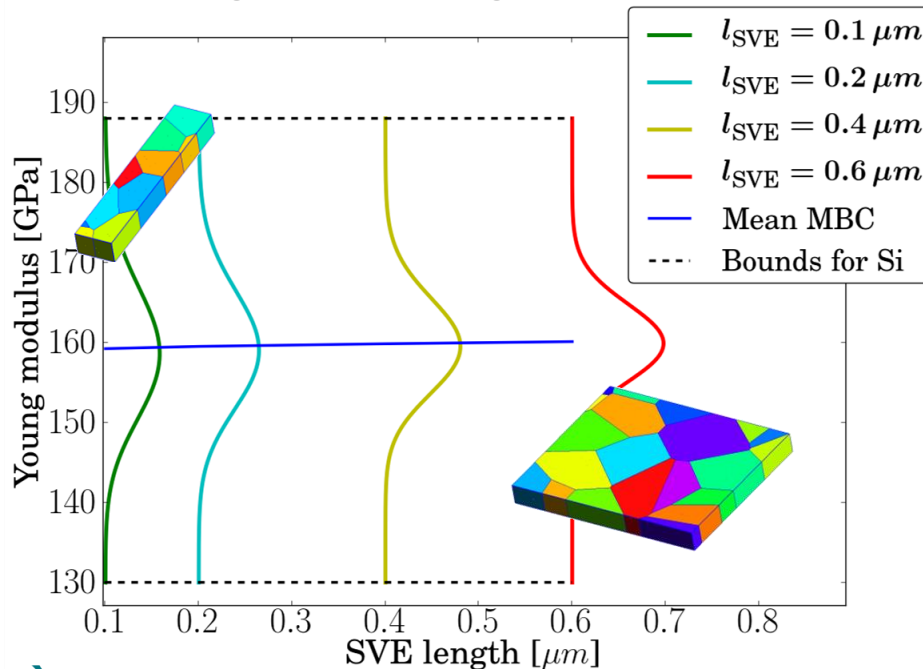
$$\sigma_{mi} = \mathbb{C}_i : \epsilon_{mi} \quad , \forall i$$

Stochastic Homogenization

$$\sigma_M = \mathbb{C}_M : \epsilon_M$$

Samples of the meso-scale homogenized elasticity tensors

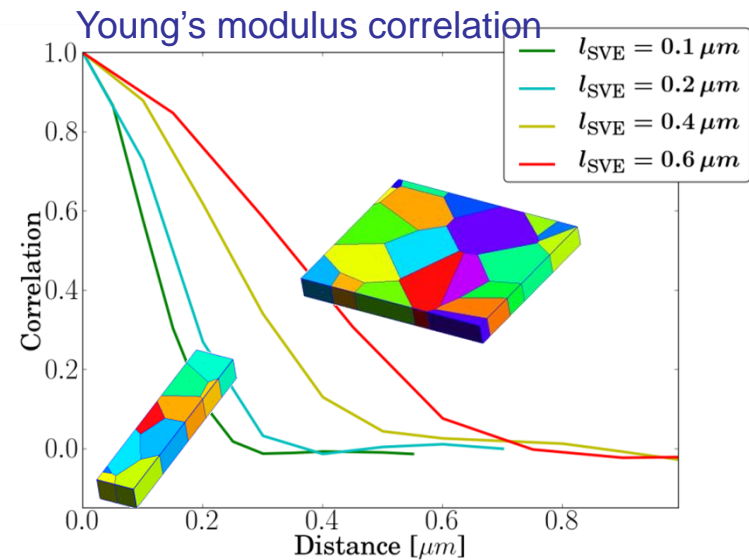
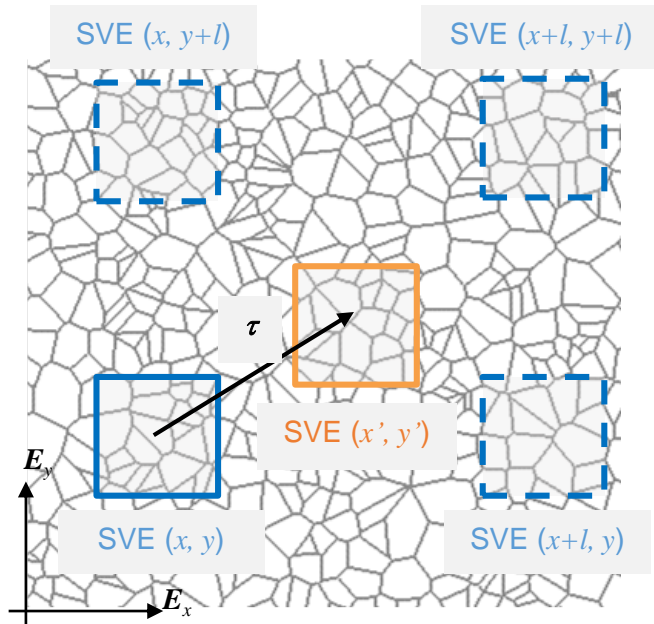
- Homogenized Young's modulus distribution



Stochastic 3-Scale Models

- Application to polycrystalline materials: The meso-scale spatial correlation
 - Use of the window technique

$$R_{\mathbb{C}}^{(rs)}(\boldsymbol{\tau}) = \frac{\mathbb{E} \left[\left(\mathbb{C}^{(r)}(\mathbf{x}) - \mathbb{E}(\mathbb{C}^{(r)}) \right) \left(\mathbb{C}^{(s)}(\mathbf{x} + \boldsymbol{\tau}) - \mathbb{E}(\mathbb{C}^{(s)}) \right) \right]}{\sqrt{\mathbb{E} \left[\left(\mathbb{C}^{(r)} - \mathbb{E}(\mathbb{C}^{(r)}) \right)^2 \right] \mathbb{E} \left[\left(\mathbb{C}^{(s)} - \mathbb{E}(\mathbb{C}^{(s)}) \right)^2 \right]}}$$

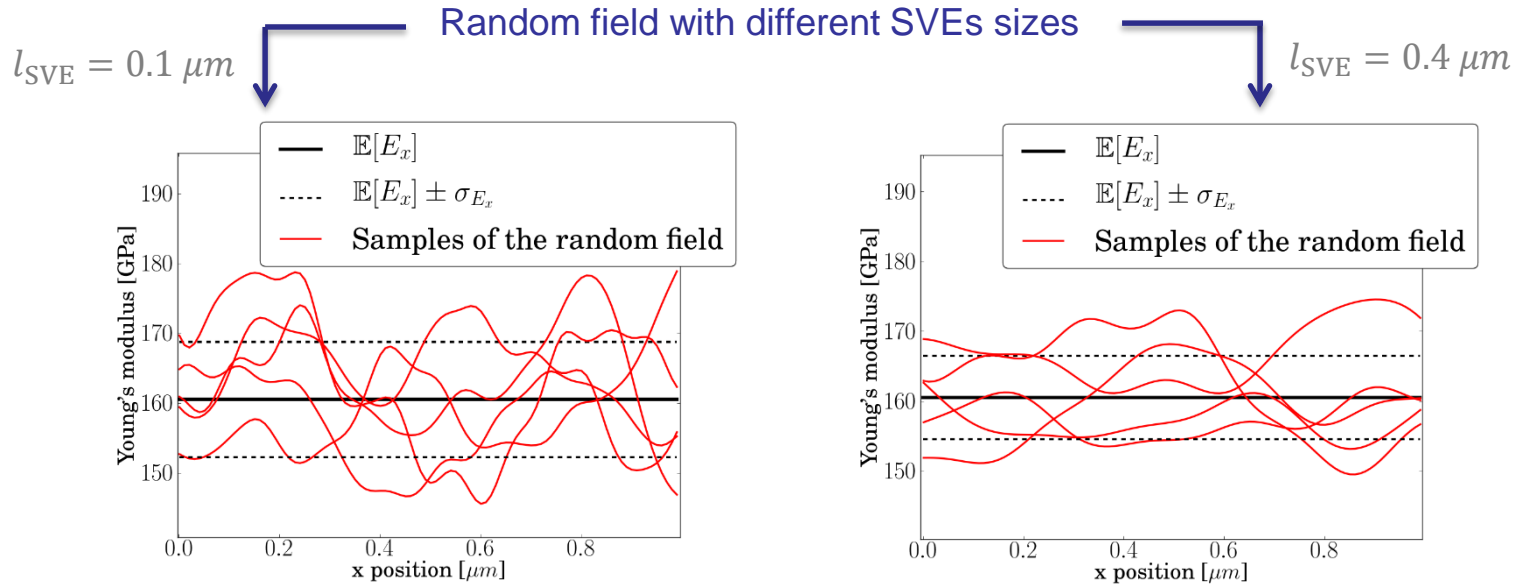


- Definition of the correlation length

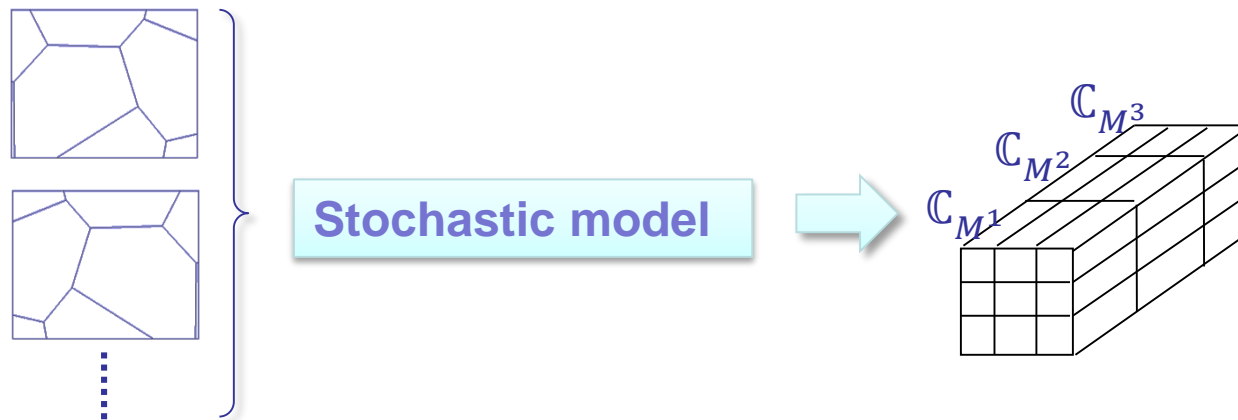
$$L_{\mathbb{C}}^{(rs)} = \frac{\int_{-\infty}^{\infty} R_{\mathbb{C}}^{(rs)}(\boldsymbol{\tau}) d\boldsymbol{\tau}}{R_{\mathbb{C}}^{(rs)}(0)}$$

Stochastic 3-Scale Models

- Application to polycrystalline materials: The meso-scale random field
 - Accounts for the meso-scale distribution & spatial correlation



- Needs to be generated using a stochastic model



- Stochastic model of Gaussian meso-scale random fields

- Define the homogenous zero-mean random field $\mathcal{A}'(x, \theta)$

- Elasticity tensor $\mathbb{C}_M(x, \theta)$ (matrix form \mathbf{C}_M) is bounded

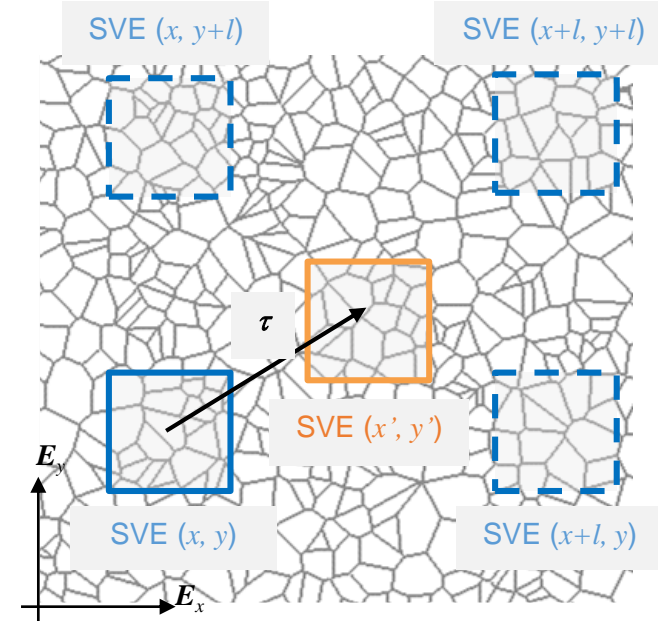
$$\boldsymbol{\varepsilon}: (\mathbb{C}_M - \mathbb{C}_L): \boldsymbol{\varepsilon} > 0 \quad \forall \boldsymbol{\varepsilon}$$

- Use a Cholesky decomposition

$$\mathbf{C}_M(x, \theta) = \mathbf{C}_L + (\bar{\mathcal{A}} + \mathcal{A}'(x, \theta))^T (\bar{\mathcal{A}} + \mathcal{A}'(x, \theta))$$

- Evaluate the covariance function

$$\begin{aligned} \tilde{R}_{\mathcal{A}'}^{(rs)}(\boldsymbol{\tau}) &= \sigma_{\mathcal{A}'(r)} \sigma_{\mathcal{A}'(s)} R_{\mathcal{A}'}^{(rs)}(\boldsymbol{\tau}) \\ &= \mathbb{E} \left[\left(\mathcal{A}'^{(r)}(x) \right) \left(\mathcal{A}'^{(s)}(x + \boldsymbol{\tau}) \right) \right] \end{aligned}$$



- Evaluate the spectral density matrix from periodized zero-padded matrix $\tilde{R}_{\mathcal{A}'}^P(\boldsymbol{\tau})$

$$\mathcal{S}_{\mathcal{A}'}^{(rs)}[\boldsymbol{\omega}^{(m)}] = \sum_n \tilde{R}_{\mathcal{A}'}^P{}^{(rs)}[\boldsymbol{\tau}^{(n)}] e^{-2\pi i \boldsymbol{\tau}^{(n)} \cdot \boldsymbol{\omega}^{(m)}} \quad \& \quad \mathcal{S}_{\mathcal{A}'}[\boldsymbol{\omega}^{(m)}] = \mathbf{H}_{\mathcal{A}'}[\boldsymbol{\omega}^{(m)}] \mathbf{H}_{\mathcal{A}'}^*[\boldsymbol{\omega}^{(m)}]$$

- Generate a Gaussian random field $\mathcal{A}'(x, \theta)$

$$\mathcal{A}'^{(r)}(x, \theta) = \sqrt{2\Delta\omega} \Re \left(\sum_s \sum_m \mathbf{H}_{\mathcal{A}'}^{(rs)}[\boldsymbol{\omega}^{(m)}] \eta^{(s,m)} e^{2\pi i (x \cdot \boldsymbol{\omega}^{(m)} + \theta^{(s,m)})} \right)$$

Stochastic 3-Scale Models

- Stochastic model of non-Gaussian meso-scale random fields

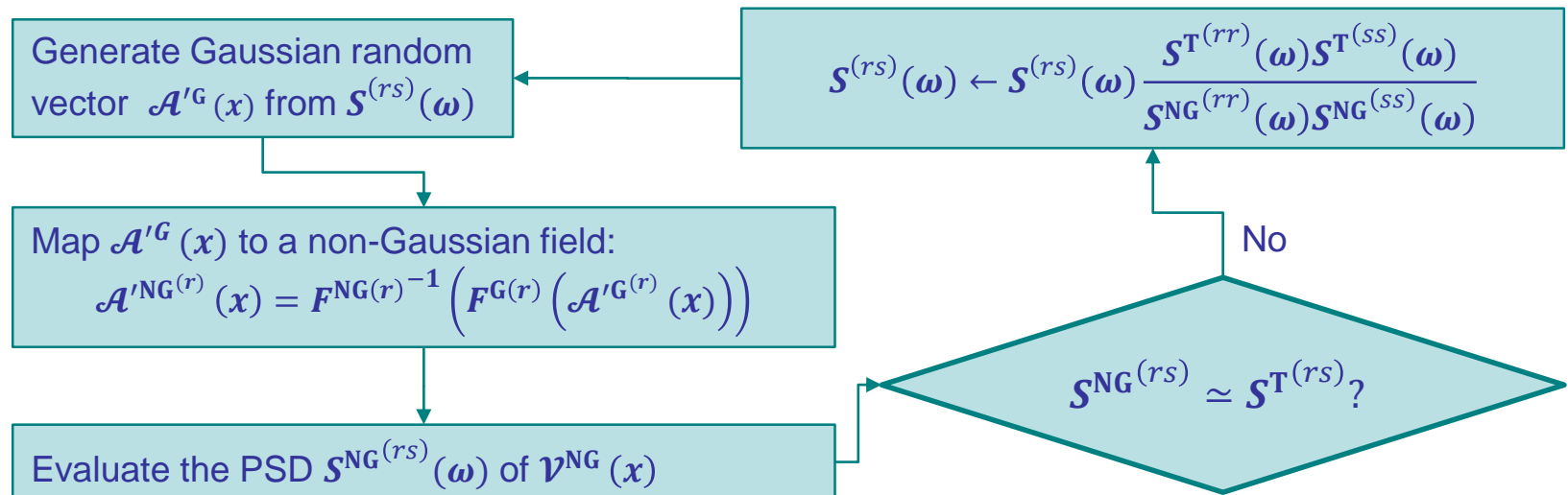
- Start from micro-sampling of the stochastic homogenization

- The continuous form of the targeted PSD function

$$\mathcal{S}^{\text{T}(rs)}(\omega) = \Delta\tau \mathcal{S}_{\mathcal{V}'}^{(rs)}[\omega^{(m)}] = \Delta\tau \sum_n \tilde{R}_{\mathcal{A}'}^{\text{P}(rs)}[\tau^{(n)}] e^{-2\pi i \tau^{(n)} \cdot \omega^{(m)}}$$

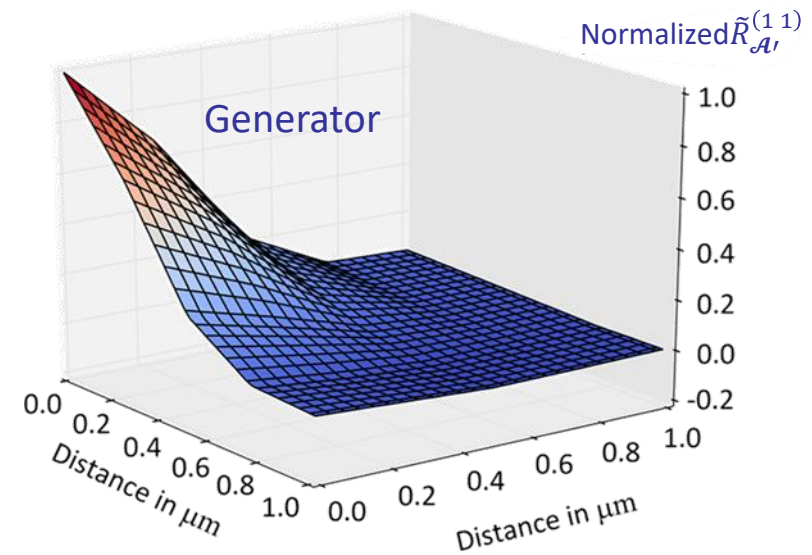
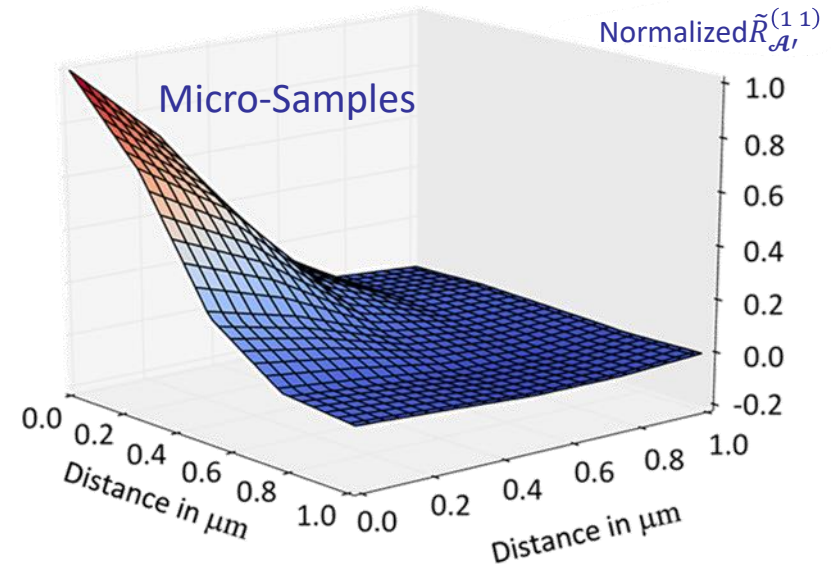
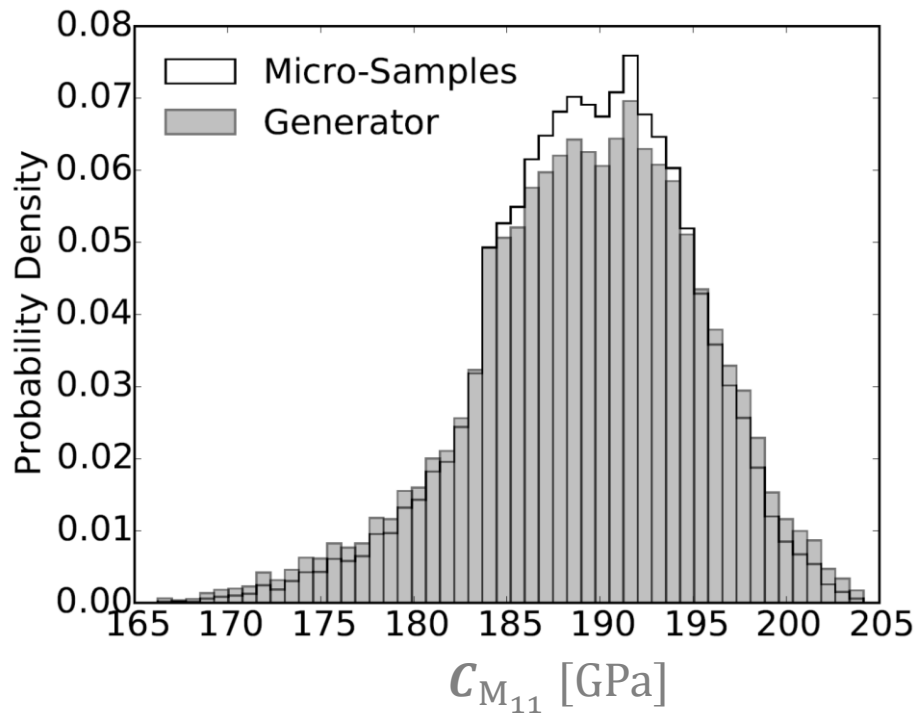
- The targeted marginal distribution density function $F^{\text{NG}(r)}$ of the random variable $\mathcal{A}'^{(r)}$
- A marginal Gaussian distribution $F^{\text{G}(r)}$ of zero-mean and targeted variance $\sigma_{\mathcal{A}'^{(r)}}$

- Iterate



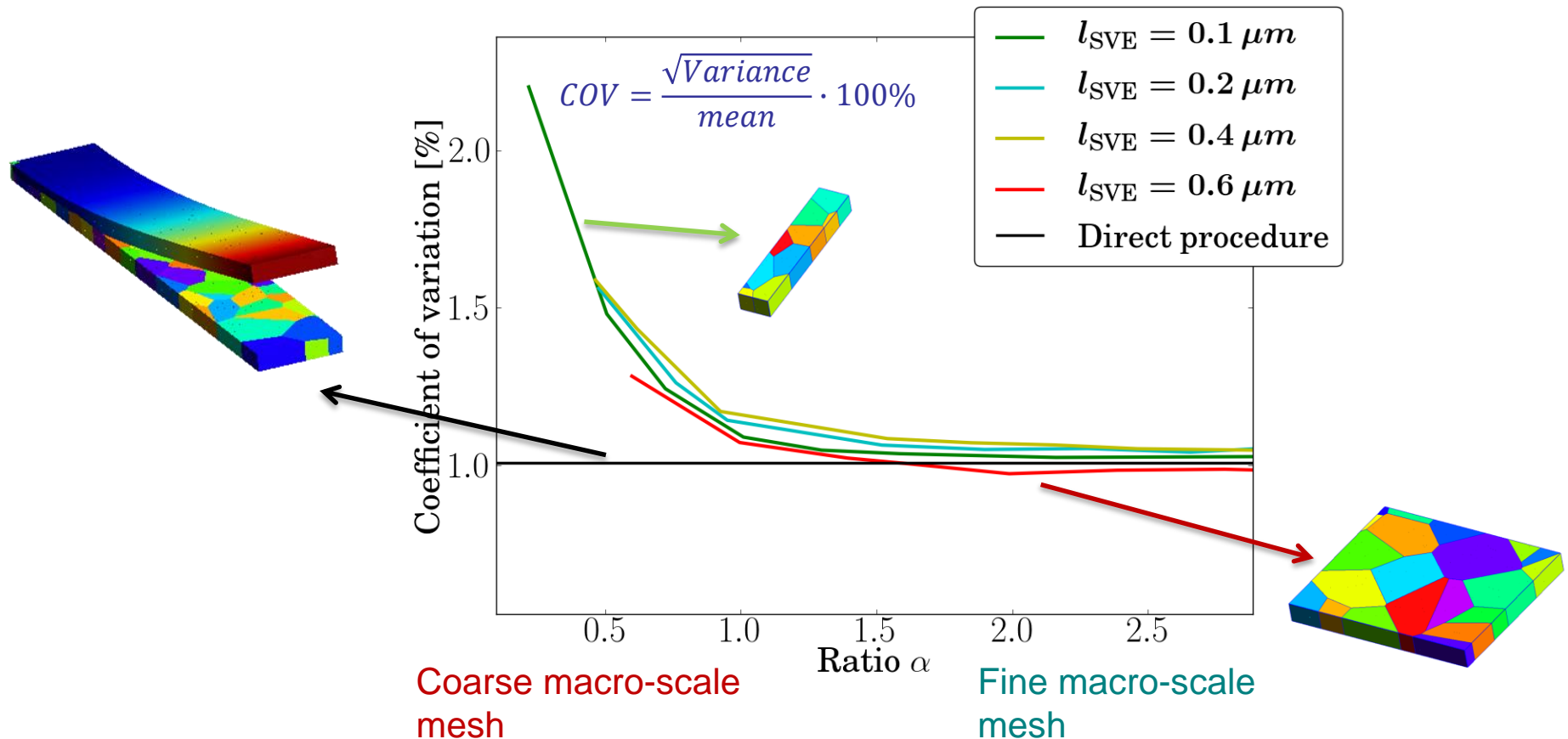
Stochastic 3-Scale Models

- The meso-scale stochastic model
 - Application to film deposited at 610 °C:
 - Comparison between micro-samples and generated fields



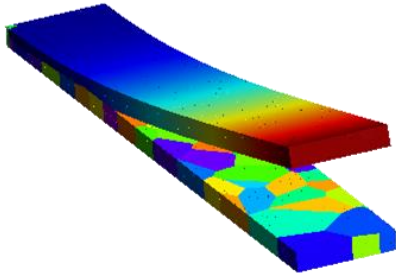
Stochastic 3-Scale Models

- Application to polycrystalline materials: The meso-scale to macro-scale transition
 - Convergence in terms of $\alpha = \frac{l_c}{l_{\text{mesh}}}$, the correlation length and macro-mesh ratio
 - The results converge
 - With the mesh size for all the SVE sizes
 - Toward the direct Monte Carlo simulations results

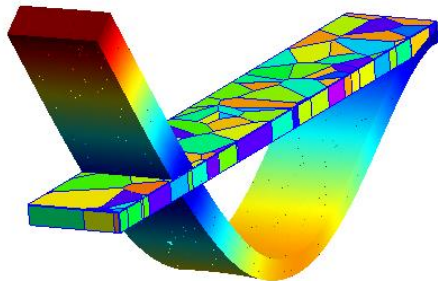


Stochastic 3-Scale Models

- Application to polycrystalline materials: The meso-scale to macro-scale transition
 - Comparison with direct Monte Carlo simulations

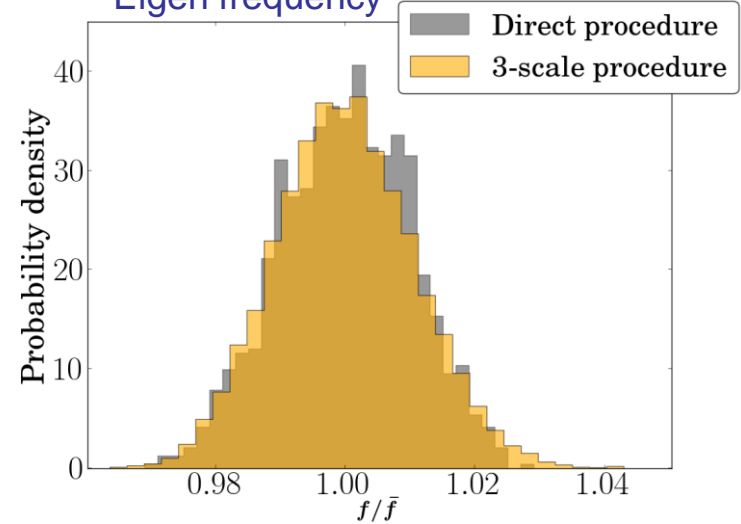


Relative difference
in the mean: 0.57 %

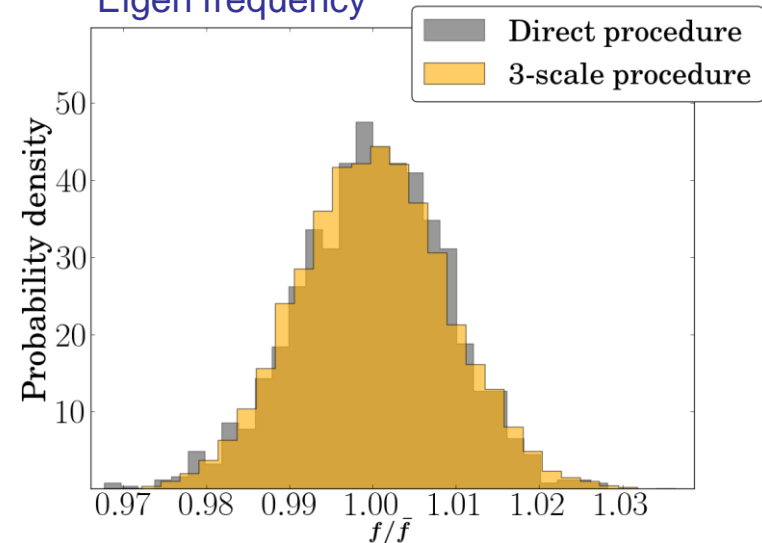


Relative difference
in the mean: 0.44 %

Eigen frequency



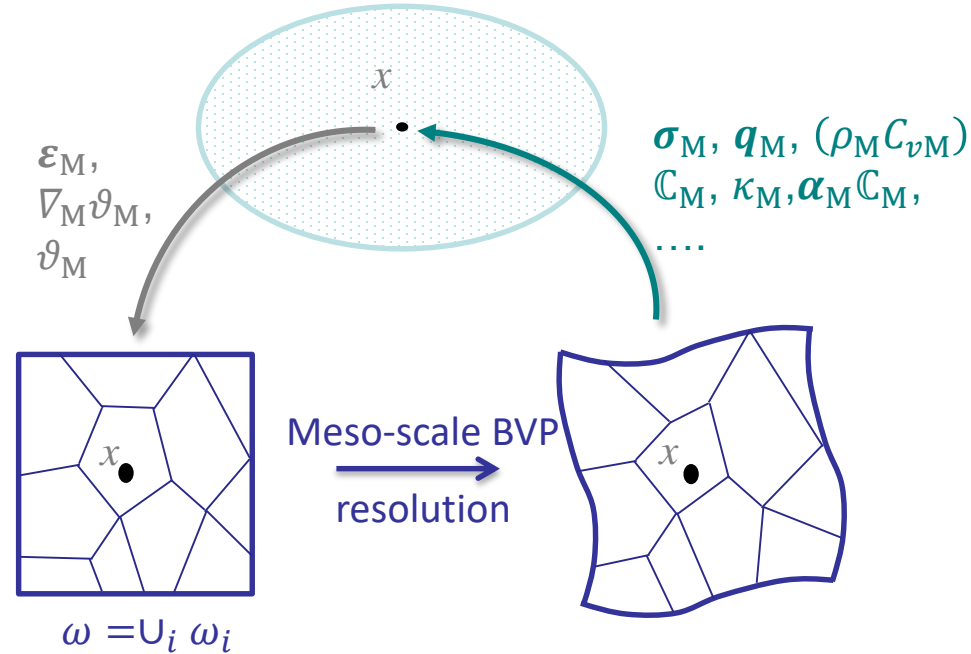
Eigen frequency



- Thermo-mechanical homogenization

- Down-scaling

$$\left\{ \begin{aligned} \varepsilon_M &= \frac{1}{V(\omega)} \int_{\omega} \varepsilon_m d\omega \\ \nabla_M \vartheta_M &= \frac{1}{V(\omega)} \int_{\omega} \nabla_m \vartheta_m d\omega \\ \vartheta_M &= \frac{1}{V(\omega)} \int_{\omega} \frac{\rho_m C_{vm}}{\rho_M C_{vM}} \vartheta_m d\omega \end{aligned} \right.$$



- Up-scaling

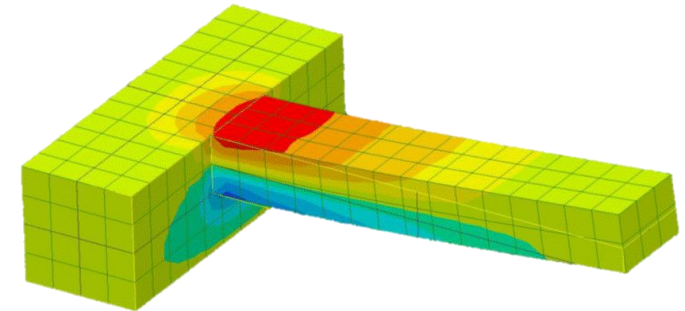
$$\left\{ \begin{aligned} \sigma_M &= \frac{1}{V(\omega)} \int_{\omega} \sigma_m d\omega \\ \mathbf{q}_M &= \frac{1}{V(\omega)} \int_{\omega} \mathbf{q}_m d\omega \\ \rho_M C_{vM} &= \frac{1}{V(\omega)} \int_{\omega} \rho_m C_{vm} dV \end{aligned} \right. \longrightarrow \left\{ \begin{aligned} \mathbb{C}_M &= \frac{\partial \sigma_M}{\partial \mathbf{u}_M \otimes \nabla_M} & \& \quad \alpha_M : \mathbb{C}_M = -\frac{\partial \sigma_M}{\partial \vartheta_M} \\ \kappa_M &= -\frac{\partial \mathbf{q}_M}{\partial \nabla_M \vartheta_M} \end{aligned} \right.$$

- Consistency \longrightarrow Satisfied by periodic boundary conditions

- Quality factor

- Micro-resonators

- Temperature changes with compression/traction
 - Energy dissipation



- Eigen values problem

- Governing equations

$$\begin{bmatrix} \mathbf{M} & \mathbf{0} \\ \mathbf{0} & \mathbf{0} \end{bmatrix} \begin{bmatrix} \ddot{\mathbf{u}} \\ \ddot{\boldsymbol{\vartheta}} \end{bmatrix} + \begin{bmatrix} \mathbf{0} & \mathbf{0} \\ \mathbf{D}_{u\boldsymbol{\vartheta}}(\boldsymbol{\theta}) & \mathbf{D}_{\boldsymbol{\vartheta}\boldsymbol{\vartheta}} \end{bmatrix} \begin{bmatrix} \dot{\mathbf{u}} \\ \dot{\boldsymbol{\vartheta}} \end{bmatrix} + \begin{bmatrix} \mathbf{K}_{uu}(\boldsymbol{\theta}) & \mathbf{K}_{u\boldsymbol{\vartheta}}(\boldsymbol{\theta}) \\ \mathbf{0} & \mathbf{K}_{\boldsymbol{\vartheta}\boldsymbol{\vartheta}}(\boldsymbol{\theta}) \end{bmatrix} \begin{bmatrix} \mathbf{u} \\ \boldsymbol{\vartheta} \end{bmatrix} = \begin{bmatrix} \mathbf{F}_u \\ \mathbf{F}_{\boldsymbol{\vartheta}} \end{bmatrix}$$

- Free vibrating problem

$$\begin{bmatrix} \mathbf{u}(t) \\ \boldsymbol{\vartheta}(t) \end{bmatrix} = \begin{bmatrix} \mathbf{u}_0 \\ \boldsymbol{\vartheta}_0 \end{bmatrix} e^{i\omega t}$$

$$\hookrightarrow \begin{bmatrix} -\mathbf{K}_{uu}(\boldsymbol{\theta}) & -\mathbf{K}_{u\boldsymbol{\vartheta}}(\boldsymbol{\theta}) & \mathbf{0} \\ \mathbf{0} & -\mathbf{K}_{\boldsymbol{\vartheta}\boldsymbol{\vartheta}}(\boldsymbol{\theta}) & \mathbf{0} \\ \mathbf{0} & \mathbf{0} & \mathbf{I} \end{bmatrix} \begin{bmatrix} \mathbf{u} \\ \boldsymbol{\vartheta} \\ \dot{\mathbf{u}} \end{bmatrix} = i\omega \begin{bmatrix} \mathbf{0} & \mathbf{0} & \mathbf{M} \\ \mathbf{D}_{\boldsymbol{\vartheta}u}(\boldsymbol{\theta}) & \mathbf{D}_{\boldsymbol{\vartheta}\boldsymbol{\vartheta}} & \mathbf{0} \\ \mathbf{I} & \mathbf{0} & \mathbf{0} \end{bmatrix} \begin{bmatrix} \mathbf{u} \\ \boldsymbol{\vartheta} \\ \dot{\mathbf{u}} \end{bmatrix}$$

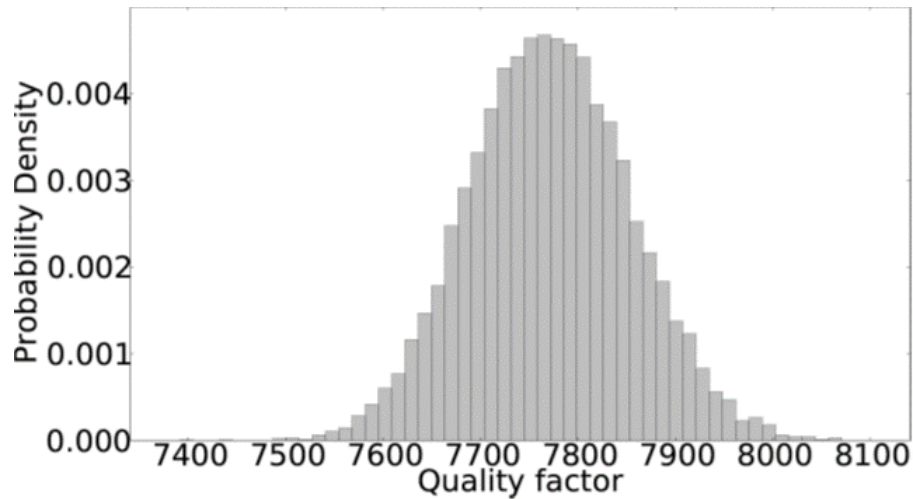
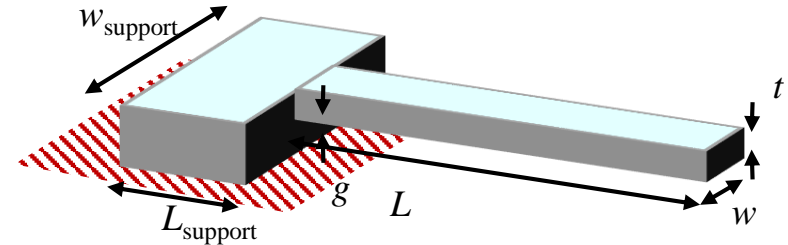
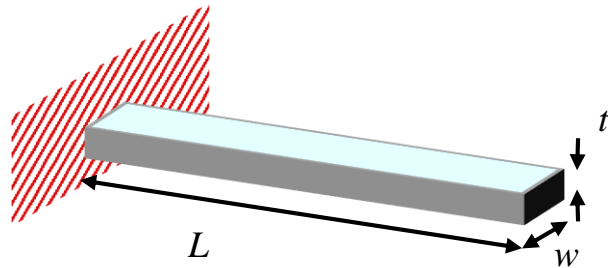
- Quality factor

- From the dissipated energy per cycle

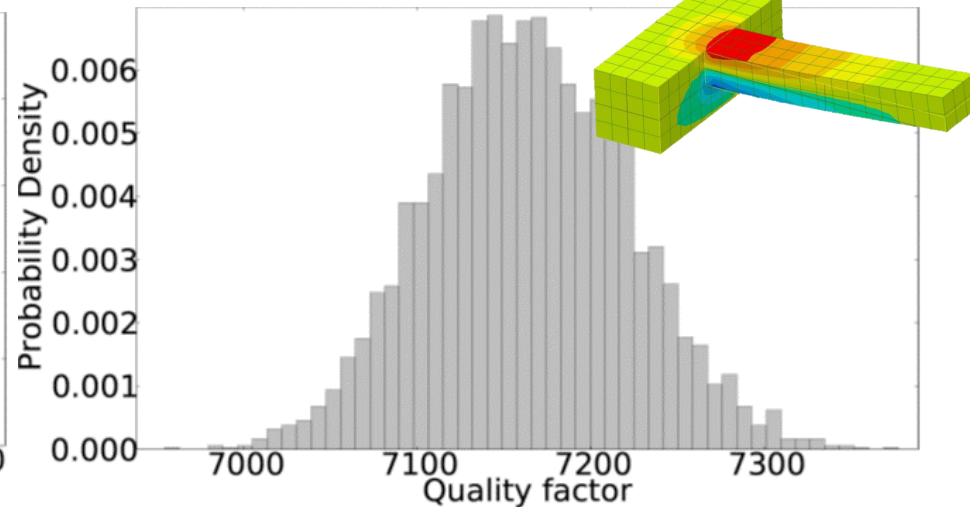
- $$Q^{-1} = \frac{2|\Im\omega|}{\sqrt{(\Re\omega)^2 + (\Im\omega)^2}}$$

Stochastic 3-Scale Models

- Application of the 3-Scale method to extract the quality factor distribution
 - 3D models readily available
 - The effect of the anchor can be studied



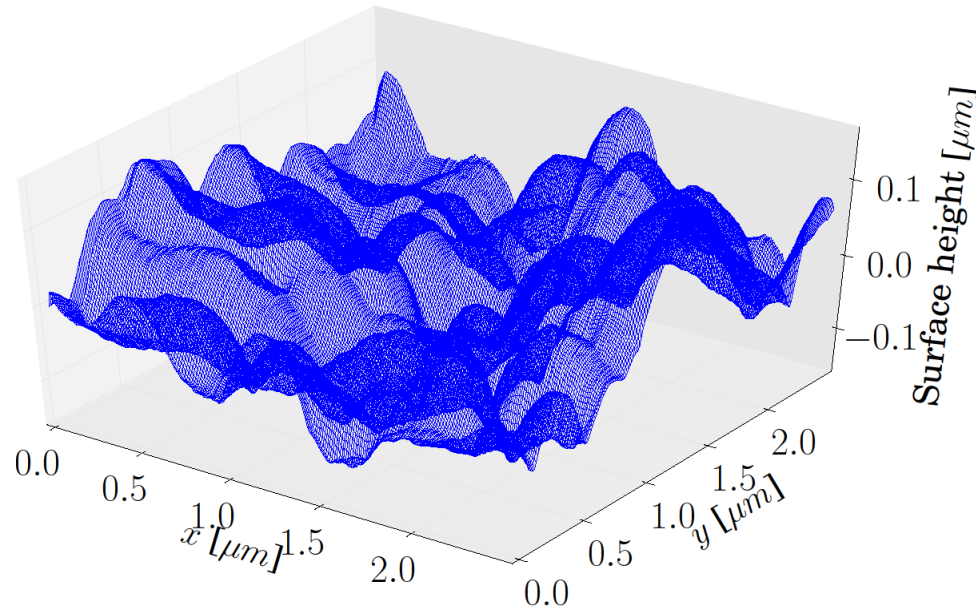
15 x 3 x 2 μm^3 -beam,
deposited at 610 °C



15 x 3 x 2 μm^3 -beam & anchor,
deposited at 610 °C

Stochastic 3-Scale Models

- Surface topology: asperity distribution
 - Upper surface topology by AFM (Atomic Force Microscope) measurements on 2 μm -thick poly-silicon films



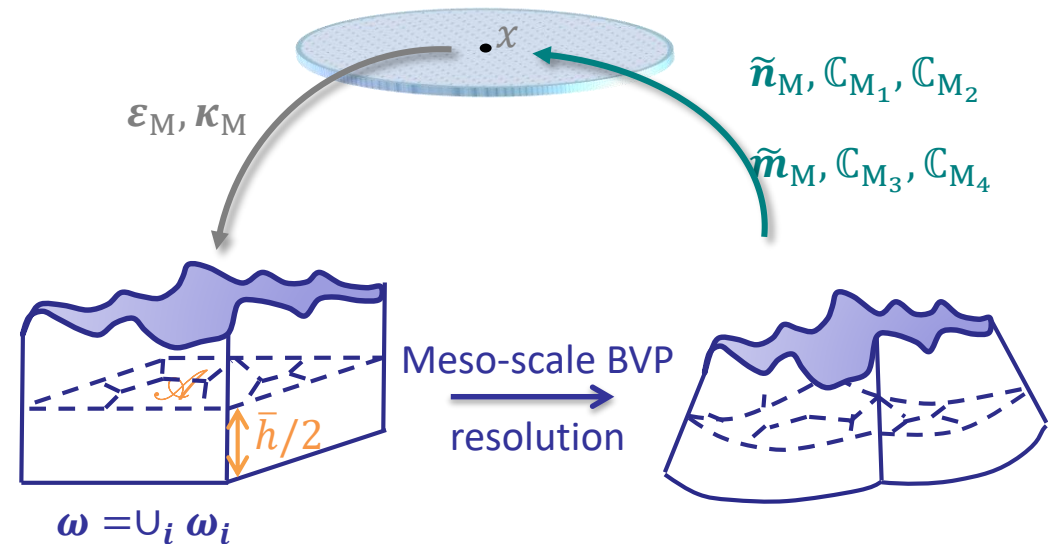
Deposition temperature [$^{\circ}\text{C}$]	580	610	630	650
Std deviation [nm]	35.6	60.3	90.7	88.3

AFM data provided by IMT Bucharest, Rodica Voicu, Angela Baracu, Raluca Muller

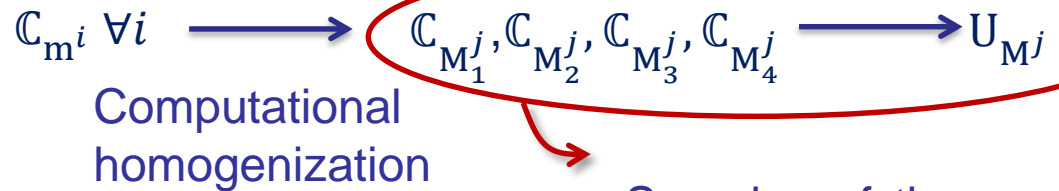
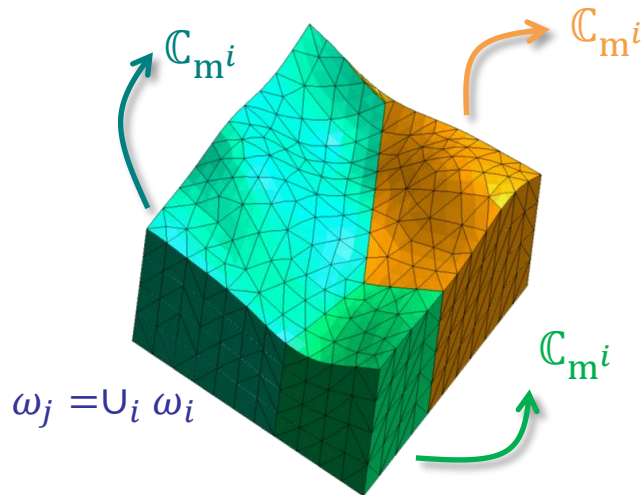
Stochastic 3-Scale Models

- Accounting for roughness
 - Second-order homogenization

$$\begin{cases} \tilde{\mathbf{n}}_M = \mathbb{C}_{M_1} : \boldsymbol{\varepsilon}_M + \mathbb{C}_{M_2} : \boldsymbol{\kappa}_M \\ \tilde{\mathbf{m}}_M = \mathbb{C}_{M_3} : \boldsymbol{\varepsilon}_M + \mathbb{C}_{M_4} : \boldsymbol{\kappa}_M \end{cases}$$



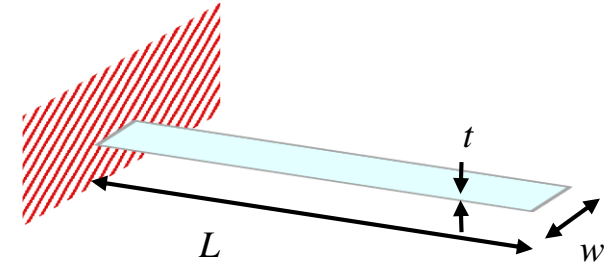
- Stochastic homogenization
 - Several SVE realizations
 - For each SVE $\omega_j = U_i \omega_i$
 - The density per unit area is now non-constant



Samples of the meso-scale homogenized elasticity matrix U_M & density $\bar{\rho}_M$

Stochastic 3-Scale Models

- Accounting for roughness
 - Cantilever of $8 \times 3 \times t \mu\text{m}^3$ deposited at $610 \text{ }^\circ\text{C}$



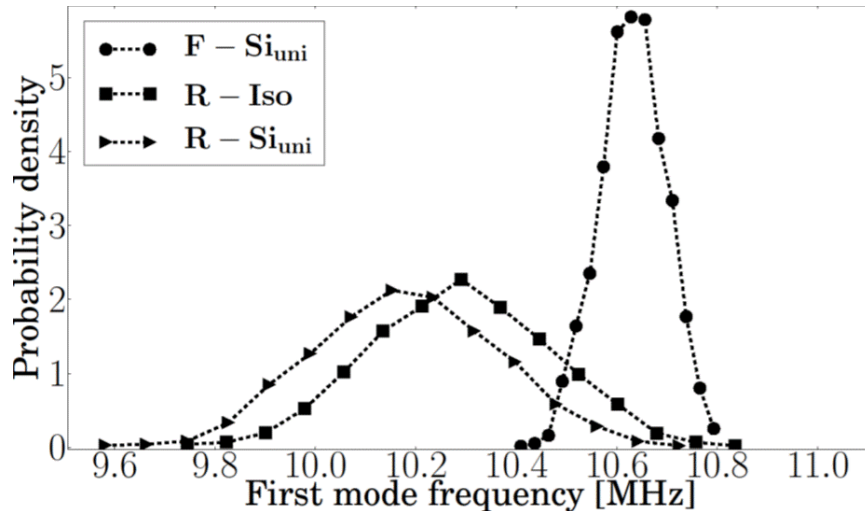
Flat SVEs (no roughness) - F

Rough SVEs (Polysilicon film deposited at $610 \text{ }^\circ\text{C}$) - R

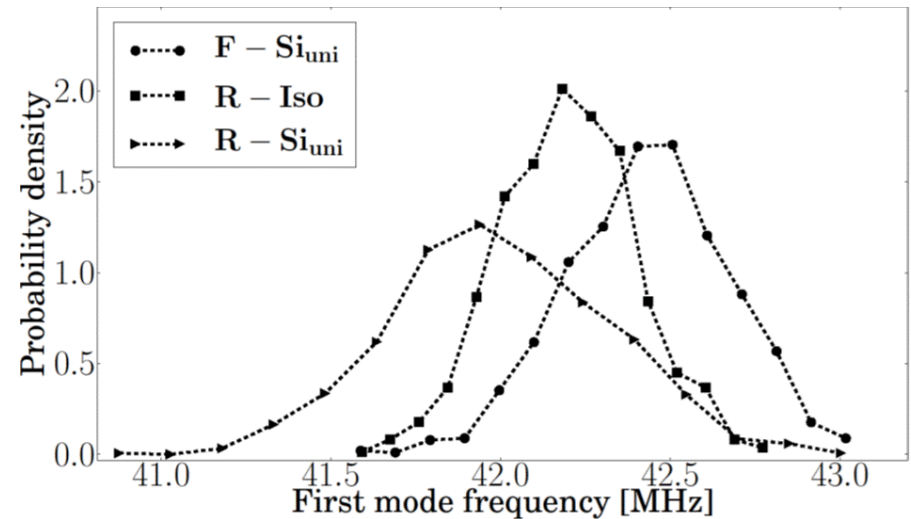
Grain orientation following XRD measurements – Si_{pref}

Grain orientation uniformly distributed – Si_{uni}

Reference isotropic material – Iso

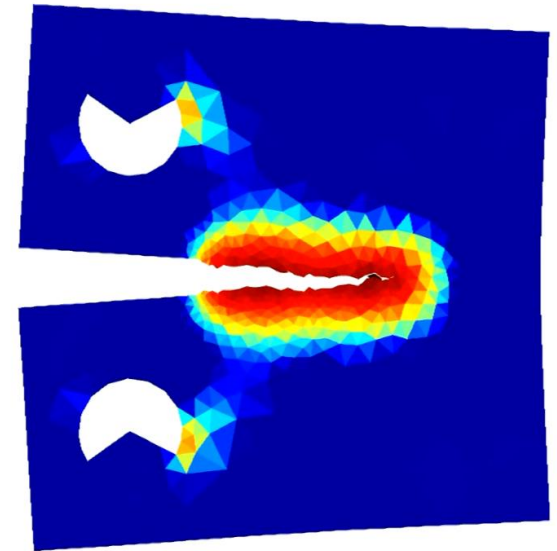
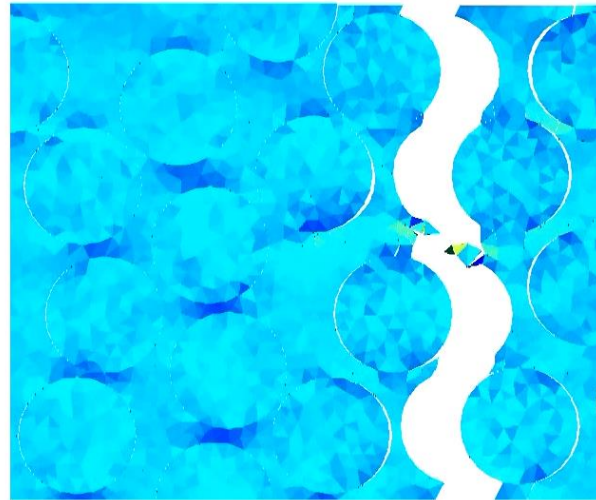
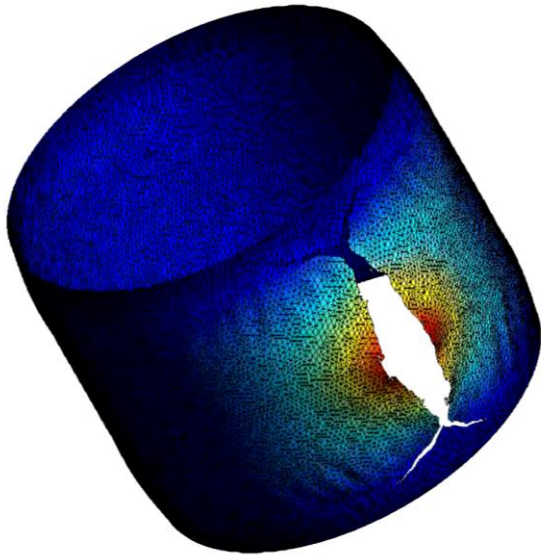


Roughness effect is the most important for $8 \times 3 \times 0.5 \mu\text{m}^3$ cantilevers



Roughness effect is of same importance as orientation for $8 \times 3 \times 2 \mu\text{m}^3$ cantilevers

- Application to robust design
 - Determination of probabilistic meso-scale properties
 - Propagate uncertainties to higher scale
 - Vibro-meter sensors:
 - Uncertainties in resonance frequency / Q factor
- 3SMVIB MNT.ERA-NET project
 - Open-Engineering, V2i, ULiège (Belgium)
 - Polit. Warszawska (Poland)
 - IMT, Univ. Cluj-Napoca (Romania)
- Publications (doi)
 - [10.1002/nme.5452](https://doi.org/10.1002/nme.5452)
 - [10.1016/j.cma.2016.07.042](https://doi.org/10.1016/j.cma.2016.07.042)
 - [10.1016/j.cma.2015.05.019](https://doi.org/10.1016/j.cma.2015.05.019)



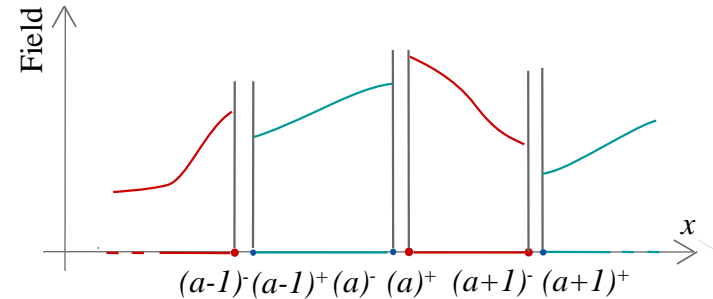
DG-Based (Multi-Scale) Fracture

The research has been funded by the Belgian National Fund for Education at the Research in Industry and Farming. SIMUCOMP The research has been funded by the Walloon Region under the agreement no 1017232 (CT-EUC 2010-10-12) in the context of the ERA-NET +, Matera + framework.

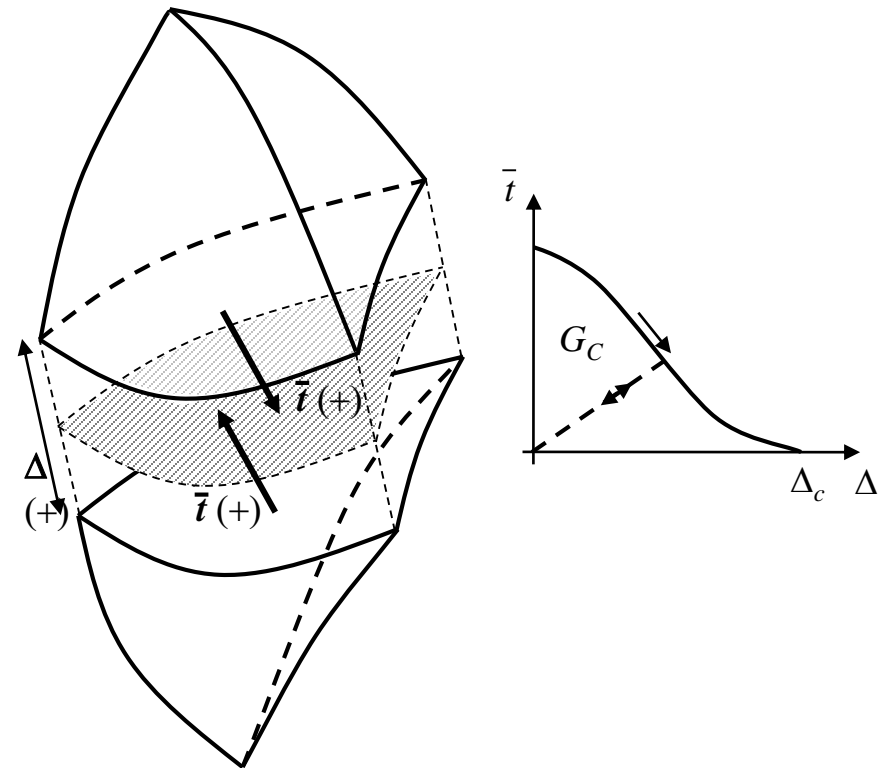
The research has been funded by the Walloon Region under the agreement no.7581-MRIPF in the context of the 16th MECATECH call.

- Hybrid DG/cohesive law formulation

- Discontinuous Galerkin method
 - Finite-element discretization
 - Same **discontinuous** polynomial approximations for the
 - **Test** functions φ_h and
 - **Trial** functions $\delta\varphi$



- Can easily be combined with a cohesive law for fracture analyses
 - Interface elements already exist
 - Easy to shift from un-fractured to fractured states
 - Remains accurate before fracture onset (DG formulation)
 - Efficient // implementation



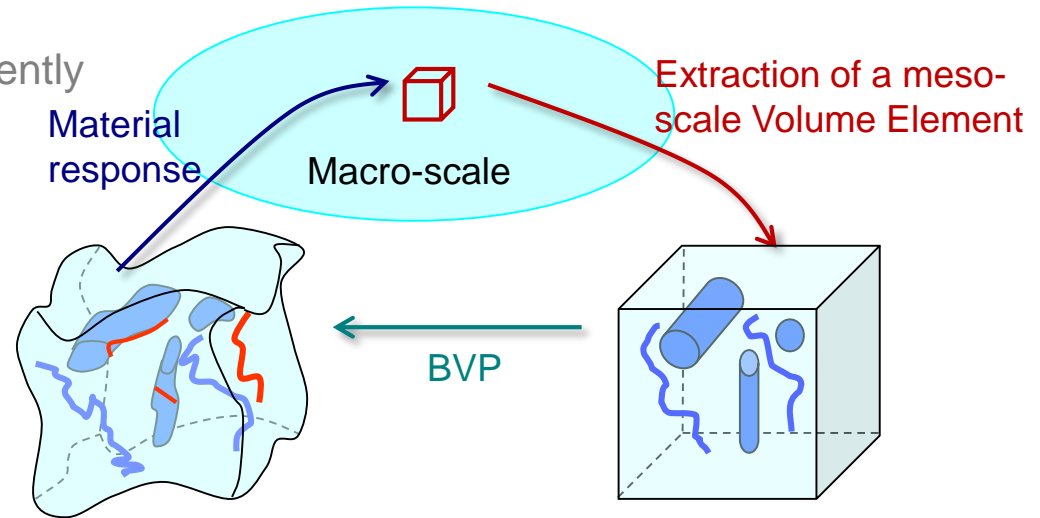
- Publications (doi)

- [10.1016/j.cma.2010.08.014](https://doi.org/10.1016/j.cma.2010.08.014)

DG-Based Multi-Scale Fracture

- Multi-scale modeling

- 2 problems are solved concurrently
 - The macro-scale problem
 - The meso-scale problem (on a meso-scale Volume Element)



- For meso-scale volume elements embedding crack propagation

$$L_{\text{macro}} \gg L_{\text{VE}} ? L_{\text{micro}}$$

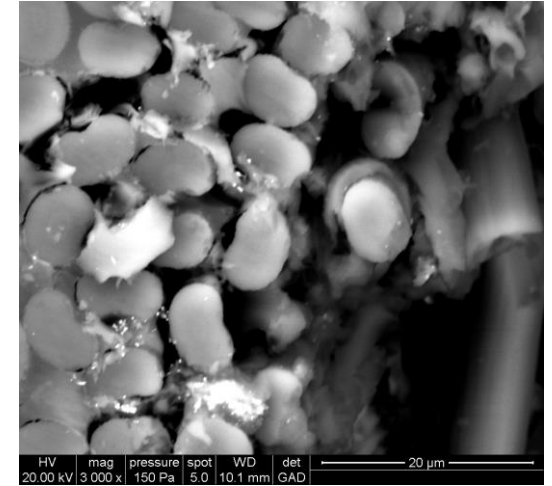
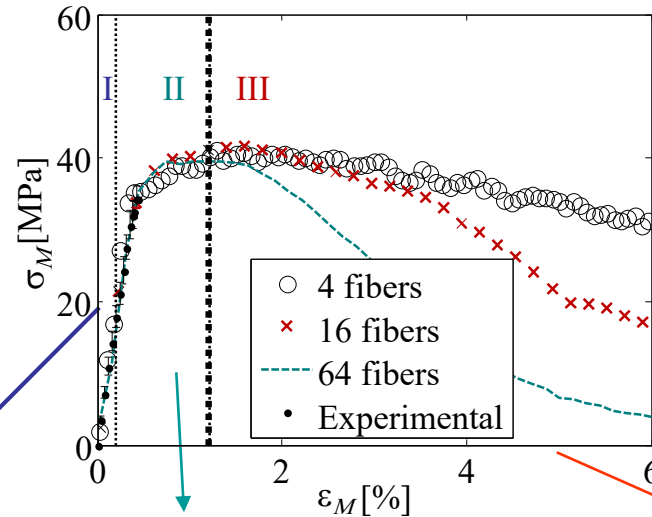
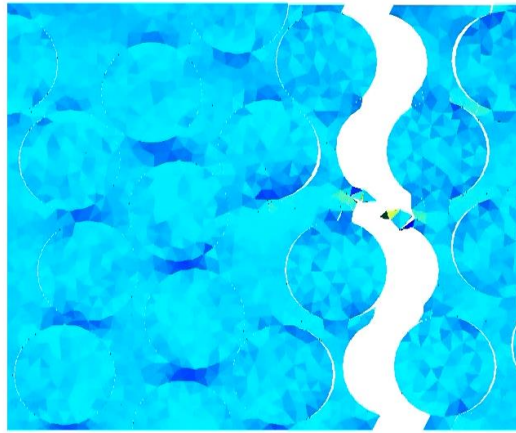
For accuracy: Size of the meso-scale volume element smaller than the characteristic length of the macro-scale loading

The crack induces a loss of statistical representativeness

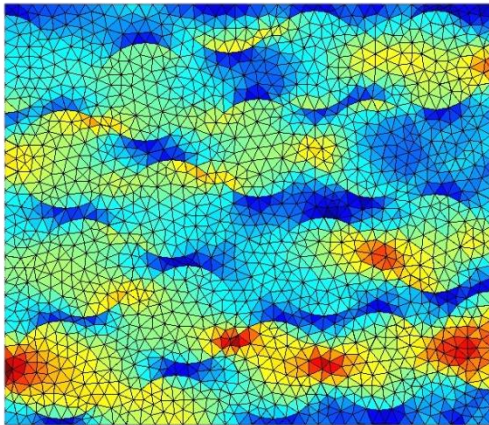
- Should recover consistency lost due to the discontinuity

DG-Based Multi-Scale Fracture

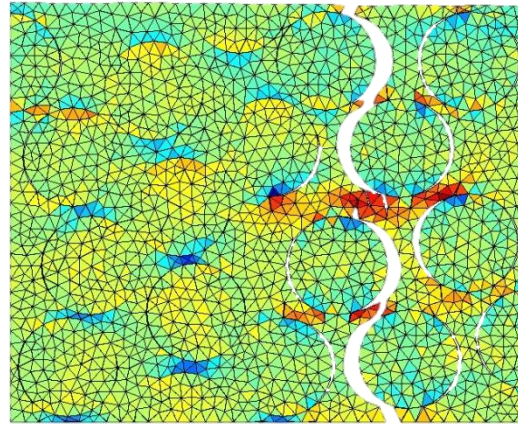
- Micro-Meso fracture model for intra-laminar failure
 - Epoxy-CF (60%), transverse loading
 - 3 stages captured



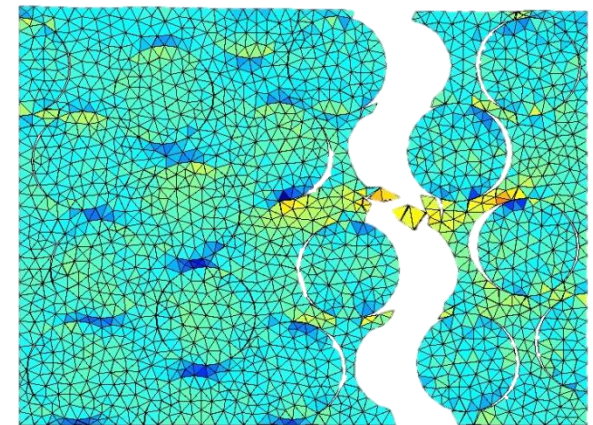
Elastic response



Damage due to debonding



Meso-crack

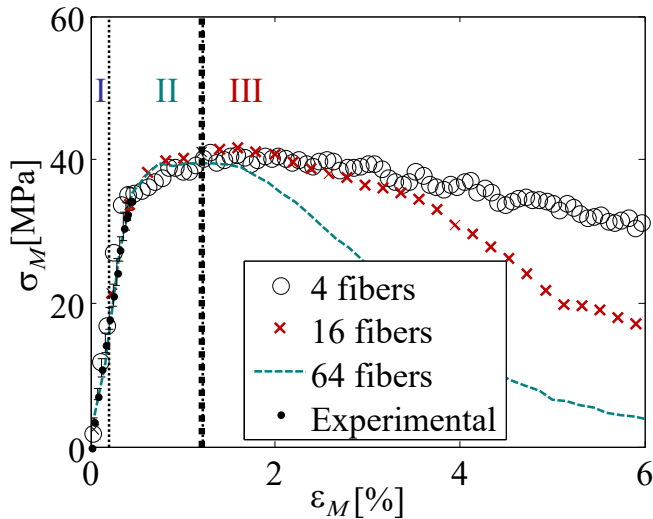


DG-Based Multi-Scale Fracture

- Micro-Meso fracture model for intra-laminar failure (2)

- Scale transition after softening onset
 - Should not depend on the RVE size
 - Extraction of the meso-scale TSL (\bar{t}_M vs. Δ_M)

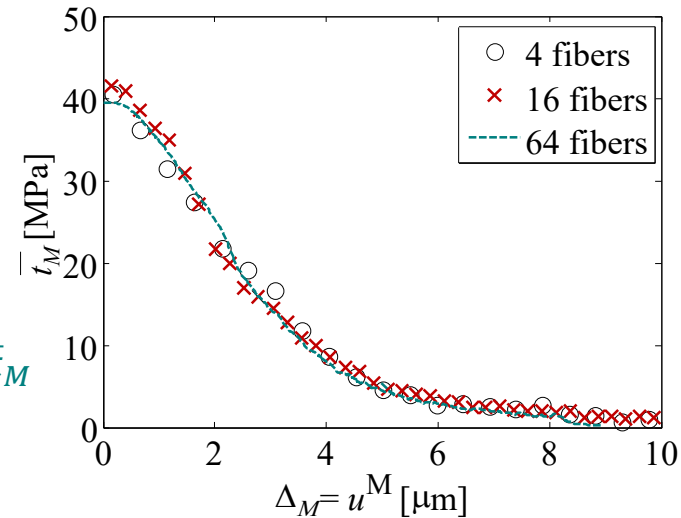
[Verhoosel et al., IJNME 2010]



$$\delta \bar{t}_M = \delta \sigma_M \cdot e_X$$



$$\delta \Delta_M = \delta u^m - L_{\text{cell}} \mathbf{C}_M^{-1} : e_X \otimes e_X \cdot \delta \bar{t}_M$$



- SIMUCOMP ERA-NET project

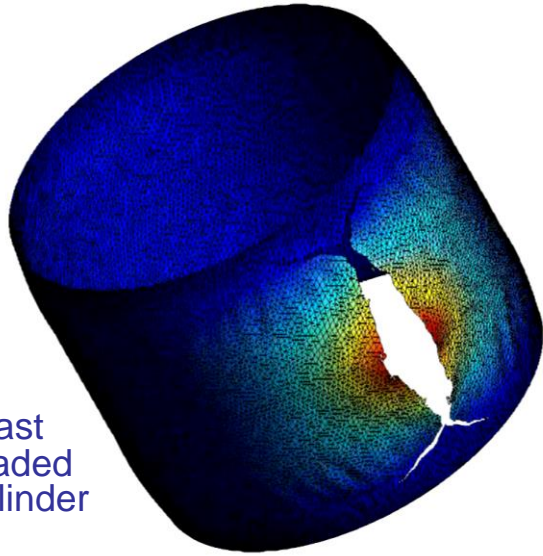
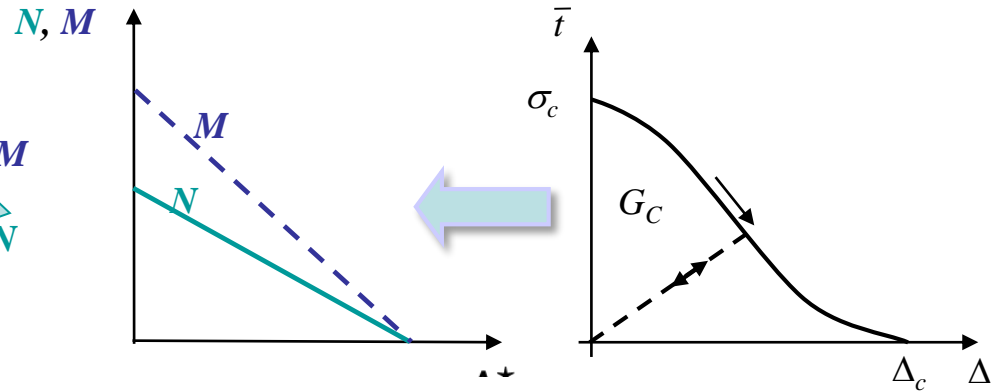
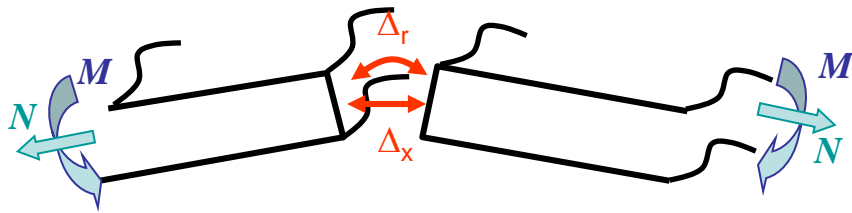
- e-Xstream, CENAERO, ULiège (Belgium)
- IMDEA Materials (Spain)
- CRP Henri-Tudor (Luxemburg)

- Publication (doi)

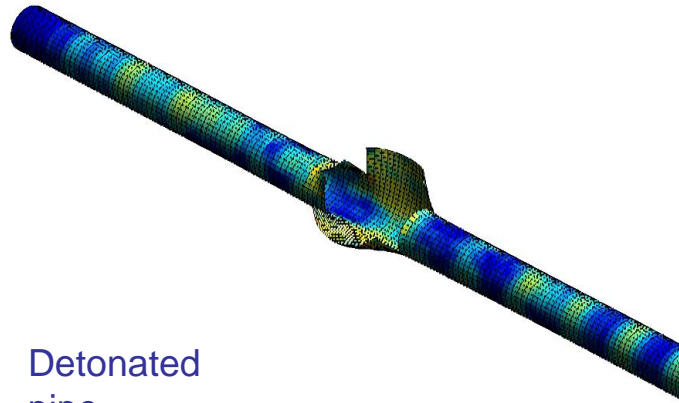
- [10.1016/j.engfracmech.2013.03.018](https://doi.org/10.1016/j.engfracmech.2013.03.018)

DG-Based Dynamic Fracture

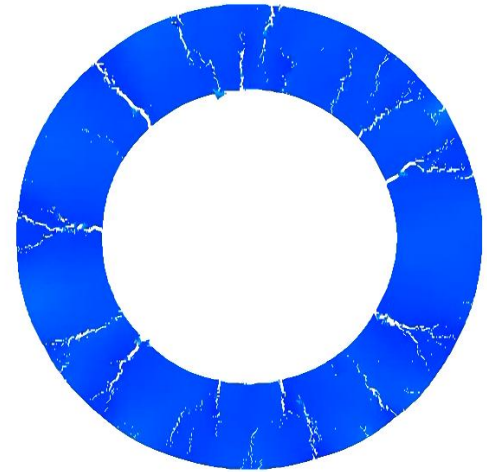
- Fracture of thin structures



Blast loaded cylinder



Detonated pipe



Fragmented disk

- FNRS-FRIA fellowship

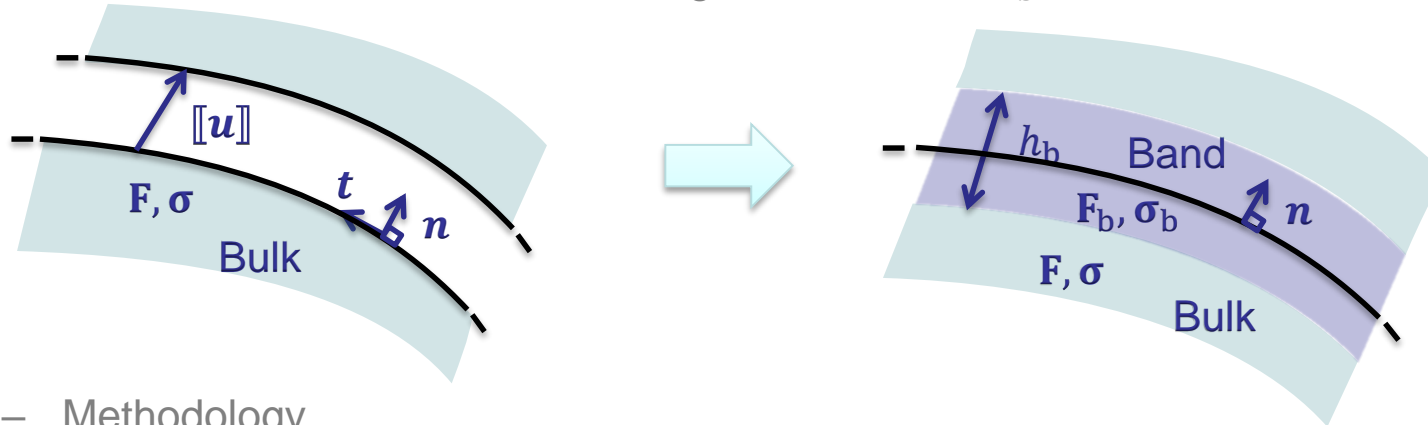
- Publications (doi)

- [10.1002/nme.4381](https://doi.org/10.1002/nme.4381)
- [10.1007/s10704-012-9748-5](https://doi.org/10.1007/s10704-012-9748-5)
- [10.1016/j.cma.2011.07.008](https://doi.org/10.1016/j.cma.2011.07.008)
- [10.1002/nme.3008](https://doi.org/10.1002/nme.3008)

DG-Based elastic damage to crack transition

- Capture triaxiality effects: Cohesive Band Model (CBM)

- Introduction of a uniform band of given thickness h_b [Remmers et al. 2013]



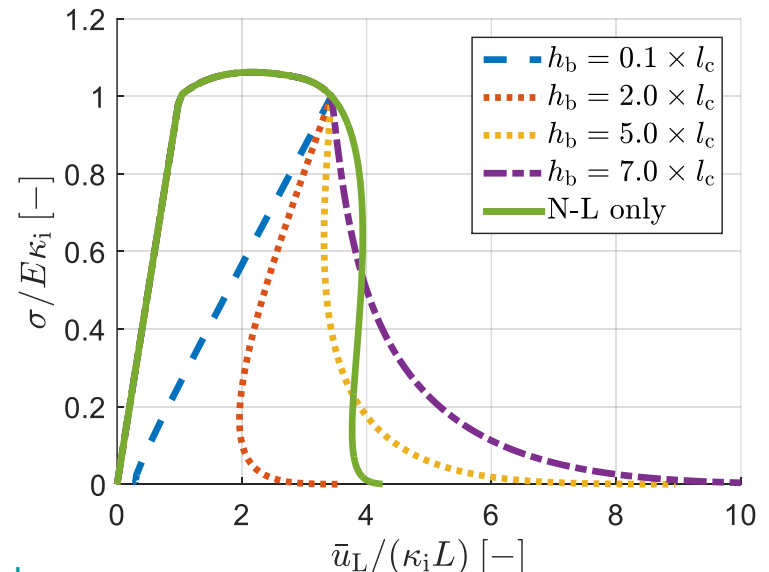
- Methodology

1. Bulk stress σ using non-local damage law
2. Compute a “band” deformation gradient

$$\mathbf{F}_b = \mathbf{F} + \frac{[[\mathbf{u}]] \otimes \mathbf{N}}{h_b} + \frac{1}{2} \nabla_T [[\mathbf{u}]]$$
3. Band stress σ_b using the (local) damage law
4. Recover traction forces $\mathbf{t}([[\mathbf{u}]], \mathbf{F}) = \sigma_b \cdot \mathbf{n}$

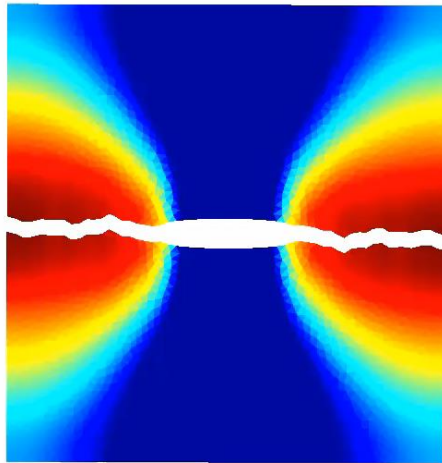
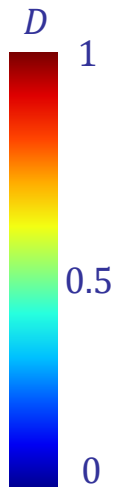
- The cohesive band thickness

- Evaluated to ensure energy consistency
- Same dissipated energy as with a damage model

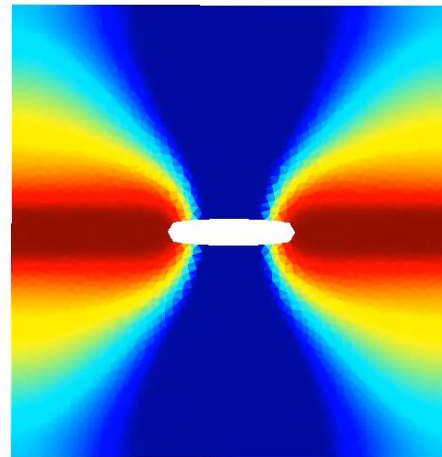


DG-Based elastic damage to crack transition

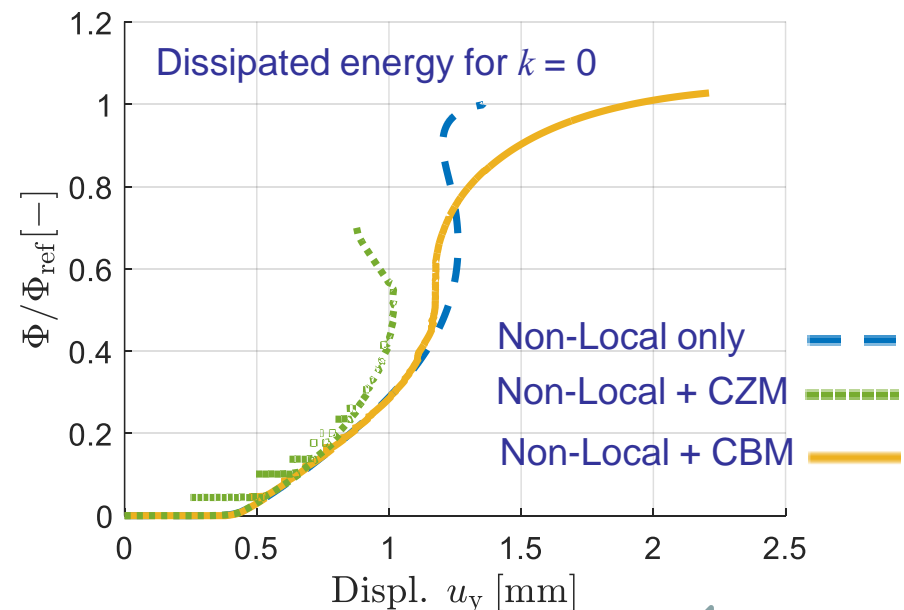
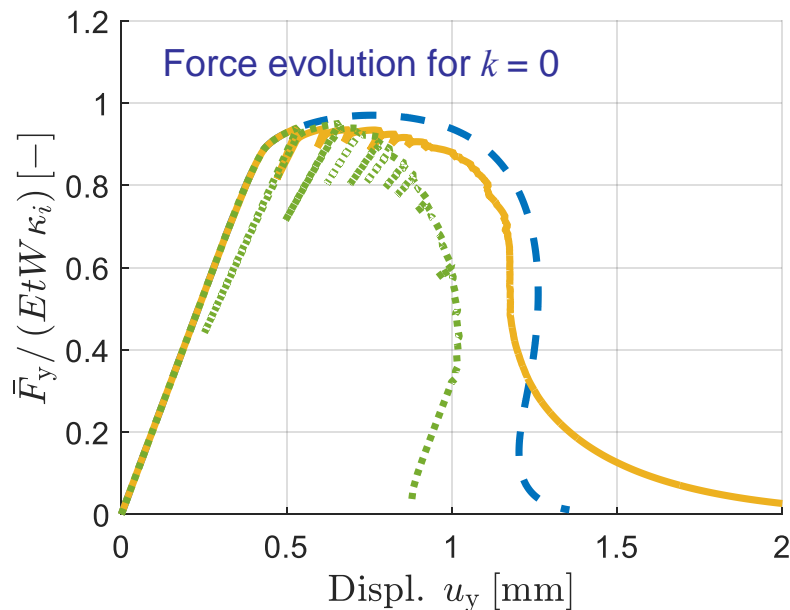
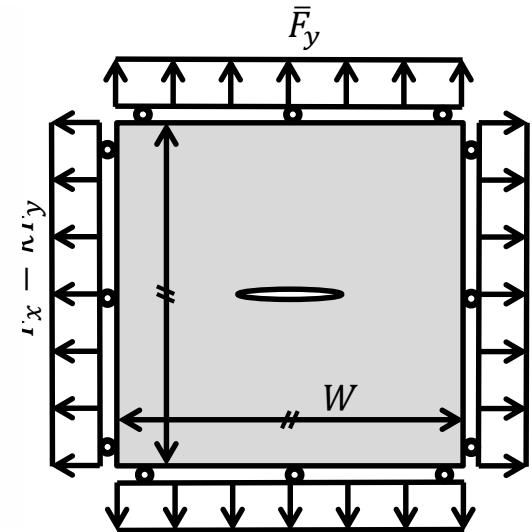
- Slit plate



Non-Local+ CBM

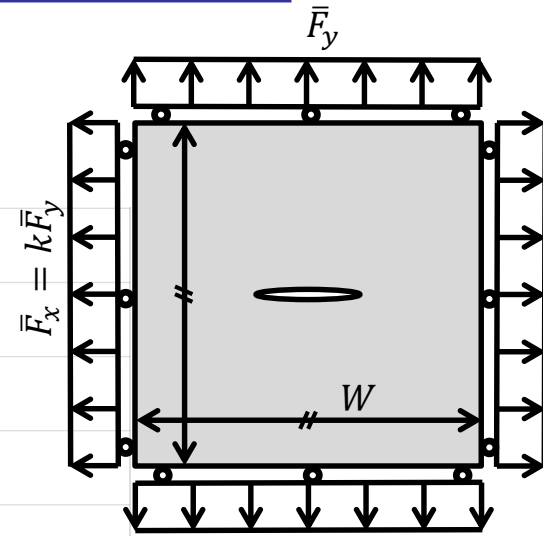
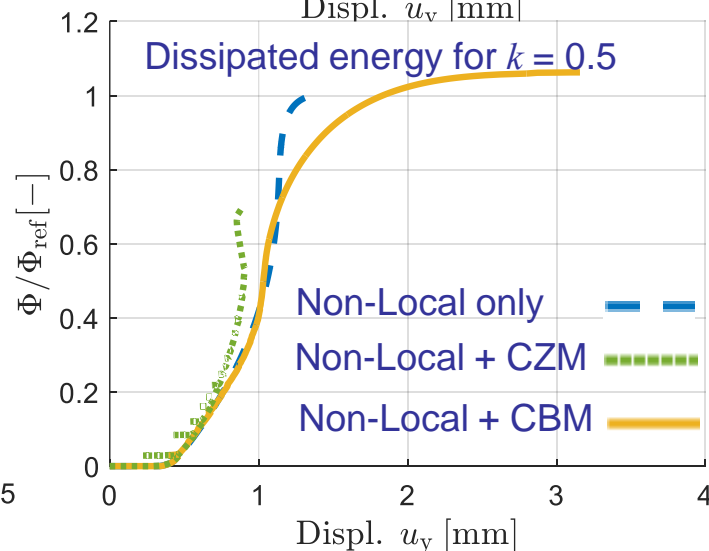
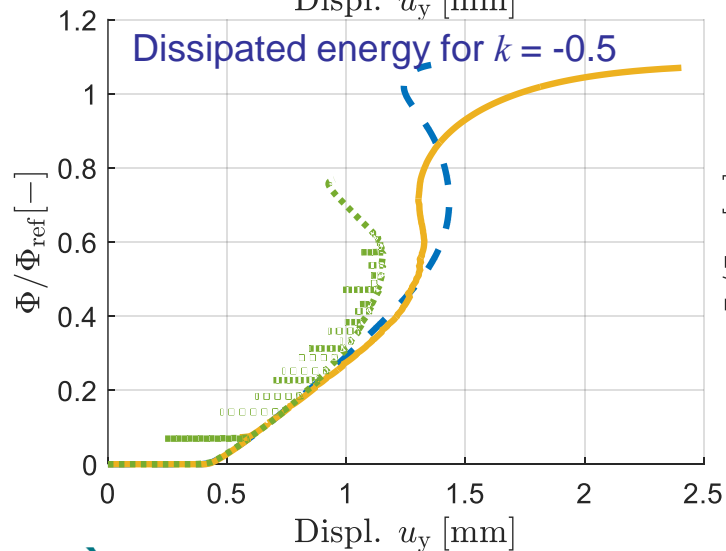
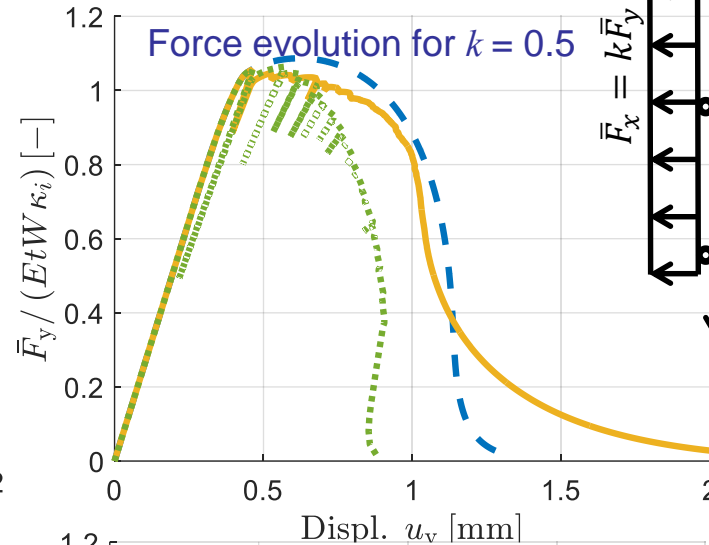
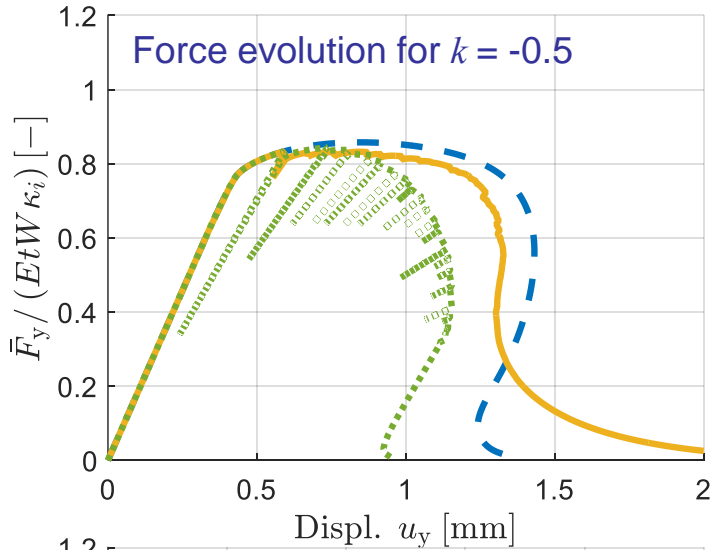


Non-Local



DG-Based elastic damage to crack transition

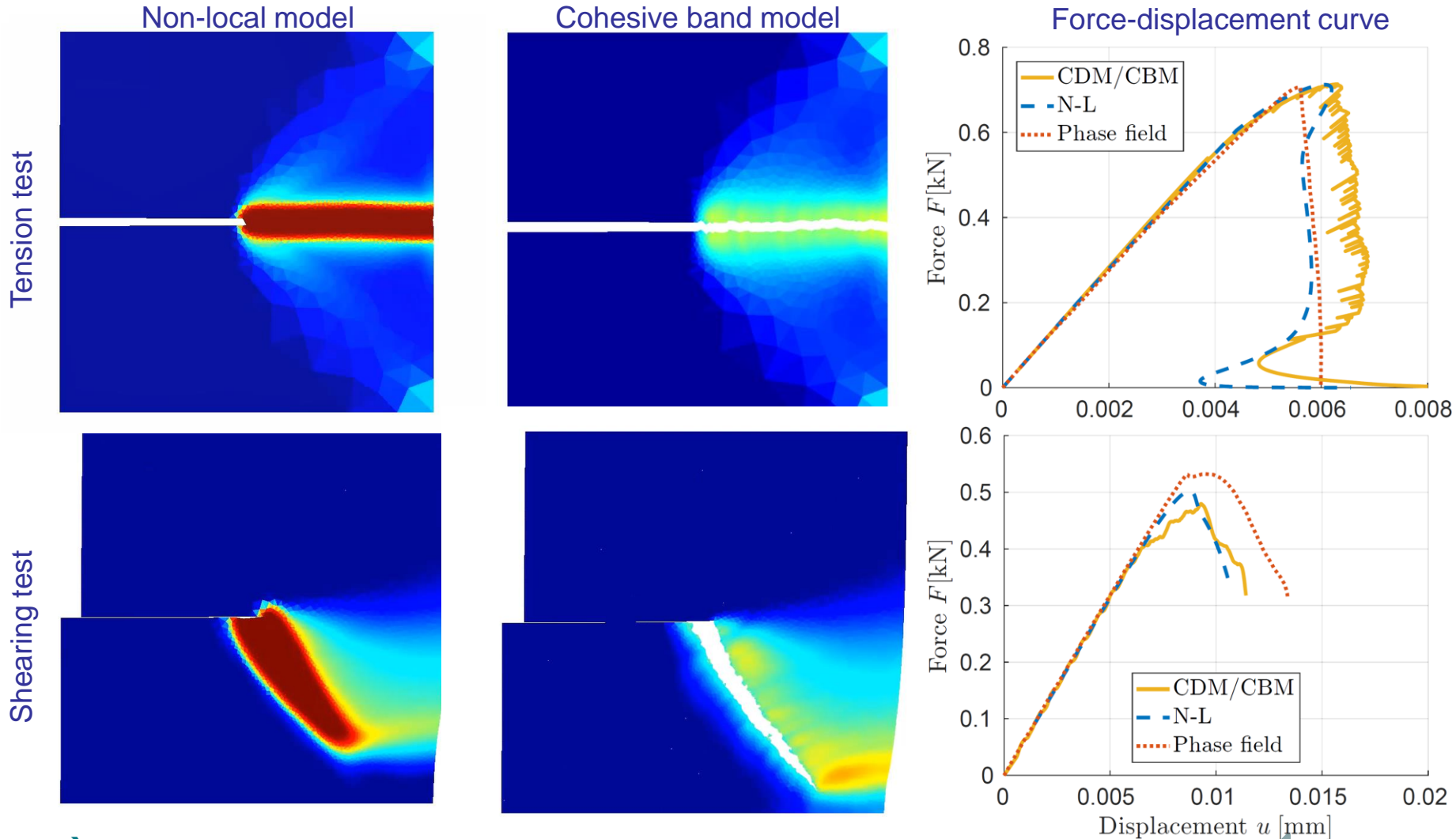
- Slit plate
 - Triaxiality effect through ratio k



DG-Based elastic damage to crack transition

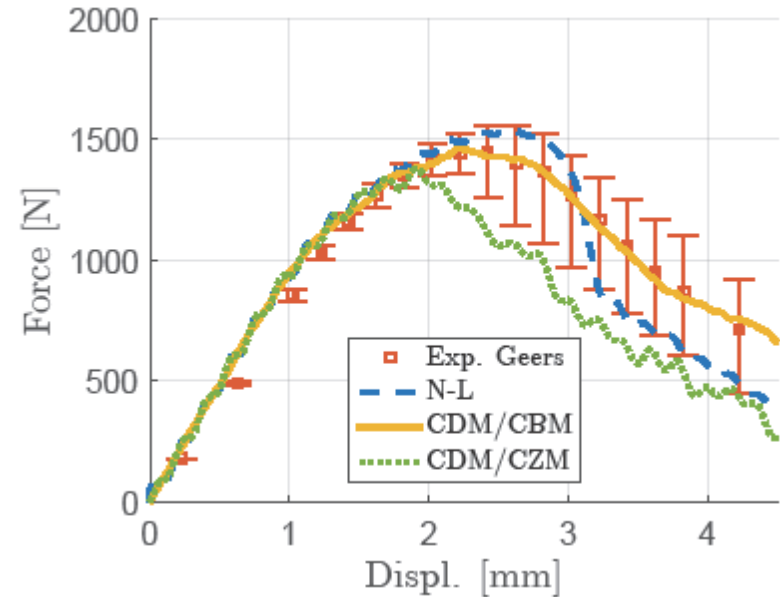
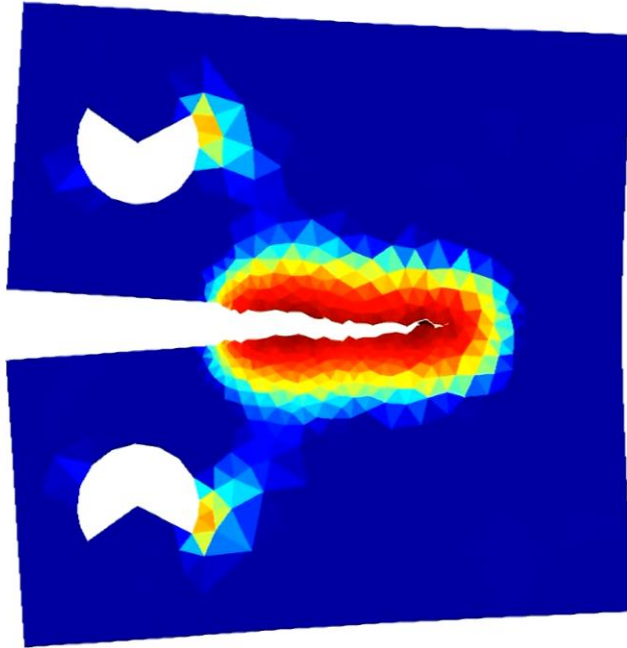
- Comparison with phase field

- Single edge notched specimen [Miehe et al. 2010]
 - Calibration of damage and CBM parameters with 1D case [Leclerc et al. 2018]

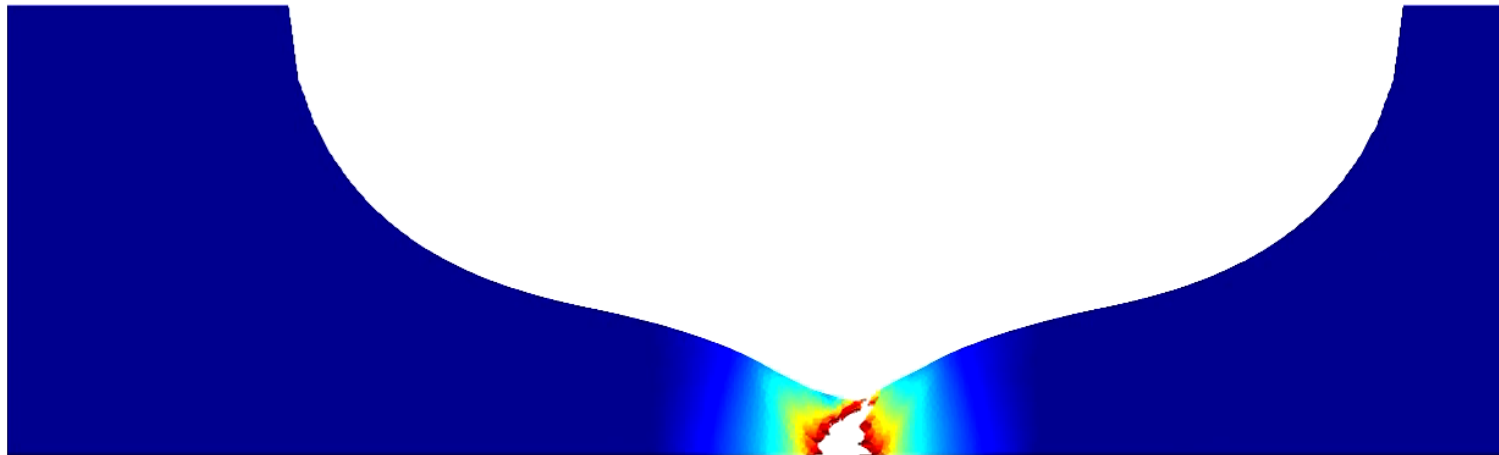


DG-Based elastic damage to crack transition

- Compact Tension Specimen:
 - Non-Local damage law combined to cohesive band model improves accuracy



- MRIPF MECATECH project
 - GD Tech, UCL, FZ, MECAR, Capital People (Belgium)
- Publication (doi)
 - [10.1002/nme.5618](https://doi.org/10.1002/nme.5618)
 - [10.1016/j.cma.2014.06.031](https://doi.org/10.1016/j.cma.2014.06.031)

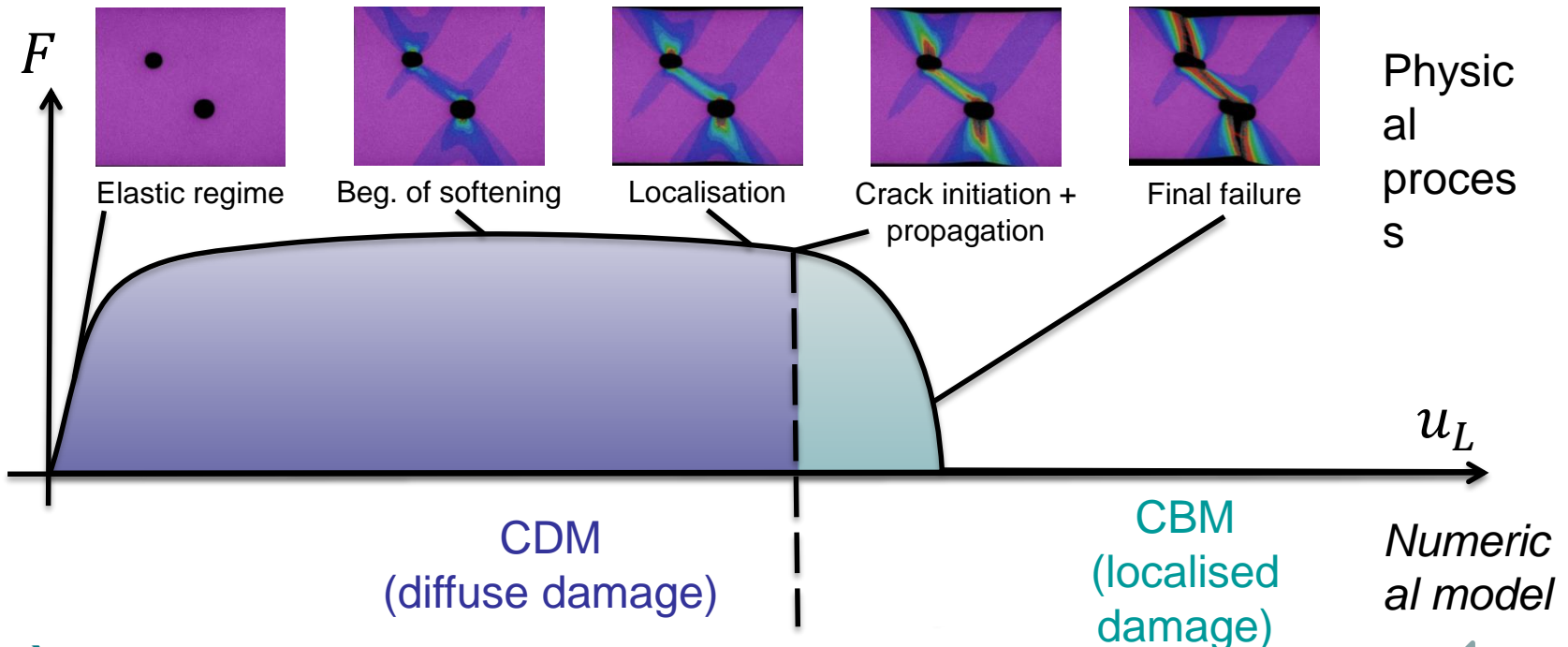


Non-local Gurson damage model to crack transition

The research has been funded by the Walloon Region under the agreement no.7581-MRIPF in the context of the 16th MECATECH call.

Non-local Gurson damage model to crack transition

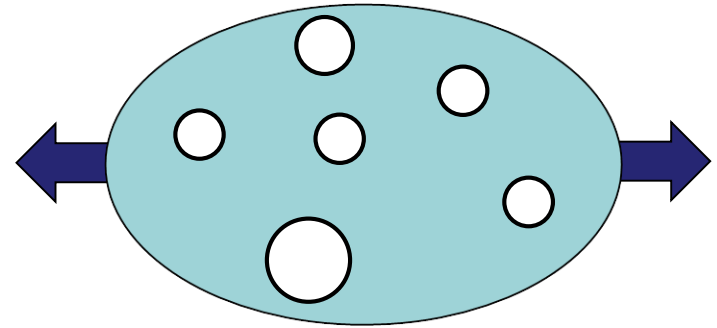
- Objective:
 - To develop high fidelity numerical methods for ductile failure
- Numerical approach:
 - Combination of 2 complementary methods in a single finite element framework:
 - continuous (damage model)
 - + transition to
 - discontinuous (cohesive band model including triaxiality / strain rate effects)



Non-local Gurson damage model to crack transition

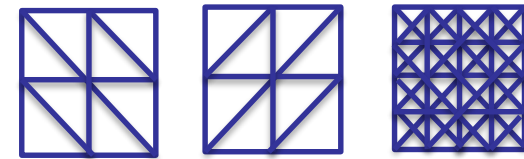
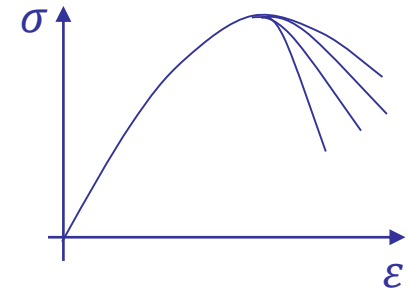
- Material changes represented via internal variables

- Constitutive law $\sigma(\boldsymbol{\varepsilon}; \mathbf{Z}(t'))$
 - Internal variables $\mathbf{Z}(t')$
- Different models
 - Lemaitre-Chaboche (degraded properties)
 - Gurson model (yield surface in terms of porosity f)



- Model implementation:

- Local form
 - Mesh dependency
- Requires non-local form [Bažant 1988]
 - Introduction of characteristic length l_c
 - Weighted average: $\tilde{Z}(\mathbf{x}) = \int_{V_c} W(\mathbf{y}; \mathbf{x}, l_c) Z(\mathbf{y}) d\mathbf{y}$
- Implicit form [Peerlings et al. 1998]
 - New degrees of freedom: \tilde{Z}
 - New Helmholtz-type equations: $\tilde{Z} - l_c^2 \Delta \tilde{Z} = Z$



The numerical results change without convergence

Non-local Gurson damage model to crack transition

- Hyperelastic-based formulation

- Multiplicative decomposition
 $\mathbf{F} = \mathbf{F}^e \cdot \mathbf{F}^p$, $\mathbf{C}^e = \mathbf{F}^{eT} \cdot \mathbf{F}^e$, $J^e = \det(\mathbf{F}^e)$

- Stress tensor definition
 - Elastic potential $\psi(\mathbf{C}^e)$
 - First Piola-Kirchhoff stress tensor

$$\mathbf{P} = 2\mathbf{F}^e \cdot \frac{\partial \psi(\mathbf{C}^e)}{\partial \mathbf{C}^e} \cdot \mathbf{F}^{p-T}$$

- Kirchhoff stress tensors
 - In current configuration
 $\boldsymbol{\kappa} = \mathbf{P} \cdot \mathbf{F}^T = 2\mathbf{F}^e \cdot \frac{\partial \psi(\mathbf{C}^e)}{\partial \mathbf{C}^e} \cdot \mathbf{F}^{eT}$

- In co-rotational space
 $\boldsymbol{\tau} = \mathbf{C}^e \cdot \mathbf{F}^{e-1} \cdot \boldsymbol{\kappa} \cdot \mathbf{F}^{e-T} = 2\mathbf{C}^e \cdot \frac{\partial \psi(\mathbf{C}^e)}{\partial \mathbf{C}^e}$

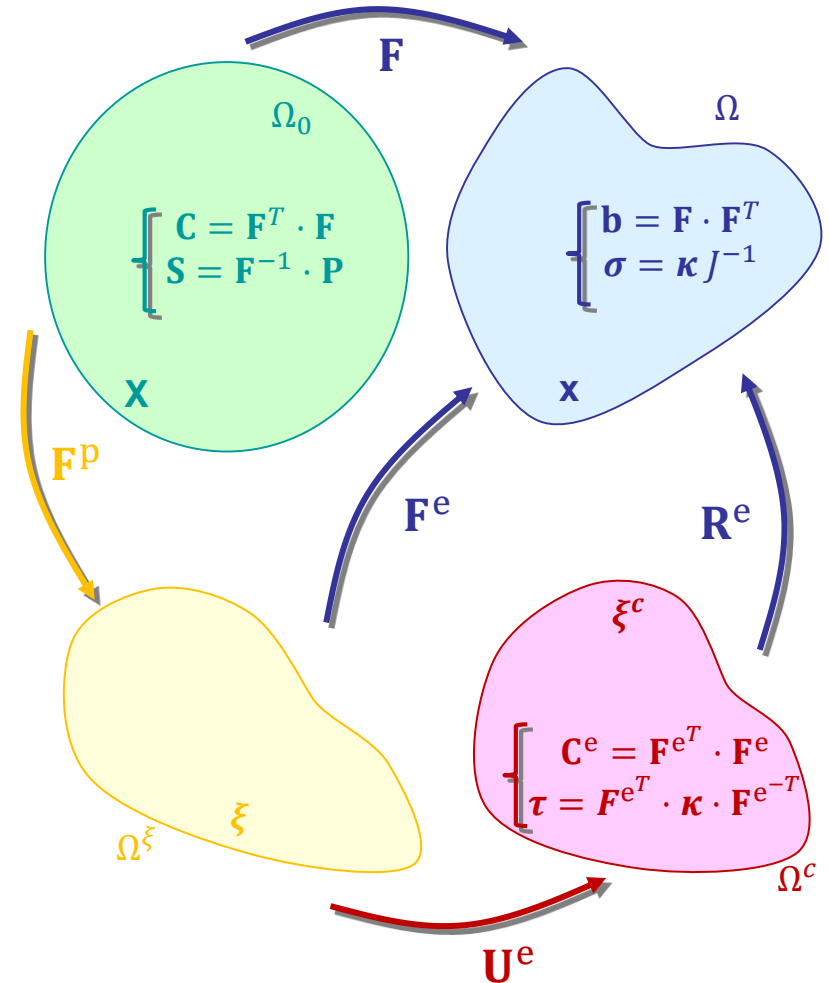
- Logarithmic deformation

- Elastic potential ψ :

$$\psi(\mathbf{C}^e) = \frac{K}{2} \ln^2(J^e) + \frac{G}{4} (\ln(\mathbf{C}^e))^{\text{dev}} : (\ln(\mathbf{C}^e))^{\text{dev}}$$

- Stress tensor in co-rotational space

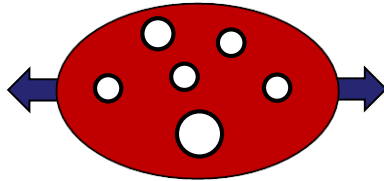
$$\boldsymbol{\tau} = \underbrace{K \ln(J^e)}_p \mathbf{I} + G (\ln(\mathbf{C}^e))^{\text{dev}}$$



Non-local Gurson damage model to crack transition

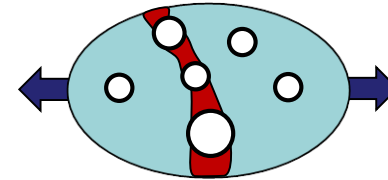
- Porous plasticity (or Gurson) approach
 - Competition between 2 plastic modes:

Growth mode:
Gurson model

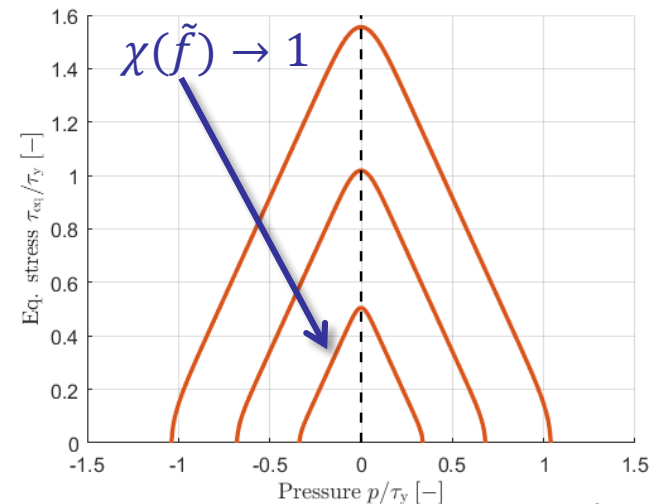
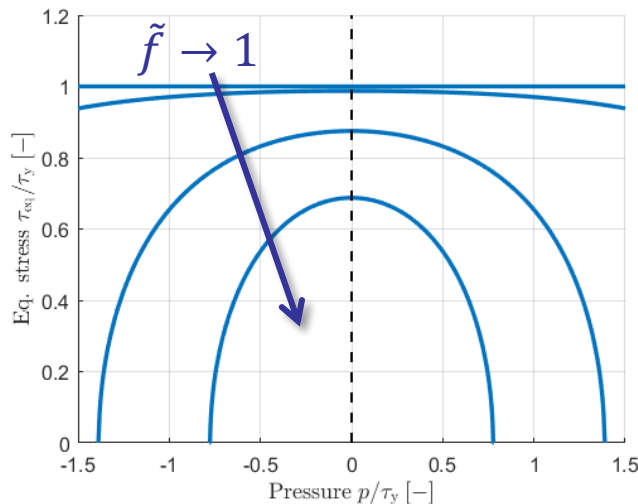


$$\phi_G = \frac{\tau_{eq}^2}{\tau_Y^2} + 2q_1 \tilde{f} \cosh\left(\frac{q_2 p}{2\tau_Y}\right) - 1 - q_3^2 \tilde{f}^2 \leq 0 \quad \text{vs}$$

Coalescence mode:
Thomason model



$$\phi_T = \frac{2}{3} \tau_{eq} + |p| - C_T^f(\chi) \tau_Y \leq 0$$

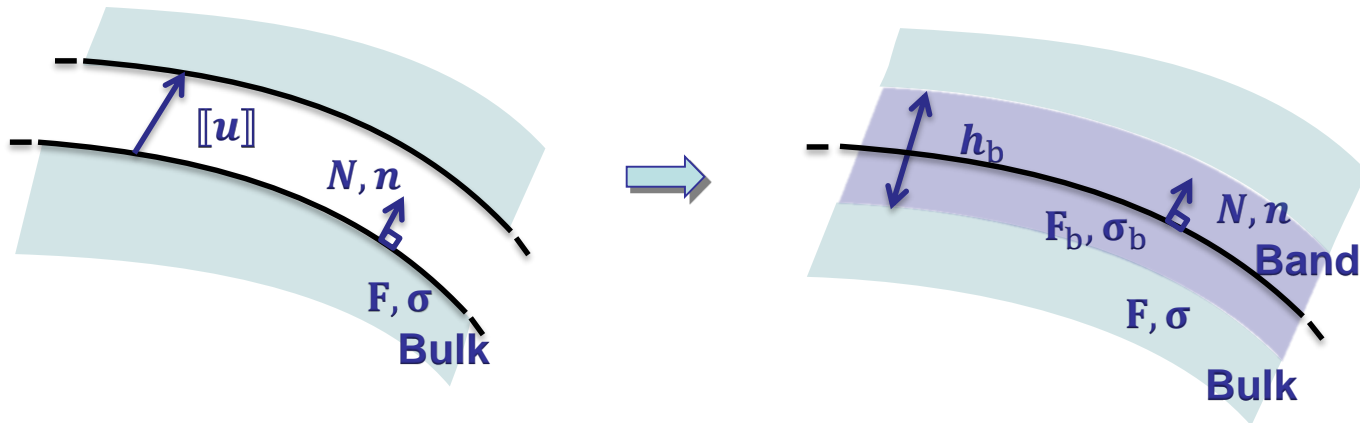


Non-local Gurson damage model to crack transition

- Hybrid DG model: use of a Cohesive Band Model (CBM)

- Principles

- Substitute TSL of CZM by the behavior of a uniform band of thickness h_b [Remmers et al. 2013]



- Localization criterion

- Thomason: $N \cdot \tau \cdot N - C_I^f \tau_y \geq 0$

- Methodology [Leclerc et al. 2018]

- Compute a band strain tensor $F_b = F + \frac{[[u]] \otimes N}{h_b} + \frac{1}{2} \nabla_T [[u]]$
- Compute a band stress tensor $\sigma_b(F_b; Z(\tau))$ using the same CDM as bulk elements
- Recover a surface traction $t([[u]], F) = \sigma_b \cdot n$

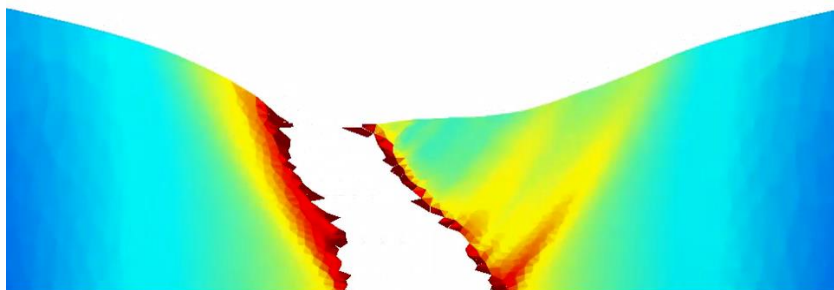
- What is the effect of h_b (band thickness)

- Recover the fracture energy

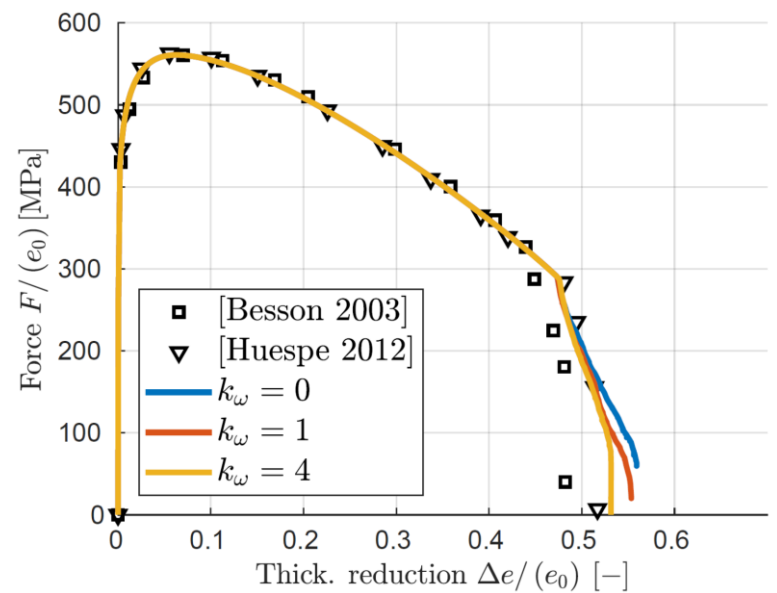
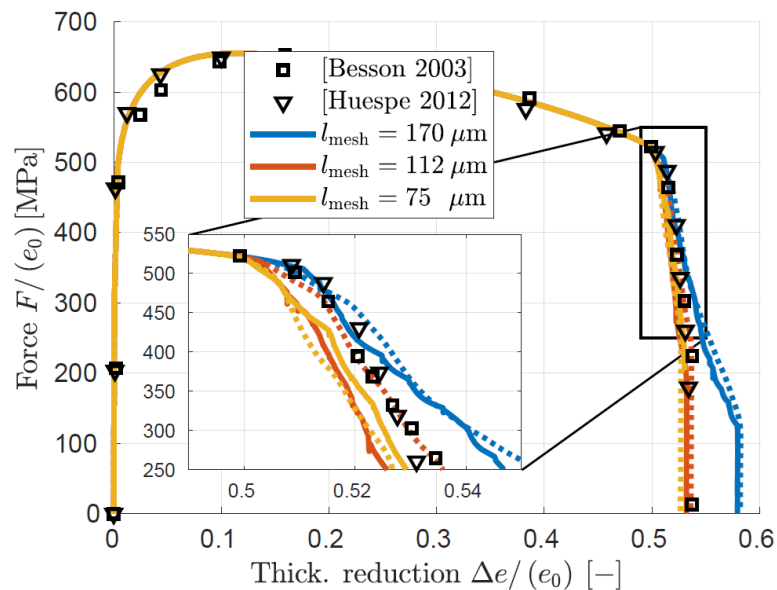
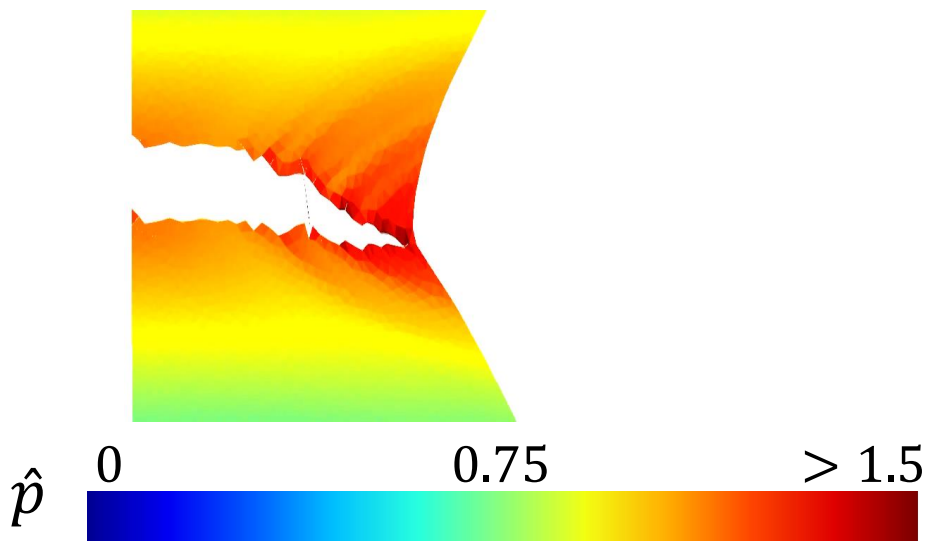
Non-local Gurson damage model to crack transition

- Comparison with literature [Huespe2012,Besson2003]

Slanted plane strain specimen

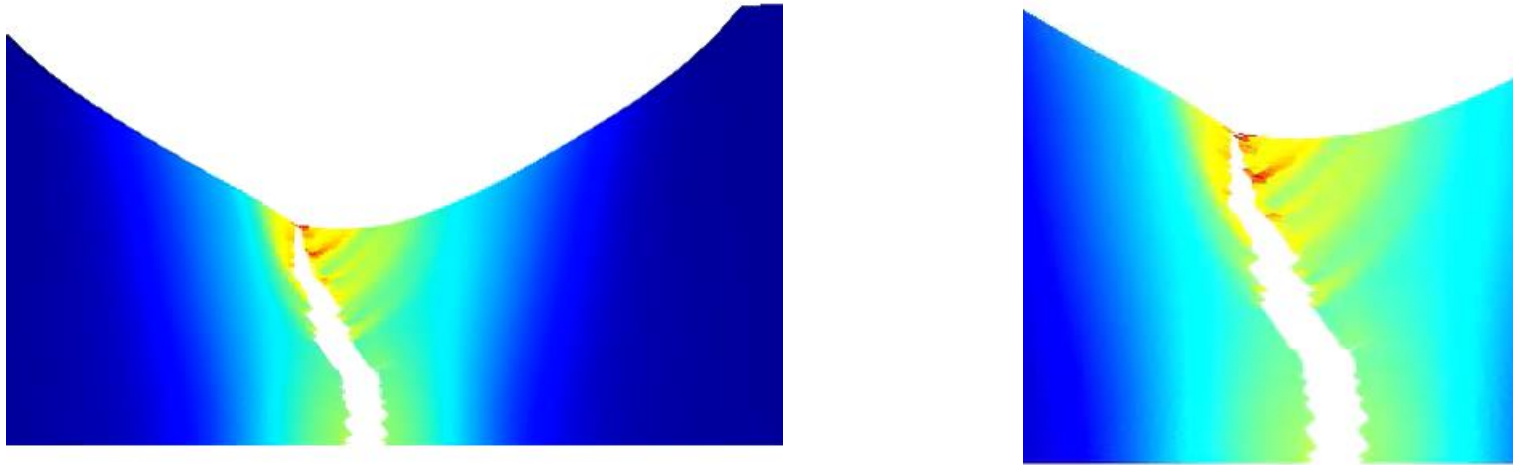


Cup-cone in round bar

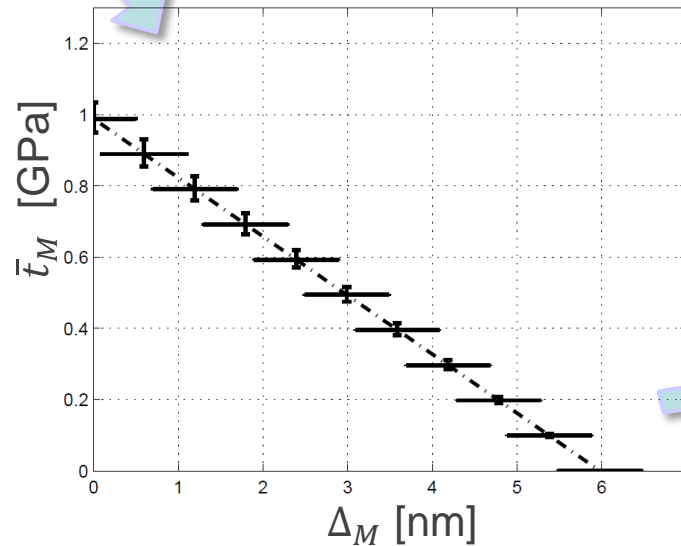
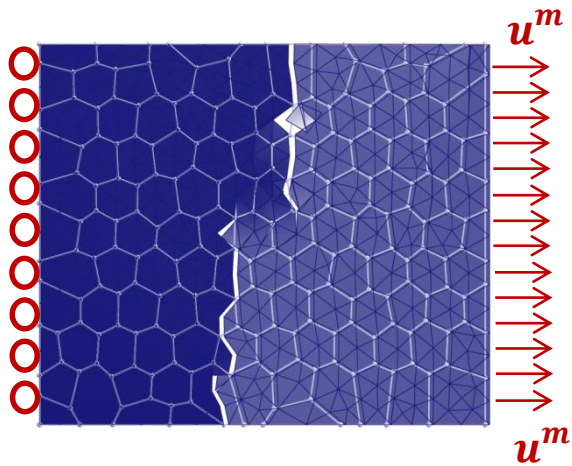


Non-local Gurson damage model to crack transition

- Notched round bar



- MRIPF MECATECH project
 - GDTech, UCL, FZ, MECAR, Capital People (Belgium)
- Publication (doi)
 - [10.1002/nme.5618](https://doi.org/10.1002/nme.5618)



Stochastic Multi-Scale Fracture of Polycrystalline Films

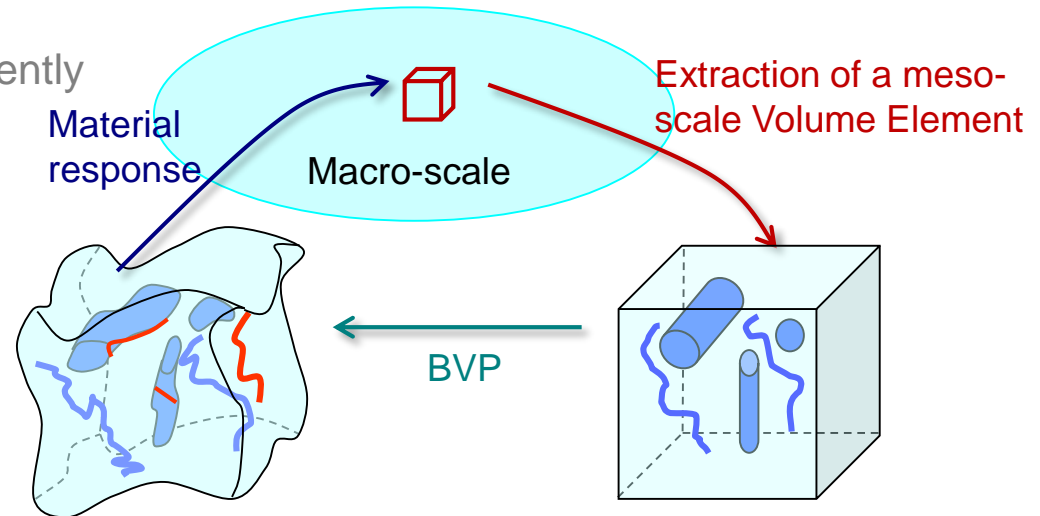
Robust design of MEMS: Financial support from F. R. S. - F. N. R. S. under the project number FRFC 2.4508.11

Stochastic Multi-Scale Fracture of Polycrystalline Films

- Multi-scale modeling

- 2 problems are solved concurrently

- The macro-scale problem
- The meso-scale problem
(on a meso-scale Volume Element)



- For meso-scale volume elements not several orders larger than the micro-structure size and embedding crack propagations

$$L_{\text{macro}} \gg L_{\text{VE}} \sim ? L_{\text{micro}}$$

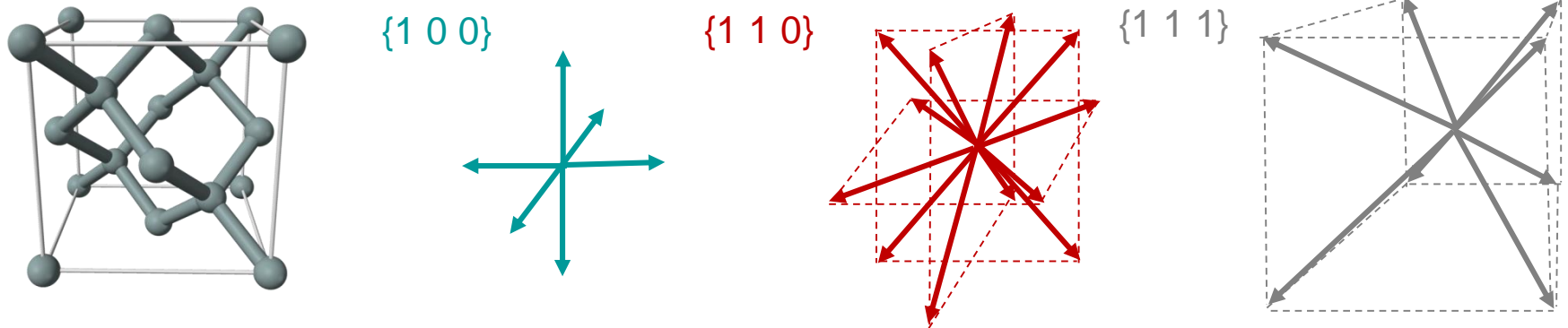
For accuracy: Size of the meso-scale volume element smaller than the characteristic length of the macro-scale loading

Meso-scale volume element no longer statistically representative:

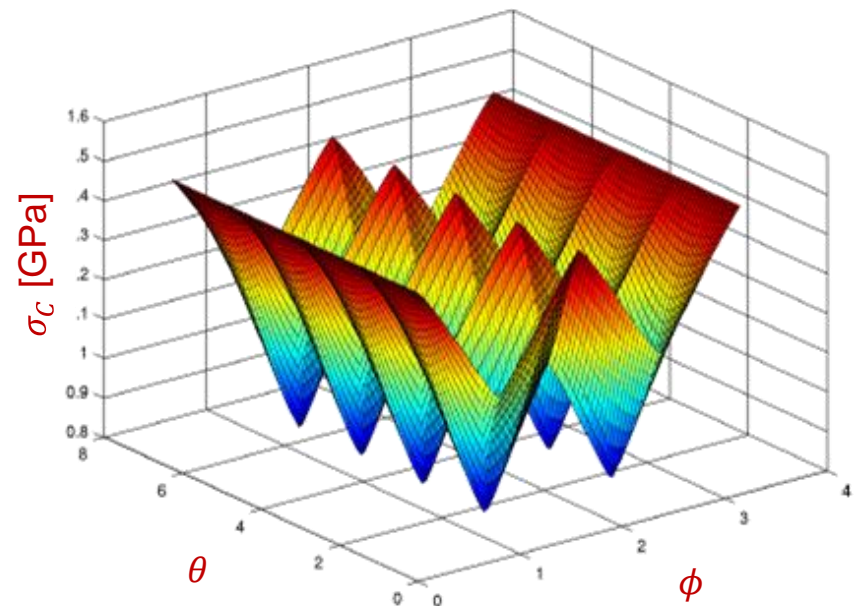
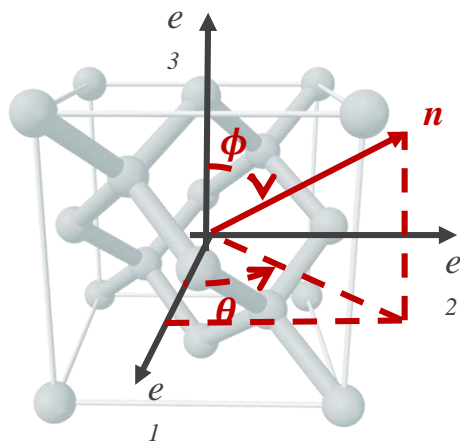
- Stochastic Volume Elements
- Should recover consistency lost due to the discontinuity

Stochastic Multi-Scale Fracture of Polycrystalline Films

- Micro-scale model: Silicon crystal
 - Different fracture strengths and critical energy release rates

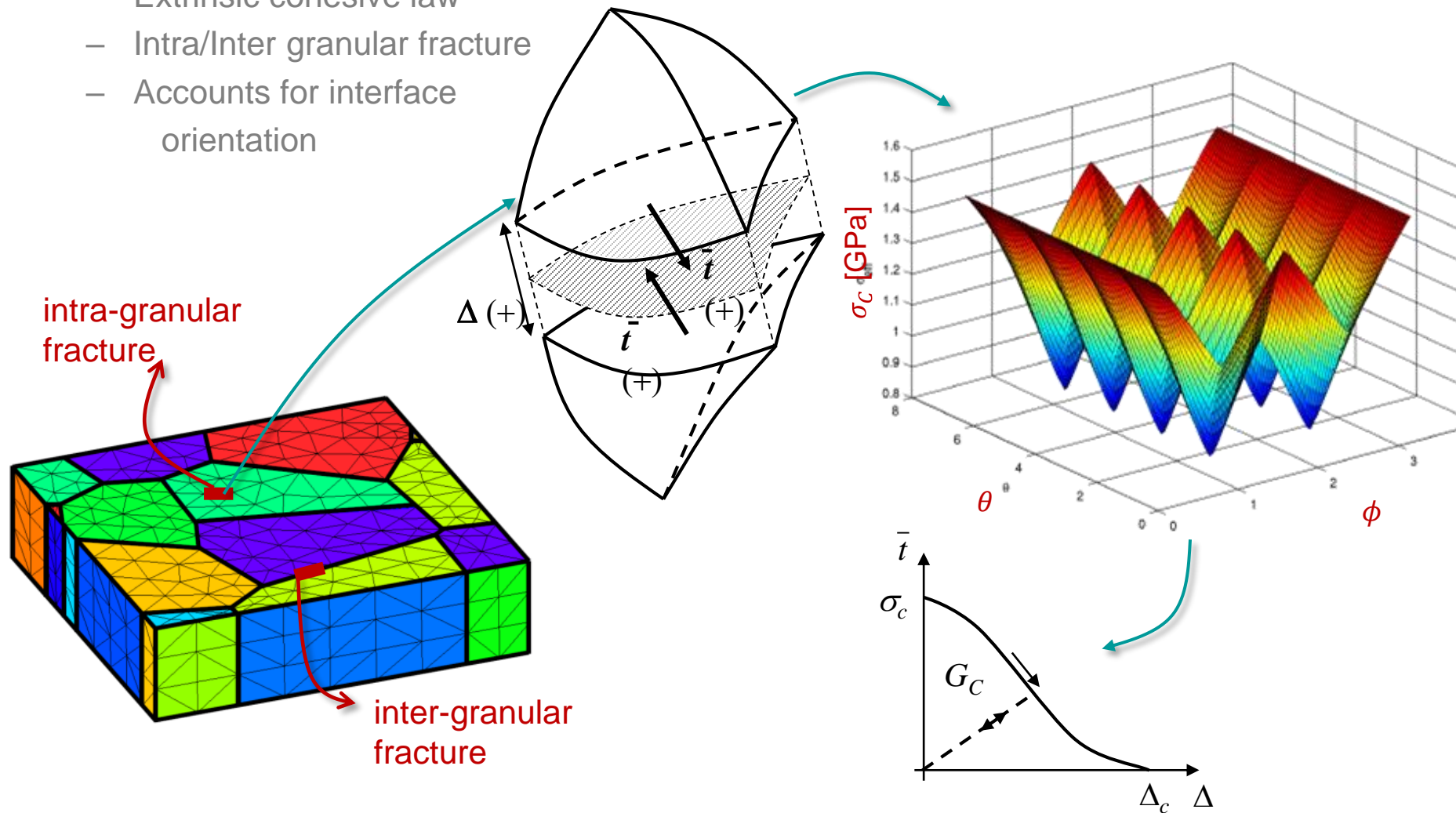


- Define a “continuous” strength mapping



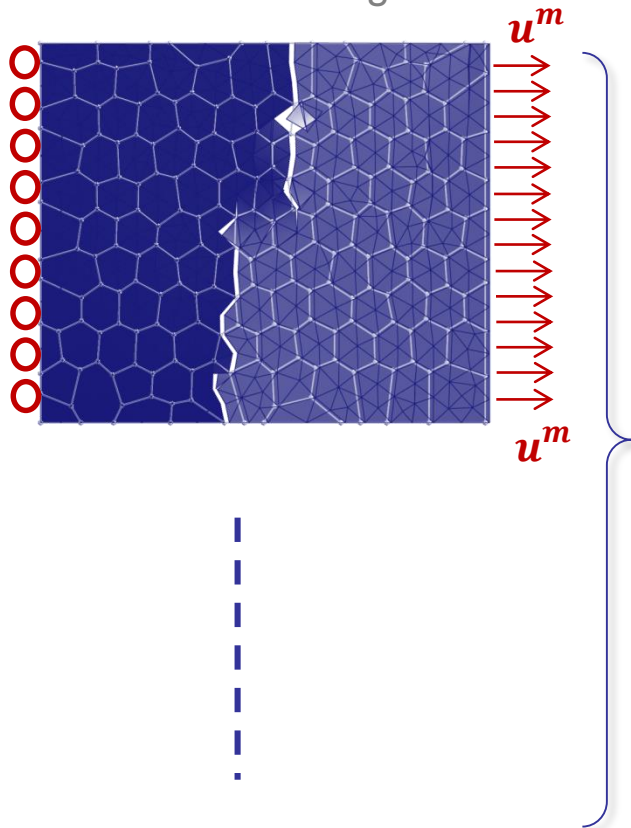
Stochastic Multi-Scale Fracture of Polycrystalline Films

- Micro-scale model: Polycrystalline films
 - [Discontinuous Galerkin method](#)
 - Extrinsic cohesive law
 - Intra/Inter granular fracture
 - Accounts for interface orientation



Stochastic Multi-Scale Fracture of Polycrystalline Films

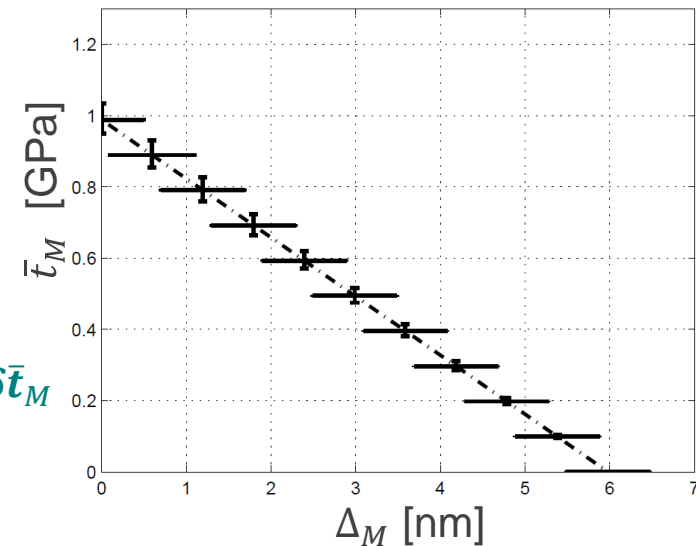
- Stochastic micro-scale to meso-scale model
 - Several SVE realizations (random grain orientation)
 - Extraction of consistent meso-scale cohesive laws
 - \bar{t}_M vs. Δ_M
 - for each SVE sample
 - Resulting meso-scale cohesive law distribution



$$\delta \bar{t}_M = \delta \sigma_M \cdot e_X$$

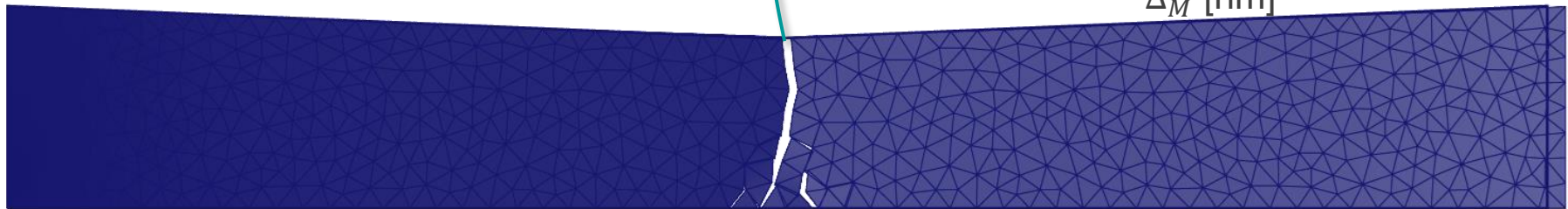
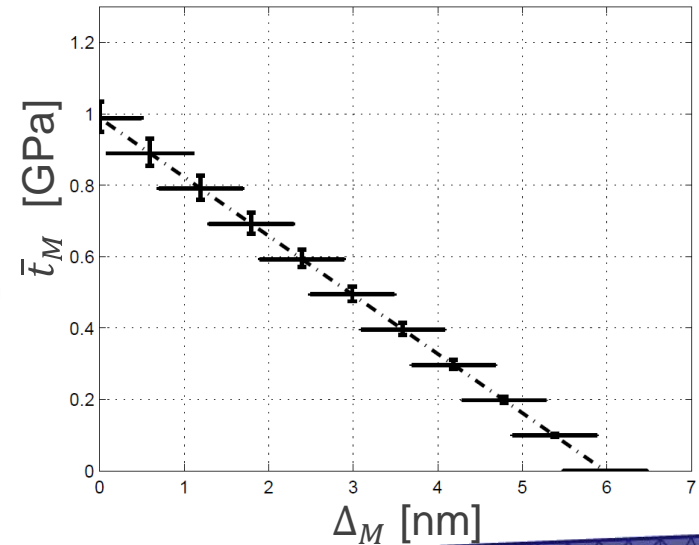


$$\delta \Delta_M = \delta u^m - L_{\text{cell}} \mathbf{C}_M^{-1} : e_X \otimes e_X \cdot \delta \bar{t}_M$$

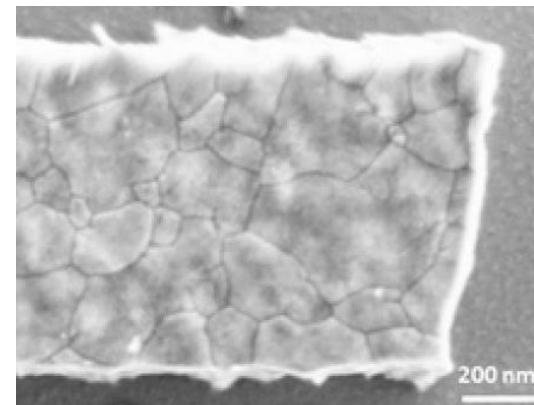


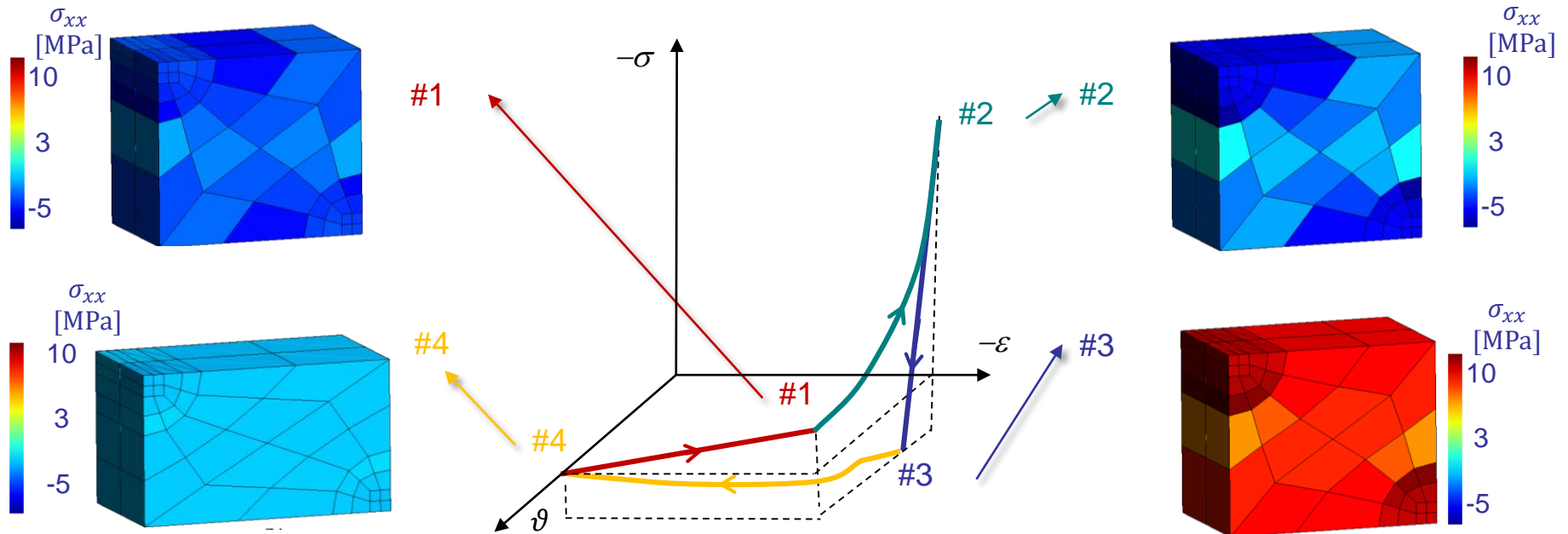
Stochastic Multi-Scale Fracture of Polycrystalline Films

- Macro-scale simulation
 - Finite element model non-conforming to the grains
 - Use homogenized (random) meso-scale cohesive laws as input



- Collaboration for experiments
 - UcL (T. Pardoen, J.-P Raskin)
- Publications
 - [10.1007/s00466-014-1083-4](https://doi.org/10.1007/s00466-014-1083-4)

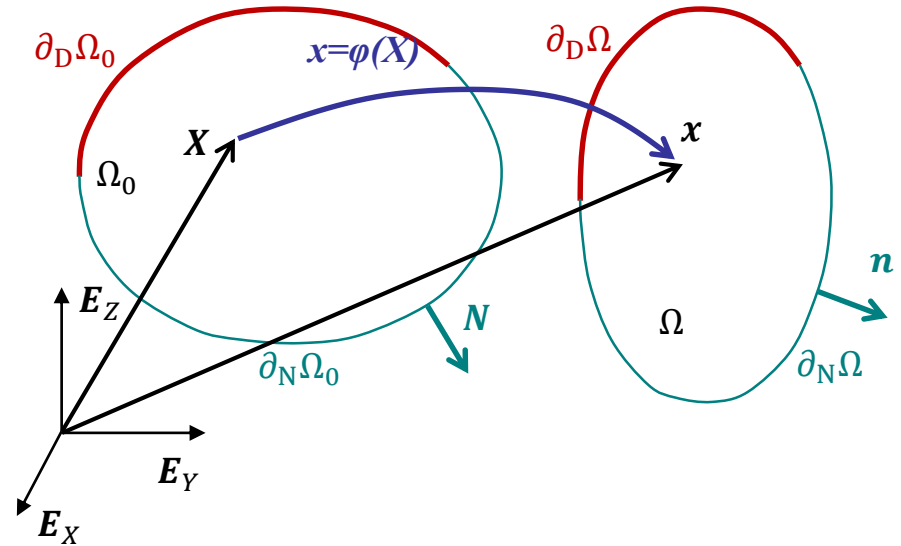




Smart Composite Materials

This project has been funded with support of the European Commission under the grant number 2012-2624/001-001-EM. This publication reflects the view only of the author, and the Commission cannot be held responsible for any use which may be made of the information contained therein.

- Electro-thermo-mechanical coupling
 - Finite field variation formulation
 - Strong coupling



Conservation of electric charge

$$\mathbf{J}_e \cdot \nabla_0 = 0$$

$$\mathbf{J}_e = \mathbf{J}_e(\mathbf{F}, \nabla_0 V, V, \nabla_0 \vartheta, \vartheta; \mathbf{Z})$$

Conservation of energy

$$\rho C_v \dot{\vartheta} - \mathcal{D} + \mathbf{J}_y \cdot \nabla_0 = 0$$

$$\mathbf{J}_y = \mathbf{q} + V \mathbf{J}_e$$

$$\mathbf{q} = \mathbf{q}(\mathbf{F}, V, \nabla_0 \vartheta, \vartheta; \mathbf{Z})$$

Conservation of momentum balance

$$\mathbf{P} \cdot \nabla_0 = 0$$

$$\mathbf{P} = \mathbf{P}(\mathbf{F}, \vartheta; \mathbf{Z})$$

$$\mathcal{D} = \beta \dot{\rho} \tau + \vartheta \frac{\partial \dot{W}^{el}}{\partial \vartheta}$$

- Two-way electro-thermal coupling

- Seebeck coefficient α
- Finite strain conductivities $\mathbf{K}(V, \vartheta) = \mathbf{F}^{-1} \cdot \mathbf{k}(V, \vartheta) \cdot \mathbf{F}^{-T} J$ & $\mathbf{L}(V, \vartheta) = \mathbf{F}^{-1} \cdot \mathbf{l}(V, \vartheta) \cdot \mathbf{F}^{-T} J$

$$\begin{pmatrix} \mathbf{J}_e \\ \mathbf{J}_y \end{pmatrix} = \begin{pmatrix} \mathbf{L}(V, \vartheta) & \alpha \mathbf{L}(V, \vartheta) \\ V \mathbf{L}(V, \vartheta) + \alpha T \mathbf{L}(V, \vartheta) & \mathbf{K}(V, \vartheta) + \alpha V \mathbf{L}(V, \vartheta) + \alpha^2 T \mathbf{L}(V, \vartheta) \end{pmatrix} \begin{pmatrix} -\nabla_0 V \\ -\nabla_0 \vartheta \end{pmatrix}$$

Non energetically

conjugated

[Liu IJES, 2012]

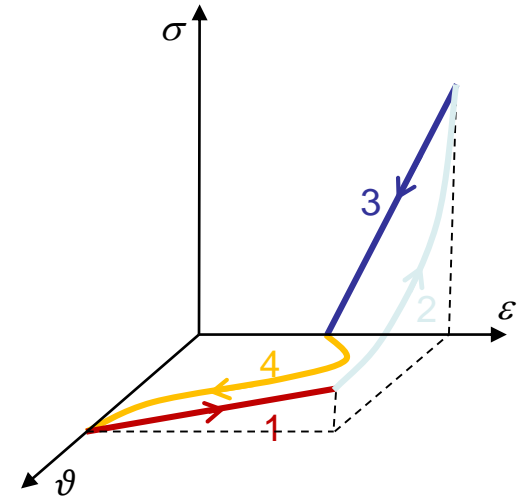
Change of
variables

$$\begin{cases} f_V = -\frac{V}{\vartheta} \\ f_\vartheta = \frac{1}{\vartheta} \end{cases}$$

$$\begin{pmatrix} \mathbf{J}_e \\ \mathbf{J}_y \end{pmatrix} = \mathbf{Z}(\mathbf{F}, f_V, f_\vartheta) \begin{pmatrix} \nabla_0 f_V \\ \nabla_0 f_\vartheta \end{pmatrix}$$

- The coefficients matrix $\mathbf{Z}(\mathbf{F}, f_V, f_\vartheta)$ is symmetric and definite positive

- Thermo-mechanical shape memory polymer
 - Deformations above glass transition temperature ϑ_g (1)
 - Fixed once cooled down below ϑ_g (2 & 3)
 - Recovery once heated up (4)



- Elasto-visco-plastic model constitutive behavior

- Different mechanisms (α)
 - Multiplicative decomposition

$$\mathbf{F}(\alpha) = \mathbf{F}^e(\alpha) \mathbf{F}^p(\alpha)$$

- Free energy

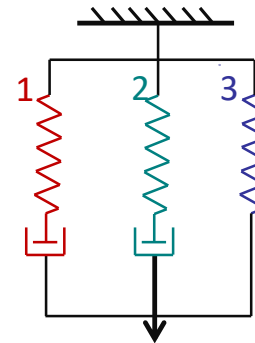
$$\psi = \sum_{\alpha} \psi^{(\alpha)}(\mathbf{C}^e(\alpha), \vartheta)$$

- Thermo-visco-plasticity

$$\tau^{(\alpha)} = \mathcal{T}(\mathbf{C}^e(\alpha), \mathbf{F}^p(\alpha), \dot{p}^{(\alpha)}, \vartheta, \xi^{(\alpha)})$$

- Stress and dissipation

$$\begin{cases} \mathbf{P} = \mathbf{P}(\mathbf{F}, \vartheta; \mathbf{F}^p(\alpha), p^{(\alpha)}, \xi^{(\alpha)}) \\ \mathcal{D} = \beta \dot{p}^{(\alpha)} \tau^{(\alpha)} \end{cases}$$

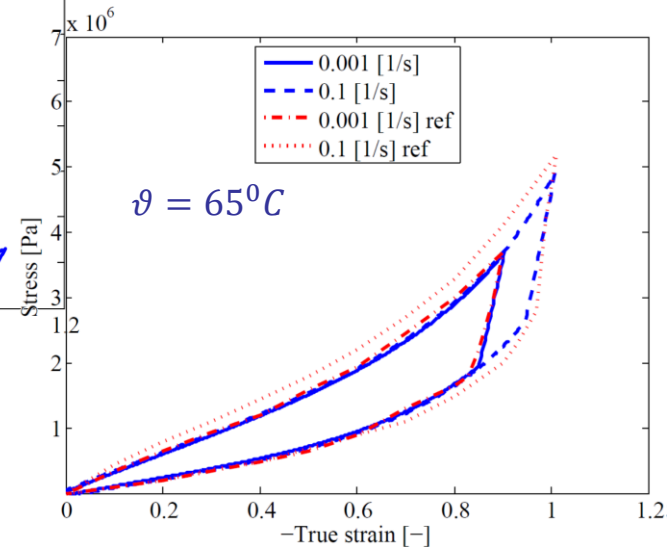
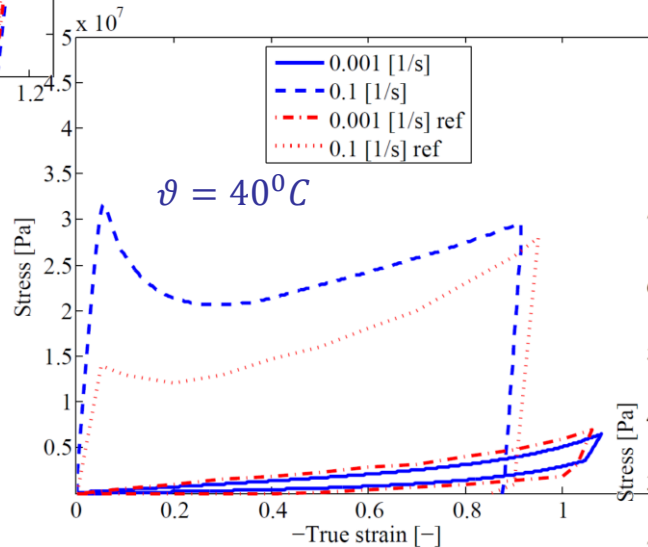
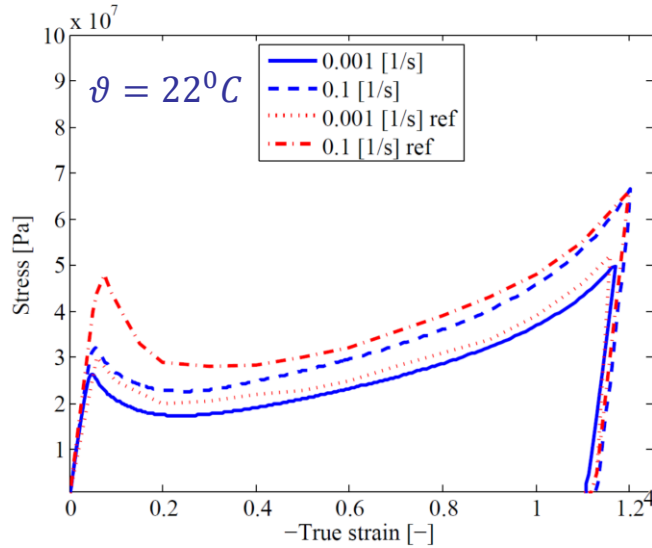


Intermolecular bonds/crosslink stretching Molecular resistance

[V. Srivastav et. al, 2010]

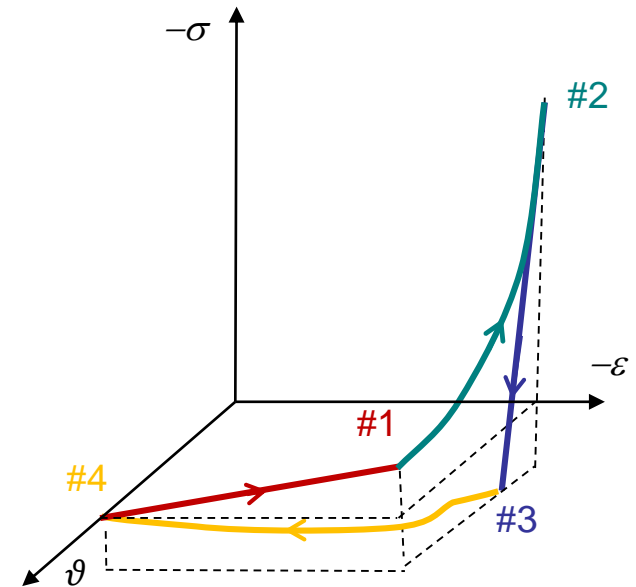
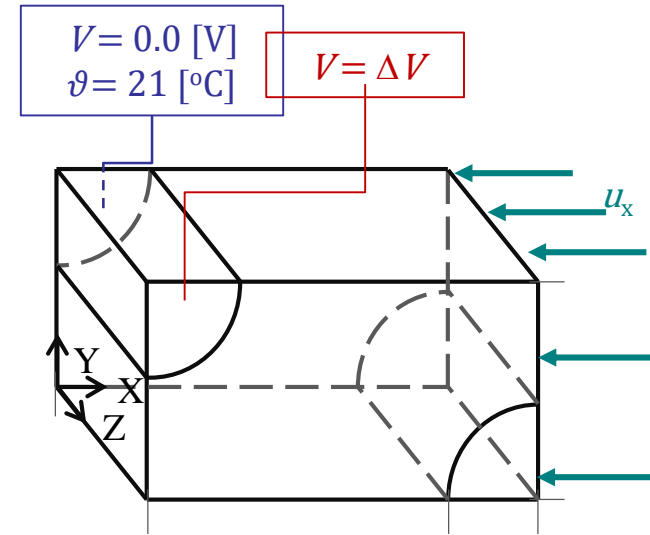
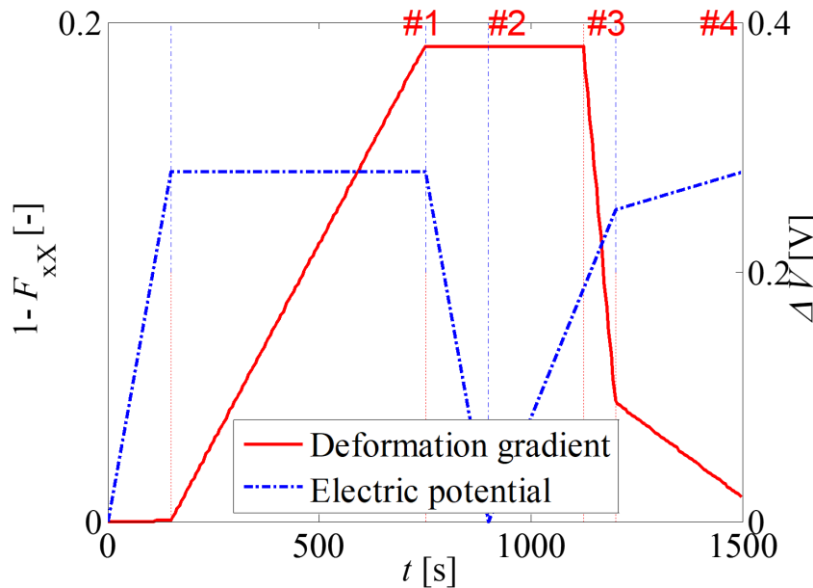
- Elasto-visco-plastic behavior of thermo-mechanical shape memory polymer

Refs. by [V. Srivastav et. al, 2010]

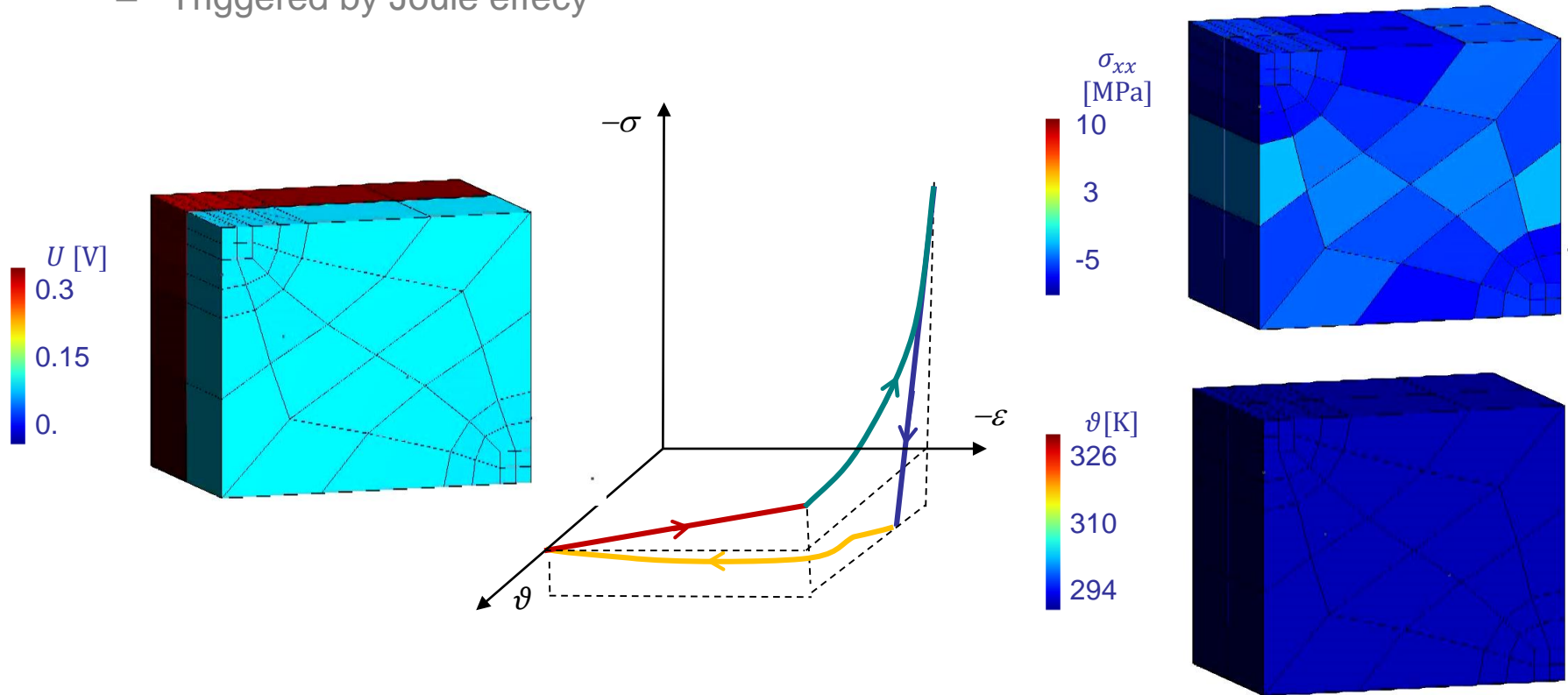


- Recovery of a shape memory composite unit cell

- Carbon Fiber reinforced SMP
- Shape memory effect triggered by Joule effect
- Test with compressive force recovery:
 - #1: Compression deformation obtained above ϑ_g
 - #2: Fixation of the deformation above ϑ_g
 - #3: Reheat above ϑ_g at constant deformation:
 - recovery force, the cell wants to expand
 - #4: Release deformation/stress
 - recovery force vanishes

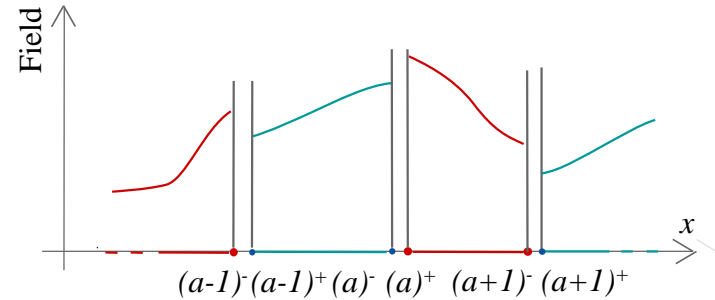


- Recovery of a shape memory composite unit cell
 - Carbon Fiber reinforced SMP
 - Triggered by Joule effecty



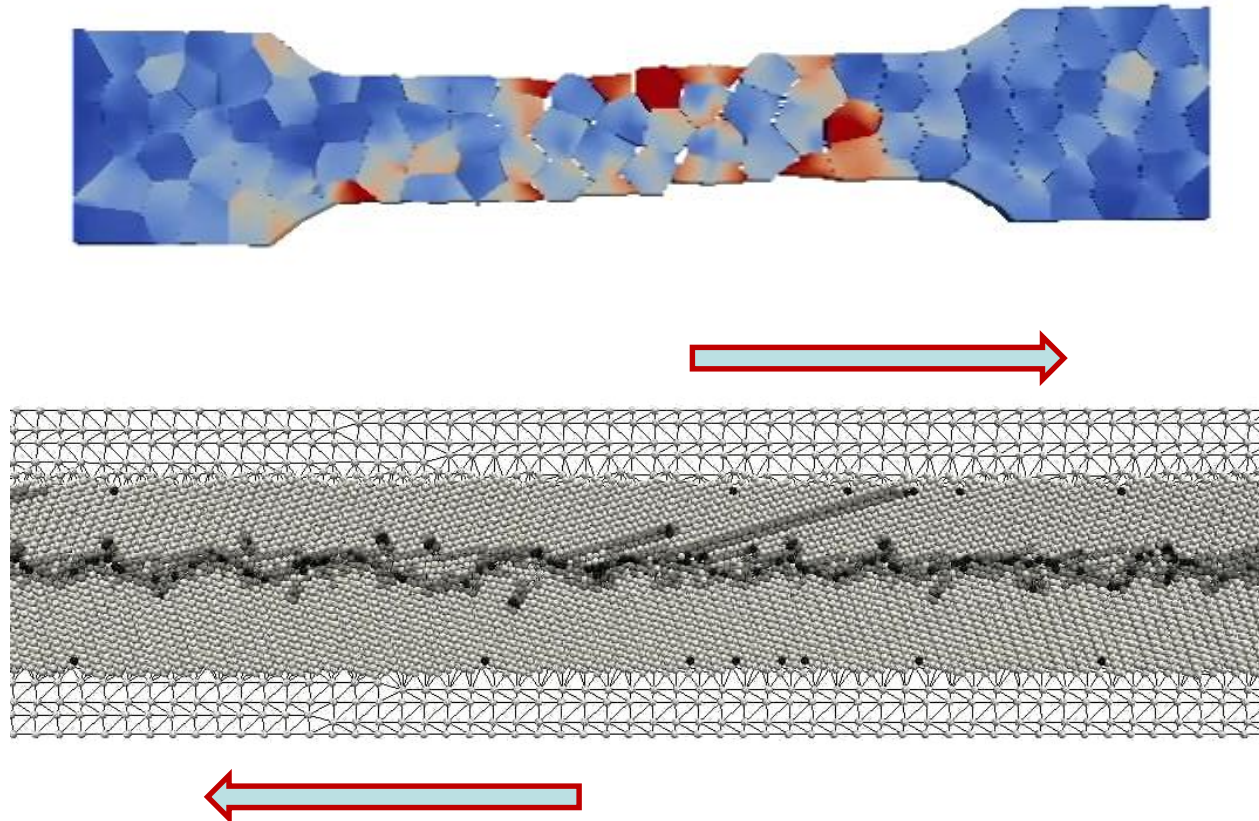
- Discontinuous Galerkin implementation

- Finite-element discretization
- Same **discontinuous** polynomial approximations for the
 - **Test** functions φ_h and
 - **Trial** functions $\delta\varphi$
- Extended to non-linear electro-thermo-mechanical coupling



- Publication (doi)

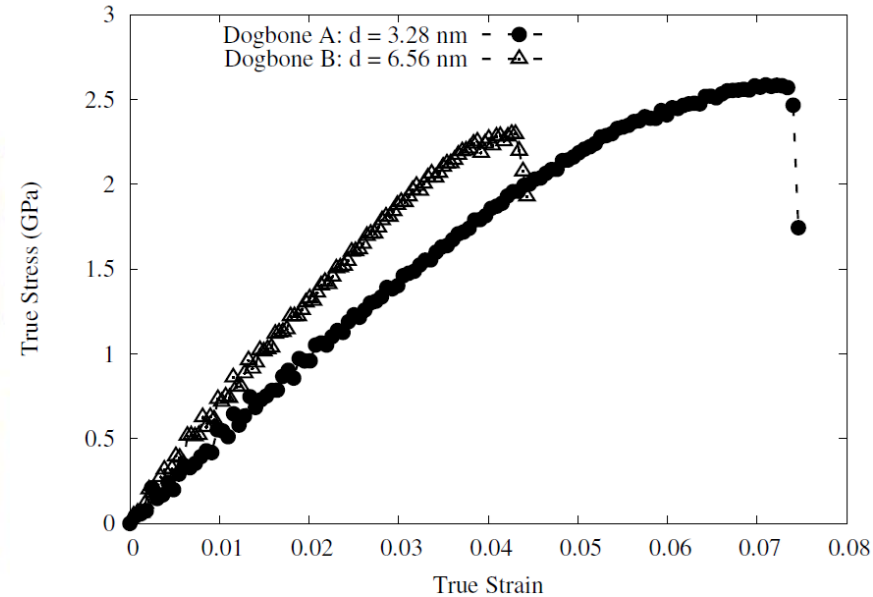
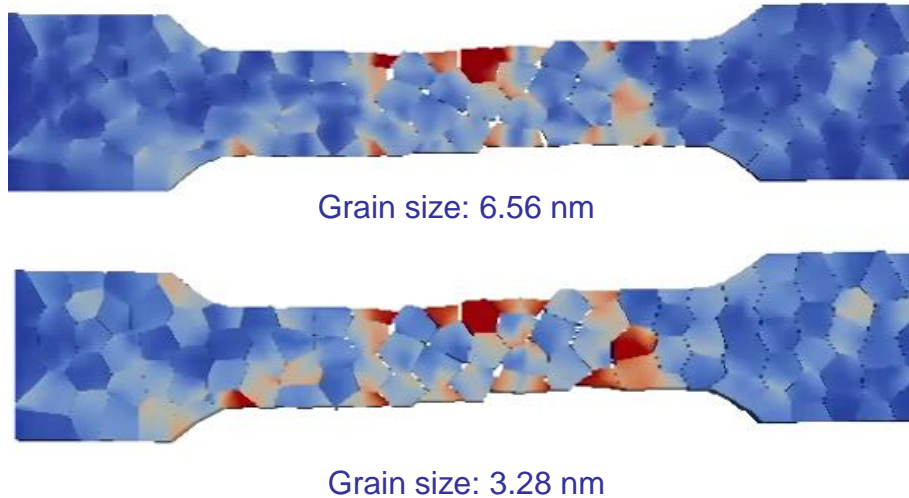
- [10.1007/s11012-017-0743-9](https://doi.org/10.1007/s11012-017-0743-9)
- [10.1016/j.jcp.2017.07.028](https://doi.org/10.1016/j.jcp.2017.07.028)



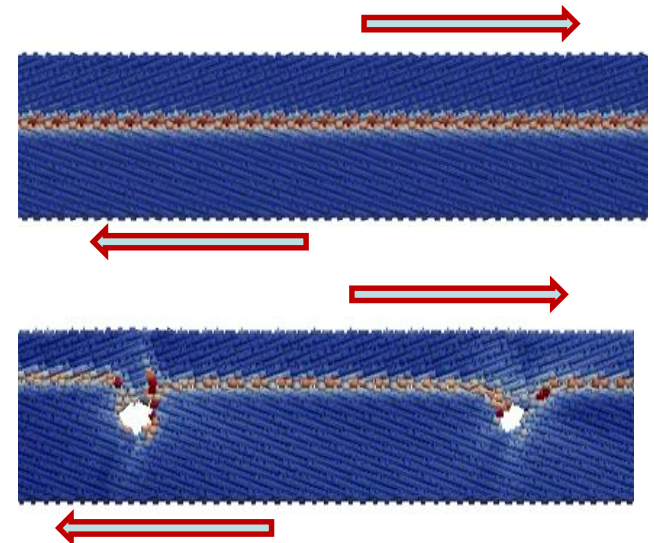
Multi-Scale Modeling of Nano-Crystal Grain Boundary Sliding

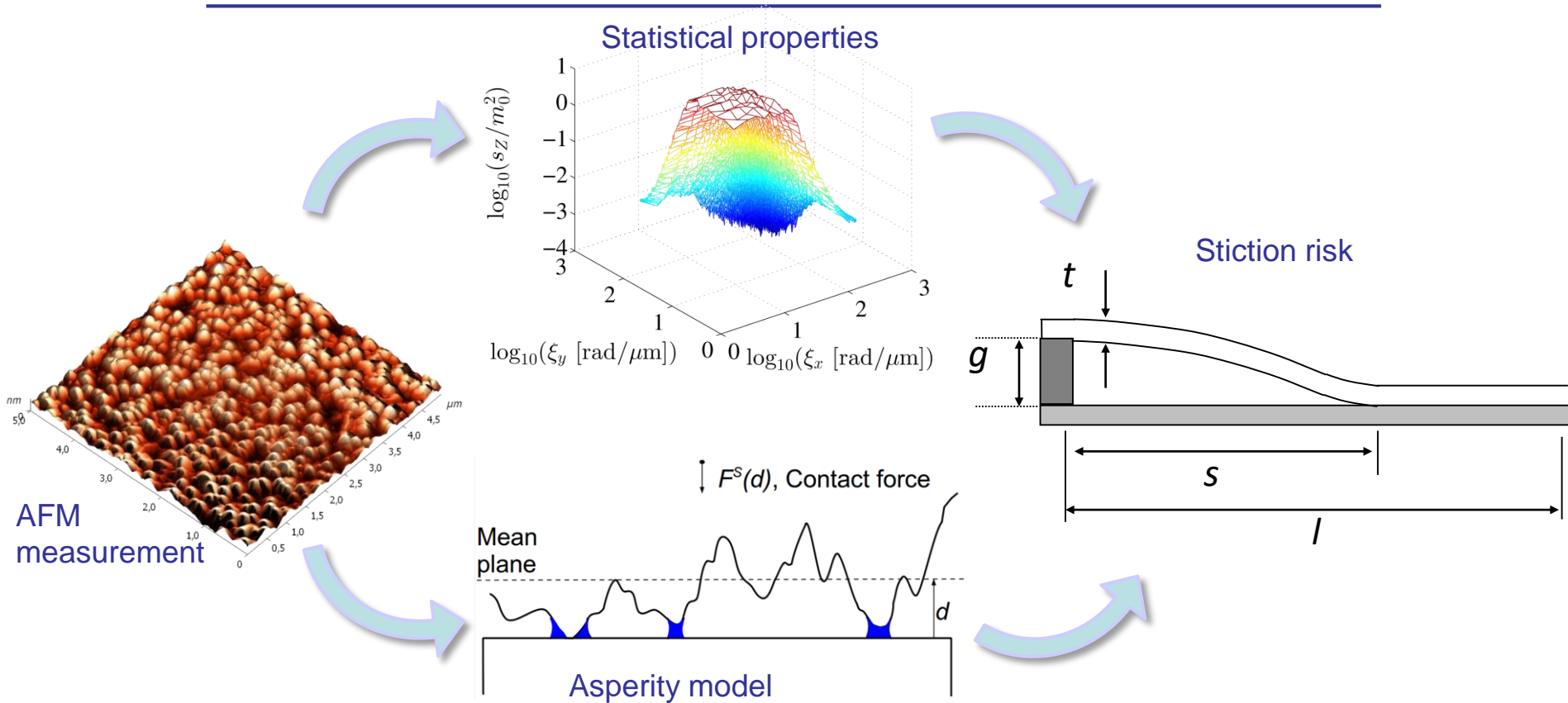
Multi-Scale Modeling of Nano-Crystal Grain Boundary Sliding

- Grain size effect
 - Competition between inter-intra granular



- Effect of nano-voids in the grain boundaries
 - Different deformation mechanism
 - Lower yield stress
- Collaboration
 - EC Nantes, Univ. of Vermont, Oxford
- Publications
 - [10.1016/j.commat.2014.03.070](https://doi.org/10.1016/j.commat.2014.03.070)
 - [10.1016/j.actamat.2013.10.056](https://doi.org/10.1016/j.actamat.2013.10.056)
 - [10.1016/j.jmps.2013.04.009](https://doi.org/10.1016/j.jmps.2013.04.009)





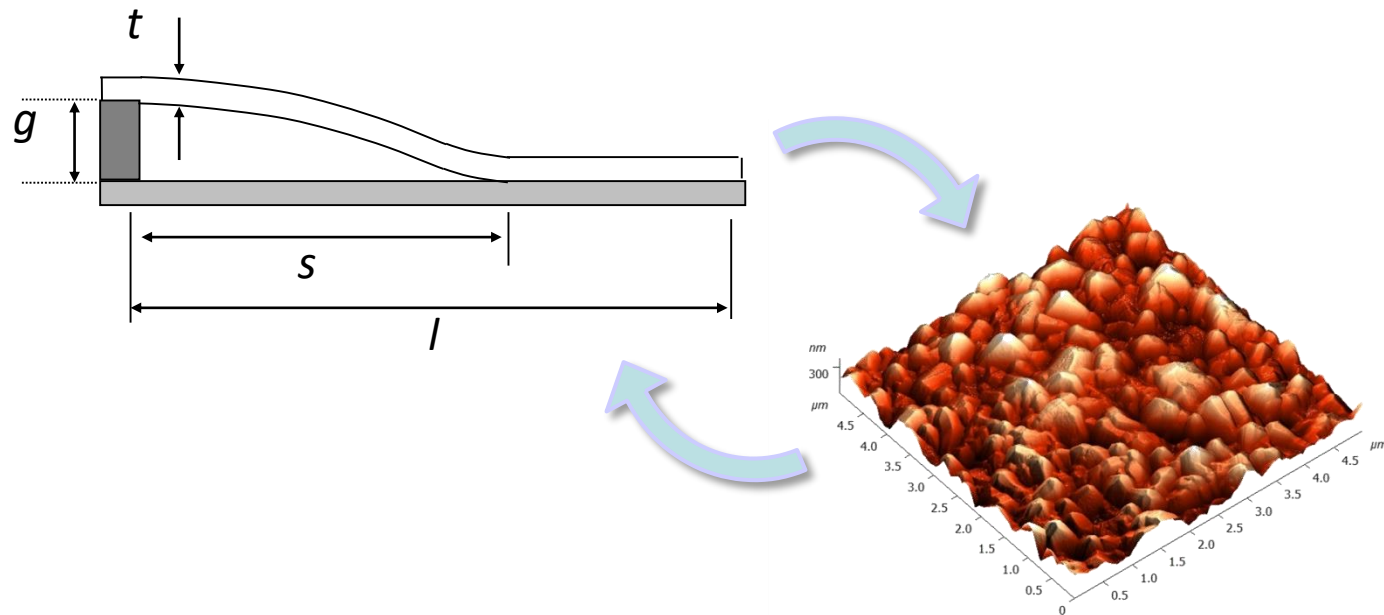
Stochastic Multi-Scale Model to Predict MEMS Stiction

3SMVIB: The research has been funded by the Walloon Region under the agreement no 1117477 (CT-INT 2011-11-14) in the context of the ERA-NET MNT framework.

The research has been funded by the Belgian National Fund for Education at the Research in Industry and Farming.

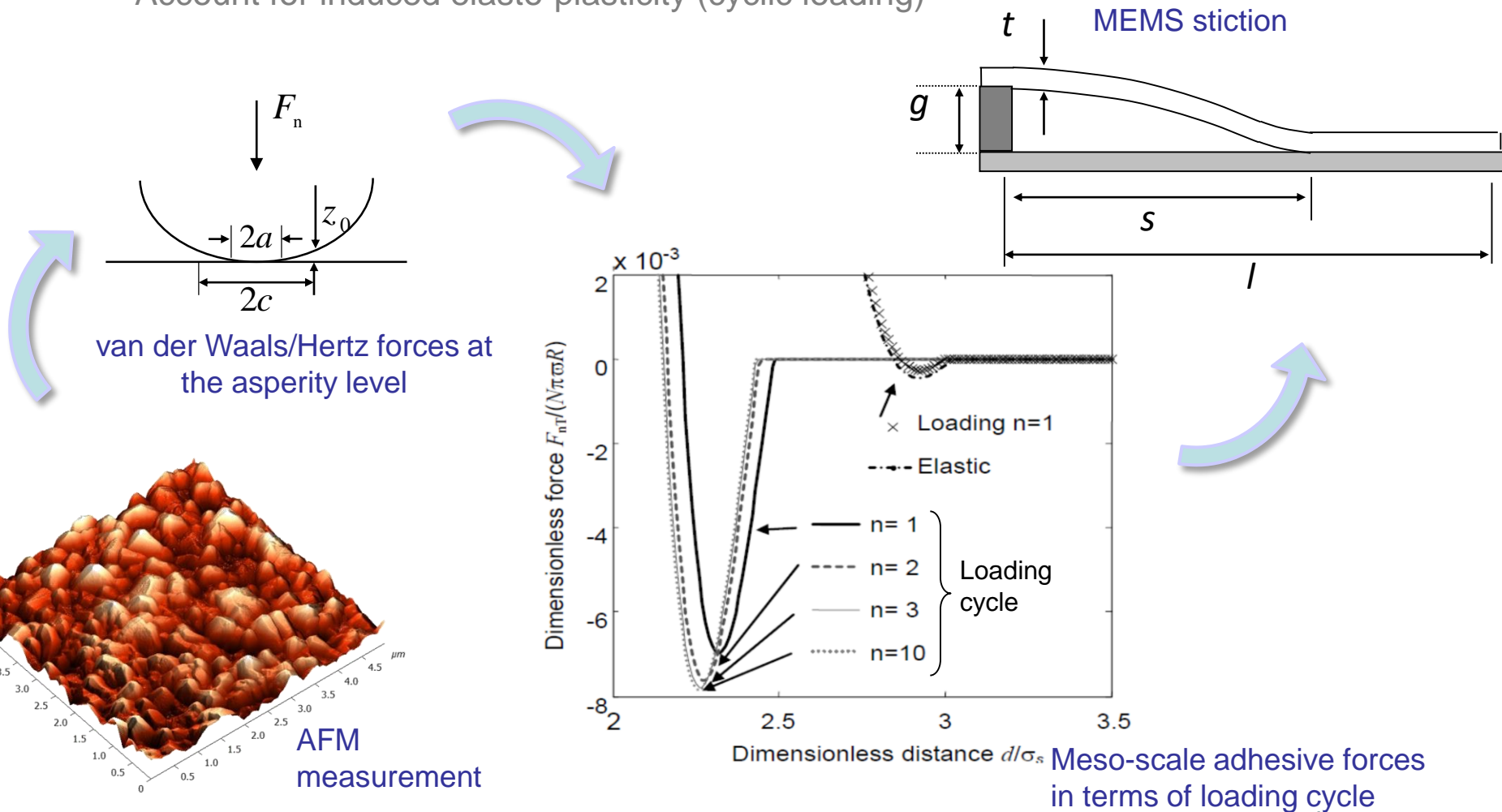
Stochastic Multi-Scale Model to Predict MEMS Stiction

- Stiction (adhesion of MEMS)
 - Different physics at the different scales
 - Elastic or Elasto-plastic behaviors
 - Due to van der Waals (dry environment) and/or capillary (humid environment) forces
- Requires surfaces topology knowledge (AFM measures)
 - Subject to uncertainties



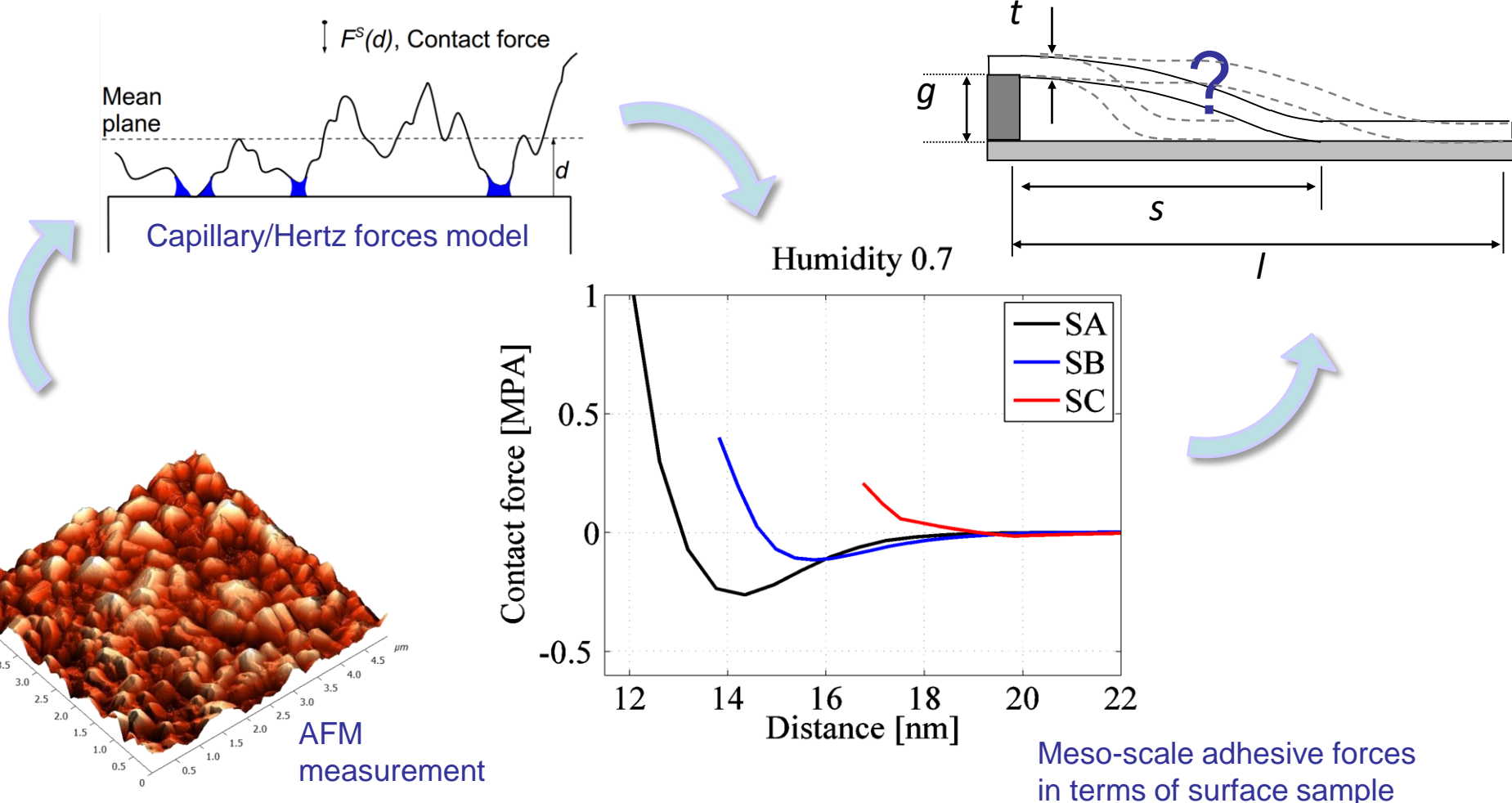
Stochastic Multi-Scale Model to Predict MEMS Stiction

- Deterministic multi-scale models for van der Waals forces
 - Extraction of meso-scale adhesive-forces
 - Using statistical representations of the rough surface (average solution)
 - Account for induced elasto-plasticity (cyclic loading)



Stochastic Multi-Scale Model to Predict MEMS Stiction

- New multi-scale models with capillary effect
 - Extraction of meso-scale adhesive-forces from a single surface measurement
 - Depends on the surface sample measurement location
 - Motivates the development of a stochastic multi-scale method



Meso-scale adhesive forces in terms of surface sample

Stochastic Multi-Scale Model to Predict MEMS Stiction

- Stochastic multi-scale model: From the AFM to virtual surfaces

Enforce statistical moments with maximum entropy method

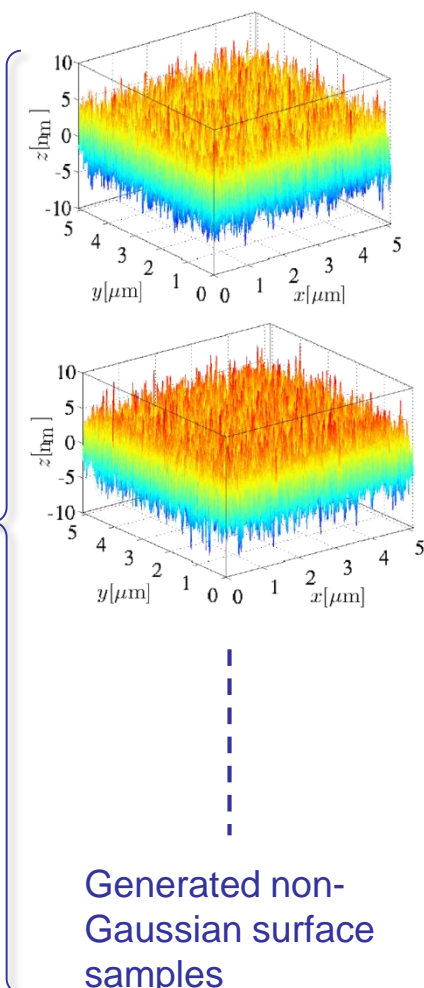
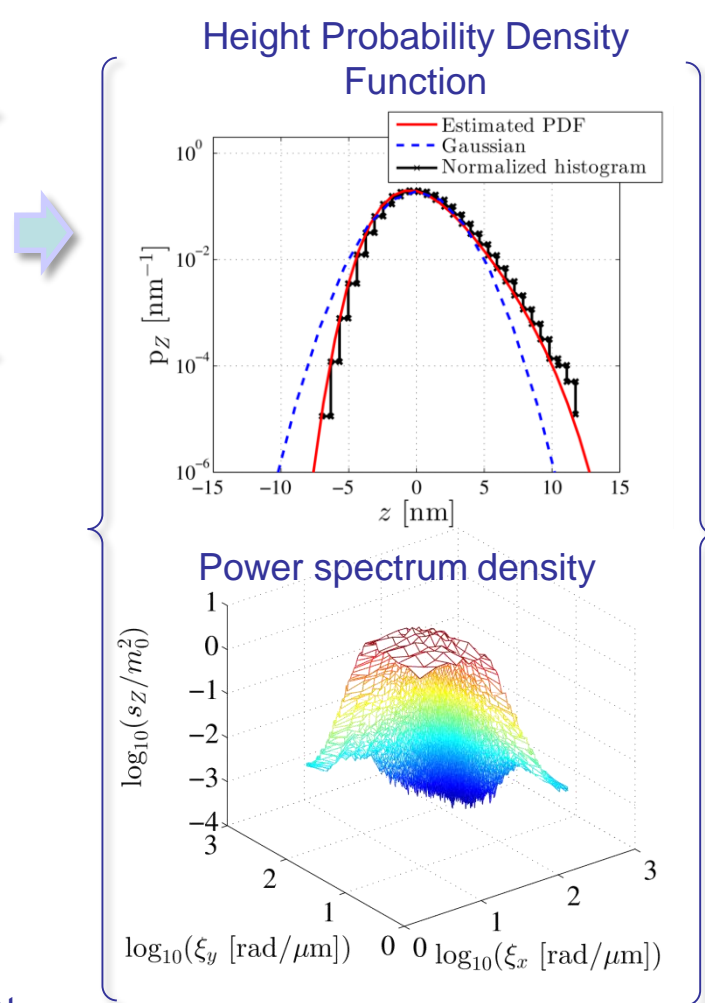
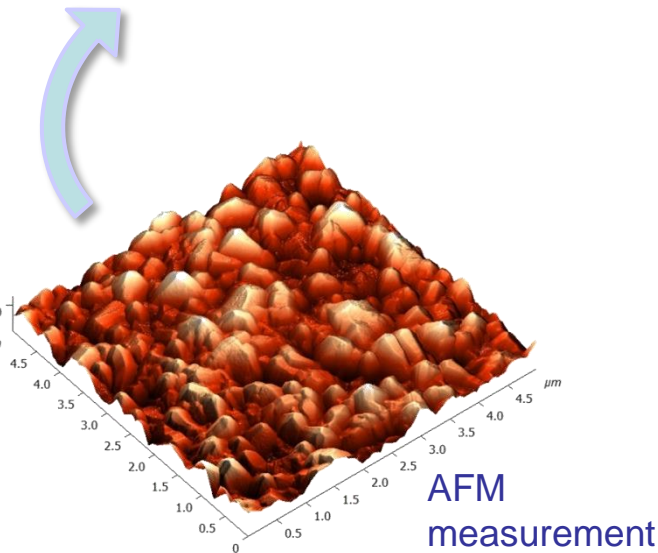
$$m_i = \int_R z^i p_Z(z) dz$$

$$p_Z = \arg \max - \int_R p_Z(z) \ln(p_Z(z)) dz$$

Evaluate PSD from covariance

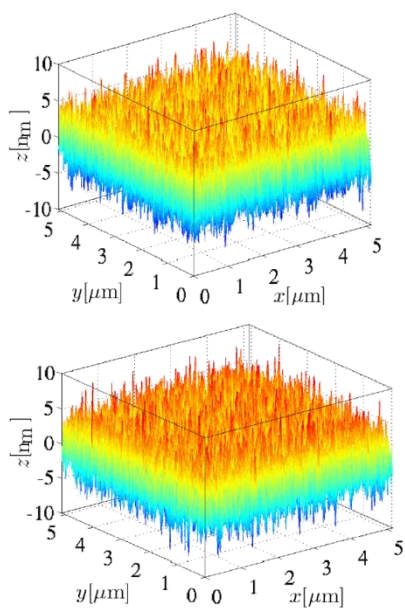
$$\tilde{R}(\boldsymbol{\tau}) = \mathbb{E}[z(\boldsymbol{x}), z(\boldsymbol{x} + \boldsymbol{\tau})]$$

$$S_Z(\boldsymbol{\tau}) = \int_{R^2} \exp(-i\boldsymbol{\zeta} \cdot \boldsymbol{\tau}) \tilde{R}_Z(\boldsymbol{\tau}) d\boldsymbol{\zeta}$$

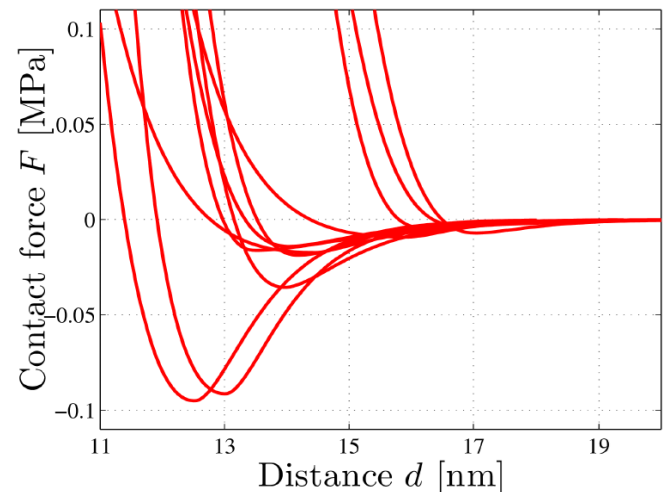
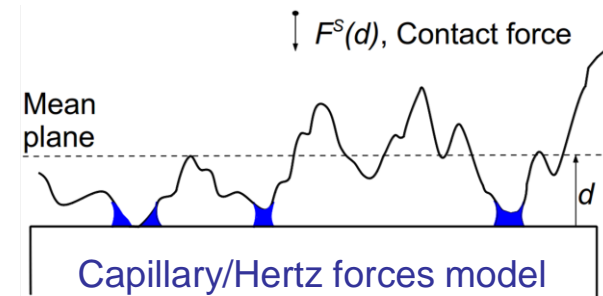
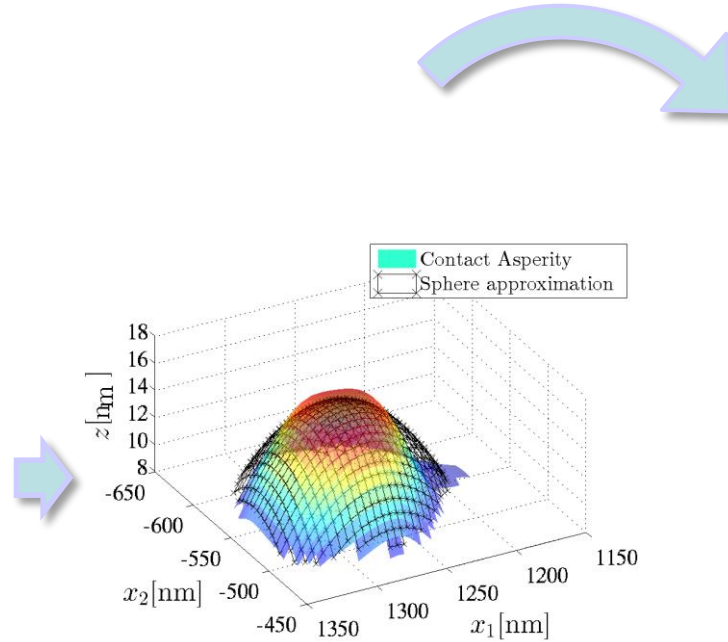


Stochastic Multi-Scale Model to Predict MEMS Stiction

- Stochastic multi-scale model: Evaluate meso-scale surface forces



Generated non-Gaussian surface samples



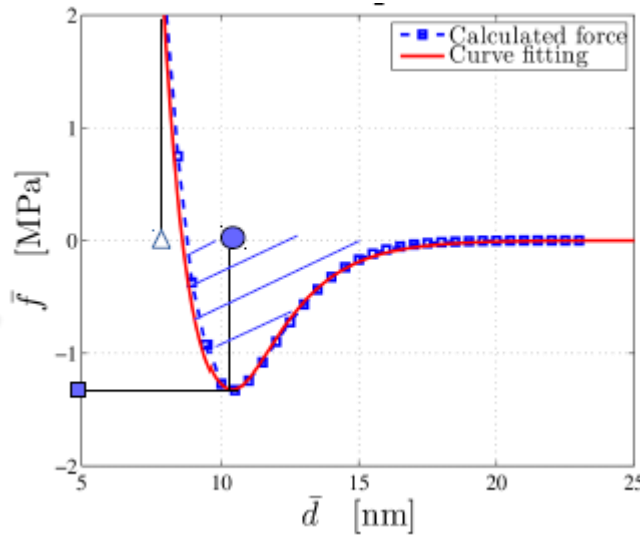
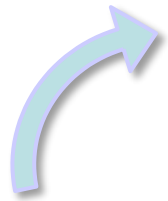
Computed meso-scale adhesive forces

Stochastic Multi-Scale Model to Predict MEMS Stiction

- Stochastic multi-scale model: Stochastic model of meso-scale adhesion forces

Definition of parameter vector v

$$\bar{f}(\bar{d}) = \Phi(\bar{d}, v)$$



Enforce physical constraints

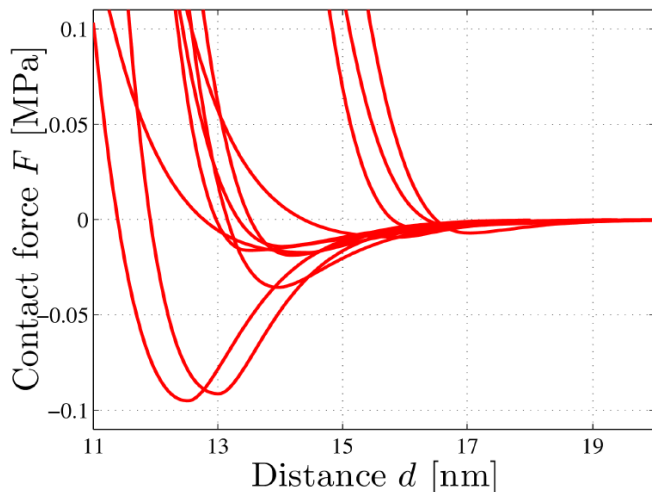
$$v^{(i)} \rightarrow q^{(i)}$$

Principal component analysis from covariance matrix $[\tilde{R}_Q]$ of vectors $q^{(i)}$

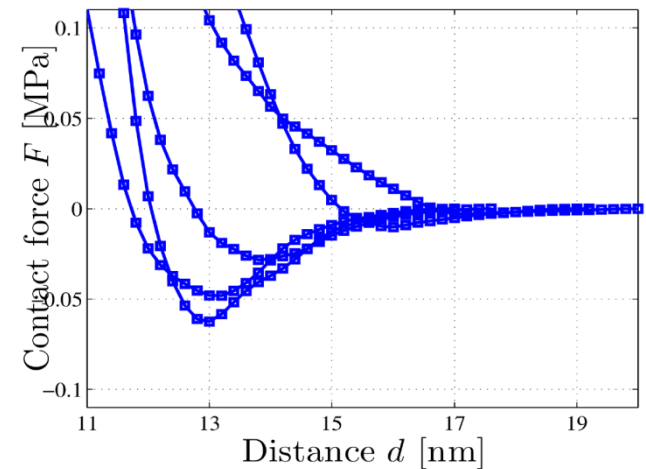
$$\eta^T = (q - \bar{q})^T [A][\lambda]^{-1/2}$$

Polynomial chaos expansion

$$\eta^{PC} = \sum c_\alpha \Psi_\alpha(\xi)$$



Computed meso-scale adhesive forces

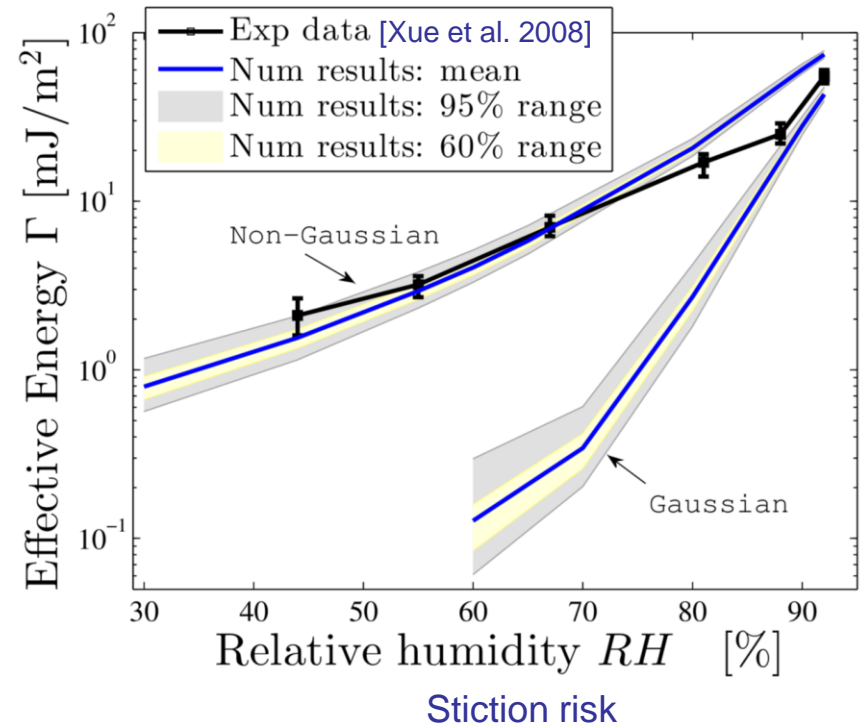
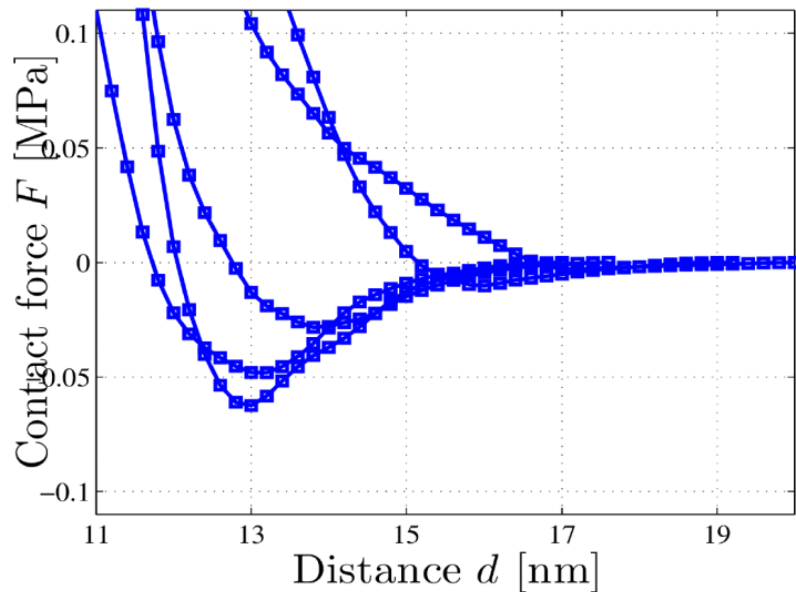
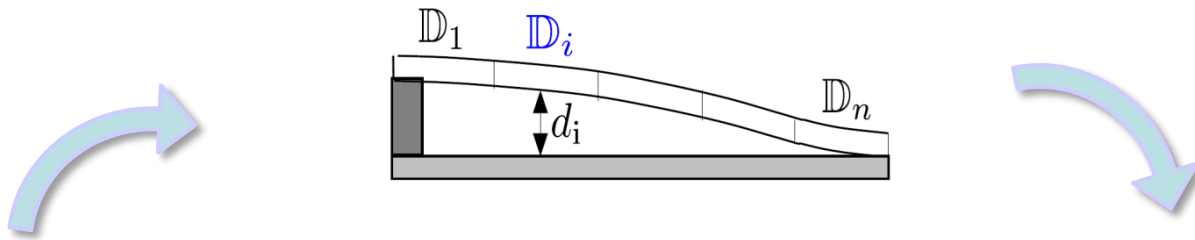


Generated adhesive forces

Stochastic Multi-Scale Model to Predict MEMS Stiction

- Stochastic multi-scale model: Stochastic MEMS stiction analyzes

Stochastic finite elements (random contact law variable)



Generated meso-scale adhesive forces

- Application to robust design
 - Determination of probabilistic meso-scale properties
 - Propagate uncertainties to higher scale
 - Vibro-meter sensors:
 - Uncertainties in stiction risk
- 3SMVIB MNT.ERA-NET project
 - Open-Engineering, V2i, ULiège (Belgium)
 - Polit. Warszawska (Poland)
 - IMT, Univ. Cluj-Napoca (Romania)
- FNRS-FRIA fellowship
- Publications (doi)
 - [10.1109/JMEMS.2018.2797133](https://doi.org/10.1109/JMEMS.2018.2797133)
 - [10.1016/j.triboint.2016.10.007](https://doi.org/10.1016/j.triboint.2016.10.007)
 - [10.1007/978-3-319-42228-2_1](https://doi.org/10.1007/978-3-319-42228-2_1)
 - [10.1016/j.cam.2015.02.022](https://doi.org/10.1016/j.cam.2015.02.022)
 - [10.1016/j.triboint.2012.08.003](https://doi.org/10.1016/j.triboint.2012.08.003)
 - [10.1007/978-1-4614-4436-7_11](https://doi.org/10.1007/978-1-4614-4436-7_11)
 - [10.1109/JMEMS.2011.2153823](https://doi.org/10.1109/JMEMS.2011.2153823)
 - [10.1063/1.3260248](https://doi.org/10.1063/1.3260248)